

Multi-wavelength Accretion
Studies of Cataclysmic
Variable Stars



Deanne
Coppejans

Multi-wavelength Accretion Studies of Cataclysmic Variable Stars

Proefschrift

ter verkrijging van de graad van doctor
aan de Radboud Universiteit Nijmegen
op gezag van de rector magnificus prof. dr. J.H.J.M. van Krieken,
volgens besluit van het college van decanen
in het openbaar te verdedigen op
Maandag 3 Oktober 2016
om 10:30 uur precies

door

Deanne Larissa Coppejans

geboren op 7 Februari 1988
te Zuid-Afrika

PROMOTOREN: Prof. dr. P.J. Groot
Prof. dr. P.A. Woudt University of Cape Town, SA

COPROMOTOR: Dr. E.G. K rding

MANUSCRIPTCOMMISSIE: Prof. dr. R. Kleiss
Prof. dr. F.W.M. Verbunt
Prof. dr. R.P. Fender University of Oxford, UK
Prof. dr. A. Achterberg
Dr. S. Scaringi MPE, Duitsland

  2016, Deanne Larissa Coppejans
Multi-wavelength Accretion Studies of Cataclysmic Variable Stars
Thesis, Radboud University Nijmegen
Printed by Ipskamp Printing
Illustrated; with bibliographic information and Dutch summary
ISBN: 978-94-028-0320-4

CONTENTS

1	Introduction	1
1.1	Cataclysmic Variables	1
1.1.1	Structure	1
1.1.2	Mass Transfer	3
1.1.3	Formation and Evolution	4
1.2	Dwarf Novae and Novalikes	6
1.2.1	Dwarf Nova Outburst Mechanism	7
1.2.2	Superoutburst Mechanism	9
1.3	Radio Emission from Cataclysmic Variables	10
2	High-speed photometry of faint Cataclysmic Variables	13
2.1	Introduction	14
2.2	Observations	15
2.3	Discussion and Conclusions	40
3	Statistical properties of dwarf novae-type Cataclysmic Variables	43
3.1	Introduction	44
3.2	CRTS	45
3.3	Classification Script	47
3.4	The Outburst Catalogue	52
3.5	Analysis and Discussion	52
3.5.1	The Orbital Period Distribution	56
3.5.2	Colour-colour Plots	57
3.5.3	Outburst Properties	57
3.5.4	Distance and Absolute Magnitude Estimates	60
3.6	Conclusion	66
3.A	Determining the Distance Upper-limit (Column 33)	67
3.A.1	Inclination	68
3.A.2	Absolute Outburst Magnitude (V_O)	69

3.A.3	Quiescent Outburst Magnitude (v_O)	69
3.A.4	Upper-limit Determination	69
4	Novalike cataclysmic variables are significant radio emitters	71
4.1	Introduction	72
4.2	Targets	73
4.3	Observations	76
4.4	Results	77
4.4.1	Total fluxes	77
4.4.2	Polarization	78
4.4.3	Variability	79
4.4.4	Spectral Indices	81
4.5	Discussion	81
4.5.1	Thermal Emission	84
4.5.2	Non-thermal Emission	86
4.5.3	Source of the Emission	87
4.6	Conclusion	88
4.A	Subappendix	90
5	Dwarf nova-type cataclysmic variables are significant radio emitters	93
5.1	Introduction	93
5.2	Targets	95
5.2.1	Z Camelopardalis (Z Cam)	97
5.2.2	RX Andromedae (RX And)	97
5.2.3	SU Ursae Majoris (SU UMa)	97
5.2.4	YZ Cancri (YZ Cnc)	97
5.2.5	U Geminorum (U Gem)	98
5.3	Observations	98
5.4	Results	99
5.4.1	Detections	99
5.4.2	Variability	101
5.4.3	Spectral Indices and Polarization	101
5.5	Discussion	101
5.5.1	DN in Outburst as Radio Emitters	101
5.5.2	Radio Emission Mechanism in DN Outbursts	107
5.5.3	What Determines the Radio Luminosity?	111
5.6	Summary	114
5.A	Subappendix	117
	Bibliography	119
	Summary	135
	Optical CV Population Studies	135
	Radio Emission from Non-magnetic CVs	136

Looking Forward	137
Samenvatting	139
Optical CV Population Studies	139
Radiostraling van Niet-magnetische CVs	140
Vooruit Kijken	141
Publication List	143
Proceedings	143
Curriculum vitae	145
Acknowledgements	147

CHAPTER 1

INTRODUCTION

1.1 Cataclysmic Variables

Cataclysmic Variables (CVs) are binary star systems in which a white dwarf accretes matter from a main-sequence secondary star via Roche-lobe overflow [see Warner, 1995, for a review]. The mass-transfer in these systems produces a broad range of variability in luminosity (in terms of amplitude and timescale). CVs are consequently exemplary targets with which to study the process of mass-transfer and accretion – important topics in astronomy, as they govern everything from the formation of stars, to the evolution of galaxies.

1.1.1 Structure

A CV consists of a white dwarf (WD) primary¹, a main-sequence star (secondary), and often an accretion disc around the WD. The orbital period of these systems is on the order of a few hours [e.g. Gänsicke et al., 2009], so the binary is semi-detached². The basic structure is illustrated in Figure 1.1.

The WD has a mass in the range 0.8 to 1.2 M_{\odot} (the median mass is $0.83 \pm 0.23 M_{\odot}$, Zorotovic et al. 2011). The secondary star has a K- or M-spectral type, and has a radius that is a few percent larger than isolated main-sequence stars [e.g. Knigge et al., 2011]. This is an effect of the mass transfer (see Section 1.1.2).

Figure 1.2 shows the potential field that determines the structure of a CV. The primary is compact and more massive than the secondary, and has a deeper gravitational potential well and subsequently a larger Roche-lobe³. The secondary star is distorted into the ‘tear-drop’ shape of the Roche-lobe by the gravitational field of the primary. The lowest energy configuration of the system is a circular orbit and tidally locked secondary star⁴. Any deviation from this configuration is eliminated by tidal forces as explained in Section 1.1.3 [e.g. Hut, 1981].

¹The terms ‘WD’ and ‘primary’ are used interchangeably to refer to the WD

²There is mass transfer between the stars

³See the caption of Figure 1.2

⁴The secondary star is tidally locked when the spin period is equal to the orbital period, so that the same side always faces the primary.

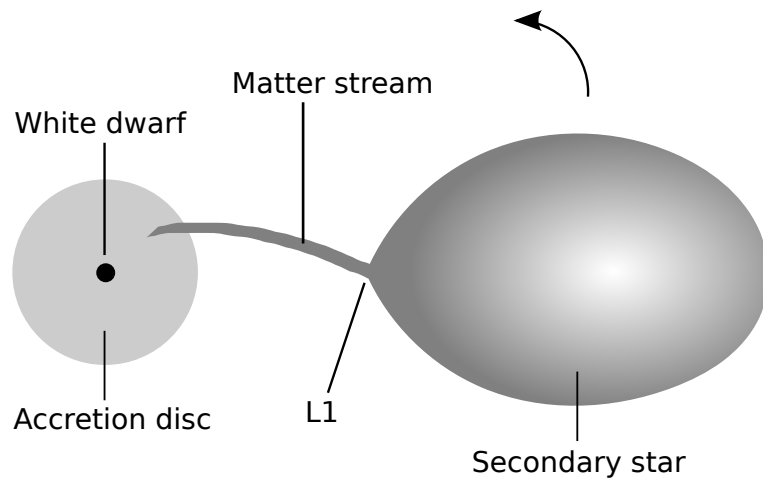


FIGURE 1.1: Illustration of the structure of a Cataclysmic Variable star (not to scale) drawn in the orbital rotation frame (the rotation direction is indicated by the arrow). L1 is the inner-Lagrangian point. The shape of the secondary star is distorted by the gravitational field of the WD. An accretion disc is not always present (see text for details).

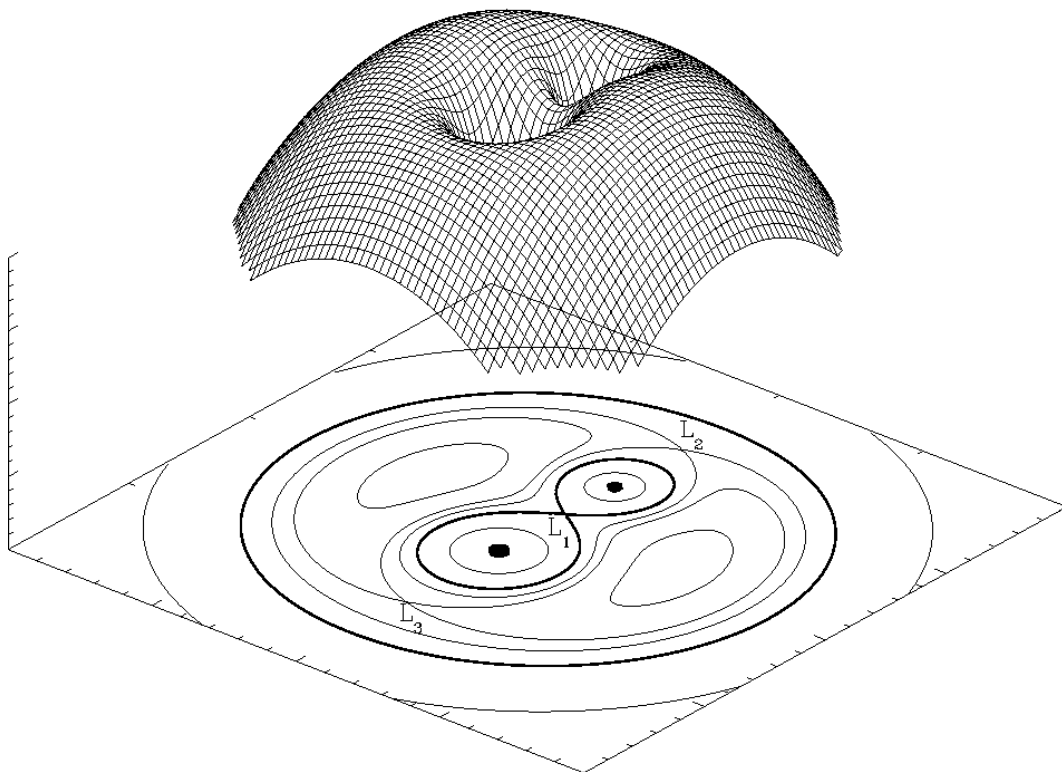


FIGURE 1.2: Illustration of the potential wells of a Cataclysmic Variable in 3D, with a 2D projection showing the equi-potential surfaces. The gravitational and centrifugal force (in the co-rotating frame) determine the potential. The equi-potential surface that appears as a ‘figure of eight’ is known as the Roche surface, and the separate lobes are referred to as the Roche-lobes. Any material within the Roche-lobe is gravitationally bound to the star. The inner-Lagrangian point (L1) is the equi-potential point where matter is transferred from the secondary to the primary. Figure from van der Sluys [2006].

1.1.2 Mass Transfer

Matter is transferred from the secondary to the primary through the inner-lagrangian point (L1 in Figure 1.2)⁵. At L1 the net gravitational and centrifugal force (in the co-rotating frame) cancel, and matter can move into the Roche-lobe of the primary due to thermal pressure. Once there, the material falls towards the primary in an accretion stream [e.g Flannery, 1975] and will eventually accrete onto the primary via an accretion disc, magnetic field lines, or a combination of both.

The magnetic field strength of the primary determines the mechanism by which material is accreted. If it is sufficiently low ($B \lesssim 10^6$ G), then the ram pressure of the gas exceeds the magnetic pressure. The matter is consequently not channelled onto magnetic field lines, but forms an accretion disc. The speed and angular momentum of the incoming matter stream carry it on a trajectory that collides with itself and the accretion disc [for detailed simulations see e.g. Kunze et al., 2001]. The collision point in the disc is referred to as the ‘hot spot’. As the supersonic stream shocks the gas at the collision point to high temperatures, it converts the excess kinetic energy in the stream to thermal energy. With this lower kinetic energy, the stream material settles into a circular orbit around the primary at the circularization radius⁶.

Within the disc the density is too low for normal viscous interactions to drain the material of angular momentum. Instead, this is accomplished through magnetic turbulence produced by shearing of the magnetic field [the Balbus-Hawley Instability or Rotational Magnetohydrodynamic Instability; Hawley & Balbus, 1991, 1992; Balbus & Hawley, 1991; Balbus et al., 1994]. The net effect of this angular momentum transfer is that the disc spreads radially inward and outward. As the WD spins at a slower rate than the inner-most orbit, there is a shock region between the two (the boundary layer) where kinetic energy is converted to heat and radiated as either soft X-ray and EUV radiation, or hard x-rays depending on the accretion rate and optical depth [e.g. Pringle, 1977; Pringle & Savonije, 1979; Tylenda, 1981; Patterson & Raymond, 1985].

In cases where the magnetic field strength of the WD is sufficiently large ($10^6 \lesssim B \lesssim 10^7$ G), the disc is truncated at the Alfvén radius. The matter is then funnelled from the disc onto the magnetic field lines and accretes onto the WD via the field lines. If the WD magnetic field is sufficiently large ($B \gtrsim 10^7$ G), an accretion disc cannot form, as the matter is directly channelled onto the field lines at the point where the ram pressure of the matter stream is exceeded by the magnetic field pressure [see Zhilkin et al., 2012, for 3D magnetohydrodynamical models using complex magnetic fields].

This manner in which material is accreted divides CVs into two main classes, namely the magnetic and non-magnetic CVs. The classes are named in reference to the magnetic field strength of the WD – not the secondary star. The magnetic systems are further sub-classified into the polars⁷ (no accretion disc), and the intermediate polars⁸ (partial accretion disc). The non-magnetics are sub-divided into the dwarf novae (DN) systems and the novalikes based on their long-term optical behaviour. The properties of the DN and novalike classes will be discussed in detail in Section 1.2.

⁵Section 1.1.3 describes how matter reaches L1

⁶The radius for which the angular momentum is equal to that of the material at the inner-Lagrangian point.

⁷Also referred to as AM Herculis stars after the defining member of the class.

⁸Also referred to as DQ Herculis stars.

1.1.3 Formation and Evolution

CVs are commonly accepted to have originated from wide binaries where an intermediate mass star has evolved to the Asymptotic Giant Branch (AGB) and overflowed its Roche-lobe [e.g Paczynski, 1976]. The binary is surrounded by the material (in a common-envelope), and spirals in to shorter orbital periods as angular momentum is lost from the orbit due to drag forces. When the common envelope is expelled due to the orbital motion, a main-sequence WD binary remains (the WD is the core of the original AGB star). This binary then evolves to shorter orbital periods through gravitational radiation and magnetic braking (as described below). At the point when the secondary star fills the Roche-lobe, mass transfer begins and the binary becomes a CV.

The evolutionary paths of non-magnetic and magnetic CVs differ. For the evolution of magnetic CVs, the reader is referred to the discussions in Pretorius et al. [2013] and the references therein. The evolution for the non-magnetic CVs will now be discussed.

In CVs the evolution is driven by angular momentum considerations. Any angular momentum loss from the secondary will reduce the spin rate of the secondary. The primary continues to produce a tidal bulge in the secondary, but as the secondary is now rotating non-synchronously with the orbit, this bulge is dragged off-axis by the secondary. The off-axis bulge results in a tidal torque, which slows the binary rotation (and spins up the secondary) until the secondary is again in a synchronous orbit. The binary orbit now has a smaller angular momentum and orbital separation. In this manner, any angular momentum loss in the secondary is transferred to the orbit [Hut, 1981].

There are two main processes by which angular momentum can be lost from the CV, namely gravitational radiation [Kraft et al., 1962; Paczyński, 1967] and magnetic braking [Verbunt & Zwaan, 1981]. According to general relativity, accelerated motion of a massive object produces a change in the curvature of space-time. In CVs, the orbital motion of the two stars produces ripples in space-time that propagate outwards as gravitational waves. The binary consequently loses angular momentum. In magnetic braking, particles in the stellar wind of the secondary are captured by its magnetic field lines. As the field lines are fixed to the secondary, this material is forced to rotate at the same angular rotation rate as the star. The particles on the field lines that extend out to the Alfvén radius escape the star and carry away angular momentum from the secondary star, and hence the binary. These Angular Momentum Loss (AML) mechanisms act to reduce the orbital period, and importantly, reduce the Roche-lobe size.

The standard model describing the evolution of CVs is the disrupted magnetic braking scenario [Rappaport et al., 1982, 1983; Spruit & Ritter, 1983]. In recent years a number of discrepancies between the observed population and that predicted by the model have arisen [see e.g. Knigge et al., 2011]. Briefly, in the standard model, CVs first evolve to shorter orbital periods (P_{orb}) and then reverse direction at an orbital period known as the ‘period minimum’ ($P_{\text{orb}}^{\text{min}}$)⁹ [Paczynski & Sienkiewicz, 1981; Rappaport et al., 1982] and thereafter evolve to longer periods. The physics responsible for this evolutionary path is now discussed.

When the secondary star is in contact with the Roche-lobe, material is transferred to the primary in the manner described in Section 1.1.2. As the material has moved closer to the center of mass of the binary (the WD), the binary (and hence the Roche-lobe of the secondary) expands to

⁹Observational and theoretical values for $P_{\text{orb}}^{\text{min}}$ differ. This will be discussed in detail later on in this section.

counteract this loss in angular momentum. In the absence of an AML mechanism, the secondary would detach from the Roche-lobe and mass transfer would cease. In CVs magnetic braking and gravitational radiation shrink the Roche-lobe and continue mass transfer. At orbital periods greater than ≈ 3 hours magnetic braking dominates. At $P_{\text{orb}} \approx 3$ hours magnetic braking is thought to cease¹⁰, and gravitational radiation acts as the AML mechanism. As will be discussed later, recent studies have found that an additional AML mechanism is necessary at these orbital periods [e.g. Knigge et al., 2011].

Until this point, the rate at which matter was removed from the secondary slightly exceeded the thermal time-scale of the star [see Knigge et al., 2011]. As a result the secondary became increasingly too large for its mass. The cessation of magnetic braking at $P_{\text{orb}} \approx 3$ hours drops the AML rate down to a point where the secondary can return to thermal equilibrium. It shrinks to the point where it is once again in thermal equilibrium, loses contact with the Roche-lobe and stops transferring matter. The CV continues to evolve to shorter periods through gravitational radiation AML, until at $P_{\text{orb}} \approx 2$ hours the secondary fills the Roche-lobe and matter transfer recommences. This interval ($2 \lesssim P_{\text{orb}} \lesssim 3$ hours) is known as the period gap, because the lack of mass transfer makes it difficult to detect CVs in this range, and so comparatively few systems with these orbital periods are known¹¹.

As the CV evolves to even shorter orbital periods, the thermal time-scale of the secondary increases at a faster rate than the mass transfer time-scale. When the mass of the secondary becomes too small to support Hydrogen burning, it becomes degenerate. From this point onwards the secondary responds to mass loss by increasing in radius [see Strömberg, 1939; Kolb & Baraffe, 1999; Howell et al., 2001] and no longer loses contact with the Roche-lobe. Unlike in the previous evolutionary stages, the CV now evolves to longer periods. From this point onwards the CV is referred to as a ‘post-bounce’ system (prior to this it is referred to as a ‘pre-bounce’ system). The turn-around point is known as the ‘period minimum’ ($P_{\text{orb}}^{\text{min}}$). Early theoretical work estimated $P_{\text{orb}}^{\text{min}} \approx 81$ min [Paczynski & Sienkiewicz, 1981], but later theoretical estimates are in the range 60-75 min [Rappaport et al., 1982; Kolb & Baraffe, 1999; Howell et al., 2001]. Observational studies, in contrast have found $P_{\text{orb}}^{\text{min}} \approx 82$ min [Gänsicke et al., 2009; Woudt et al., 2012].

There are a number of features in the CV population that the standard evolutionary model does not correctly predict. *First*, the period minimum is observed at $P_{\text{orb}}^{\text{min}} \approx 82$ min [Gänsicke et al., 2009; Woudt et al., 2012] instead of the theoretically predicted 60-75 min. *Second*, the predicted ratio of long-period to short-period pre-bounce CVs does not match observations [e.g. Kolb, 1993; Patterson, 1998; Pretorius & Knigge, 2008a,b]. *Third*, although post-bounce CVs are predicted to constitute 40-70% of the CV population [e.g. Littlefair et al., 2008] only a few candidates have been identified [e.g. Howell & Ciardi, 2001] or confirmed [Hernández Santisteban et al., 2016]. Additionally, there is now evidence for magnetic braking in fully convective low-mass stars [e.g. Barnes, 2003; Reiners & Basri, 2008, 2009; Donati & Landstreet, 2009].

A number of solutions to these problems have been proposed. For example, one solution is to evoke an additional (or enhanced) AML mechanism below the period gap [Patterson, 1998; Pretorius et al., 2007; Knigge et al., 2011]. For additional suggestions, the interested reader can

¹⁰It was previously believed that the secondary becomes fully convective at this point [e.g. Copeland et al., 1970]

¹¹This can be seen in the orbital period distribution in Figure 3.6.

see e.g. Andronov et al. [2003]; Ivanova & Taam [2003]; King & Schenker [2002].

The improvement of the evolutionary models is important to both the CV community and the broader astronomical community. For example, the mass accretion rate in CVs is a key factor in determining what fraction of supernova 1a¹² are produced by accretion onto a WD [the single degenerate scenario, Whelan & Iben, 1973; Nomoto, 1982]. See Toonen et al. [2014] for further details on this topic.

A key requirement for testing these solutions and improving the evolutionary model is an unbiased sample of CVs. The evolutionary models are derived and constrained based on the observed orbital period distribution of CVs (e.g. Figure 3.6). As such, they are sensitive to the selection biases inherent in detecting, classifying and characterising CVs. The survey sensitivity and cadence, colour or variability selection criteria, and x-ray luminosity, are just a few of the criteria that bias the known population of CVs. Larger samples of characterised CVs that are discovered and classified through on a variety of techniques are necessary to create a more complete sample with which to constrain evolutionary models. Large surveys, along with dedicated follow-up efforts are the solution to this problem. A number of sensitive, large-scale surveys have come online in recent years and more are planned for the near future. The Catalina Real-time Transient Survey (CRTS; Drake et al. 2009) and the Sloan Digital Sky Survey (SDSS; Aihara et al. 2011) for example, have detected large numbers of CVs based on their variability and colour.

To produce a large, (more) unbiased sample of CVs, the new systems detected in these modern, sensitive surveys need to be followed-up and characterised. In Chapter 2, I present photometric follow-up observations of a sample of 20 CVs identified by the CRTS. In Chapter 3, I present a script that automatically classifies, and estimates properties for, CVs based on long-term photometric data. Subsequently I present a catalogue of properties for 1031 CVs determined by running this script on the CRTS survey data.

1.2 Dwarf Novae and Novalikes

One of the most noticeable features in the long-term light curves of CVs is the dwarf nova outburst¹³. Outbursts are intermittent intervals during which the CV is significantly brighter than the faint quiescent state. The outburst amplitudes are typically in the range 2–6 mag in the known CV population, but outbursts with amplitudes of up to $\Delta V \sim 8$ mag have been observed [e.g. Warner, 1995; Otulakowska-Hypka et al., 2016]. The duration is typically less than 25 days, but outbursts of length 50 days [e.g. Otulakowska-Hypka et al., 2016] have been observed. The interval between outbursts is on the order of days to decades depending on the class of CV [Warner, 1995]. This timescale is not strictly periodic, but each system has a characteristic recurrence time [e.g. Cannizzo et al., 2012; Otulakowska-Hypka & Olech, 2013]. Some CVs also show an additional class of outbursts – the superoutbursts. Superoutbursts are more luminous and last longer than the normal outbursts in a given CV [see Otulakowska-Hypka & Olech, 2013, for a detailed comparison of the outburst and superoutburst properties].

¹²Thermonuclear explosions of a WD progenitor

¹³The terms ‘dwarf nova outburst’ and ‘outburst’ are used interchangeably throughout the remainder of this work.

The non-magnetic CVs are roughly divided into two main classes based on the presence (or absence) of DN outbursts. The CVs that show outbursts (or superoutbursts) are called ‘dwarf novae’ (DN), and those that do not are called ‘novalikes’¹⁴.

1.2.1 Dwarf Nova Outburst Mechanism

The additional luminosity generated during an outburst comes from the release of gravitational energy produced by an increased mass transfer rate through the accretion rate [Osaki, 1974; Smak, 1971]. Originally there were two models describing mechanisms to trigger the increased mass transfer rate, but it is now commonly accepted that outbursts are triggered primarily by a thermal-viscous instability in the accretion disc.

Briefly, the alternative model (the ‘Enhanced Mass Transfer Model’, EMT) posited that an instability in the secondary star increased the mass transfer rate into the disc, and consequently increased the mass transfer rate within the disc [Paczynski et al., 1969; Bath, 1975; Papaloizou & Bath, 1975; Bath & Pringle, 1981]. There are a number of reasons why this model is no longer considered plausible. Primarily, there is no accepted physical mechanism for triggering the instability in the secondary, and the lack of DN outbursts in the novalike class of non-magnetic CVs could not be explained¹⁵ [e.g Gontikakis & Hameury, 1993; Hameury et al., 1998; Cannizzo, 1993; Ichikawa & Osaki, 1992; Warner, 1995].

The standard model for the outburst triggering mechanism is the ‘Disc Instability Model’ (DIM, Smak 1971; Osaki 1974; Höshi 1979). In this model, a thermal-viscous instability switches the accretion disc between a hot ionized state (outburst) and a cool unionised state (quiescence). This mechanism will now be described qualitatively. For a full analytical treatment and summary, see Warner [1995] or Lasota [2001].

Consider a single annulus in the disc. In a state of thermal equilibrium, the viscous heating will balance the radiation from the surface of the annulus. In the temperature-surface density plane (or the mass transfer rate-surface density plane) the thermal equilibrium states trace out a relationship that is referred to as a ‘S-curve’ [e.g. Höshi, 1979; Meyer & Meyer-Hofmeister, 1981]. This is shown schematically in Figure 1.3. If the annulus lies in a state to the right of the curve, viscous heating will raise the temperature and it will return to thermal equilibrium. Similarly, in an annulus that lies to the left of the curve, the disc will cool radiatively and return to thermal equilibrium.

In this diagram there are two stable branches – the A–B line and the C–D line. On either of these branches, an increase in the surface density will increase the temperature through viscous heating. On the lower-branch the annulus is in a cool, unionised state, with a low mass transfer rate (quiescence). On the upper-branch the annulus is in a hot, ionised state with a high-mass transfer rate (outburst). The mechanism that switches the annulus between these states is the thermal-viscous instability.

¹⁴According to the DIM (see Section 1.2.1), the mass transfer rate in the novalike class is sufficiently high to maintain the disc in a constant state of outburst outburst.

¹⁵The Novalike class, and the physical explanation for the lack of outbursts in this class, will be explained at the end of this section.

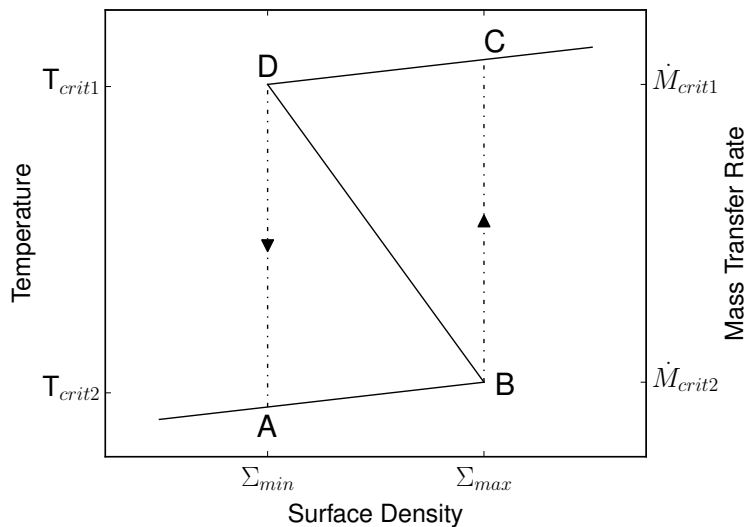


FIGURE 1.3: Illustration qualitatively describing the Disc Instability Model S-curve relationship between surface density (mass per disc area) and temperature, or mass transfer rate. On the solid curve the system is in thermal equilibrium. The dotted lines indicate the thermal instabilities. The precise thermal equilibrium curve is dependent on the viscosity parameter, radius of the annulus, chemical abundance, and model used [e.g. Meyer & Meyer-Hofmeister, 1981; Pojmanski, 1986]. Figure adapted from Warner [1995] and Hellier [2001].

Initially consider an annulus with a surface density (Σ) and Temperature (T) such that it lies on the quiescent branch (line A–B in Figure 1.3). If the rate of matter transfer into the annulus (\dot{M}_{in}) exceeds the rate at which matter is transferred out of the annulus (\dot{M}_{out}) then the surface density and temperature will increase and the annulus moves towards point B in Figure 1.3. At this point the temperature is sufficiently high for the hydrogen to be partially ionized ($T \sim 5000$ K), and the opacity is steeply dependent on temperature ([Faulkner et al., 1983; Cannizzo, 1984]). Further viscous heating increases the opacity and ionizes the remaining hydrogen. As the time-scale on which the opacity rises is shorter than that required for the viscous exchange of material between annuli, the temperature rises at approximately constant Σ to point C in Figure 1.3. The annulus is now in a hot, ionized state. The viscosity (and hence the mass transfer rate) is higher, as the Rotational Magnetohydrodynamic Instability [Hawley & Balbus, 1991, 1992; Balbus & Hawley, 1991; Balbus et al., 1994] is more effective due to the higher abundance of ions. At this stage $\dot{M}_{out} > \dot{M}_{in}$, and the surface density and temperature decline as matter drains from the annulus. Once the annulus reaches state D in the figure, the temperature is no longer sufficient to maintain the fully ionized annulus and it rapidly cools to state A (quiescence).

An annulus of the disc can cycle between quiescence and outburst in this manner. Importantly, an outburst in one annulus will raise the temperature in the adjacent annuli and cause them to transition into outburst. In turn they trigger adjacent annuli, and a heating wave travelling to smaller (and larger) radii causes the accretion disc to transition into outburst. When the outermost annuli drop below Σ_{min} , they trigger a cooling wave inwards and the accretion disc returns to quiescence. See e.g. Meyer [1984]; Lin et al. [1985]; Mineshige & Osaki [1985] for more

details.

This basic DIM has been updated over the years to include effects such as a non-uniform mass transfer rate from the secondary, irradiation of the disc and secondary and tidal instabilities [e.g. Smak, 2000]¹⁶. It is also used to explain the outbursts in the low mass X-ray Binaries [Dubus et al., 2001]. For discussions on the successes and shortcomings of this model see Lasota [e.g. 2001]¹⁷.

1.2.2 Superoutburst Mechanism

There are three main models describing the mechanism that triggers superoutbursts. These respectively invoke the pure thermal-viscous instability of the DIM, a tidal instability, or an enhanced mass transfer rate due to irradiation of the secondary star.

The Thermal-viscous Limit Cycle Instability [van Paradijs, 1983; Cannizzo et al., 2010, 2012] postulates that superoutbursts are simply extended outbursts described by the DIM. The difference lies in the fraction of the disc that participates in the outburst. In this model, the outburst is triggered in the inner disc and a heating wave propagates outwards. In the DN outbursts, this wave does not reach the outer disc because there is insufficient matter to support the heating wave at large radii. Over successive outbursts, matter and angular momentum consequently accumulate in the outer disc. A superoutburst is triggered when the heating wave reaches the outer disc radii, which produces a longer, brighter outburst.

In the Thermal Tidal Instability model [TTI, Whitehurst, 1988; Osaki, 1989, 1996; Osaki & Meyer, 2003] successive DN outbursts extend the radius of the disc. At sufficiently large radii the gravitational attraction of the secondary star on the orbiting material becomes significant. At the radius where the disc material orbits with a period of $\frac{1}{3}P_{\text{orb}}$, the material will resonate with the secondary and be driven into elliptical orbits. This increases the viscous heating, and prolongs the outburst into a superoutburst.

The Enhanced Mass Transfer model [EMT, Vogt, 1983; Smak, 1984; Osaki, 1985] states that the secondary star is irradiated during the DN outburst. This increases the mass transfer rate to the disc and subsequently prolongs the outburst to produce a superoutburst.

The TTI model is more evident in the literature, but there is not yet consensus on which model, or which combination of models, is responsible for superoutbursts. For recent discussions on the strengths and deficiencies in each model see Smak [2000, 2008, 2009]; Schreiber et al. [2004]; Viallet & Hameury [2007, 2008]; Cannizzo et al. [2010]; Osaki & Kato [2013]. For an application to the AM CVn¹⁸ systems see Kotko et al. [2012] and Cannizzo & Nelemans [2015].

¹⁶See also Section 1.2.2

¹⁷The outbursts in the DN SS Cyg are commonly cited as a key counter-example to the DIM, as the mass transfer rate is too high (according to the DIM) to produce DN outbursts in this system. Note that later radio observations by Miller-Jones et al. [2013] proved that this discrepancy was produced by an incorrect distance determination, and the true mass transfer rate is in line with the DIM.

¹⁸Binaries in which a white dwarf accretes hydrogen-poor matter from a compact companion [e.g. Levitan et al., 2015].

1.3 Radio Emission from Cataclysmic Variables

Interacting binaries produce radio emission through a variety of mechanisms, such as winds, shocks, jets, and magnetic field interactions [e.g. Hjellming et al., 1979; Ramsay et al., 2007; Rupen et al., 2008; Slee et al., 2008; Deneva et al., 2016; Plotkin et al., 2016]. Radio emission has been detected from novae [Hjellming & Wade, 1970; Weston et al., 2016] and from magnetic CVs [e.g. Mason & Gray, 2007], but prior to this thesis non-magnetic CVs¹⁹ were accepted to not be radio emitters, as only five had been detected at radio wavelengths [Benz et al., 1996; K rding et al., 2008] out of the thousands of known CVs.

At least 7 magnetic CVs, including polars and intermediate polars, have been detected at radio wavelengths, and of these only three are persistent radio emitters²⁰ [Mason & Gray, 2007]. These systems include AM Her [e.g. Chanmugam & Dulk, 1982; Dulk et al., 1983; Mason & Gray, 2007], V834 Cen [Wright et al., 1988], ST LMi [Pavelin et al., 1994], AR UMa [Gray & Mason, 2005; Mason & Gray, 2007], AE Aqr [e.g. Bookbinder & Lamb, 1987; Meintjes & Venter, 2005], DQ Her and BG CMi [Pavelin et al., 1994]. The radio emission from these magnetic CVs is non-thermal, variable, and in some cases has shown strong flares and high circular polarization (CP) fractions [e.g. Dulk et al., 1983; Chanmugam, 1987]. Models for the radio emission mechanism include gyrosynchrotron emission in the white dwarf magnetosphere [Chanmugam & Dulk, 1982], cyclotron maser emission operating at the surface of the secondary [Dulk et al., 1983; Chanmugam, 1987] and synchrotron emission from ejected clumps of material (for AE Aqr, Wynn et al. 1997; Meintjes & Venter 2005).

A large number of radio surveys of non-magnetic CVs were conducted in the 1980s [e.g. Benz et al., 1983; Benz & Guedel, 1989; Cordova et al., 1983; Fuerst et al., 1986; Echevarria, 1987; Nelson & Spencer, 1988; Turner, 1985]. During this time only three non-magnetic CVs (EM Cyg, SU UMa and TY PSc) were detected and the emission was not persistent [Benz et al., 1996]. The 3σ upper-limits on the non-detections were typically 0.1–0.3 mJy.

Benz et al. [1983] detected SU UMa at a flux density of 1.3 mJy at 4.75 GHz. Observations from two separate outbursts, taken during the decline phase, were combined to make this detection. In quiescence Benz et al. obtained an upper-limit of 0.4 mJy. SU UMa was not detected in further observations by Fuerst et al. [1986]; Nelson & Spencer [1988] and Echevarria [1987]. In Chapter 5 the validity of the 1.3 mJy detection of this source is questioned. TY PSc was detected in the range 3–10 mJy by Turner [1985] at 2.5 GHz, and not detected in follow-up observations by Benz & Guedel [1989]. Turner [1985] also claimed a detection of the system UZ Boo at 2.4 mJy, but both Benz & Guedel [1989] and Nelson & Spencer [1988] found a separate radio source within the beam width of this observation. EM Cyg was detected at 4.9 GHz [Benz & Guedel, 1989]. Benz & Guedel detected it three days into the outburst at 140 μ Jy, and then 37 hours later at 340 μ Jy.

A number of radio emission mechanisms have been proposed for non-magnetic CVs. Thermal emission from a cloud surrounding the dwarf nova produced by an outburst wind has been suggested [e.g. Cordova et al., 1983; Fuerst et al., 1986]. The brightness temperature of the detected

¹⁹The reader is reminded that CVs are classified into the magnetics and non-magnetics solely according to the magnetic field strength of the WD (see Section 1.1.2). The terms ‘non-magnetic’ and ‘magnetic’ do not refer to the magnetic field strength of other components (such as the disc or secondary star).

²⁰The persistent radio emitters are AM Her, AE Aqr and AR UMa

sources is too high to be thermal emission however [e.g. Benz & Guedel, 1989]. Benz & Guedel [1989] found that maser emission produced by non-thermal electrons reflected in the magnetic field in the WD is the most likely explanation for the radio emission in EM Cyg. Benz & Guedel considered the disc, and secondary star, as possible sources for the maser emission, but favoured the WD, as the maser instability has a significantly slower growth in these regions and is likely to be dominated by other processes. According to Benz et al. [1996] the short, sporadic bursts of radio emission from non-magnetic CVs is best explained by cyclotron maser emission. Gyrosynchrotron or synchrotron produced by (for example) a disruption of the DN magnetosphere has also been suggested [e.g. Fuerst et al., 1986]. Small number statistics, with low sensitivity detections and lack of polarization, variability and spectral information made it difficult to constrain and test these models previously.

The low radio detection rates of CVs established their reputation as ‘non-radio emitters’. One important implication that followed from this, was the idea that CVs do not launch jets. Jets have been detected in most classes of compact accreting objects, from Active Galactic Nuclei (AGN) and XRBs [e.g. Fender et al., 2004; Migliari & Fender, 2006], to novae [e.g. Retter, 2004; Sokoloski et al., 2008; Weston et al., 2016] and symbiotics²¹ [e.g. Brocksopp et al., 2004]. The lack of jets in CVs was consequently used to constrain jet-launching models [e.g. Livio, 1999; Soker & Lasota, 2004].

A long hiatus in radio studies of CVs followed these low detection rates in the 1980s. During this time, it was established that there is an empirical relation between the accretion mode and the strength and type of outflow in X-ray binaries [e.g. Corbel et al., 2001; Fender et al., 2004; Fender & Belloni, 2012; Migliari & Fender, 2006]. K rding et al. [2006] extended this to the AGN by describing the relation in terms of a ‘Disc Fraction Luminosity Diagram’ (DFLD), in which the radio luminosity is related to the fraction that the power law component contributes to the total luminosity. The outbursts of XRBs and CVs are described by the same mechanism and they share phenomenology, so K rding et al. [2008] extended the DFLD to CVs, and predicted that CVs should show a radio flare on the rise to outburst, associated with a jet.

K rding et al. [2008] observed the DN SS Cyg at 8.6 and 1.4 GHz during outburst in April 2007 and detected a 1.1 mJy flare shortly after the rise to outburst which faded to 0.3 mJy on a timescale of hours. This flare was detected in subsequent outburst observations by Miller-Jones et al. [2011] and Russell et al. [2016]. Russell et al. confirmed that the radio light curve of SS Cyg is repeatable over outbursts. Based on the timing, brightness temperatures, spectral indices, and simultaneous multi-wavelength observations, all three studies concluded that the observed radio emission is synchrotron emission from a transient jet.

Previous radio observations of dwarf novae did not cover the early rise phase of the outburst [e.g. Benz et al., 1996] and K rding et al. [2008] attributed the lack of prior radio detections to the timing of the observations. Although SS Cyg was argued to be unique for many years as the observed accretion rate was claimed to be too high to be explained by the DIM, Miller-Jones et al. [2013] used radio observations to prove that the previous distance estimate (and hence mass accretion rate) were overestimated.

Following the detection of SS Cyg, K rding et al. [2011] observed three novalikes with the VLA

²¹Binary systems in which a white dwarf accretes from a red giant companion.

and detected V3885 Sgr at 0.16 ± 0.01 Jy at 5.5 GHz and at 0.11 ± 0.02 Jy at 9 GHz, but did not detect AC Cnc or IX Vel. K rding et al. concluded that the radio emission from V3885 Sgr was most likely synchrotron emission based on the spectral index and upper-limit on the polarization fraction of $\sim 28\%$.

In summary, the status quo before this thesis was that 5 non-magnetic CVs had been detected at radio wavelengths, and importantly, contrary to previous ideas, evidence for a jet had been found in the CV SS Cyg. In Chapter 4 and 5 I present radio observations of 9 non-magnetic CVs (8 of which were detected). These results prove that non-magnetic CVs are radio-emitters at a luminosity that is higher than can be expected based on the spectral energy distribution of the white dwarf, secondary star, and accretion disc components. Furthermore, the radio emission from SS Cyg is not unique in type, luminosity, or variability time-scales.

HIGH-SPEED PHOTOMETRY OF FAINT CATAclySMIC VARIABLES - VIII. TARGETS FROM THE CATALINA REAL-TIME TRANSIENT SURVEY

Deanne L. Coppejans, Patrick A. Woudt, Brian Warner, Elmar K rding, Sally A. Macfarlane,
Matthew P.E. Schurch, Marissa M. Kotze, Hannes B. Breytenbach, Amanda A. S. Gulbis and
Rocco Coppejans

MNRAS 437, 510–523 (2014)

Abstract

Time series photometry of 20 Cataclysmic Variables detected by the Catalina Real-time Transient Survey is presented. 14 of these systems have not been observed previously and only two have been examined in-depth. From the observations we determined 12 new orbital periods and independently found a further two. Eight of the CVs are eclipsing systems, five of which have eclipse depths of more than 0.9 mag. Included in the sample are six SU UMa systems (three of which show superhumps in our photometry), a polar (SSS1944-42) and one system (CSS1417-18) that displays an abnormally fast decline from outburst.

2.1 Introduction

We present the latest results of a photometric follow-up study of faint Cataclysmic Variable stars (CVs; see Warner 1995) mostly in the southern hemisphere. Specifically, in this paper we discuss the observations of 20 CVs identified by the Catalina Real-time Transient Survey (CRTS; see Drake et al. 2009).

This work forms part of a survey with the aim of characterising newly identified CVs, determining their orbital periods, searching for sub-orbital periodicities and selecting targets for in-depth studies on large telescopes and multi-wavelength campaigns. In the previous papers in this series (see Woudt et al. 2012 and references therein), the focus was on faint nova remnants and CVs identified by the Sloan Digital Sky Survey (SDSS, e.g. Aihara et al. 2011). Recently, it has shifted to CVs discovered by the CRTS [Woudt et al., 2012].

The CRTS is a large scale transient survey that observes 30 000 deg² of the sky in search of transients (see Djorgovski et al. 2011). They make use of data from the Catalina Sky Survey [Christensen et al., 2012], which searches for Near-Earth Objects. The observing strategy is to observe a field four times at 10-minute intervals, then return to the field up to four times per lunation [Djorgovski et al., 2011]. Transients are detected by looking for variations of more than 2 mag in the *V* filter. As most of the fields have 7- to 8-year baselines and the CRTS can reach a depth of *V* \sim 23 by co-adding images (although individual pointings reach *V* \sim 19 to 21), a variety of transients are discovered. Amongst these are supernovae, blazars, flare stars and CVs.

As evidenced by the number of CVs the CRTS has detected - more than 1000 to date (September 2013)¹ - the CRTS is particularly efficient at finding them. This is for a number of reasons. For example, the magnitude variation cut-off limit of 2 mag, which was designed to restrict the number of artifacts and pulsating variables, is approximately the minimum amplitude of a dwarf nova outburst, so large numbers of Dwarf Novae (DNe) are detected. This range also ensures that the high inclination systems with deep eclipses are detected, as well as a number of magnetic systems that show high and low states. As the CRTS commonly reaches down to *V* \sim 21, or fainter if the object has a high state brighter than this limit, it will find faint CVs such as the double degenerate AM CVn (AM Canum Venaticorum) systems. Also advantageous to our photometric follow-up study, is the excellent coverage in the southern hemisphere.

Follow-up observations on the objects identified by large scale surveys, such as the CRTS, are becoming increasingly necessary as existing projects continue to detect new transients and surveys such as the Large Synoptic Survey Telescope (LSST; Sweeney et al. 2009) are planned. On average, from 2008 to 2012 the CRTS detected 45 new CVs per quarter. For CVs, finding the orbital periods for a greater sample of systems is necessary for evolutionary studies (e.g. Gänsicke et al. 2009). Additionally, amongst the newly discovered CVs will be systems that need to be observed with larger telescopes (e.g., SALT: Woudt et al. 2010) and multi-wavelength campaigns (e.g. CC Sculptoris: Woudt et al. 2012b). Particularly important are the eclipsing systems, from which we can obtain system characteristics such as the mass ratio through eclipse deconvolution (Littlefair et al. 2008; Savoury et al. 2011). Photometric surveys, such as the kind presented in this paper, help to identify these targets.

¹See <http://nessi.cacr.caltech.edu/catalina/Stats.html>

In this paper, in section 2.2 we describe the observing procedure, the instrumentation and the data reduction. The results of each of the individual CVs follow. Section 2.3 contains a summary and discussion of the results.

2.2 Observations

Differential photometry was performed using the University of Cape Town (UCT) CCD [O’Donoghue, 1995] and the new Sutherland High-speed Optical Cameras (SHOC; Gulbis et al. 2011, Coppejans et al. 2013) mounted on the 74-in and 40-in reflector telescopes of the South African Astronomical Observatory (SAAO).

For the first time in this series of papers, we have used the SHOC systems. Two instruments utilizing Andor iXon 888 cameras are available for use at the SAAO. The field of view is 2.85×2.85 arcmin² on the 40-in telescope and 1.29×1.29 arcmin² on the 74-in², as compared to 1.23×1.82 arcmin² and 0.57×0.83 arcmin² on the UCT CCD.

For these observations both the UCT CCD and SHOC were used in frame-transfer mode and SHOC was operated in 1MHz conventional mode with 2.4 preamplifier gain. No filters were used, but the data were calibrated to the Sloan r photometric system. Papers I to VI in this series used hot white dwarfs as calibration standards [Landolt, 1992], which gave V accurate to ~ 0.1 mag [Woudt et al., 2012]. Using the survey archival data we compared the calibration offset using hot white dwarfs and those using SDSS photometry of comparison stars on the target field on nights when both were available. Over the range $g - r = 0.2$ to 1.0, it was found that there was a stable zero-point offset of 0.12 ± 0.05 mag between V and SDSS r - which is consistent with the photometric transformation in Jester et al. [2005]. Subsequently, we calibrated our white light photometry to the r photometric system using SDSS stars on the target field that have $g - r$ colours in the range 0.2-1.0. The calibration is accurate to ~ 0.1 mag. In the cases where a suitable calibration star was not observed over the course of the evening, we applied the calibration determined for another night during the observing run. The runs calibrated in this way are labelled with a colon in the observing log (Table 2.1).

The observing procedure varies according to the behaviour of a given CV. A target is initially observed for a few hours (~ 4 h). If the light curve shows modulation, then it is observed further over consecutive nights. If there are no modulations present or the CV appears to have a long orbital period (greater than 5 hours), then no further observations are taken as the telescope time can be spent more profitably. Longer-term monitoring (weeks to years) is carried out in order to reduce the error margin on orbital periods or to observe CVs in an alternate outburst state in order to obtain a superhump period, an orbital period or to examine Quasi-Periodic Oscillations (QPOs) and Dwarf Nova Oscillations (DNOs).

Data reductions were performed with the program Duphot for the UCT CCD [O’Donoghue, 1995] and in IRAF [Tody, 1986] using standard reduction routines for the SHOC observations.

Two different techniques were used to find periodicities (such as the orbital period) in the photometry. The CVs which had sinusoidal light curves were analyzed by Fourier Analysis using

²See <http://shoc.sao.ac.za/>

the Starlink Period package³. Those with non-sinusoidal light curves (e.g. the eclipsing systems) were analyzed by Phase Dispersion Minimization (PDM, Stellingwerf 1978). The former technique has been explained in detail in previous papers in this series. Briefly, PDM determines the true period by folding the light curve on a series of test periods and determining which produces the least scatter. In order to quantify the scatter, each folded light curve is binned and the overall variance of all the bins is divided by the variance of the unbinned data. The result - the PDM statistic Θ - will be close to 1 for false periods and be small for true periods. A PDM periodogram will thus have local minima at the true periods (see for example Figure 2.2). Full details are given in Stellingwerf [1978].

The distinction in treatment between the non-sinusoidal and sinusoidal systems is due to the fact that in attempting to fit sharp features by a series of sinusoids, Fourier Analysis spreads the power to harmonics of the period, thereby reducing the power of the fundamental. PDM does not suffer from this problem.

Unless otherwise stated, before the PDM periodogram or Fourier Transform (FT) is calculated, the individual runs are linearly detrended and mean-subtracted. This reduces the spurious noise at low frequencies introduced by observing the CV over the same airmass range over consecutive nights.

In order to determine an uncertainty on the periods obtained from the FT, a sine-curve is fitted to the photometry using the FT period as an initial guess. By varying the period, a Markov Chain Monte Carlo Method (MCMC) - specifically the Metropolis Hastings algorithm (Metropolis et al. 1953 and Hastings 1970) - then samples the probability distribution of solutions. The median value and standard deviation of this distribution are then quoted as the period and uncertainty respectively. In cases where there are additional strong peaks in the FT, more than one sine-wave is fitted simultaneously.

For those systems which have highly non-sinusoidal light curves, the uncertainty cannot be determined in this way. The uncertainty derived from PDM for these CVs is obtained by bootstrapping using the Monte Carlo Algorithm for case resampling [Efron, 1979]. The sampling distribution for the period is estimated by creating new light curves by selecting N of the N data points (repetition is allowed) and performing PDM on each new sample. As is the case for the FT, the period and uncertainty given in this paper are the median and standard deviation of the bootstrap distribution.

A variety of other techniques are used to select the correct period from the FT/PDM periodogram and determine the reality of a peak. These include phase-folding, using the window function - which shows the aliasing structure introduced by sampling - and the Fisher randomisation test [Linnell Nemeč & Nemeč, 1985]. In the latter, the amplitude values on the light curves are shuffled to create a large number of new light curves and FTs are calculated for each. The probability of a period being real and equal to the quoted value on the original FT is then determined by looking at the proportion of shuffled light curves that gave a higher peak at that frequency.

The observing log is given in Table 2.1. Each CRTS transient has an ID of the form CSS yymmdd:hmmss±ddmmss. The first three letters indicate in which of the three component

³<http://www.starlink.rl.ac.uk/docs/sun167.htx/sun167.html>

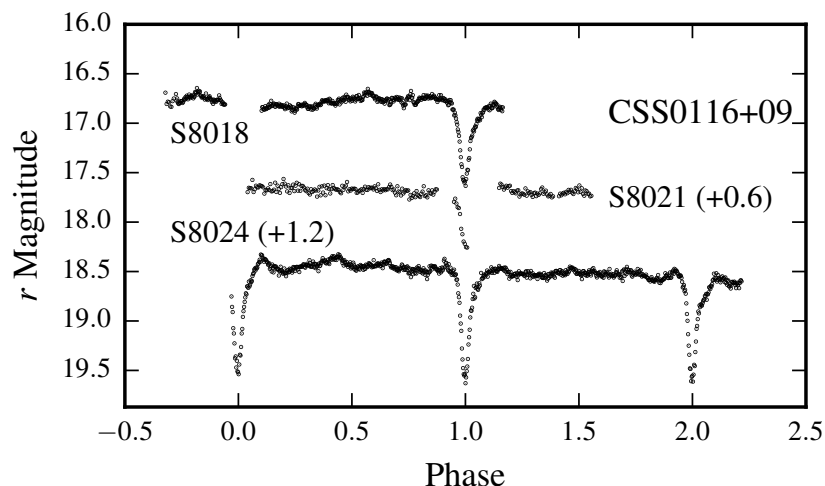


FIGURE 2.1: Light curves for CSS0116+09 taken on the decline from outburst, showing deep eclipses. The runs are offset vertically for display purposes by the magnitude indicated in parentheses. The gaps in the light curves were caused by passing cloud.

surveys it was discovered (CSS: Catalina Sky Survey, MLS: Mount Lemmon Survey and SSS: Siding Springs Survey, see Djorgovski et al. 2011). The following six digits indicate the date on which it was classified. The Right Ascension and Declination follow the colon. In the observing log and the discussion the ID is abbreviated to the form CSS hhmm±dd.

CSS0116+09 (CSS081220:011614+092216)

CSS0116+09 was discovered by the CRTS on December 20, 2008 when it was observed in outburst at $\Delta V \sim 3$ mag. It has a counterpart in Data Release 8 of the Sloan Digital Sky Survey (SDSS, Aihara et al. [2011]) with $u=19.0$, $g=19.1$ and $r=19.0$. Thorstensen & Skinner [2012] further observed it at $B - V=0.24 \pm 0.06$, $V=18.89 \pm 0.02$, $V - I=0.64 \pm 0.03$. Based on its colour, they confirmed its CRTS classification as a CV.

We caught CSS0116+09 on the decline from outburst in November 2010 and in quiescence on two further observing runs (see Tab. 1). The outburst light curves are given in Fig. 2.1 and show CSS0116+09 to be a deeply eclipsing system.

The PDM periodogram (see Fig. 2.2) of these observations together with those taken in quiescence a week later (S8033 and S8040), gives an orbital period of 0.0657 ± 0.0001 d. Bootstrapping the results gives $P_{orb}=0.06582 \pm 0.00005$ d, where the orbital period and uncertainty are the median and standard deviation of the distribution respectively. The ephemeris for minimum light is⁴

$$HJD_{\min} = 2455528.3681 + 0^d.06582(\pm 5)E. \quad (2.1)$$

Plot A of Fig. 2.3 shows the average light curve of S8033 and S8040 folded on the orbital period. The average of runs S8098 and S8100 is shown in Plot B of the figure. Unfortunately these runs were too far removed in time to reduce the uncertainty in Eq. 2.1. From S8040 to

⁴E is the cycle number and the error on the last digit is quoted in parentheses, for example $0.06582(\pm 5)$ denotes an error of 0.00005.

TABLE 2.1: Observing log

Object	Type	Run	Date	HJD start +2450000	length (h)	t_{in} (s)	Tel.	r (mag)
CSS0116+09	DN	S8018 ^o	27 Nov. 2010	5528.2811	2.3485	30	40-in	16.8 ^m
		S8021 ^o	28 Nov. 2010	5529.2925	2.3928	30	40-in	17.1 ^m
		S8024 ^o	29 Nov. 2010	5530.2755	3.5503	15	40-in	17.3 ^m
		S8033	5 Dec. 2010	5536.2887	1.1579	20,25	74-in	18.9 ^m
		S8040	8 Dec. 2010	5539.3026	2.0642	25	74-in	19.1 ^m
		S8098 ^s	5 Oct. 2011	5840.4774	2.8041	20	74-in	18.8 ^m
CSS0411-09	SU	S7891 ^u	21 Dec. 2009	5187.2848	3.6556	8	74-in	15.3
		S7893 ^u	22 Dec. 2009	5188.2872	1.4372	8	74-in	15.3:
		S7898 ^u	24 Dec. 2009	5190.2908	1.4061	8	74-in	15.7:
CSS0438+00	DN	S8022	28 Nov. 2010	5529.4480	2.0579	30	40-in	19.2 ^m
		S8025	29 Nov. 2010	5530.4410	3.7803	20	40-in	19.3 ^m
		S8050	26 Dec. 2010	5557.3107	1.3357	70	74-in	19.5 ^m
CSS0449-18	DN	S8059	30 Jan. 2011	5592.3146	3.6642	45	40-in	17.9 ^m
		S8061	31 Jan. 2011	5593.2846	3.1261	45	40-in	17.8 ^m
		S8062	1 Feb. 2011	5594.2851	4.3161	45	40-in	17.9 ^m
		S8063	6 Feb. 2011	5599.3015	3.1400	45	40-in	17.9 ^m
SSS0501-48	DN	S8144 ^s	21 Jan. 2012	5948.2779	0.4890	20	74-in	17.3
		S8145 ^s	22 Jan. 2012	5949.2795	5.5672	20	74-in	17.2
		S8147 ^s	23 Jan. 2012	5950.2802	5.3910	20	74-in	17.3
CSS0558+00	DN	S8031	4 Dec. 2010	5535.4867	1.0567	40	74-in	19.2
		S8041	8 Dec. 2010	5539.3984	4.5805	40	74-in	19.4
		S8042	9 Dec. 2010	5540.3889	4.6192	40,50,60	74-in	19.6
		S8044	12 Dec. 2010	5543.4696	2.8842	60	74-in	19.3
		S8048	24 Dec. 2010	5555.4143	2.4899	40	74-in	18.9
CSS0902-11	DN	S7927 ^o	22 Mar. 2010	5278.2856	1.1053	6	74-in	16.5:
		S7932	31 Mar. 2010	5287.2415	5.0953	30	40-in	17.8:
		S7934	1 Apr. 2010	5288.2411	4.4381	30	40-in	17.8
		S8032	4 Dec. 2010	5535.5401	0.9011	20	74-in	17.6
CSS0942-19	SU?	S8039	7 Dec. 2010	5538.5174	1.5656	10	74-in	17.7:
		S8082	11 May 2011	5693.2133	4.1458	60	74-in	19.6
		S8085	12 May 2011	5694.2114	4.1342	60	74-in	19.5
CSS1052-06	SU	S8088	13 May 2011	5695.2133	3.9792	60	74-in	19.3
		S7949 ^u	8 Apr. 2010	5295.2194	3.4922	10	40-in	16.0
		S7952 ^u	9 Apr. 2010	5296.2272	1.9869	10	40-in	16.3:
		S7955 ^u	10 Apr. 2010	5297.4247	0.6506	10	40-in	16.4
		S7964	13 Apr. 2010	5300.3142	3.2947	20	40-in	18.7

Notes: t_{in} : Integration time, DN: Dwarf Nova, SU: SU Ursae Majoris, P: Polar, ^sobservations were taken with the SHOC camera (as opposed to the UCT CCD), ^osystem was in outburst, ^usystem was in superoutburst, ^mmean magnitude out of eclipse, : denotes an uncertain value (see Sec. 2.2 for details).

Object	Type	Run	Date	HJD start +2450000	length (h)	t_{in} (s)	Tel.	r (mag)
SSS1128-34	DN	S8091	14 May 2011	5696.2570	4.9031	30	74-in	18.7:
		S8094 ^o	15 May 2011	5697.2270	3.1458	40	74-in	16.0:
		S8095 ^o	16 May 2011	5698.2932	2.5563	40	74-in	16.0:
CSS1221-10	DN	S8056	28 Jan. 2011	5590.5679	1.4753	90	40-in	19.3:
		S8058	29 Jan. 2011	5591.4973	3.0451	120	40-in	19.3:
		S8060	30 Jan. 2011	5592.5197	1.8894	100	40-in	19.3:
		S8064	6 Feb. 2011	5599.4637	3.9494	120	40-in	19.4:
		S8066	7 Feb. 2011	5600.4846	1.2688	120	40-in	19.7:
		S8068	5 Mar. 2011	5626.4949	3.6354	120	40-in	19.6:
		S8069	6 Mar. 2011	5627.3897	4.5690	120	40-in	19.4:
		S8071	8 Mar. 2011	5629.3847	6.4775	120	40-in	19.4
SSS1224-41	DN	S8162 ^s	28 Feb. 2012	5986.5230	2.4560	120	40-in	19.4 ^m
		S8177 ^s	17 Mar. 2012	6004.4454	5.1158	120	74-in	19.3 ^m
		S8180 ^s	18 Mar. 2012	6005.4696	4.1647	120	74-in	19.3 ^m
		S8182 ^s	19 Mar. 2012	6006.3926	6.0487	120	74-in	19.3 ^m
		S8185 ^s	20 Mar. 2012	6007.4541	4.5465	120	74-in	19.3 ^m
SSS1340-35	DN	S8188 ^s	20 Apr. 2012	6038.3205	2.9894	60	40-in	18.4 ^m
CSS1417-18	SU	S7992 ^o	6 Jul. 2010	5384.2382	2.3681	20	74-in	16.8
		S7993 ^o	7 Jul. 2010	5385.2267	2.5268	20	74-in	18.8
		S8080	10 May 2011	5692.3198	4.5998	120	74-in	19.9
		S8083	11 May 2011	5693.4119	3.0331	120	74-in	20
		S8089	13 May 2011	5695.4009	3.0666	120	74-in	19.7
CSS1556-08	DN	S8078 ^o	9 May 2011	5691.4659	4.3199	10	74-in	16.9:
		S8081	10 May 2011	5692.5194	2.9558	10	74-in	18.0
		S8086	12 May 2011	5694.3974	3.7759	10	74-in	18.4:
CSS1727+13	DN	S7967	19 May 2010	5336.5160	2.3258	45	74-in	19.0:
		S7970	20 May 2010	5337.4814	3.4521	45	74-in	19.7:
		S7972	21 May 2010	5338.4636	3.0020	45	74-in	19.7:
		S7976	22 May 2010	5339.4875	2.1676	55	74-in	19.7:
SSS1944-42	P	S8084	11 May 2011	5693.5527	2.9464	10	74-in	17.4
		S8087	12 May 2011	5694.5753	2.4897	10	74-in	17.6:
		S8090	13 May 2011	5695.5555	3.1700	10	74-in	17.2
SSS2003-28	SU	S8093	14 May 2011	5696.5973	2.0719	35	74-in	19.1: ^m
		S8096 ^o	16 May 2011	5698.5522	2.9172	90,100	74-in	16.4: ^m
CSS2054-19	SU	S8005 ^u	31 Oct. 2010	5501.2447	4.0508	45	74-in	16.5:
		S8008 ^u	1 Nov. 2010	5502.2457	3.4636	45	74-in	16.7
		S8010 ^u	2 Nov. 2010	5503.2729	2.5758	30	74-in	17.3:
CSS2108-03	DN	S8107 ^s	11 Oct. 2011	5846.2343	4.5482	30	74-in	17.7 ^m
		S8109 ^s	15 Oct. 2011	5850.2412	2.4834	60	40-in	17.6 ^m
		S8111 ^s	16 Oct. 2011	5851.2308	3.7767	60	40-in	17.6 ^m
		S8113 ^s	19 Oct. 2011	5854.2789	0.6000	60	40-in	17.8 ^m

Notes: t_{in} : Integration time, DN: Dwarf Nova, SU: SU Ursae Majoris, P: Polar, ^sobservations were taken with the SHOC camera (as opposed to the UCT CCD), ^osystem was in outburst, ^usystem was in superoutburst, ^mmean magnitude out of eclipse, : denotes an uncertain value (see Sec. 2.2 for details).

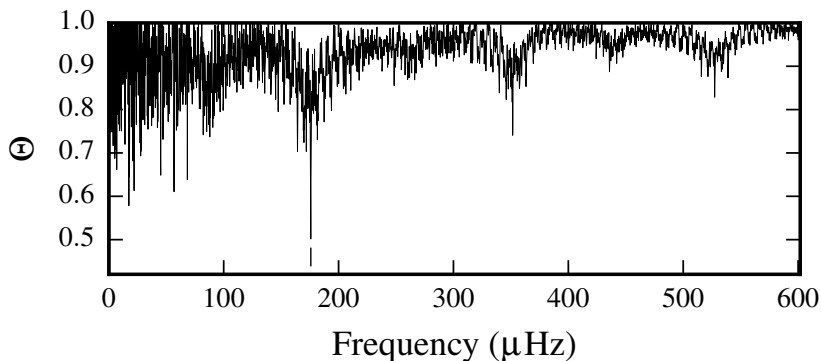


FIGURE 2.2: Phase Dispersion Minimization periodogram for combined runs S8018, S8021, S8024, S8033 and S8040 of CSS0116+09. The orbital period at $175.84 \pm 0.13 \mu\text{Hz}$ is indicated by a vertical bar.

S8098, the uncertainty on the eclipse timing amounted to more than a period and so combining these runs would have introduced a cycle ambiguity.

The eclipse depth of the light curves ranges from 0.8 mag to 1.4 mag. It is at its minimum in outburst, when the accretion disc contributes a larger fraction of the light. This depth indicates that CSS0116+09 has an inclination of greater than approximately 70° .

CSS0411-09 (CSS091215:041134-090729)

The CRTS light curve⁵ of CSS0411-09 has a number of high amplitude outbursts (up to 3.8 mag) over the 8-year baseline. No follow-up work had been undertaken on this object prior to this paper.

Based on our observations and the quoted CRTS quiescent magnitude of $V=19.4$, we observed the system during an outburst of more than 4 mag. The light curves (Fig. 2.4) show superhumps with amplitudes decreasing from approximately 0.5 to 0.3 mag over four days - indicating that this was a superoutburst and that CSS0411-09 is of the SU UMa class.

The combined FT of runs S7891, S7893 and S7898 is shown in the upper panel of Fig. 2.5. Only the mean was subtracted from each run, not the linear trend. The middle panel shows the window function, which reveals some structure in the FT and accounts for the broadness of the alias structure. Power at the first ($349.18 \pm 0.05 \mu\text{Hz}$) and second harmonic ($523.93 \pm 0.10 \mu\text{Hz}$) of the main peak at $174.40 \pm 0.02 \mu\text{Hz}$ allows the unambiguous identification of the superhump period of 0.06637 ± 0.00004 d. The PDM periodogram (see bottom panel of Fig. 2.5) gives a consistent solution. Bootstrapping the PDM gives $P_{SH} = 0.06633 \pm 0.00001$ d.

Using $P_{SH} = 0.06633 \pm 0.00001$ d and equation 1 of Gänsicke et al. [2009] gives an approximate orbital period of $0.0645(\pm 5)$ d for CSS0411-09.

The FT of run S7898 (shown in Fig. 2.6), when CSS0411-09 started its descent towards quiescence (0.4 mag fainter than the previous observation two days earlier), shows a clear peak at 25.58 ± 0.04 s with an amplitude of 4 mmag. The amplitude and frequency of this rapid optical modulation is typical of dwarf nova oscillations (see Warner 2004).

⁵<http://nessi.cacr.caltech.edu/catalina/AICV.html>

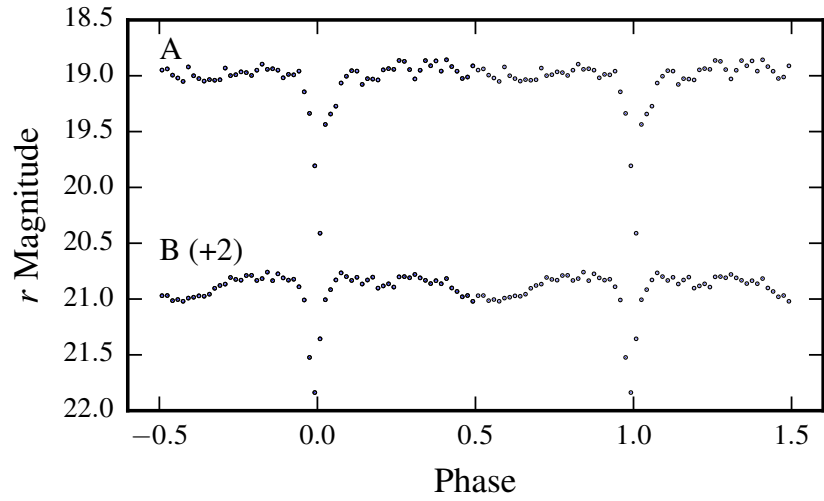


FIGURE 2.3: Average binned light curves of the quiescent runs of CSS0116+09 folded on the orbital period. Each orbit is plotted twice for display purposes. Plot A: Average of S8033 and S8040. Plot B: Average of S8098 and S8100, offset by 2 mag for display purposes.

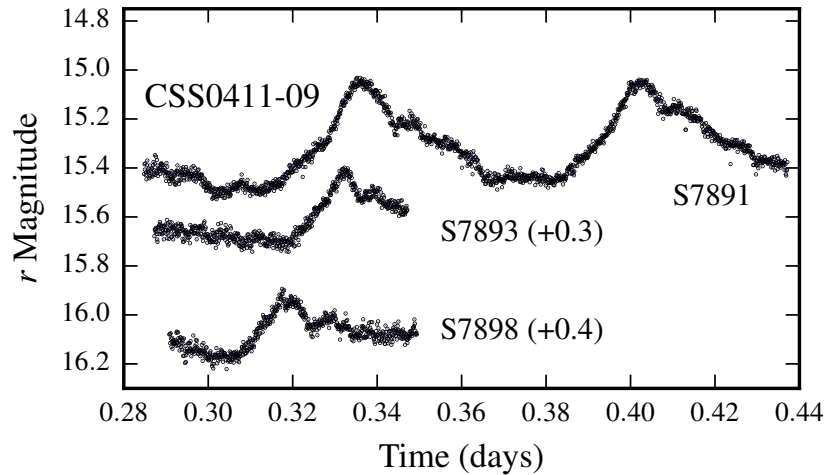


FIGURE 2.4: Observations of CSS0411-09 taken during superoutburst, showing superhumps (saw-tooth shaped profiles in the light curve produced by a precessing elliptical disc). Runs S7893 and S7898 have been displaced vertically by 0.3 and 0.4 mag respectively. The time given is the fractional part of the Heliocentric Julian Date.

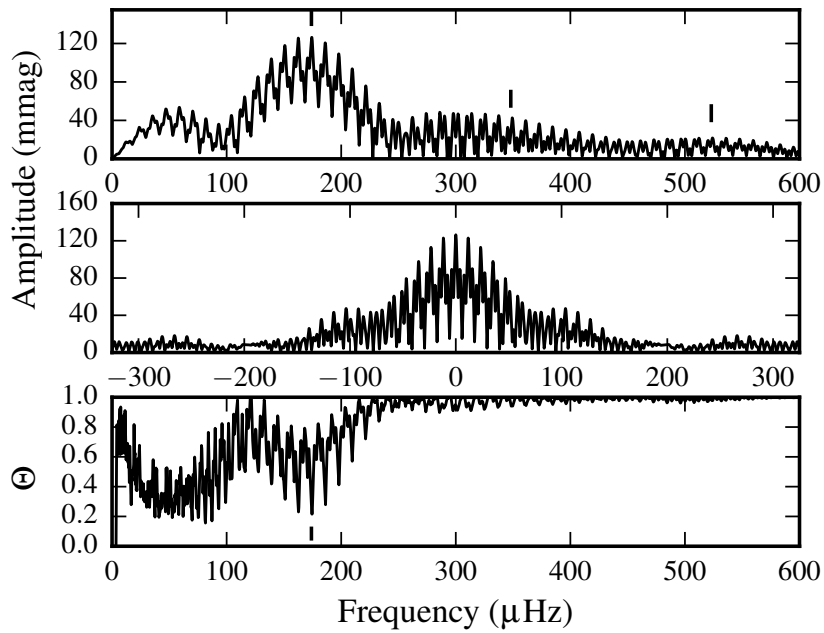


FIGURE 2.5: Upper panel: The FT of CSS0411-09 (combined runs S7891, S7893 and S7898). The superhump period at $174.40 \pm 0.02 \mu\text{Hz}$, and its first and second harmonics are marked. Middle panel: The corresponding window function shows the alias structure in the FT. Lower panel: PDM periodogram of the combined runs, with the superhump period marked.

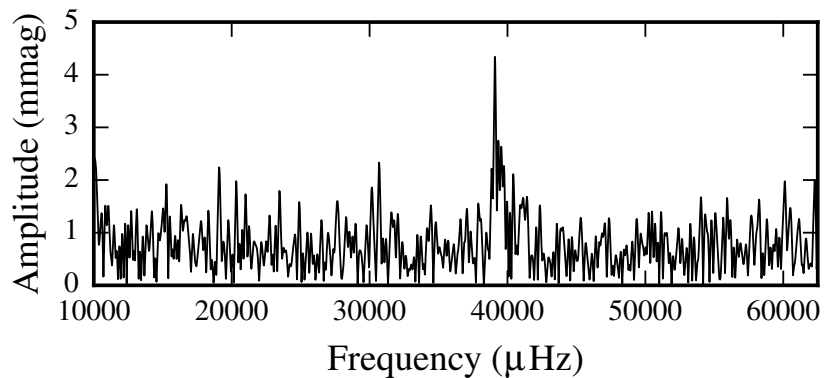


FIGURE 2.6: FT of run S7898 on CSS0411-09, showing a DNO at $39093 \mu\text{Hz}$ (25.58 s).

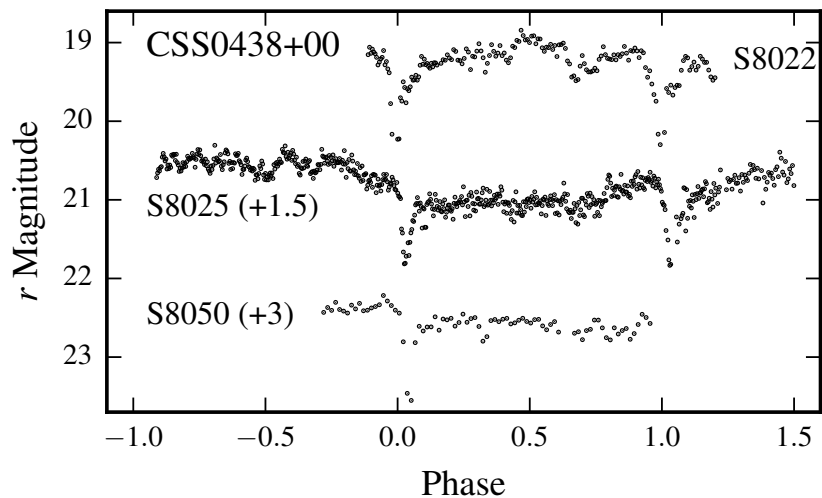


FIGURE 2.7: Light curves for CSS0438+00. Run S8050 was taken on the 74-in telescope with the UCT CCD. We observed this source under stable conditions only, as we were unable to fit a comparison star into the field-of-view and could not perform differential photometry. S8025 and S8050 are displaced vertically.

CSS0438+00 (CSS100218:043829+004016)

Over the course of the 6.5-year CRTS observations of CSS0438+00, three outbursts have been recorded. The first was observed at $\Delta V \sim 2.5$ mag above the quiescent magnitude ($V=19.3$) and the second, at $\Delta V \sim 2$ mag. It is within the SDSS survey area and was observed in quiescence at $u=19.4$, $g=19.5$ and $r=19.4$ mag.

Fig. 2.7 gives light curves for the three observing runs we obtained for CSS0438+00. It shows an eclipse depth of ~ 1 mag - indicative of a system with an inclination greater than approximately 70° .

The magnitude of the system, when out of eclipse, varies between orbits (for example, compare S8025 before and after phase 0). This type of variation is usually attributed to changes in the mass transfer rate from the secondary. In the combined PDM periodogram of S8022 and S8025 it produced a very high amplitude peak at 0.131 d. Prewhitening at this frequency gave an orbital period of 0.0657 d.

Taking the median and standard deviation of the bootstrapped sample as the orbital period and uncertainty, yields an ephemeris for minimum light of

$$HJD_{\min} = 2\,455\,529.45527 + 0^{\text{d}}.06546(\pm 9)E . \quad (2.2)$$

Unfortunately S8050 could not be used to reduce the uncertainty on P_{orb} . Over the 27 days between S8025 and S8050, the uncertainty on the orbital period accumulated to the point where there was a cycle ambiguity.

CSS0449-18 (CSS110114:044903-184129)

CSS0449-18 shows frequent outbursts in its CRTS light curve, despite the fact that it is not as well sampled as the other CSS systems. The quiescent magnitude is quoted at $V=17.7$ and the

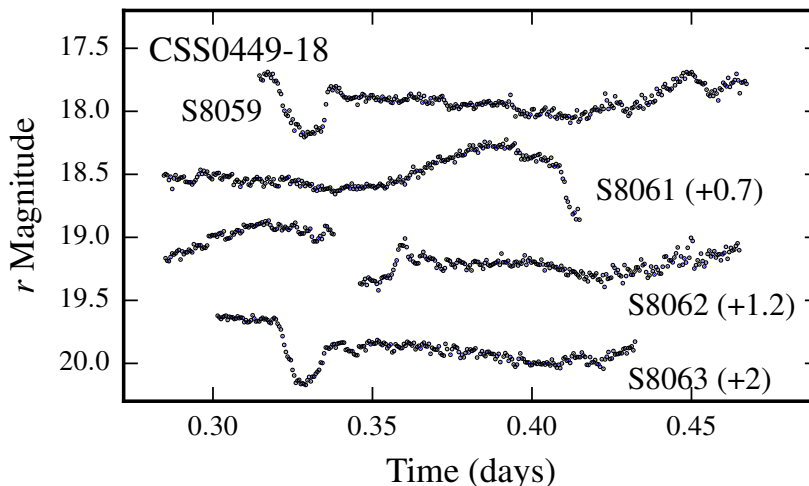


FIGURE 2.8: Photometry for CSS0449-18. S8059 is shown at the correct brightness, the remaining runs are displaced by the magnitude indicated in parentheses. The shallow, rounded eclipses are reminiscent of those of U Gem. Passing cloud caused the interruptions in the light curves.

outbursts were captured up to 2.8 mag above quiescence.

Our photometry was taken at close to minimum light. The light curves show orbital humps and rounded, shallow eclipses (see Fig. 2.8) that vary in profile from night to night. This indicates that it is likely that only the bright spot and part of the accretion disc were eclipsed.

From bootstrapping the PDM, we obtain an orbital period of $P_{orb} = 0.15554 \pm 0.00004$ d. The ephemeris for minimum light is

$$HJD_{\min} = 2455\,592.32760 + 0^{\text{d}}.15554(\pm 4)E. \quad (2.3)$$

The average light curve is shown in Fig. 2.9. The eclipses have a depth of $r \sim 0.4$ mag and a duration of approximately 26 min. They resemble those of U Gem (see for example Zhang &

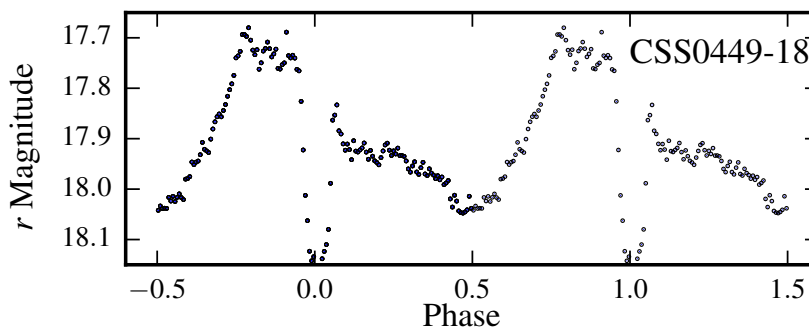


FIGURE 2.9: Average binned light curve of runs S8059, S8061, S8062 and S8063 of CSS0449-18, folded on the ephemeris given in Eq. 2.3. The average is plotted twice for display purposes.

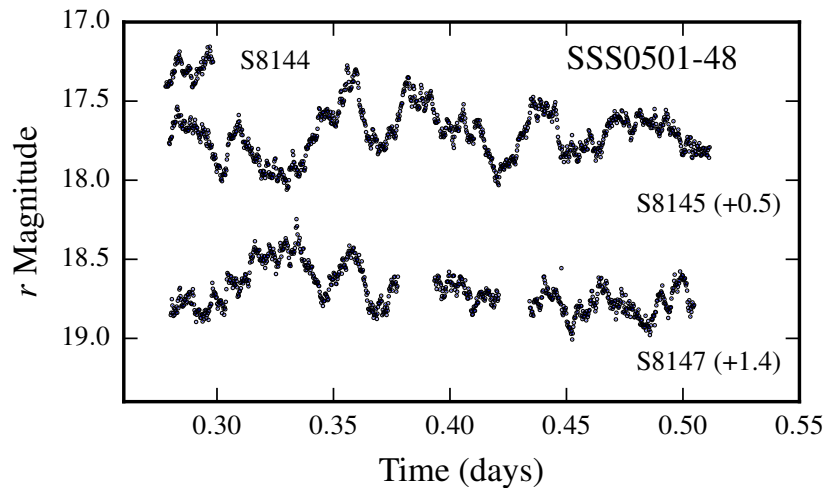


FIGURE 2.10: Light curves for SSS0501-48 dominated by flickering; no periodic modulations were found. S8145 and S8147 were 5.56 h and 5.39 h long respectively and are displaced vertically by 0.5 and 1.4 mag for display purposes.

Robinson 1987 and Warner & Nather 1971), consequently the inclination angle should be similar to the $\sim 72^\circ$ estimated for U Gem by Unda-Sanzana et al. [2006].

SSS0501-48 (SSS120112:050157-483901)

SSS0501-48 shows a variation in its quiescent magnitude in the CRTS light curve, ranging between $V \sim 16.7$ and 19 mag. Two outbursts were also recorded up to $V \sim 15.3$.

A substantial amount of flickering can be seen in our observations of SSS0501-48 (see Fig. 2.10), which could partly explain the scatter seen in the CRTS quiescent magnitudes. Despite the long length of the observing runs, the FTs did not show any periodic behaviour.

CSS0558+00 (CSS100114:055843+000626)

CSS0558+00 was discovered on January 14, 2010 during an outburst of approximately $\Delta V = 2.4$ mag. Two previous outbursts were also recorded in the CRTS archival data. It has a counterpart in the SDSS DR8 with $u=20.6$, $g=20.3$ and $r=19.0$. Spectroscopic follow-up observations were carried out by Thorstensen & Skinner [2012], who observed it during an outburst that was not captured by the CRTS. The single spectrum they obtained was typical of a dwarf nova in outburst and showed weak, broad $H\alpha$ line in emission.

We observed this system during quiescence. Each of the runs showed flickering (see Fig. 2.11), which caused broad, low-amplitude peaks in the individual FTs. Figure 2.12 gives the FT and PDM periodogram for the four longest runs. Both contained a peak at 0.06809 d and at the first harmonic. A Fisher Randomization test on the fundamental gives a false alarm probability (FAP) lying between 0 and 0.01 with 95% confidence, that this period is not present in the data. It gives the same FAP that the period is not equal to the quoted value. These two results confirm that the 0.06809 d period is real.

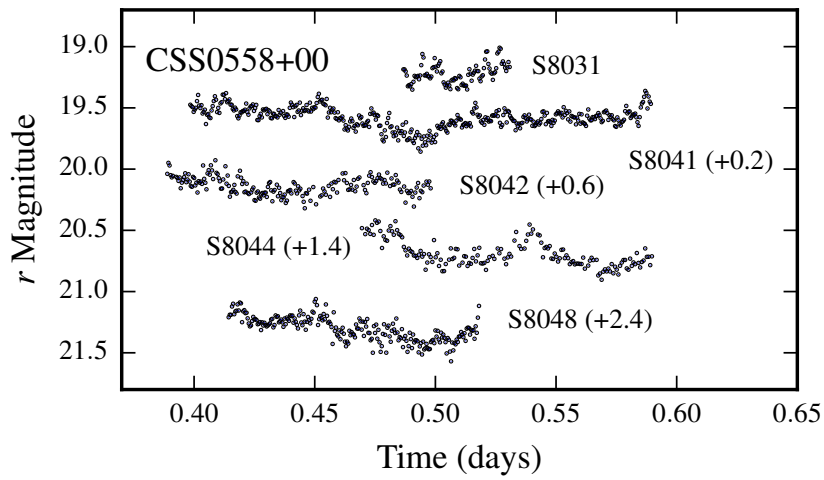


FIGURE 2.11: Light curves for CSS0558+00 taken in quiescence. The run lengths range between 1 h (S8031) and 4.6 h (S8041). Each run is offset vertically by the magnitude indicated in parentheses.

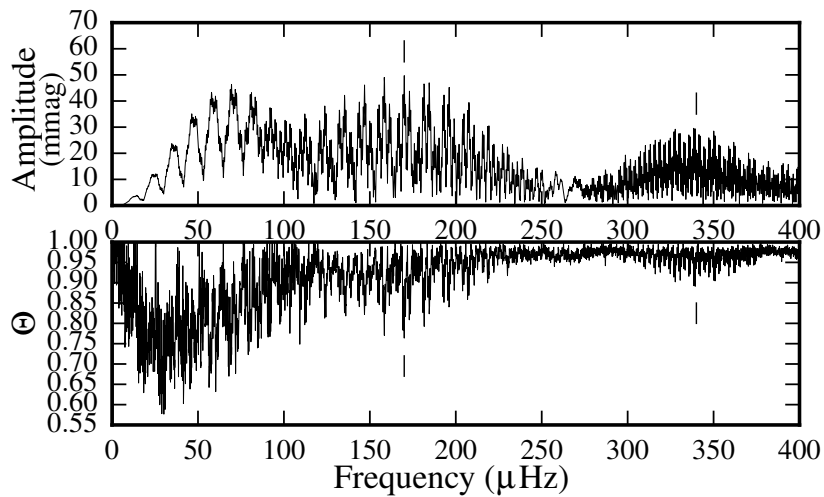


FIGURE 2.12: FT (top panel) and PDM periodogram (bottom panel) of the combined runs S8041, S8042, S8044 and S8048 of CSS0558+00. The orbital period (at $170.01 \pm 0.03 \mu\text{Hz}$) and its first harmonic are marked. The power at lower frequencies is caused by the finite length of the runs.

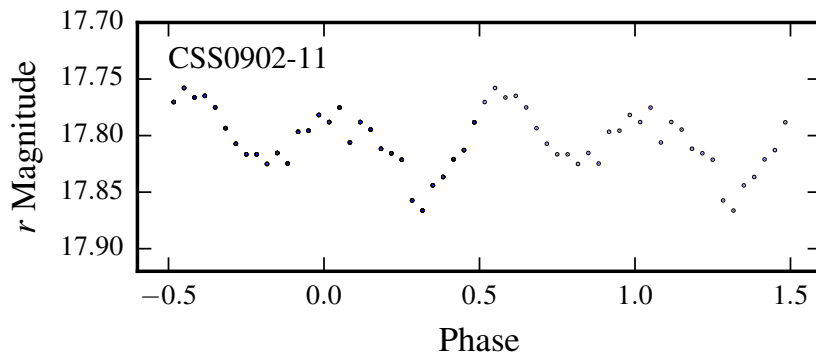


FIGURE 2.13: Average binned light curve of the two longest runs on CSS0902-11, folded on the 6.62 ± 0.01 h modulation detected by Thorstensen & Skinner [2012]. The data-length of the two runs, S7932 and S7934, were 5.1 h and 4.4 h respectively.

Bootstrapping the PDM gives an orbital period of $0.06808(\pm 1)$ d. Phasefolding the observations gives the ephemeris for maximum light as

$$HJD_{max} = 2\,455\,539.4522 + 0^d.06808(\pm 1)E . \quad (2.4)$$

CSS0902-11 (CSS090210:090210-113032)

The quiescent magnitude for CSS0902-11, as given by the CRTS, is $V=17.5$ mag. It was discovered on February 1, 2009 when it went into a 2.8 mag or higher outburst.

Thorstensen & Skinner [2012] took time series spectroscopy of this CV, from which they estimated it to be at a distance of $1100(+350,-260)$ pc and have a secondary star of spectral type $K7 \pm 1$ and magnitude $V \sim 18.5$. Additionally, based on the small velocity amplitude of the secondary (100 ± 6 km s $^{-1}$), they predicted that the system would not be eclipsing. This is confirmed by our photometry.

Their absorption spectra showed a clear 6.62 ± 0.01 h modulation. Only two of our runs approached this length - at 5.1 and 4.4 h respectively. The combined FT gives a period of 3.3 ± 0.1 h, half that of Thorstensen & Skinner's value. Phase-folding our two longest runs (S7932 and S7934) on the 6.62 h period (Fig. 2.13) shows that CSS0902-11 is a double hump system. Only one orbital hump was covered entirely in each of our two runs, which produced significant power in the FT at half the orbital period. In conclusion, our photometry is consistent with the 6.62 h orbital period detected by Thorstensen & Skinner [2012].

CSS0942-19 (CSS090117:094252-193652)

The CRTS light curve for CSS0942-19 is sparsely sampled, but shows two outbursts with amplitudes of approximately 4 mag. Judging from the large amplitudes, these may have been superoutbursts. This system was also caught in outburst by the Palomar Quest Sky Survey [Djorgovski et al., 2008].

We observed CSS0942-19 in quiescence in May 2011 at $V \sim 19.5$ (see Tab. 1) four months after the last recorded outburst by CRTS. The PDM periodogram of the combined runs on this object (see Fig. 2.14), shows strong peaks at the orbital frequency (78.7 ± 0.7 μ Hz) and at its first

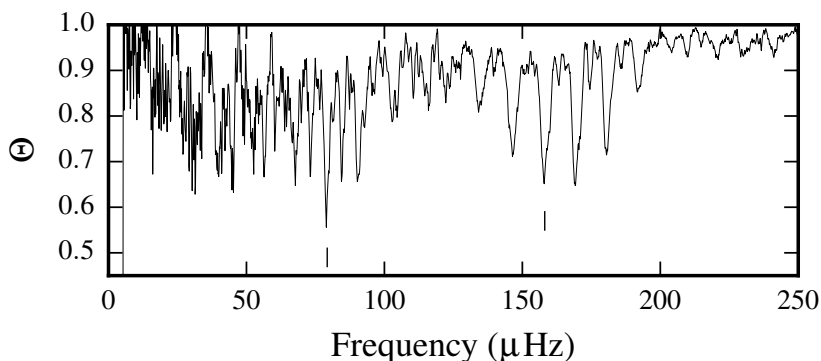


FIGURE 2.14: PDM periodogram of runs S8082, S8085 and S8088 on CSS0942-19. The peaks at the fundamental and first harmonic are marked.

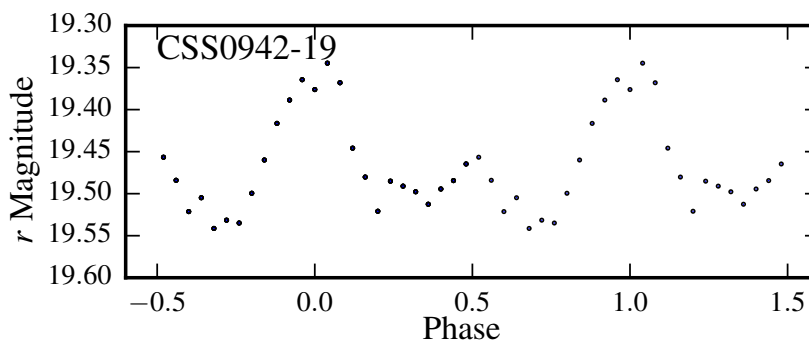


FIGURE 2.15: The average binned light curve of CSS0942-19, folded on the 0.147 ± 0.001 d photometric period.

harmonic. Bootstrapping the PDM, we obtain an orbital period and ephemeris for maximum light of

$$HJD_{max} = 2\,455\,693.2442 + 0^d.147(\pm 1)E . \quad (2.5)$$

The average light curve of CSS0942-19, folded on this ephemeris, is shown in Fig. 2.15.

CSS1052-06 (CSS100408:105215-064326)

Since CSS1052-06 was detected by the CRTS on April 8, 2010, numerous outbursts of approximately $\Delta V=3$ mag have been captured. No follow-up observations have been performed on it prior to this paper.

During our first three observing runs (S7949, S7952 and S7955), CSS1052-06 was in superoutburst and superhumps were present (see Fig. 2.16). Three days later, during S7964, the system had returned to quiescence.

The FT and the PDM periodogram of the two long runs in superoutburst are given in Fig. 2.17. The highest (or lowest in the case of the PDM) peaks coincide. Bootstrapping the PDM gives a superhump period of $0.07938(\pm 3)$ d. A Fisher randomisation test gives a false alarm probability, that the quoted period is different to the true period, of between 0 and 0.01 with a 95% confidence level.

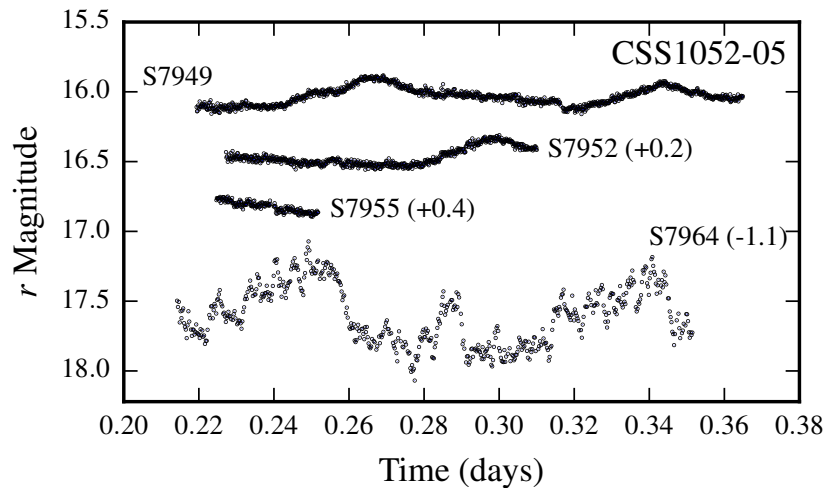


FIGURE 2.16: Light curves for CSS1052-06. S7949, S7952 and S7955 were taken during superoutburst and show superhumps. S7964 was taken in quiescence. For display purposes S7952, S7955 and S7964 have been displaced vertically by 0.2, 0.4 and -1.1 mag respectively.

Using the relation between the superhump and orbital periods in equation 1 of Gänsicke et al. [2009], the approximate orbital period for this system is 0.0765 ± 0.0005 d. The FT of the quiescent run S7964 did not show a peak at this period. This could be attributed to the large flickering in the light curve and the run length of less than two orbits.

SSS1128-34 (SSS110327:112815-344807)

The CRTS have detected multiple outbursts of SSS1128-34 since it was first observed in 2006. Their light curve gives an average quiescent magnitude of $V \sim 19$, although the individual observations range from $V \sim 18$ to $V \sim 19.8$. This range is produced by the orbital variation, as shown in our photometry in Fig. 2.18.

Each of the light curves show a clear double hump structure. The orbital hump of amplitude ~ 0.4 mag at phase 1 is produced by the bright spot orbiting into and out of our line of sight. The smaller hump at phase 0.5 is probably produced by the bright spot shining through a semi-transparent disc.

During our initial run (S8091), SSS1128-34 was in quiescence. The following day the system was 1.7 mag brighter and S8094 and S8095 were taken in outburst.

In the FT of the combined runs, the orbital period ($0.096(\pm 1)$ d) was chosen from two possible aliases of approximately equal height, based on the power of their respective first harmonics (see Fig. 2.19). The double hump structure produces large amounts of power at the first harmonic, so the ambiguity in the fundamental is removed because only one of the two likely orbital periods has a strong first harmonic. Only the mean, not the linear trend, was subtracted from these runs before calculating the FT, as removing the linear trend would greatly affect the shape of S8094 and S8095.

Using the Metropolis-Hastings algorithm to sample the period probability distribution (based

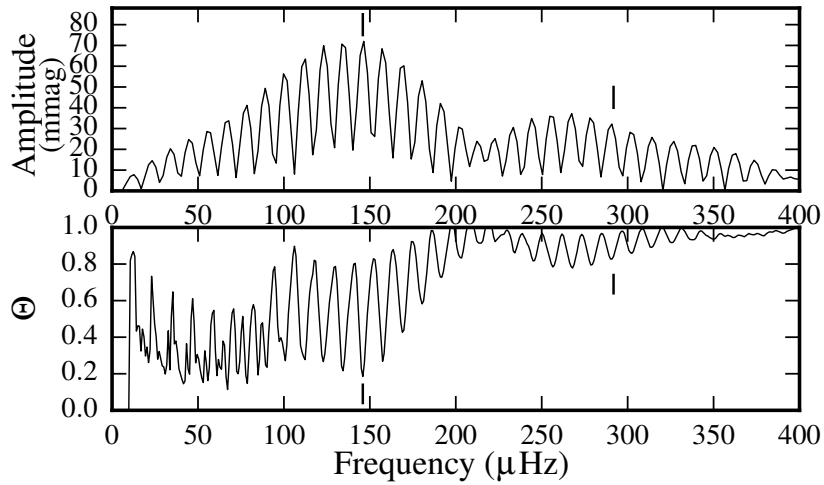


FIGURE 2.17: FT (top panel) and PDM periodogram (bottom panel) of S7949 and S7952 for CSS1052-06. Only the mean was subtracted from each run; they were not linearly detrended. The superhump period (0.07938 d) and its first harmonic are marked.

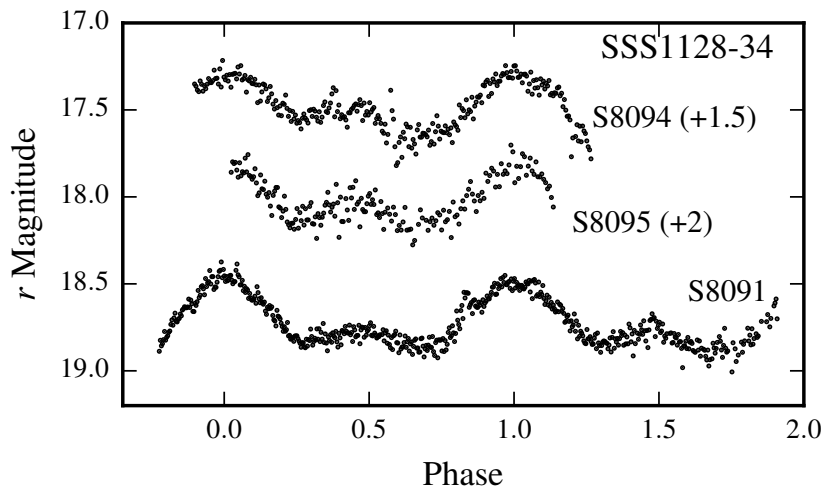


FIGURE 2.18: Light curves for SSS1128-34 phased on the orbital period (0.0985 d). S8091 was taken during quiescence, whereas S8094 and S8095 were taken in outburst. The latter two runs were displaced vertically for display.

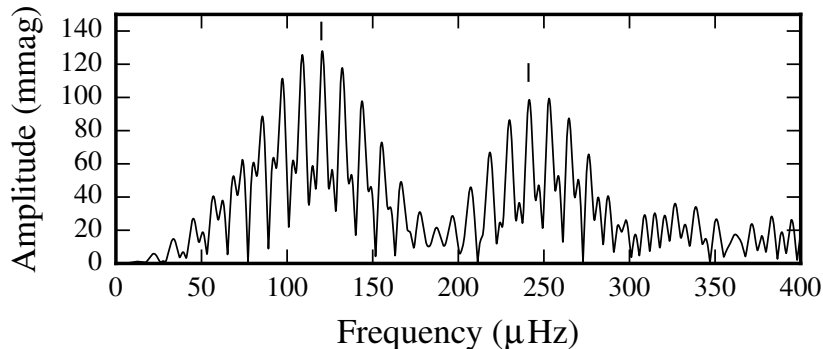


FIGURE 2.19: FT of the combined runs S8091, S8094 and S8095 of SSS1128-34. The orbital period and its first harmonic are marked.

on sine-curve fitting of the light curve), we get $P_{orb} = 0.0985 \pm 0.0001$ d. The period from the FT was used as the initial guess and the median and standard deviation are quoted as the period and uncertainty. The ephemeris for maximum light for these observations is

$$HJD_{max} = 2\,455\,696.2785 \pm 0.0985(\pm 1)E, \quad (2.6)$$

which places SSS1128-34 in the period gap.

CSS1221-10 (CSS080324:122100-102735)

The CRTS detected CSS1221-10 when it went into an outburst of magnitude $\Delta V \sim 3.5$ on March 24, 2008. It does not have a counterpart in the SDSS.

As seen in Fig. 2.20, CSS1221-10 has shallow eclipses with varying profiles reminiscent of those seen in CSS0449-18 (Fig. 2.8). This indicates that the system has a low inclination and is showing grazing eclipses.

The first harmonic of the orbital period was clear in the PDM periodogram of the combined runs S8056, S8058, S8064, S8068, S8069 and S8071. The ephemeris for minimum light is

$$HJD_{min} = 2\,455\,590.5743 + 0^d.14615(\pm 1)E, \quad (2.7)$$

where the uncertainty on the orbital period was obtained by bootstrapping the results. Fig. 2.21 displays the folded average light curve of the observations. The eclipse depth is approximately 0.2 mag and the system shows an orbital hump.

SSS1224-41 (SSS120215:122443-410158)

The CRTS quiescent value for SSS1224-41 is $V = 19.1$, but the light curve shows scatter between 17 and 20.6. This is due to outbursts and, as we see in our photometry, eclipses.

We obtained five runs on SSS1224-41 over February and March 2012. The corresponding light curves, with their ~ 0.6 mag eclipses, are shown in Fig. 2.22. As it turns out, run S8182 was 142s short of a complete orbital cycle.

The PDM periodogram showed peaks at the orbital period (0.2537 d) and its first harmonic. Bootstrapping the results to refine the orbital period and determine the uncertainty, as well as

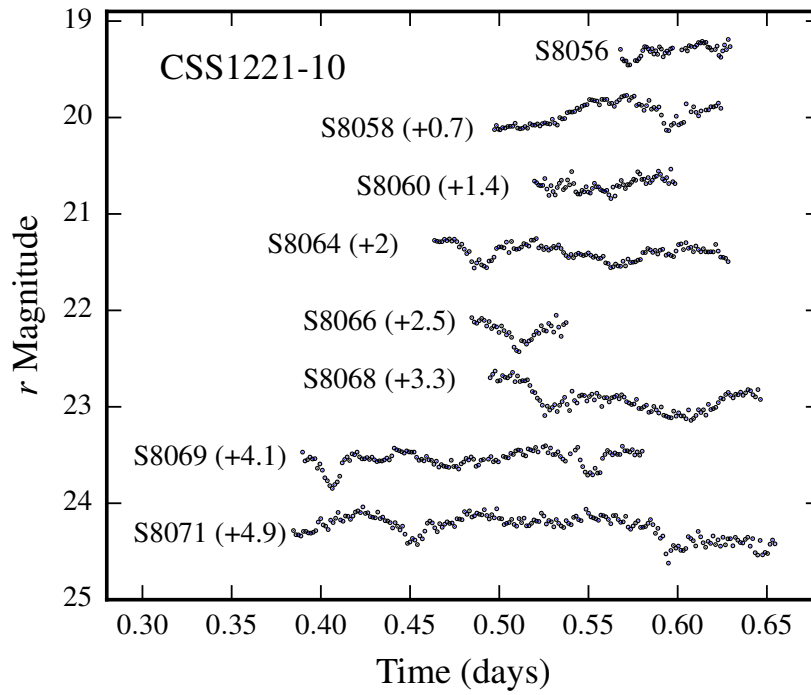


FIGURE 2.20: Light curves for CSS1221-10, showing grazing eclipses. The runs range in length from 1.3 h (S8066) to 6.5 h (S8071). Each run is shifted vertically by the magnitude indicated in parentheses.

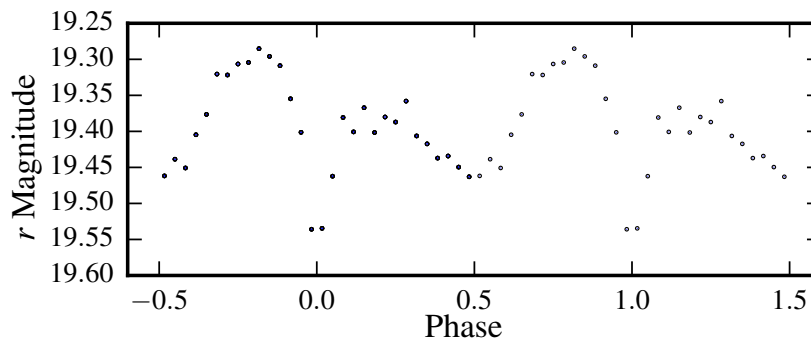


FIGURE 2.21: Averaged and binned light curve for CSS1221-10, folded on the 0.14615 d orbital period. Two orbits are shown for display purposes.

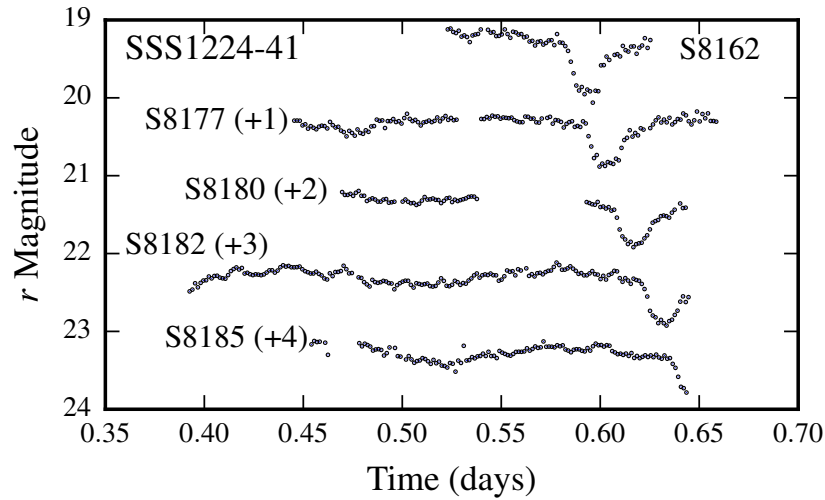


FIGURE 2.22: Light curves of SSS1224-41 showing ~ 0.6 mag eclipses. The gaps in the light curves were caused by passing cloud. The indicated vertical offsets are for display purposes.

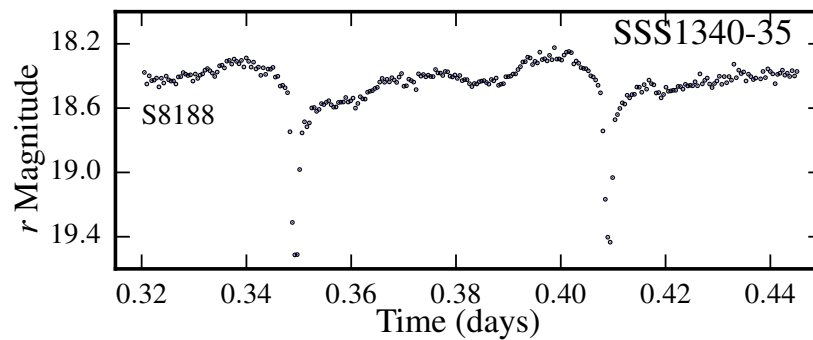


FIGURE 2.23: Light curve of SSS1340-35. The eclipse depth is $r \sim 0.9$, indicating a system inclination of greater than approximately 70° .

phase-folding the observations, gave an ephemeris for minimum light of

$$HJD_{\min} = 2\,455\,986.5934 + 0^{\text{d}}.25367(\pm 3)E . \quad (2.8)$$

SSS1340-35 (SSS120402:134015-350512)

SSS1224-41 has a quiescent magnitude of $V \sim 18.4$ mag, but has a number of points that were taken at $V \leq 20$. As shown by our photometry, these points were taken during eclipse.

We obtained one run on SSS1340-35, which contained two eclipses of depth ~ 0.9 mag (see Fig. 2.23). The corresponding PDM periodogram gives an orbital period of $0.059(\pm 1)$ d, where the uncertainty was obtained by bootstrapping. The ephemeris for minimum light is

$$HJD_{\min} = 2\,456\,038.3492 + 0^{\text{d}}.059(\pm 1)E . \quad (2.9)$$

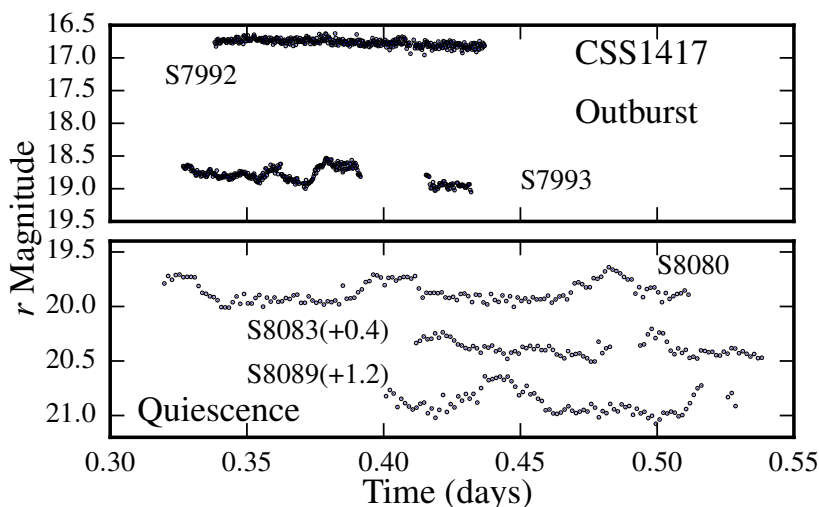


FIGURE 2.24: Light curves for CSS1417-18. The top panel contains those taken in outburst and the bottom panel contains those taken in quiescence. S8083 and S8089 have been displaced vertically by 0.4 and 1.2 mag respectively.

CSS1417-18 (CSS080425:141712-180328)

The CRTS detected one superoutburst of CSS1417-18 at $V \approx 15$ - approximately 5 magnitudes higher than the SDSS DR8 quiescent magnitude of $r=20.3$. We obtained two sets of observations of this object, one in outburst at $r=16.8$ and one in quiescence at $r=20$. This outburst was not captured by the CRTS.

All the observations are given in Fig. 2.24. Consider first the quiescent light curves shown in the bottom panel. They show a clear orbital hump profile with a ~ 0.2 mag amplitude. Using the highest amplitude peak in the FT as the initial guess for sine-curve fitting, the MCMC method produced a distribution of periods with median value 0.0845 d and standard deviation 0.0001 d, which we quote as the orbital period and uncertainty. The ephemeris for maximum light is

$$HJD_{max} = 2\,455\,692.3254 + 0^d.0845(\pm 1)E . \quad (2.10)$$

Now consider the two runs taken in outburst. S7992 did not show a modulation near the orbital period because, at $r=16.8$, the high disc luminosity overwhelmed all other variations. The gap in S7993, caused by passing cloud, was too large to pick up an orbital variation in this run.

In the one day separating S7992 and S7993, CSS1417-18 declined in magnitude by $r=2$ mag. In dwarf novae (DNe) the decline rate from outburst is related to the orbital period via equation 3.5 in Warner [1995]:

$$\tau_d = 0.53P_{orb}^{0.84}(h) \text{ d mag}^{-1} . \quad (2.11)$$

Using the 0.0845 d orbital period obtained from the quiescent runs, we would expect a decline rate of $\sim 0.96 \text{ mag d}^{-1}$, instead of the observed 2 mag d^{-1} . This value falls below the scatter on the plot of $\log(\tau_d)$ versus $\log(P_{orb})$ for DNe (see Figure 3.11 of Warner [1995]). Further observations of this system in decline are needed.

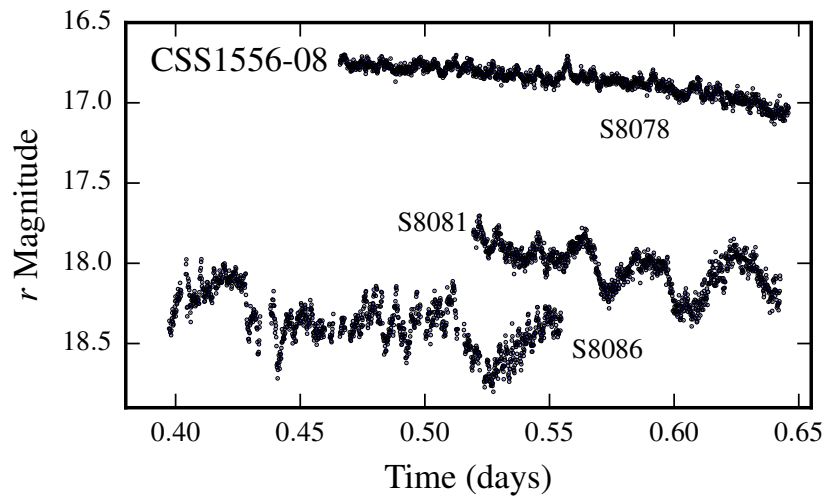


FIGURE 2.25: Light curves for CSS1556-08. Run S8078 is in outburst.

CSS1556-08 (CSS090321:155631-080440)

CSS1556-08 is listed as $V=18.4$ by the CRTS. On January 31, 2011, Thorstensen & Skinner [2012] took two spectra of it showing broad $H\alpha$ and $H\beta$ lines in emission. In March 2012 it went into superoutburst at $V\approx 15.3$ mag, which was observed by Oshima [2012a], Oshima [2012b] and Kato et al. [2013] (the system is referred to as OT J155631.0-080440). Oshima [2012a] gave an initial value for the superhump period as 0.1 d, which was then refined to 0.08933 ± 0.00006 d by Oshima [2012b]. Kato et al. [2013] determined the superhump period to be 0.089309 ± 0.000053 d. The average profile phased on this period is shown in figure 70 of Kato et al. [2013].

Our photometry of CSS1556-8 includes one run in outburst (S8078) and two in quiescence (S8086 and S8081) - it is shown in Fig. 2.25.

Using equation 1 from Gänsicke et al. [2009] and the 0.089309 ± 0.000053 d superhump period from Kato et al. [2013], gives an estimate for the orbital period as 0.0856 ± 0.0006 d. Although this period is present in the FTs of S8078 and of S8081 and S8086 combined, it is not the highest power alias and does not have any high power harmonics.

CSS1727+13 (CSS090929:172734+130513)

The CRTS quiescent magnitude for CSS1727+13 is listed as $V=19.5$, but is probably lower because many of the observations only yielded upper limits - most of them at $V\sim 20.3$.

Thorstensen & Skinner [2012] observed this object spectroscopically. Based on the FWHM of the $H\alpha$ line (1200 km s^{-1}), they concluded that CSS1727+13 has an intermediate inclination. Our light curves (Fig. 2.26) show flickering, but the FT and PDM of the combined runs only show low amplitude, broad peaks.

SSS1944-42 (SSS100805:194428-420209)

The ~ 7 -year long CRTS light curve for SSS1944-42 shows two low states and a high state lasting from August 2009 to June 2011; no outbursts have been captured. This behaviour is typical of a

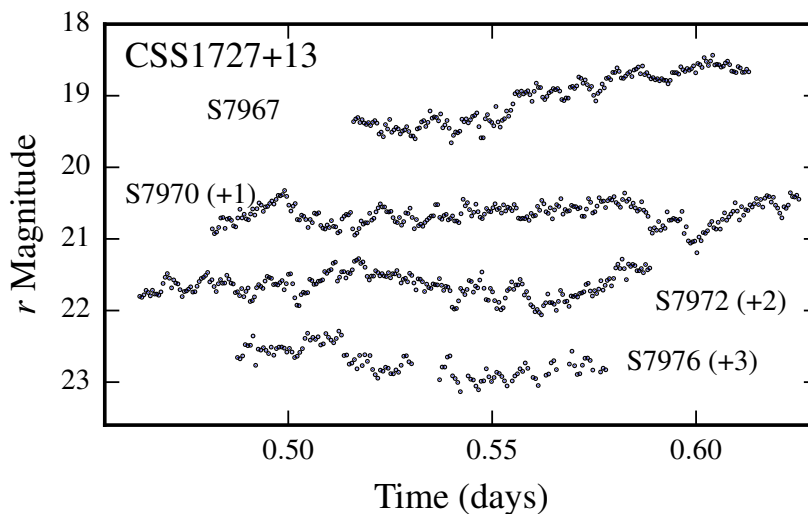


FIGURE 2.26: Light curves for CSS1727+13. No coherent modulations were indicated by the FT. Vertical offsets are indicated in parentheses.

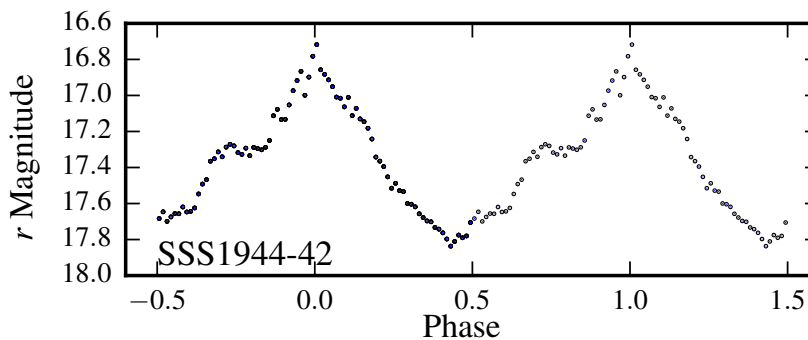


FIGURE 2.27: Average, binned light curve of SSS1944 folded on the ephemeris in Eq. 2.12. Two orbits are shown for display purposes.

magnetic system and the absence of outbursts indicates that it may be a polar. Our observations were taken during the high state.

Only the mean of each of the individual runs was subtracted, not the linear trend. The PDM periodogram of the combined runs has a peak at the orbital period (0.063855 d). Bootstrapping yields $P_{orb} = 0.06385 \pm 0.00002$ d. The ephemeris for maximum light for this system is

$$HJD_{max} = 2455693.6148 + 0^d.06385(\pm 2)E. \quad (2.12)$$

Fig. 2.27 shows the average light curve folded on this ephemeris.

SSS2003-28 (SSS100615:200331-284941)

Over the course of the CRTS observations (from April 2005 to September 2012), only one outburst has been recorded for this object. It occurred on the 15th of June 2010, when the system rose to $V=15.4$ from the listed quiescent value of $V=18.8$.

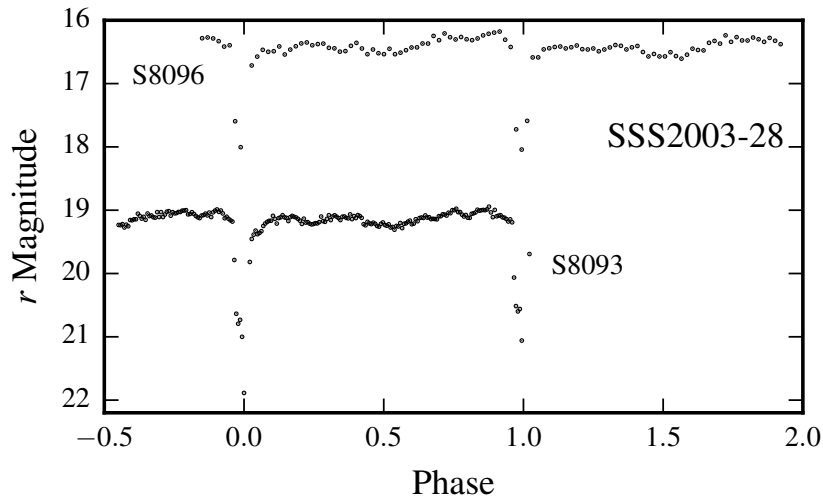


FIGURE 2.28: Lightcurves of SSS2003-28 folded on the orbital period. S8096 was taken during outburst. The average eclipse depth is approximately 1.9 mag.

On the 16th of May 2011, we caught this system in an outburst that was not captured by the CRTS. This run (S8096), as well as the quiescent run taken two days previously, are both displayed in Fig. 2.28. The photometry shows eclipses of depth $r \sim 1.9$, indicating an inclination of greater than approximately 70° .

The ephemeris for the time of mid-eclipse for these observations is

$$HJD_{\min} = 2\,455\,696.6236 + 0^{\text{d}}.05871(\pm 4)E, \quad (2.13)$$

where the orbital period and uncertainty were obtained by bootstrapping the PDM.

CSS2054-19 (CSS090829:205408-194027)

Since the detection of CSS2054-19 on the 29th of August 2009, numerous outbursts have been captured by the CRTS, the highest amplitude being $\Delta V = 3.5$ above the quoted quiescent value. The large amplitudes indicated that this may be an SU UMa system. Our observations confirm this. The photometry (Fig. 2.29) shows superhumps of amplitude ~ 0.2 mag, indicating that CSS2054-19 was in superoutburst.

The FT of the combined runs on this object gave two possible aliases for the superhump period, namely 0.096 ± 0.001 d and 0.0872 ± 0.0009 d, where the former was marginally higher. The corresponding PDM periodogram gave the same results (see Fig. 2.30). Bootstrapping the PDM produced a peak at both aliases. The first peak, at 0.09598 ± 0.00008 d, accounted for 88.5% of the data points, while the second peak (at 0.08752 ± 0.00008 d) accounted for the remainder. Based on these results, we have a preference for the 0.09598 ± 0.00008 d period, but can't exclude the one day alias.

Using $P_{SH} = 0.09598 \pm 0.00008$ d, equation 1 of Gänsicke et al. [2009] estimates an orbital period of 0.0917 ± 0.0006 d. This estimate would place CSS2054-19 within the period gap.

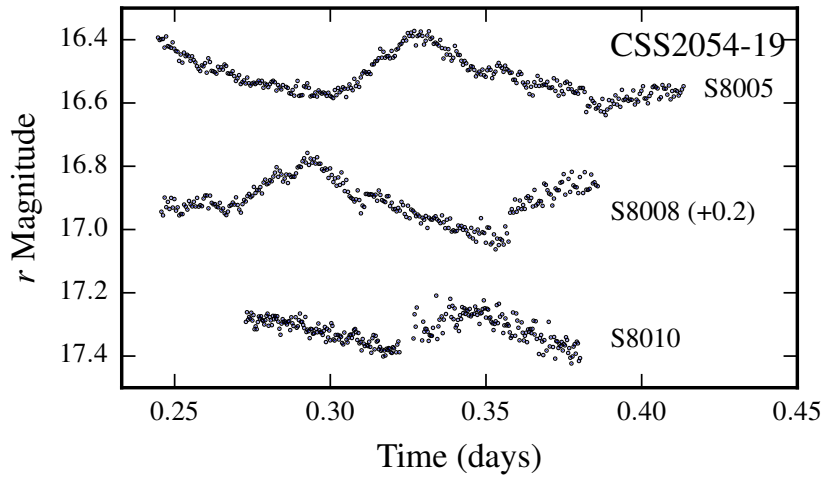


FIGURE 2.29: Light curves for CSS2054-19 taken during outburst, showing superhumps of amplitude ~ 0.2 mag. S8005 and S8010 are displayed at the correct brightness; S8008 has been shifted by 0.2 mag.

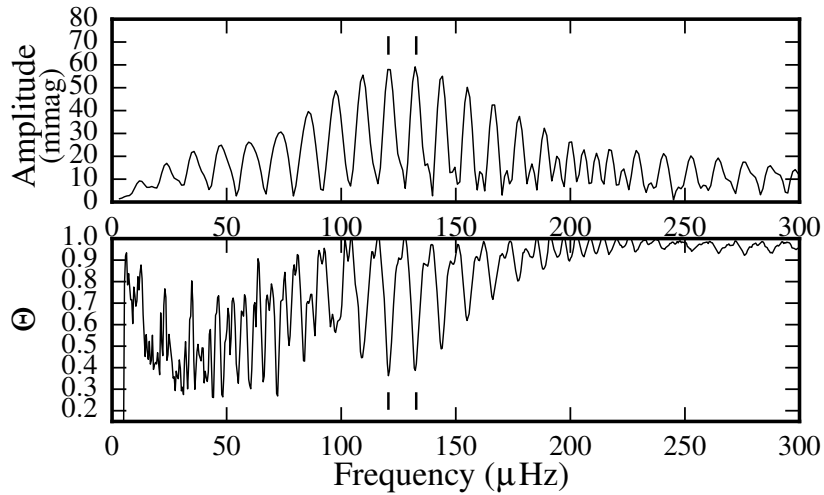


FIGURE 2.30: FT (top panel) and PDM periodogram (bottom panel) of the combined runs S8005, S8008 and S8010 of CSS2054-19. The vertical bars mark the two possible aliases for the superhump period, at 0.096 ± 0.001 d and 0.0872 ± 0.0009 d.

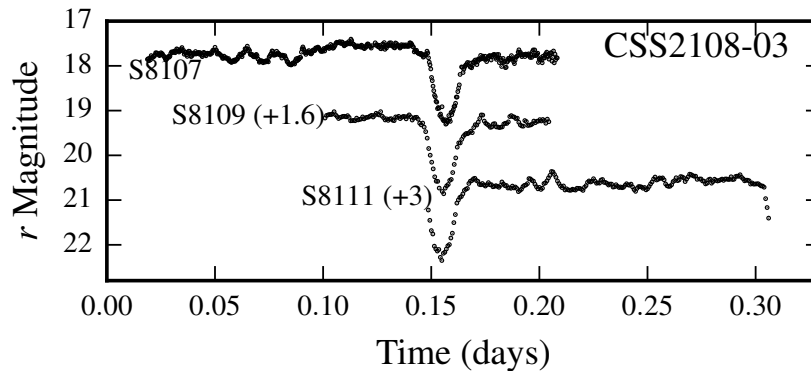


FIGURE 2.31: Light curves for CSS2108-03 folded on the ephemeris given in Eq. 2.14. The shortest run (S8113) is not shown. S8109 and S8111 have been shifted by 1.6 and 3 mag for display purposes.

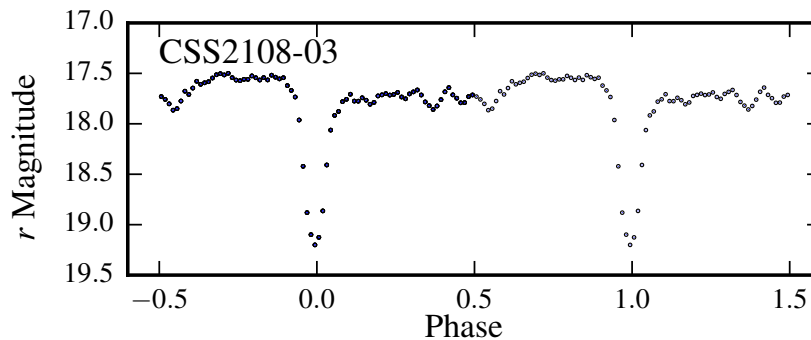


FIGURE 2.32: Average, binned light curve for CSS2108-03, folded on the ephemeris given in Eq. 2.14. The eclipse depth is ~ 1.5 mag.

CSS2108-03 (CSS110513:210846-035031)

The CRTS light curve for CSS2108-03 gives the quiescent magnitude as $V=18$ and its highest amplitude outburst at $V=14.9$. Its counterpart in the SDSS DR8 was observed in quiescence at $u=18.7$, $g=18.6$ and $r=18$ [Aihara et al., 2011]. The CRTS light curve for this object gives strong indications that it is an eclipsing system, as it has a number of points that are found more than a magnitude below quiescence. The faintest point is an upper-limit for detection at $V=20.7$. Photometry on CSS2108-03 confirms this, showing deep eclipses and large amplitude flickering (see Fig. 2.31).

Kato [2013] observed this system photometrically and determined an $P_{\text{orb}} = 0.156926798(\pm 9)$ d. Independently we determined an orbital period of $0.15699(\pm 5)$ d by bootstrapping the PDM of runs S8107, S8109 and S8111 combined. The ephemeris of minimum light for our observations is

$$HJD_{\text{min}} = 2455846.3725 + 0^{\text{d}}.15699(\pm 5)E . \quad (2.14)$$

The average of the runs folded on this ephemeris is presented in Fig. 2.32. It has an eclipse depth of ~ 1.5 mag.

TABLE 2.2: Summary of results

Object	Type	P_{morb} (d)	P_{SH} (d)	r	Remarks
CSS0116+09	DN	0.06582(± 5)	-	18.9 ^{m,q} , 17.1 ^{m,o}	Eclipsing, depth~1.4 mag
CSS0411-09	SU	-	0.06633(± 1)	15.4 ^o	Superhump
CSS0438+00	DN	0.06546(± 9)	-	19.3 ^{m,q}	Eclipsing, depth~1 mag
CSS0449-18	DN	0.15554(± 4)	-	17.9 ^{m,q}	Eclipsing, depth~0.4 mag
SSS0501-48	DN	-	-	17.3 ^q	
CSS0558+00	DN	0.06808(± 1)	-	19.3 ^q	
CSS0902-11	DN	0.2758(± 4) ^a	-	17.7 ^q , 16.5 ^o	
CSS0942-19	SU?	0.147(± 1)	-	19.5 ^q	
CSS1052-06	SU	-	0.07938(± 3)	16.2 ^o , 18.7 ^q	Superhump
SSS1128-34	DN	0.0985(± 1)	-	18.7 ^q , 16 ^o	
CSS1221-10	DN	0.14615(± 1)	-	19.4 ^{q,m}	Eclipsing, depth~0.2 mag
SSS1224-41	DN	0.25367(± 3)	-	19.3 ^{q,m}	Eclipsing, depth~0.6 mag
SSS1340-35	DN	0.059(± 1)	-	18.4 ^{q,m}	Eclipsing, depth~0.9 mag
CSS1417-18	SU	0.0845(± 1)	-	17.8 ^o , 19.9 ^q	Fast decline from outburst
CSS1556-08	SU	-	0.089309(± 53) ^b	16.9 ^o , 18.2 ^q	
CSS1727+13	DN	-	-	19.5 ^q	
SSS1944-42	P	0.06385(± 2)	-	17.4 ^q	
SSS2003-28	SU	0.05871(± 4)	-	19.1 ^{q,m} , 16.4 ^{o,m}	Eclipsing, depth~1.9 mag
CSS2054-19	SU	-	0.09598(± 8) ^c	16.8 ^o	Superhump
CSS2108-03	DN	0.15699(± 5) ^d	-	17.7 ^{q,m}	Eclipsing, depth~1.5 mag

Notes: Uncertainties on the last decimal are given in parentheses. DN: Dwarf Nova, SU: SU Ursae Majoris, P: Polar, ^mmean magnitude out of eclipse, ^ooutburst magnitude, ^qquiescent magnitude, ^aperiod determined by Thorstensen & Skinner [2012], ^bperiod from Kato et al. [2013], ^cone day alias is at 0.08752(± 8) d, ^dKato [2013] independently found $P_{morb} = 0.156926798(\pm 9)$ d

2.3 Discussion and Conclusions

We observed 20 CVs identified by the CRTS with the aim of classifying them, determining orbital periods and selecting targets for further observations with large telescopes. Of these 20 systems, only 6 have been observed prior to this work. Four systems were confirmed to be CVs by means of spectra and standardized photometry and a superhump period was determined for one of these (CSS1556-08, Kato et al. 2013). CSS0902-11 has been followed-up in detail with time-series spectroscopy [Thorstensen & Skinner, 2012] and CSS2108-03 was observed photometrically by Kato [2013].

The results are summarised in Tab. 2. We determined 12 new orbital periods and independently discovered periods for a further two CVs, namely CSS0902-11 and CSS2108-03. For three of the systems (CSS0411-09, CSS1052-06 and CSS2054-19), we determined superhump periods. CSS1556-08 had a pre-determined superhump period (Oshima 2012b and Kato et al. 2013), but we could not determine an orbital period from our photometry. The remaining 2 CVs did not show any periodic modulations.

Most of the CVs were DNe systems. This is as we should expect, as the CRTS identifies transients based on their variability. There was also a polar in the sample (SSS1944-42), that

was picked up by the CRTS because it showed high and low states that differed by more than a magnitude.

The orbital periods of these CVs fall predominantly below the period gap (see Knigge 2006 and Knigge et al. 2011), but there were two within the gap (SSS1128-34 and possibly CSS2054-19) and six above it. The predominance of CVs with periods below the period gap in the CRTS dataset is not fully explained. Thorstensen & Skinner [2012] discussed this bias. They compared the cumulative distribution functions of the outburst amplitudes of the CRTS CVs and those in the survey region that were listed in RKcat [Ritter & Kolb, 2003] that were not detected by the CRTS. They found that the CRTS shows a bias against low amplitude outbursts up to 6 mag. CVs with larger outburst amplitudes spend more time above the 2 mag cut-off limit that the CRTS employs and are thus more likely to be detected. Furthermore, they plotted the outburst amplitude versus the orbital period for CVs within the CRTS footprint (values from RKCat) and found a trend for short period DNe to have larger outbursts. Combined, these two findings indicate that there is a bias in the CRTS towards shorter period systems [Thorstensen & Skinner, 2012].

Eight of the CVs in this sample were eclipsing systems. As mentioned in Section 2.2, the long-term CRTS light curves of the deeply eclipsing systems sometimes give indications of the eclipses. As each field is observed three times at 10-min intervals, it is possible that one or two of the observations are taken in eclipse. If it is sufficiently deep, these points can show up on the long-term light curve at a magnitude or more below the quiescent level. Of the five systems with eclipse depths of more than 0.9 mag in our sample, four showed these characteristics.

A number of the CVs presented in this paper provide promising targets for more in-depth studies with larger telescopes - such as the eclipsing systems (CSS0116+09, CSS0438+00, CSS0449-18, CSS1221-10, SSS1224-41, SSS1340-35, SSS2003-28 and CSS2108-03), which through eclipse deconvolution can yield parameters such as the inclination and mass ratio. CSS1417-18 shows an unusually fast decline from outburst. The new orbital periods will also contribute towards population and evolutionary studies.

Acknowledgements

We thank the anonymous referee for the suggestions and comments which helped to improve this paper.

The authors also gratefully acknowledge funding from the South African Square Kilometre Array Project, the Erasmus Mundus Programme SAPIENT, the National Research Foundation of South Africa (NRF), the Nederlandse Organisatie voor Wetenschappelijk Onderzoek, the University of Cape Town, the National Astrophysics and Space Science Programme, the South African Astronomical Observatory (SAAO) and the Claude Leon Foundation Postdoctoral Fellowship program. Funding for the SHOC camera was provided by the NRF, specifically the Research Infrastructure Support Programme's National Equipment Programme (grant UID # 74428).

This research uses observations made at the SAAO and has also made use of NASA's Astrophysics Data System Bibliographic Services and of SDSS-III data. Funding for SDSS-III has been provided by the Alfred P. Sloan Foundation, the Participating Institutions (see <http://www.sdss3.org>), the National Science Foundation, and the U.S. Department of Energy

Office of Science.

The CSS survey is funded by the National Aeronautics and Space Administration under Grant No. NNG05GF22G issued through the Science Mission Directorate Near-Earth Objects Observations Program. The CRTS survey is supported by the U.S. National Science Foundation under grants AST-0909182 and AST-1313422.

Thank you to Thuso Simon for his Markov Chain Monte Carlo code.

STATISTICAL PROPERTIES OF DWARF NOVAE-TYPE CATAclySMIC VARIABLES: THE OUTBURST CATALOGUE

Deanne L. Coppejans, Elmar G. K rding, Christian Knigge, Magaretha L. Pretorius, Patrick A. Woudt, Paul J. Groot, Cameron L. Van Eck, Andrew J. Drake

MNRAS 456, 4441–4454 (2016)

Abstract

The Outburst Catalogue contains a wide variety of observational properties for 722 dwarf nova-type (DN) cataclysmic variables (CVs) and 309 CVs of other types from the Catalina Real-time Transient Survey. In particular, it includes the apparent outburst and quiescent V -band magnitudes, duty cycles, limits on the recurrence time, upper- and lower-limits on the distance and absolute quiescent magnitudes, colour information, orbital parameters, and X-ray counterparts. These properties were determined by means of a classification script presented in this paper. The DN in the catalogue show a correlation between the outburst duty cycle and the orbital period (and outburst recurrence time), as well as between the quiescent absolute magnitude and the orbital period (and duty cycle). This is the largest sample of dwarf nova properties collected to date. Besides serving as a useful reference for individual systems and a means of selecting objects for targetted studies, it will prove valuable for statistical studies that aim to shed light on the formation and evolution of cataclysmic variables.

3.1 Introduction

Cataclysmic Variable stars (CVs) are interacting binary systems which comprise a white dwarf (WD) primary and a red dwarf secondary star (see Warner 1995 for a review). Mass transfer occurs via Roche-lobe overflow, and accretion onto the surface of the primary can either proceed via an accretion disc (the non-magnetic systems), or via magnetic field line-channeling from the Alfvén radius if the magnetic field strength is sufficiently high (the magnetic systems).

The main CV subclasses are primarily defined according to their long-term photometric behaviour and the magnetic field strength of the WD. In many of the non-magnetic systems ($B_{\text{WD}} \lesssim 10^6$ G), the accretion disc switches between a cool, un-ionised state and a hot, ionised state with a high mass-transfer rate. This is commonly accepted to be caused by a thermal-viscous instability (Smak 1971; Osaki 1974; Höshi 1979). The interludes where the disc is bright and hot are known as dwarf nova outbursts (hereafter referred to as outbursts). Outbursts typically recur on timescales of days to decades, last for about a week and have outburst amplitudes of 2–8 magnitudes in the optical, but there are large variations between CVs in all three of these properties. The CVs that show these outbursts are known as dwarf novae (DN). Non-magnetic CVs in which the mass-transfer rate from the secondary (\dot{M}) is sufficiently high to maintain the disc in a hot state, are the novalikes. Some novalikes are known to show occasional low-states lasting weeks to years (e.g. Groot et al. 2001; Honeycutt & Kafka 2004). The polars and intermediate polars form the two classes of magnetic CVs. In intermediate polars ($10^6 \lesssim B_{\text{WD}} \lesssim 10^7$ G) a partial accretion disc is present (it is truncated at the Alfvén radius), whereas in polars the magnetic field strength is sufficiently high ($B_{\text{WD}} \gtrsim 10^7$ G) that material is fed directly from the secondary onto magnetic field lines at the point where the magnetic pressure exceeds the ram pressure.

In the last few years a number of discrepancies have emerged in the evolutionary model for (particularly) the non-magnetic CVs. First, it was predicted that there should be a spike in the number of CVs at the minimum orbital period, $P_{\text{orb}}^{\text{min}} \approx 65$ mins [Paczynski & Sienkiewicz, 1981; Rappaport et al., 1982; Kolb & Baraffe, 1999; Howell et al., 2001]. This period spike has now been detected and confirmed observationally, but at the longer orbital period (P_{orb}) of approximately 82 mins [Gänsicke et al., 2009; Woudt et al., 2012; Drake et al., 2014]. A CV initially evolves to shorter P_{orb} via a loss of angular momentum by magnetic braking and gravitational radiation. During this time, the mass-loss rate from the secondary drives it increasingly out of thermal-equilibrium until the thermal-timescale exceeds the mass-loss timescale and it expands in response to mass loss – thereby increasing P_{orb} . Consequently the evolutionary direction changes at $P_{\text{orb}}^{\text{min}}$, and a large number of CVs is expected at this orbital period (the period spike). In order to reconcile the observed and predicted values for $P_{\text{orb}}^{\text{min}}$, enhanced angular momentum loss at short orbital periods has been suggested [Knigge et al., 2011]. Second, a large population of CVs that have evolved past $P_{\text{orb}}^{\text{min}}$ (post period-minimum CVs) is predicted. The fraction of post-bounce CVs is expected to be 40-70%, however, only a few candidates have been identified to date (e.g. Littlefair et al. 2008).

Deep, long-term, time-domain surveys offer a solution to these problems, as they are detecting larger, deeper, and less-biased samples of CVs. Examples of these surveys include the Catalina Real-time Transient Survey (CRTS, Drake et al. 2009), the Palomar Quest digital synoptic sky survey (PQ, Djorgovski et al. 2008) and the Palomar Transient Factory (PTF, Law et al. 2009; Rau

et al. 2009), as well as the upcoming Large Scale Synoptic Telescope (LSST, Tyson 2002). The overall strategy of these surveys is to detect variable objects through multi-epoch observations, but the observing cadence, sky coverage and variability criteria differ between the surveys. CVs are detected in large numbers by these surveys due to their range of variability amplitudes and time-scales: from sub-second to minute variability (below $\Delta V \sim 10^{-3}$ mag, e.g. Woudt & Warner 2002; Scaringi 2014), orbital modulations on time-scales of minutes to hours ($\Delta V \lesssim 3$ mag, e.g. Coppejans et al. 2014), to outbursts ($\Delta V \sim 8$ mag, which include dwarf nova outbursts and the longer, brighter superoutbursts – see Warner 1995). Additionally, thermo-nuclear runaways on the surface of the WD (Novae) produce amplitude variations of up to $\Delta V \sim 10$ mag (for a review, see Bode 2010).

The CRTS, in particular, has detected more than 1000 CVs to date, each with a light curve spanning ~ 8 to 9 years. We have used these long-term light curves to estimate the duty cycle and constrain the outburst recurrence time for a large sample of CVs. These properties will help constrain the mass-transfer rate and angular momentum loss (AML) rate in the overall population. Better-constrained AML rates will improve evolutionary models and our understanding of the post-bounce population, and help to reconcile the observed and predicted position of the period minimum.

Our catalogue was constructed with a goal towards answering these, and related, questions that require large samples of CV properties to answer. Additionally it is meant as a reference for individual systems and a means of selecting CVs for targeted campaigns, based on their outburst properties.

In Section 3.2 we discuss the CRTS survey in detail. Section 3.3 describes the classification script, and Section 3.4 outlines the contents of our catalogue. The catalogue is then characterised in Section 3.5.

3.2 CRTS

The Catalina Real-time Transient Survey (CRTS) identifies transients in the data from the Catalina Sky Survey¹ (Larson et al. 1998, 2003; Johnson et al. 2014b) – a photometric survey that searches for Potentially Hazardous Asteroids (PHAs) and Near Earth Objects (NEOs). Three sub-surveys constitute the Catalina Sky Survey, namely the original CSS (Catalina Schmidt Survey), the MLS (Mt. Lemmon Survey) based in Arizona, and the SSS (Siding Spring Survey) in Australia, which ended on 5 July 2014. Each has a dedicated telescope with a 4k back-illuminated, unfiltered CCD camera [Djorgovski et al., 2010]. The field of view and typical limiting magnitude for each survey (at ~ 30 s integrations) are 8.2° and $V \sim 19.5$ mag for the CSS, 1.1° and $V \sim 21.5$ mag for the MLS, and 4° and $V \sim 19$ mag for the SSS. Together these surveys cover $30,000 \text{ deg}^2$ ($-70^\circ < \delta < 70^\circ$, see Drake et al. 2014 for more details). The Galactic plane ($|b| < 15^\circ$) is avoided due to overcrowding, as are the Magellanic Clouds.

Each observation consists of four images (frames) that are separated by ≈ 10 minutes. The observing cadence is typically 1-4 times per lunation (depending on the sub-survey and field).

¹<http://www.lpl.arizona.edu/css/>

Aperture photometry is performed using SExtractor software [Bertin & Arnouts, 1996] and converted to V -band magnitudes using standard stars as described in Drake et al. [2013].

The CRTS began processing CSS data on 8 November 2007, MLS data on 6 November 2009 and 5 May 2010 for SSS data [Drake et al., 2014]. Although there is Catalina Sky Survey data preceding these dates, the CRTS only use these data in the transient classification process – any object that was only variable during this time will not have been identified as a CRTS transient.

To identify variability, the CRTS makes catalogues of the objects in each image and compare these to previously recorded magnitudes; they do not use image subtraction. An object needs to pass a number of tests to be classified as a transient. In each set of four frames (one epoch), it needs to be positionally coincident in at least three of the frames. This eliminates high proper motion objects (movement of $> 0.1' \text{ min}^{-1}$ between frames), which are generally solar system objects. Additionally it needs to be a point source, and cannot be saturated ($V \gtrsim 12.5$ mag), or blended (the pixel scale is $2.5''$).

Objects that pass these tests are then compared to deep co-added image catalogues. There is one co-add per CRTS field and it is the median of 20 images taken at the beginning of the CRTS survey. The co-adds typically reach down to $V \sim 21.5$ mag for the CSS, $V \sim 22.5 - 23$ mag for the MLS and $V \sim 20$ mag for the SSS.

The criteria for classifying a transient have evolved over the course of the survey to detect more transients and filter out periodic variable stars (see Drake et al. 2014). Initially an object needed to be either ≥ 2 mag brighter than the co-add or had to be absent in the co-add [Drake et al., 2009]. This requirement changed to ≥ 1 mag brighter than the co-add (or absent in the co-add). Currently, an object needs to be ≥ 0.65 mag brighter than the co-add (or absent in the co-add), with a $\geq 3\sigma$ flux change in comparison to its CRTS light curve [Drake et al., 2014]. The new criteria have not been applied to previously processed data. The candidate transient is then compared to archival data from the SDSS, the USNO-B (US Naval Observatory B catalogue, Monet et al. 2003) and the Palomar-Quest Synoptic Sky Survey [PQ, Djorgovski et al., 2008] in order to discard further artifacts, for example those that were missing in the co-adds because they were blended. As a final check against artifacts, new transients are examined by eye and assigned a classification of CV, supernova (SN), quasar, asteroid or flare star, blazar, AGN, or unknown.

We now describe the CRTS classification procedure in relation to CVs; for details regarding other classes of transients see Drake et al. [2009, 2014]. If available, the classification given in the Virtual Observatory (VO, Quinn et al. 2004; Borne 2013) is used, otherwise spectra and photometry from SDSS, USNO-B and PQ, along with the CRTS light curves are used in the classification. A number of features are taken into account when classifying an object as a CV. Multiple outbursts, rapid declines, a return to quiescence within a short time, a variable quiescent level, and a blue point-source counterpart in the SDSS, all increase the probability of a transient being classified as a CV. Colour-cuts are not used. Objects that show only one outburst could be either CVs or SN, although CVs are generally brighter on average and more likely to be seen in quiescence. If an object with a single outburst has a background galaxy, it is classified as a SN (as SN are likely to be followed up, misclassifications are generally caught). If it is not clear whether an object with a single outburst is a CV or SN, it is placed in the ‘CV or SN’ category in the CRTS. Note that since the CRTS do not routinely reclassify, a CV that shows another outburst

after the classification may still be in the ‘CV or SN’ category. CRTS follow-up photometry and spectroscopy has been performed for some of the CVs [Drake et al., 2014].

The CRTS data is open access, so the images and light curves are available to the public. The discovery date, magnitude, change in magnitude, classification and images from other surveys are also included. This has led to a number of photometric and spectroscopic CV follow-up studies (e.g. Thorstensen & Skinner 2012; Woudt et al. 2012; Kato et al. 2013; Breedt et al. 2014; Coppejans et al. 2014; Szkody et al. 2014 and references therein). These surveys indicate that more than 95% of objects classified as CVs were correctly classified [Breedt et al., 2014; Drake et al., 2014]. Any misclassification noted in the ATels or literature is corrected in the CRTS database.

Up to October 2015, the CRTS had detected a total of 10,782 transients. This total includes 1252 CVs, 2570 supernovae, 1476 CVs/supernovae, 638 asteroids/flares, 373 blazars and 2968 AGN. An up-to-date tally is given on the CRTS website².

3.3 Classification Script

The 8–9 year CRTS CV light curves offer a good means to estimate and constrain outburst properties for DN, such as the duty cycle, recurrence time, outburst amplitude, and apparent quiescent and outburst magnitudes.

Due to the difficulties involved with making these estimates from magnitude-limited, irregularly-sampled data, previous estimates for these properties have been made by eye (e.g. Breedt et al. 2014; Drake et al. 2014). Scripting this procedure is advantageous for a number of reasons. It defines hard classification criteria. This makes it possible to determine completeness, compare the sample to other databases and, importantly, update it when new observations become available. Using a script also makes it possible to trace outbursts and estimate recurrence times.

We have written a script, hereafter referred to as ‘the classification script’, that uses light curves to classify a CV as a ‘DN’ or ‘non-DN’, and subsequently estimate and define limits for the duty cycle, outburst recurrence time, apparent outburst and quiescent magnitudes, and distance. Only those transients that had already been classified as CVs by the CRTS have been run through the script. A flowchart describing the procedure is shown in Figure 3.1.

The CRTS input light curves for the classification script are generated from the published light curves and the observing log. The latter is necessary to determine the times when the objects were not detected (the non-detections/upper-limits are not included in the current CRTS data release). The exact magnitude of the upper-limit is not important for the classification script, so it is recorded at the average limiting magnitude of the survey³ (SSS: $V = 19$ mag, MLS: $V = 21.5$ mag, CSS: $V = 19.5$ mag).

The first steps in the script are to average the light curve, and to determine if there are enough data points to attempt a classification. Each light curve is averaged by day (by set of four CRTS observations separated by 10 minutes) in order to reduce the scatter introduced by eclipses and variability. A minimum of 10 detections, or 15 non-detections, are then required to proceed.

²<http://crts.caltech.edu/>

³See <http://crts.caltech.edu/Telescopes.html>

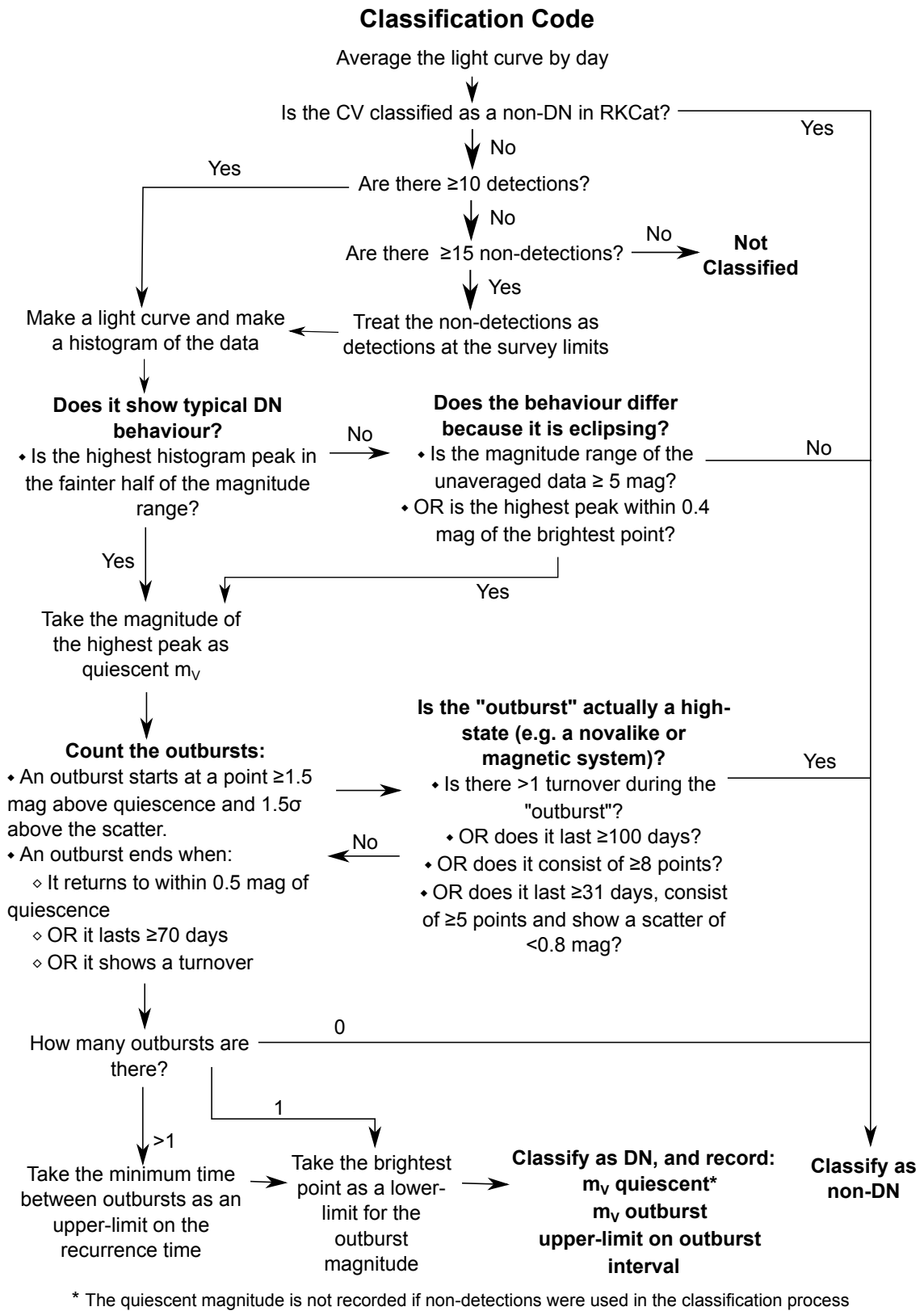


FIGURE 3.1: Flowchart depicting the process followed by the classification script, whereby a CV is classified as 'DN' or 'non-DN' based on the light curve. Outburst properties are subsequently estimated for the DN systems.

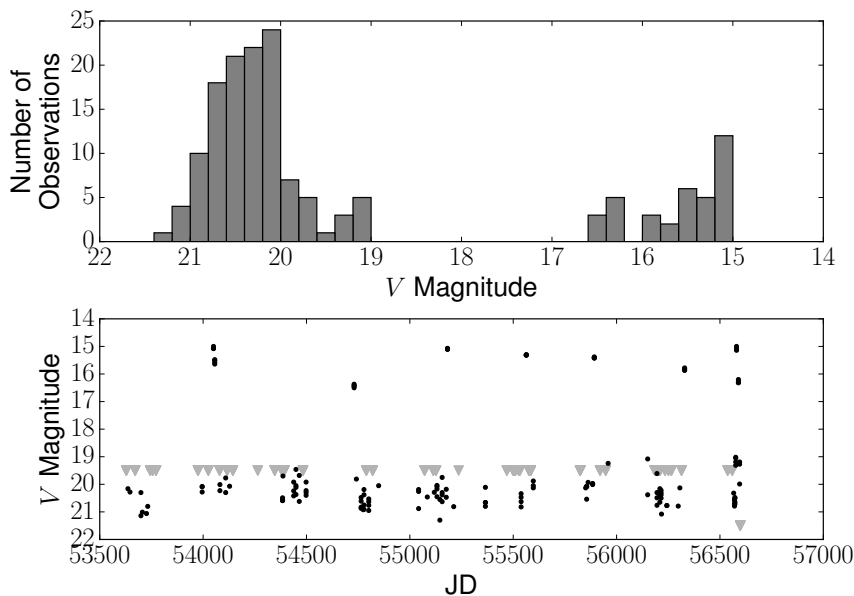


FIGURE 3.2: Illustration of the initial classification step (see Figure 3.1), where the light curve (bottom panel) is histogrammed by magnitude (top panel) in order to determine whether it shows standard DN-type behaviour. In this example the CV was given the initial classification of ‘DN’, because the higher histogram peak is in the fainter half of the magnitude range – as one would expect from a DN that spends the majority of its time in quiescence. Subsequent tests in the script confirmed the ‘DN’ classification, counted 7 outbursts, and estimated $v_Q = 20.1$ mag and $v_O < 15.5$ mag. Note that the non-detections in the lightcurves are shown at the typical detection limit of the survey (currently the CRTS data release does not provide upper limits).

Through a series of tests, the script assigns one of two possible classifications to every CV, namely ‘DN’ or ‘non-DN’. The former consists of all CVs that show outbursts, while the latter consists of non-outbursting CVs such as polars and novalikes.

An initial, tentative classification is assigned based on the histogram of the light curve. A typical DN is predominantly in quiescence, so a histogram of its light curve will reflect this and have a higher peak in the fainter half of the magnitude range (see Figure 3.2). Light curves that do not show these properties are typically of CVs that show extended high-states, such as novalikes and magnetic CVs, and are assigned the classification ‘non-DN’. This means that some DN with very high duty cycles ($> 50\%$), and intermediate polars that show outbursts as well as high-states, can be incorrectly classified as ‘non-DN’. Although few eclipses are expected in the averaged data, CVs are flagged as potential eclipsers if the magnitude range exceeds $\Delta V = 5$ mag, or the highest peak is within $V = 0.4$ mag of the brightest point (which will be the case if there are no outbursts). The $\Delta V = 5$ magnitude limit will miss the shallower eclipsers (e.g. grazing eclipses of the disc), but it is set to prevent the magnetic CVs and those with large orbital modulations from masquerading as eclipsers.

DN and potential eclipsers then undergo a second round of classification. In order to test the ‘DN’ classification, the script traces and counts the outbursts, and then runs a number of checks to ensure that the outbursts are not high-states. Tracing the outbursts is necessary, as the

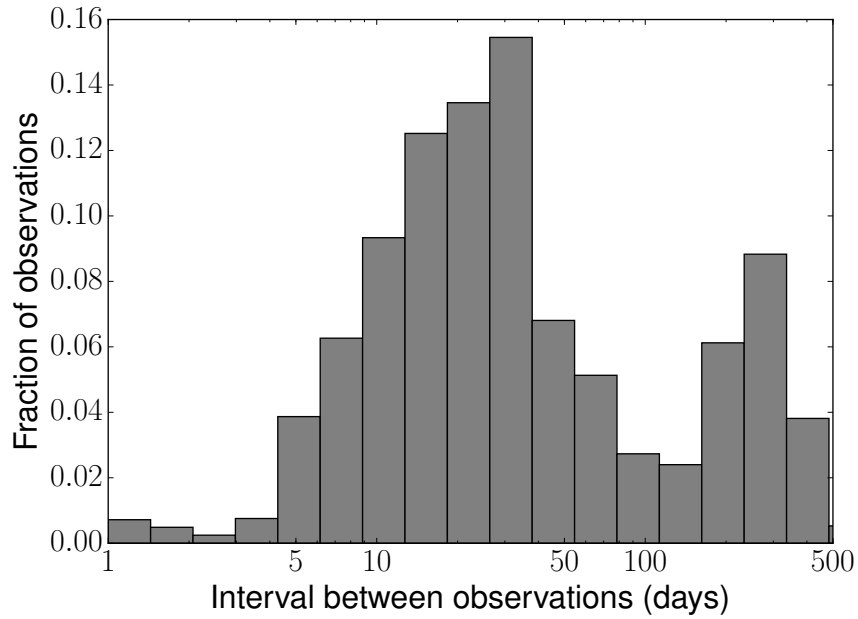


FIGURE 3.3: Distribution showing the interval, in days, between CRTS observations. The median interval was 28 days, 16% of the intervals were less than 10 days, and 61% were between 10 and 100 days.

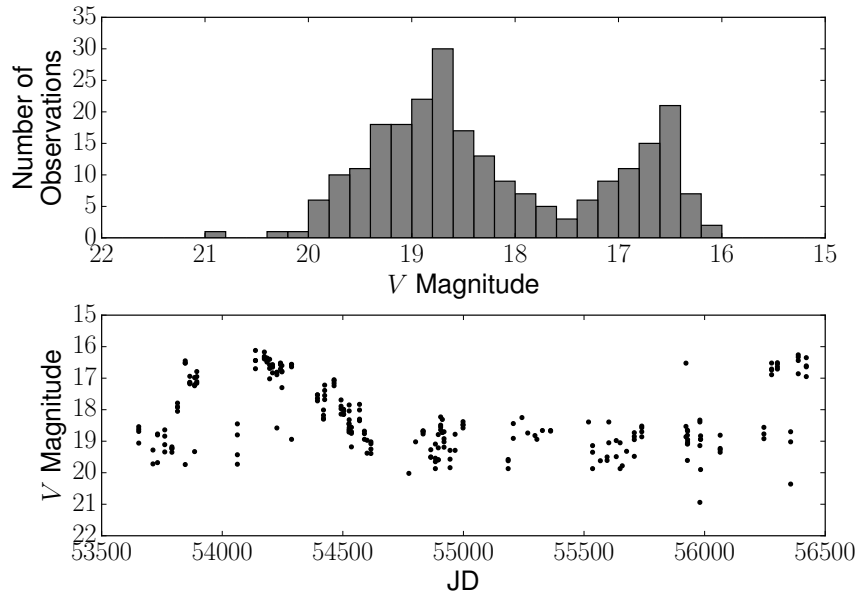


FIGURE 3.4: Example of a light curve that was designated as ‘non-DN’ by the classification script because it shows high-states and low-states in the light curve (see Figure 3.1). Magnetic CVs typically show high-states in their optical light curves.

CRTS light curve may be sampled up to four times per month (see Figure 3.3), and it is therefore insufficient to count every bright point as a separate outburst, as outbursts can last for more than a week. Assuming (temporarily) that the ‘DN’ classification is correct, the apparent quiescent magnitude (v_Q) is set equal to the magnitude of the highest peak of the histogram. Thereafter the script identifies the outbursts. Tracing through the light curve, an outburst ‘starts’ at the first point that is $\Delta V = 1.5$ mag brighter than v_Q and 1.5σ above the scatter. The outburst is then traced until either (1) the lightcurve drops to within 1.5 mag of v_Q , or (2) lasts more than 70 days, or (3) shows a turnover⁴.

With this procedure it is possible to mistake high-states for outbursts, so each potential outburst is tested. If an ‘outburst’ shows any of the following properties, the CV classification is changed to ‘non-DN’. (1) If there is more than 1 turn-over per outburst, or (2) if an outburst lasts more than 100 days, or (3) consists of more than 8 light curve points, or (4) lasts more than 30 days, consists of more than 5 points and shows a scatter of < 0.8 mag, then it is likely a high-state. Figure 3.4 shows an example of a CV that was classified as a ‘DN’ in the initial step, but was flagged as a ‘non-DN’ in this step because high-states were found. Additionally, any CV that shows no outbursts is classified as ‘non-DN’.

Once the classification is complete, the script estimates the outburst properties for every CV classified as a DN. The brightest outburst point is taken as the apparent magnitude in outburst (v_O), and v_Q is set equal to the magnitude of the highest histogram peak. As the CRTS did not necessarily detect the CV at the peak of outburst, v_O should be considered a faint-limit. The duty cycle is estimated as the fraction of time spent in outburst (number of days in outburst divided by the total number of days observed – non-detections included⁵). The shortest time between two outbursts is taken as an upper-limit on the recurrence time, since the CRTS may have missed intervening outbursts due to the sampling cadence⁶.

All the limits and criteria used in the script were defined in order to maximize the number of classifications and avoid misclassifications.

To determine the accuracy and efficiency with which the script classifies DN, we compared the classifications to those in the Catalogue of Cataclysmic Binaries, Low-Mass X-Ray Binaries and Related Objects [Ritter & Kolb, 2003], hereafter referred to as RKCcat. Of the 252 CRTS CVs with RKCcat classifications, 243 had clear ‘DN’ or ‘non-DN’ classifications in RKCcat. For this purpose, ‘DN’ RKCcat classifications include dwarf novae (DN, UG, ZC), SU UMa stars (SU, WZ), ER UMa stars (ER), or systems showing superhumps (NS,SH)⁷. ‘Non-DN’ RKCcat classifications include novalikes (NL, SW, UX, VY), polars (AM, AS) and intermediate polar (IP, DQ)⁸. For

⁴A stage where the light curve shows a decrease, and subsequent increase, in brightness. As the light curve is averaged by day, and not sampled on consecutive days, a turnover is not expected within an outburst. Although some WZ Sge-type DN do show post superoutburst re-brightenings (e.g. Kato et al. 2009; Nakata et al. 2013), few turnovers are expected in the dataset due to the CRTS sampling cadence.

⁵Note that image artifacts and saturation can cause a non-detection.

⁶A comparison of our recurrence time upper-limits to the recurrence-times listed in RKCcat (19 DN in common) indicates that our upper-limit is approximately equal to the true recurrence time if 5 or more outbursts are observed in the light curve.

⁷See <http://www.mpa-garching.mpg.de/RKcat/> for further details on the classifications

⁸In the case that a CV is classified as both ‘DN’ and ‘non-DN’ in RKCcat, for example IP DN, it is given the classification ‘DN’

comparison purposes we assume that the RKCAt classifications are all correct, but there may be DN with very long recurrence times that are misclassified as NL.

Of these 243 common CVs, 209 were classified as ‘DN’ by the classification script and 28 were classified as ‘non-DN’. The accuracy of the ‘DN’ sample is 95.7% (200 out of 209 were also classified as ‘DN’ in RKCAt). The 9 incorrect DN were polars according to RKCAt, and all had large amplitude, short-duration high-states (similar to DN outbursts) in their lightcurves⁹. The efficiency with which the script finds DN is lower, as the accuracy of the ‘non-DN’ classification was only 67.9% (19 of the 28 were correctly classified as ‘non-DN’ according to RKCAt). There are a number of reasons for the lower efficiency. First, the light curve may not be sufficiently well-sampled to catch the outbursts. Second, the quiescent level may be undetectable. In this case, the script will mistake the outburst points for a quiescent level and count zero outbursts. This was the case for the majority of the DN mistaken for non-DN, as they were SU UMa stars with high amplitude outbursts and non-detectable quiescent levels. Currently the CRTS do not provide upper-limits for their non-detections, but in future CRTS data releases we will use the non-detections to correct this bias. Third (as mentioned previously), DN with very high duty cycles can also be mistaken for polars. The efficiency with which the code detects DN could be increased by relaxing the classification conditions, but it would decrease the accuracy. Relaxing the conditions under which a CV is classified as a ‘DN’ would increase the efficiency, but it would also decrease the $\approx 96\%$ accuracy of the ‘DN’ classifications.

3.4 The Outburst Catalogue

The Outburst Catalogue contains outburst properties (duty cycle, apparent V -band magnitudes in quiescence (v_Q) and outburst (v_O), and upper-limits on the recurrence time), system parameters, distance estimates, colour information, and X-ray counterparts where applicable, for 1031 CVs (of which 722 are DN), and 7 known AM CVn¹⁰. This is the largest sample of estimates for these properties, which are seldom available, but often necessary when analysing particular systems or selecting objects for targetted observations/studies.

The data-set used to make this catalogue is the Catalina Surveys Data Release 2 (CSDR2), covering the dates 2005-04-04 to 2013-10-31 (CSS), 2005-06-12 to 2014-01-23 (MLS) and 2005-04-19 to 2013-07-22 (SSS). A histogram of the number of observations per CV in this dataset is shown in Figure 3.5, and as mentioned previously, Figure 3.3 shows the length of the intervals between CRTS observations. Table 3.1 describes the columns in the Outburst Catalogue, which can be accessed online and at the Strasbourg astronomical Data Center¹¹ (CDS).

3.5 Analysis and Discussion

In all subsequent analysis, the 7 known AM CVns have been excluded, as these systems have a different evolutionary path and outburst characteristics to CVs [e.g. Levitan et al., 2015].

⁹The classification for these 9 CVs has been corrected to ‘non-DN’ in the Outburst Catalogue

¹⁰Helium-rich, ultra-compact binary systems.

¹¹<http://cdsarc.u-strasbg.fr/>

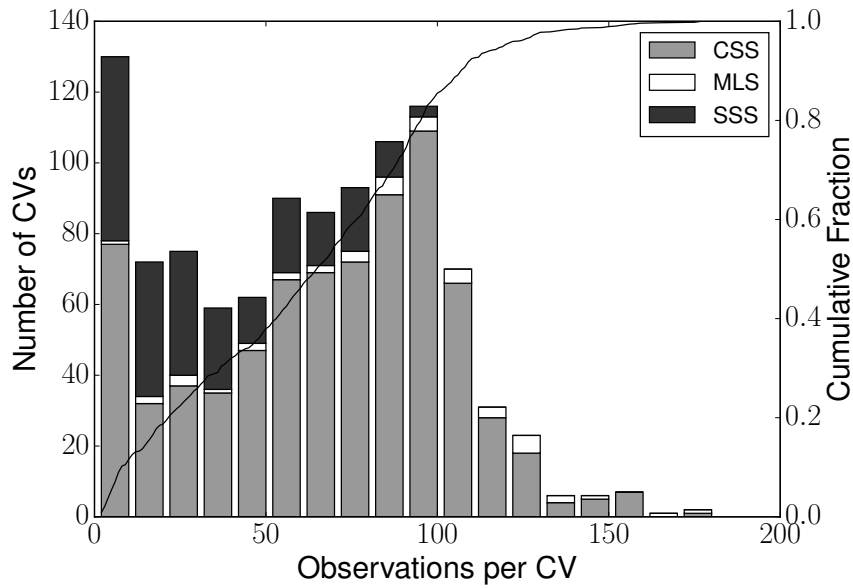


FIGURE 3.5: Distribution showing the number of CRTS observations per CV over the time-range used to make this catalogue, as well as the normalised cumulative distribution. The sampling cadence is uneven, and varies as a function of time and position on-sky. The variation between the sub-surveys is as a result of the different survey lengths and observing strategies (see Drake et al. 2014). Note that CVs with non-unique CRTS identifiers are only plotted once – if a CV is detected in more than one sub-survey it will be plotted under its CSS identifier.

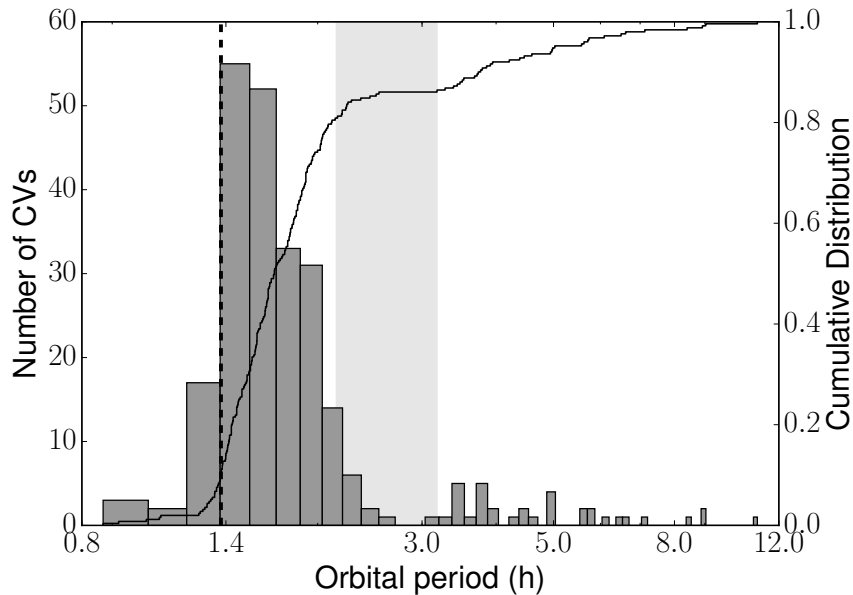


FIGURE 3.6: Orbital period distribution of the CRTS CVs with known P_{orb} in RKCcat [Ritter & Kolb, 2003]. The cumulative distribution is indicated by the solid line, the shaded region indicates the period gap (with boundaries at 2.15 and 3.18 hours, Knigge 2006) and the dotted line indicates the period minimum determined from the SDSS CVs (≈ 82 min, Gänsicke et al. 2009). The nova X Serpentis ($P_{\text{orb}} = 35.52$ d, see Thorstensen & Taylor 2000) has been omitted for clarity.

TABLE 3.1: Contents of the Outburst Catalogue

Column	Column Description	Units	# CVs with entry ^a
1	CRTS ID	–	1031
2	Alternative Names	–	1031
3	RA	deg	1031
4	DEC	deg	1031
5	CRTS sub-surveys	–	1031
6	Classification ^b	–	898
7	RKCat classification ^c	–	252
8	Spectrum ^d	–	242
9	P_{orb}	h	143
10	P_{SH}	h	179
11	P_{orb} from P_{SH}^e	h	109
12	Inclination	deg	17
13	# CRTS Observations	–	1031
14	# CRTS detections	–	1031
15	# Outbursts ^b	–	715 ^f
16	Apparent outburst magnitude faint-limit ^b ($v_{\text{O}}^{\text{lim},f}$)	mag	715 ^f
17	Apparent quiescent magnitude ^b (v_{Q})	mag	614 ^f
18	Recurrence time upper-limit ^b ($t_{\text{recur}}^{\text{lim},u}$)	days	570 ^f
19	Duty Cycle ^b	–	715 ^f
20–24	SDSS u, g, r, i, z	mag	94
25–28	WISE $w1, w2, w3, w4$	mag	332
29–31	2MASS J, H, K	mag	147
32–35	UKIDSS Y, J, H, K	mag	39
36	Distance lower-limit ^g	pc	88
37	Distance upper-limit ^h	pc	206 ^f
38	Bright-limit on absolute quiescent magnitude ⁱ ($V_{\text{Q}}^{\text{lim},b}$)	mag	71
39	Faint-limit on absolute quiescent magnitude ^j ($V_{\text{Q}}^{\text{lim},f}$)	mag	197 ^f
40–41	ROSAT 0.1–2.4 keV count rate and error	counts/s	35
42–44	Chandra 0.5–7 keV flux and upper- and lower-limits	mW/m ²	2
45–46	XMM 0.2–12 keV flux and error	mW/m ²	17

Notes: Catalogue is available online. ^aNumber of CVs with an entry in column (out of 1031 CVs – the 7 known AM CVns are excluded). ^bDetermined by the classification script (CS, Section 3.3). ^cClassifications from RKCat [Ritter & Kolb, 2003]. ^d242 CVs have spectra in Breedt et al. [2014]. ^eEstimated using $P_{\text{orb}} = 0.9162(52)P_{\text{SH}} + 5.39(52)$ (Gänsicke et al. 2009, periods in minutes). ^fOf 722 CVs classified as DN by the CS. ^gThe apparent and absolute magnitudes of the secondary are taken as the WISE (or UKIDSS) K -band value, and estimated from P_{orb} and the donor sequence [Knigge et al., 2011] respectively. This typically underestimates the true distance by a factor 1.75, as the secondary only contributes $\sim 33\%$ of the K -band [Knigge, 2006]. ^hDistance derived from $v_{\text{O}}^{\text{lim},f}$ (column 16), and the absolute magnitude in outburst (V_{O}) from the $P_{\text{orb}}-V_{\text{O}}$ relation [Warner, 1987; Patterson, 2011]. This is multiplied by two for a robust upper-limit (Appendix 3.A). ⁱDerived from column 36 and 17. ^jDerived from column 37 and 17. *Catalogue References:* 9–10, 12: RKCat, Ritter & Kolb [2003]. 20–24: Sloan Digital Sky Survey data release 8 [Aihara et al., 2011]. 25–28: Wide-field Infrared Survey Explorer All-Sky data release [Cutri & et al., 2012]. 29–31: Two Micron All-Sky Survey All-Sky Catalogue of Point Sources [Cutri et al., 2003; Skrutskie et al., 2006]. 32–35: United Kingdom Infra-red Deep Sky Survey data release 10 [Lawrence et al., 2007]. 40–41: Röntgensatellit All-sky survey faint, and bright, source catalogues [Voges et al., 1999, 2000]. 42–44: Chandra Source Catalogue 1.1 [Evans et al., 2010]. 45–46: 3XMM-DR4 catalogue [Watson et al., 2009; Rosen et al., 2015]. Only unique matches within a cone search of radius 1.2'' (SDSS), 3'' (WISE), 2'' (2MASS), 1.2'' (UKIDSS), 10'' (ROSAT), 2'' (Chandra) and 4'' (XMM), were recorded.

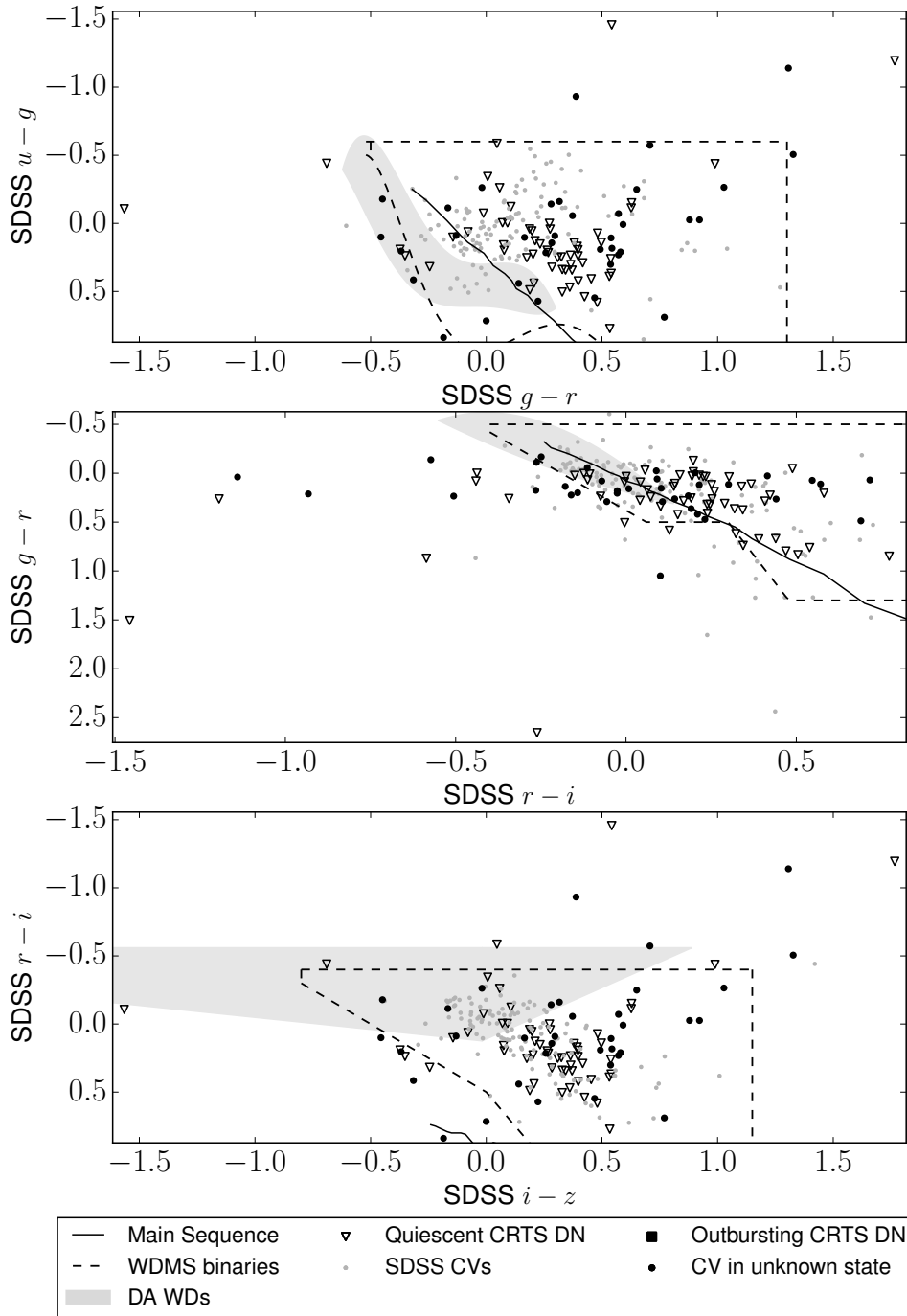


FIGURE 3.7: Colour-colour distributions for the CRTS CVs, using colour information from SDSS DR8 [Aihara et al., 2011]. Where possible, we have distinguished between the colours during outburst and quiescence (see text). Those identified as ‘non-DN’ by our script are labelled as ‘CV in unknown state’. Selection boxes for other classes of objects are shown for reference. SDSS CVs: Colour selected CVs from the SDSS [Gänsicke et al., 2009]. Main Sequence: Star colours from models optimized through comparison to the Praesepe cluster [Kraus & Hillenbrand, 2007]. DA WDs: Observational colour-colour cuts for WDs with Hydrogen-rich atmospheres based on SDSS DR7 [Girven et al., 2011]. WDMS binaries: White Dwarf Main-sequence binaries selected from SDSS DR8 [Rebassa-Mansergas et al., 2013]. Only colours for those CVs with a clean photometry flag in the SDSS were recorded in the catalogue. The extreme outliers are most likely to be as a result of photometric errors.

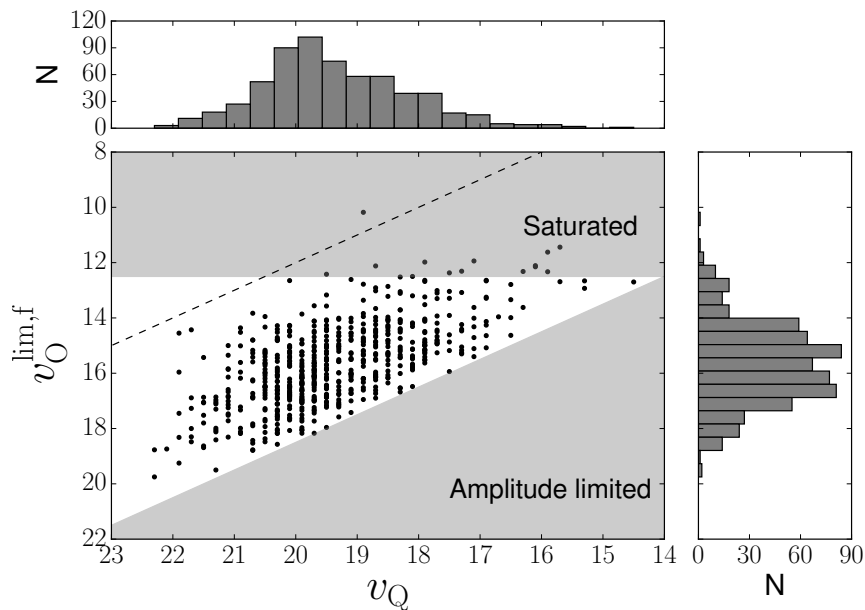


FIGURE 3.8: Distribution of the apparent outburst and quiescent magnitudes, with selection effects indicated. The upper shaded region indicates the range for which the object is saturated in the CRTS image and flagged out as an artifact. Note that the exact saturation level varies according to seeing conditions and sub-survey. The lower shaded region indicates the range where the outburst amplitude is less than 1.5 mag, and hence not considered an outburst by the classification code. The official detection limits for the CRTS are quoted as $V = 21.5$ mag (MLS), $V = 19.5$ mag (CSS) and $V = 19.0$ (SSS), although it is clear from the figure that it can see much deeper when the conditions are good – the faintest detections in the database are at 22.9 (MLS), 23 (CSS) and 22.2 (SSS). The deep co-added reference images for each field are typically at $V = 21.5$ (CSS), $V = 22.5$ (MLS) and $V = 20$ (SSS). An outburst amplitude of $\Delta V = 8$ mag is indicated by the dotted line.

3.5.1 The Orbital Period Distribution

Figure 3.6 shows the orbital period distribution of the CRTS CVs. The sample shows a clear peak that is consistent with the period spike determined from the SDSS CVs (80–86 mins, Gänsicke et al. 2009). There are 14 CVs with orbital periods shorter than 80 mins. According to RKCcat, 5 are WZ Sge-type CVs and the remainder are SU UMa-type CVs. See Breedt et al. [2014] for a detailed discussion of these systems.

The figure also shows that the CRTS is detecting a large population of CVs with P_{orb} below the period gap. This has been noted previously in the literature (e.g. Woudt et al. 2012; Thorstensen & Skinner 2012; Drake et al. 2014). Since it is expected that the short orbital-period systems should dominate the population and that the fraction of DN above the period gap should be smaller (e.g. Knigge et al. 2011), the deeper surveys are now revealing more of the intrinsic population (e.g. Breedt et al. 2014; Gänsicke et al. 2009).

3.5.2 Colour-colour Plots

Colour-colour plots for the CVs with SDSS DR8 photometry are shown in Figure 3.7. Where possible, we have distinguished between DN that were observed in quiescence and DN observed in outburst by the SDSS. Drake et al. [2014] determined that the CRTS V -band and SDSS i -band correspond most closely, with an average difference of -0.01 mag with $\sigma = 0.33$ mag. Consequently we determined a DN to be in outburst if $i \leq v_O$ or $v_Q - i \geq 1.5$ mag, or in quiescence otherwise. Only 1 DN was found to be in outburst at the time of the SDSS observations (CSS080409:174714+150048 had $v_Q - i = 2.5$ mag), but there are likely to be more in outburst, or on the rise to outburst, that do not meet our cautious definition of what constitutes an outburst. There is however, a CRTS bias against detecting DN that were in outburst in the SDSS, as the SDSS magnitude is used as a baseline for determining variability (see Wils et al. 2010). CVs that were not classified as DN are plotted as in an unknown state. The SDSS colour-selected CVs [Gänsicke et al., 2009], and the variability-selected CRTS CVs do have the same locus in the plots, but the CRTS CVs cover a larger range of colours.

3.5.3 Outburst Properties

Out of the 1031 CVs, 722 were classified as DN by the classification code. We now characterise the outburst properties of this sample and discuss the selection effects.

Figure 3.8 shows the distribution of quiescent and outburst apparent magnitudes. The median $v_O^{\text{lim},f} = 15.7$ mag, $v_Q = 19.5$ mag, and $\Delta V = 3.6$ mag which corresponds to an lower-limit for the outburst amplitude of $\Delta V^{\text{lim},l} = 2.8$ mag. The largest DN outburst amplitude is expected to be $\Delta V \approx 8$ mag, but much of the $\Delta V > 8$ mag phase space falls above the CRTS saturation limit. The CRTS and classification script variability criteria also limit the outburst amplitude to $\Delta V \geq 1.5$ mag.

The sample does not show a correlation between $\Delta V^{\text{lim},l}$, and the duty cycle (see Figure 3.9). This is still the case if only the well-sampled DN are considered, so it is unlikely that the scatter is purely a result of the sampling and saturation limit. The CRTS is biased towards detecting the high duty cycle DN – as pointed out by Breedt et al. [2014], they have in fact discovered most of the high duty cycle DN, but are still detecting low duty-cycle DN.

In the lower panel of the figure, there are indications that shorter recurrence times have smaller outburst amplitudes. A Spearman rank-order correlation test on the well-sampled points gives $\rho = 0.26$ and $p = 1.9\%$. This means that the sample shows a weak positive correlation¹² and the probability (p) that the null hypothesis that two uncorrelated datasets would produce this ρ value is 1.9%.

Figure 3.10 shows a correlation between the duty cycle (dc) and $t_{\text{recur}}^{\text{lim},u}$. If only the well-sampled DN are considered, then they related according to

$$\log(dc) = -0.31(\pm 0.04) \log(t_{\text{recur}}^{\text{lim},u}) - 0.58(\pm 0.09), \quad (3.1)$$

and the duty cycle is lower for DN with longer outburst recurrence times (the outburst duration does not increase in proportion to the recurrence time). The Spearman rank-order correlation

¹² $\rho = 1$ (or $\rho = -1$) indicates a perfect monotonic correlation with a positive (or negative) trend.

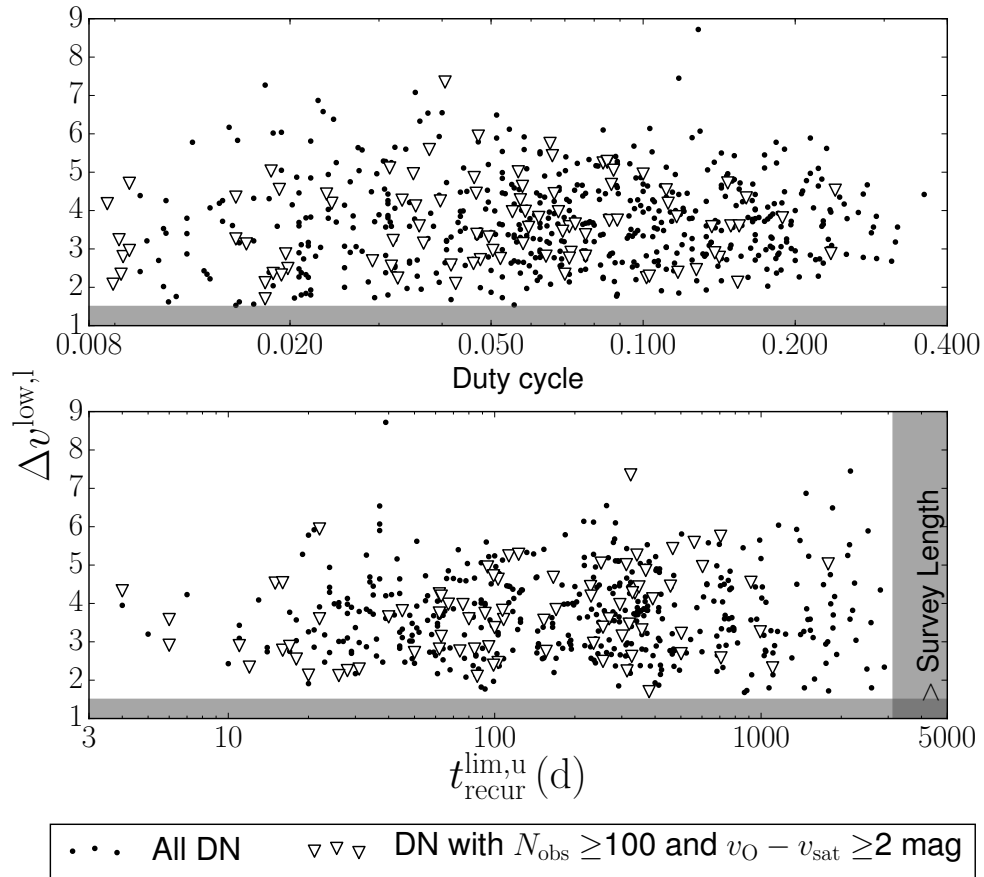


FIGURE 3.9: Distribution of the outburst amplitude lower-limit with duty cycle (top panel), and the upper-limit on the recurrence time (lower panel). The shaded regions indicate where the range exceeds the survey length, and where the outburst amplitude is smaller than 1.5 mag. The well-sampled DN (those with more than 100 CRTS observations that did not have $v_{\text{O}}^{\text{lim},f}$ within 2 mag of the saturation limit) are indicated to show that the observational effects are not masking correlations between the properties. The density fluctuations in the recurrence time limit are as a result of CRTS observing cycles due to seasonal variations.

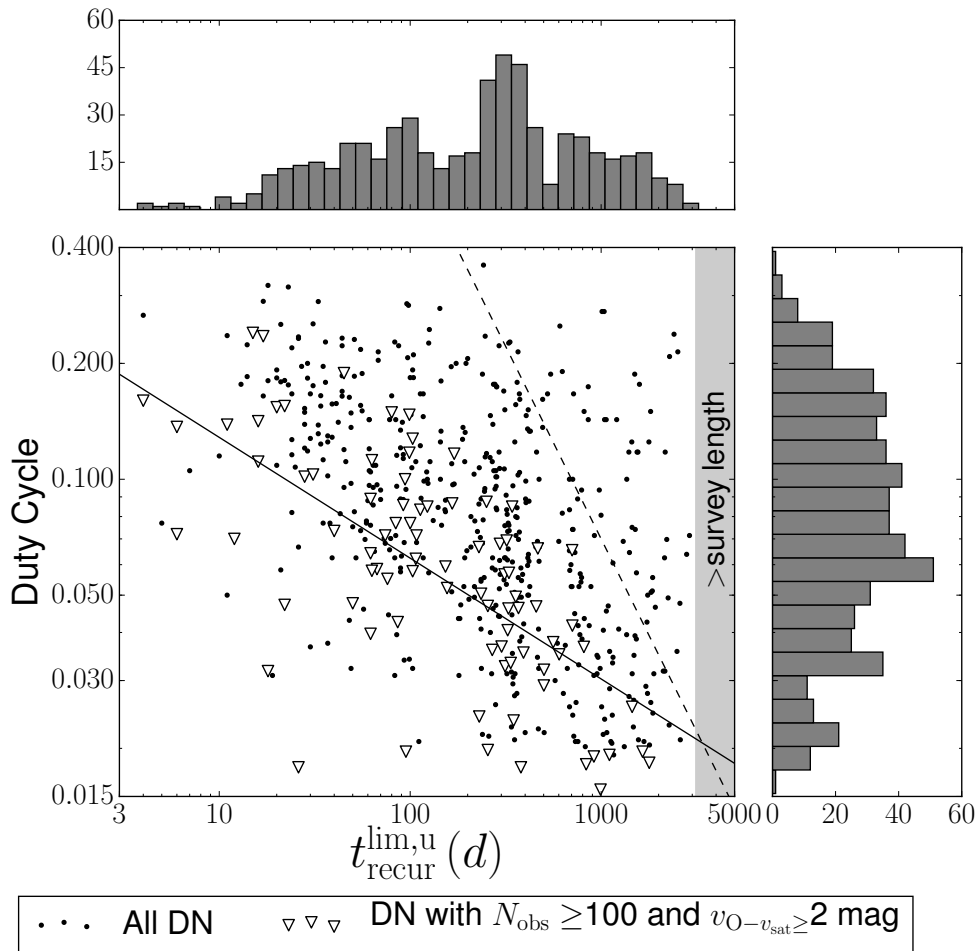


FIGURE 3.10: Distribution of the duty cycle and the upper-limit on the recurrence time, showing a strong correlation between the duty cycle and $t_{\text{recur}}^{\text{lim,u}}$ (solid line). The shaded region indicates the range where the recurrence-time exceeds the survey length. Outbursts are limited to 100 days by the classification script in order to distinguish between high- and low-states. This restriction is indicated by the dashed line. Poor sampling can make the duty cycle appear larger if a large fraction of outburst points are observed.

coefficients are $\rho = -0.6646$ and $p = 5.4 \times 10^{-12}$, so the sample shows a strong negative correlation. Note however, that there is a selection bias against short recurrence-time, low duty cycle DN, due to the CRTS cadence and the ability of the classification script to distinguish between outbursts and high-states.

The median duty cycle and $t_{\text{recur}}^{\text{lim,u}}$ are 5.8% and 138 days respectively for the well-sampled DN. For the overall population the median values are 8% and 250 days. There are, however, several selection effects that influence this distribution. A DN with a high duty cycle is more likely to be detected and classified as a CV by the CRTS as it is highly variable. Only those objects that appear bright with respect to the co-adds are flagged as transients, but a high duty cycle is unlikely to reduce the detection probability – as a DN would need to have an extremely high duty cycle to be in outburst in the CRTS reference image (which is composed of ≈ 20 coadded images). Additionally, the duty cycle would need to exceed 50% to be incorrectly classified by the classification script¹³. In contrast, the classification script introduces a bias against high duty cycles for the poorly sampled light curves. If the quiescent state between outbursts is not observed, separate outbursts can be mistaken for high-states, and the CV classified as ‘non-DN’. The recurrence time limit distribution also shows clear density fluctuations, which are produced by seasonal cycles in the CRTS observations. For example, fewer DN with a recurrence time of a year will be detected, because a fraction of them will have outbursts during the time when they are not observed by the CRTS.

Outburst properties such as the amplitude, recurrence time, and duty cycle depend on the mass-transfer rate and the orbital period (as P_{orb} determines the size of the accretion disc). Figure 3.11 shows the distributions of these properties with P_{orb} . Above the period gap, the angular momentum loss mechanism is magnetic braking, whereas below the gap it is predominantly gravitational radiation (see Knigge et al. 2011). These two regimes consequently have different mass-transfer rates, so we treat them separately. Below the period gap, the duty cycle shows a significant positive trend with P_{orb} (Spearman rank-order correlation coefficients are $\rho = 0.41$ and $p = 4 \times 10^{-8}$). A linear-least squares fit give a relationship of

$$\log(dc) = 1.9(\pm 0.4) \log(P_{\text{orb}}) - 1.63(\pm 0.08), \quad (3.2)$$

where P_{orb} is in hours. Although $t_{\text{recur}}^{\text{lim,u}}$ shows a significant negative trend with P_{orb} (Spearman rank-order correlation coefficients: $\rho = -0.22$ and $p = 0.01$), $\Delta V^{\text{lim,l}}$ does not.

Britt et al. [2015] found a relationship between the duty cycle and X-ray luminosities of DN. Unfortunately, given the uncertainty on our distance estimates, it is not possible to tell if this sample showed the same relationship.

3.5.4 Distance and Absolute Magnitude Estimates

As described in detail in Table 3.1 and Appendix 3.A (but repeated here briefly for clarity), two methods were used to determine distance limits. The upper-limit is derived by multiplying the distance estimate from the $P_{\text{orb}} - V_{\text{max}}$ relation [Warner, 1987; Patterson, 2011] by a factor two, in order to compensate for the lack of known orbital inclinations. The lower-limit is derived using

¹³For a duty cycle exceeding 50%, the majority of the light curve points would be in outburst and consequently the highest histogram peak would be in the brighter half of the magnitude range – see Section 3.3

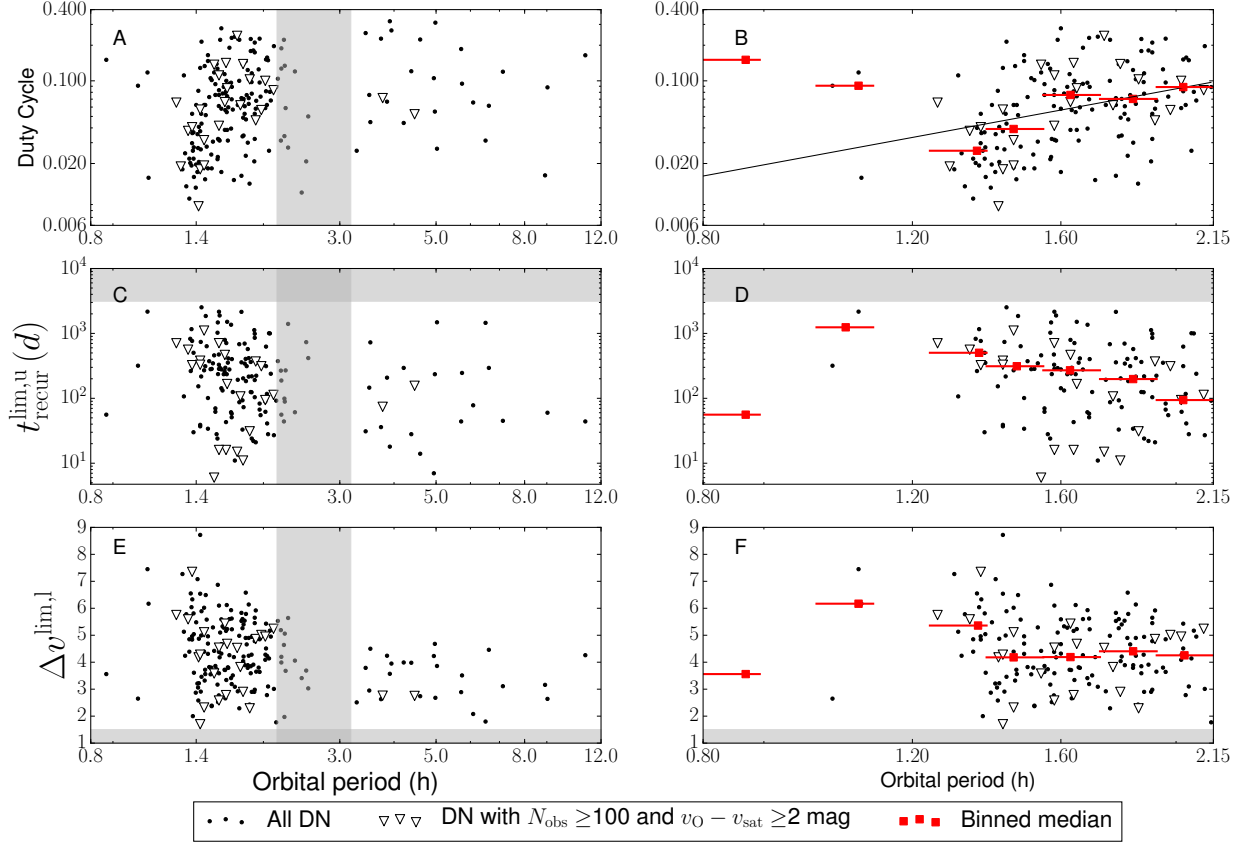


FIGURE 3.11: The dependence of the outburst properties (duty cycle, upper-limit on the recurrence time, and lower-limit on the outburst amplitude) on the orbital period. The panels on the left show the full P_{orb} range, while the panels on the right show the range $P_{\text{orb}} < 2.15$ h. Red squares indicate the median value within a given logarithmic period bin (the size of which is indicated by the error bars), to show the trend. The shaded regions indicate the period gap and survey limits. The nova X Serpentis ($P_{\text{orb}} = 35.52$ d, see Thorstensen & Taylor 2000) has been omitted for clarity.

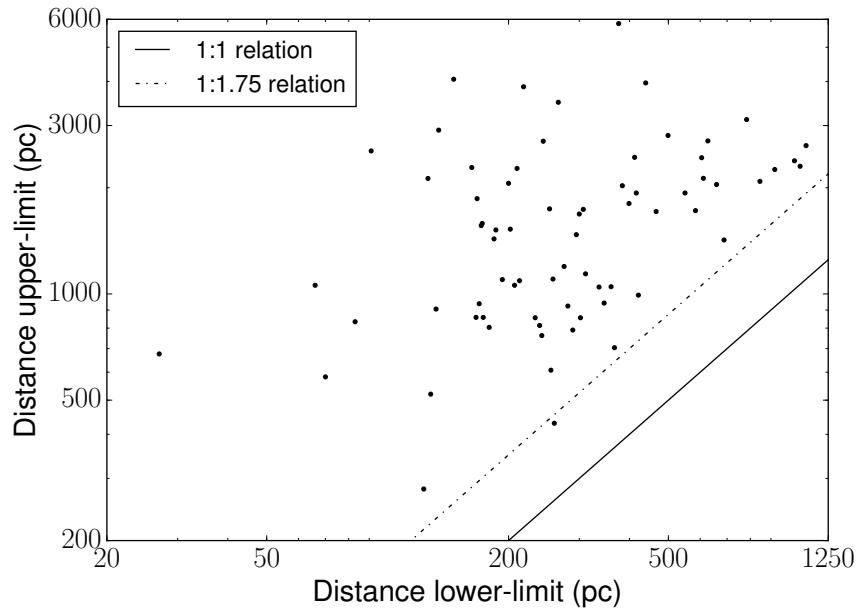


FIGURE 3.12: Distance range for the sample of DN with known orbital periods and K -band magnitudes. The upper-limit is determined using the $P_{\text{orb}}-M_{V_{\text{max}}}$ relation, and the lower-limit is determined using the the 2MASS (or UKIDSS) K -band magnitude – see text for further details. For reference the 1:1, and 1:1.75, line are plotted. Note that the functional form of the relationship between the two distance limits would still be the same if the distance estimates were plotted, as the limits and estimates differ by a constant (see text for details).

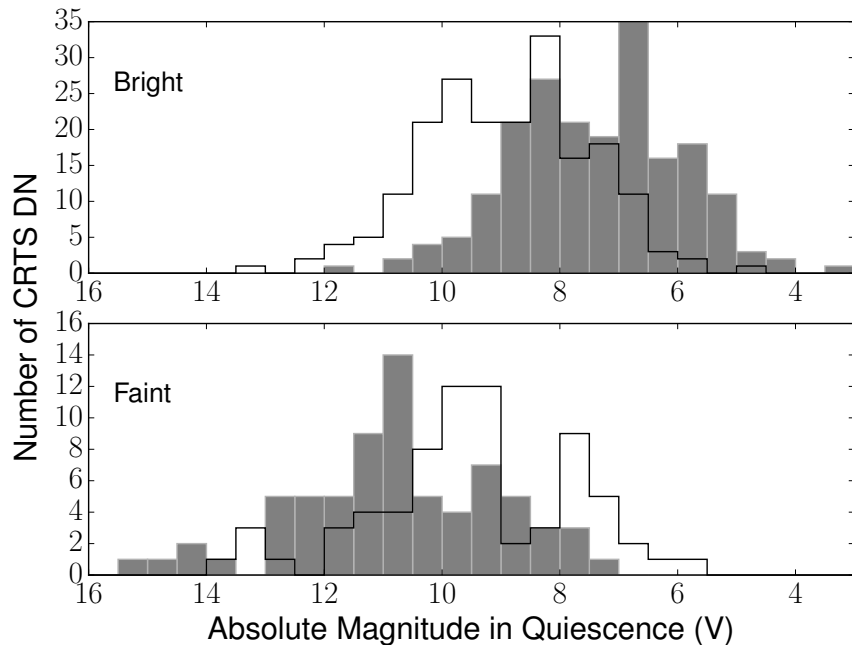


FIGURE 3.13: Distribution of the quiescent absolute magnitudes for the DN with distance limits. Top panel: Bright limit for the quiescent absolute magnitude ($V_Q^{\text{lim},b}$). The solid line gives the equivalent estimate (V_Q^b). Bottom panel: Faint limit for the quiescent absolute magnitude ($V_Q^{\text{lim},f}$). The solid line gives the equivalent estimate (V_Q^f).

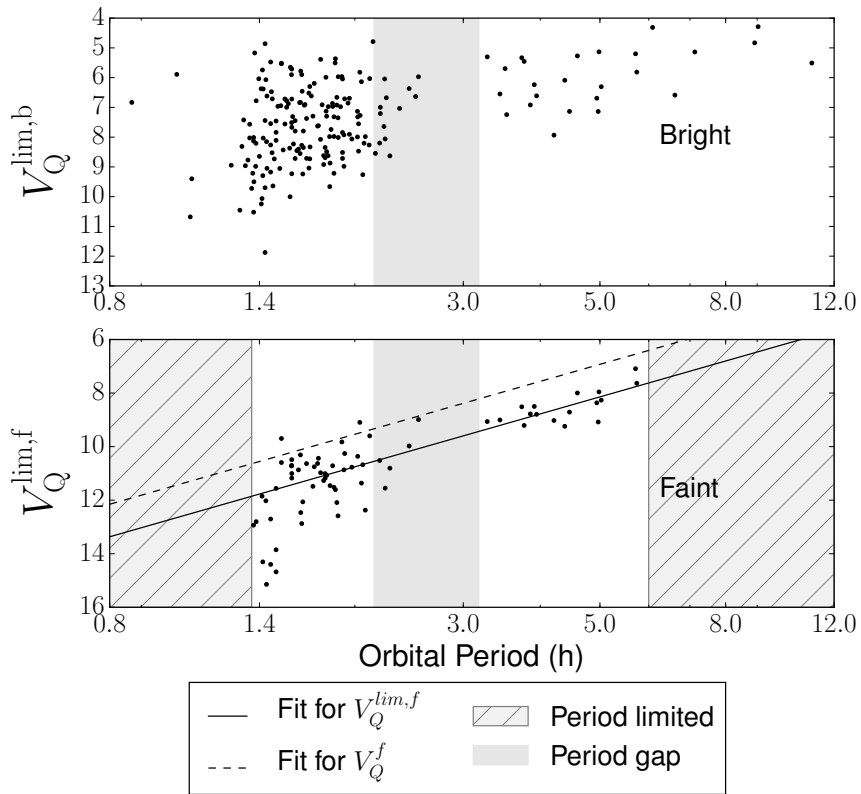


FIGURE 3.14: Variation of the quiescent absolute magnitudes with P_{orb} . See text for a description of the symbols. The period gap is indicated by the gray region in both panels. Top panel: $V_Q^{\text{lim},b}$ is directly derived from P_{orb} , so this is plotted purely for comparison purposes. Bottom panel: The solid and dashed lines indicate the linear-least squares fit to $V_Q^{\text{lim},f}$, and V_Q^f respectively. The range of orbital periods for which this distance determination method is not appropriate is indicated by the hatched region.

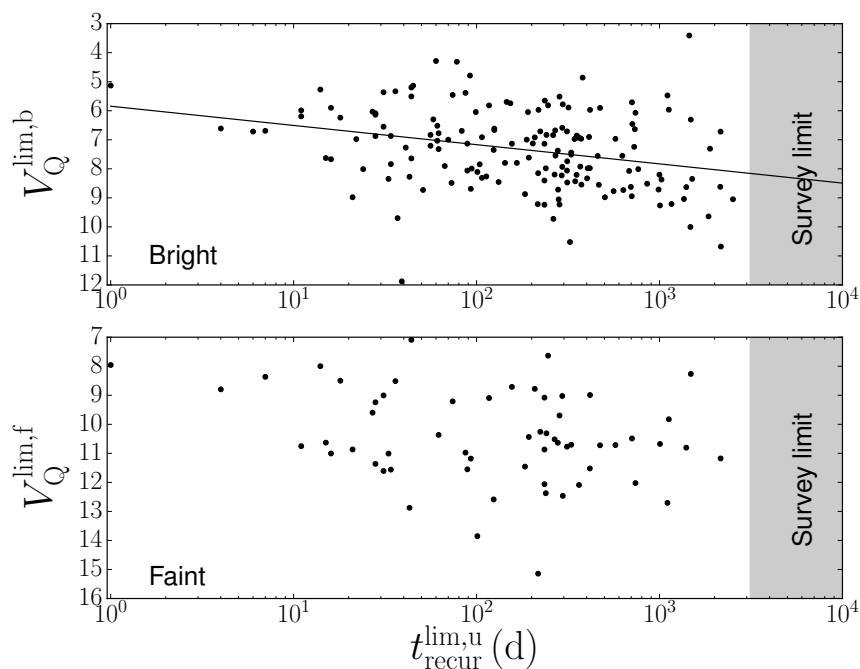


FIGURE 3.15: Distribution of the bright- and faint-limit of the absolute magnitude in quiescence with respect to the upper-limit on the outburst recurrence time. The solid line indicates the linear-least squares fit.

the 2MASS (or UKIDSS) K -band magnitudes and an estimate of the absolute magnitude of the secondary from the donor-sequence from Knigge et al. [2011].

The distance limits for the DN in this sample are shown in Figure 3.12. The maximum distance of this sample appears to be less than 6000 pc. Consider, however, that in order to determine $v_{\text{O}}^{\text{lim},1}$ and hence the distance, v_{Q} needs to be brighter than the CRTS detection limit. This excludes the (fainter) DN that the CRTS detected only in outburst. Additionally, only those DN with distance lower-limits are shown, so the detection limits of 2MASS and UKIDSS are imposed on the plot as well. The CRTS is consequently probing a larger volume of DN than indicated by the distance limits in this catalogue.

Figure 3.12 also shows a scarcity of CVs at short distances (< 500 pc). The distance lower-limit is expected to underestimate the true distance by a factor 1.75, as the K -band magnitude is expected to contribute $\sim 33\%$ of the light (see Table 3.1). Nearby CVs are likely to be bright and saturated in outburst in the CRTS images, and consequently flagged as image artifacts, so the CRTS DN population will not be complete at small distances.

The distribution for the quiescent absolute magnitude (V_{Q}) limits derived from the distance limits and v_{Q} are shown in Figure 3.13 – please see the caption for a description of the V_{Q} symbols. For the bright and faint limits, the median is $V_{\text{Q}}^{\text{lim},b} = 7.3$ mag and $V_{\text{Q}}^{\text{lim},f} = 10.7$ mag respectively. Using the distance estimates (instead of the limits) to calculate V_{Q} , produces median values of $V_{\text{Q}}^b = 8.9$ mag and $V_{\text{Q}}^f = 9.5$ mag respectively, which are in good agreement.

The faintest limits in the distribution ($V_{\text{Q}}^{\text{lim},f} \gtrsim 14$) are not physical, as the temperature of the WD would imply a cooling time approaching the Hubble time. As the only quantity determined from the light curves for this estimate is v_{Q} , poor sampling cannot explain this discrepancy. It

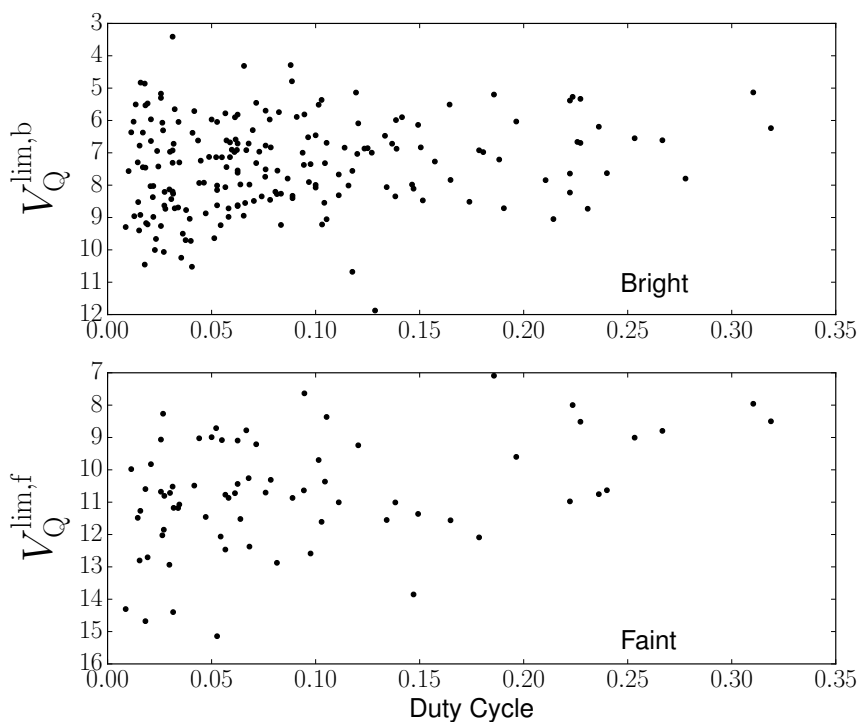


FIGURE 3.16: Distribution of the bright- and faint-limit of the absolute magnitude in quiescence as a function of the duty cycle.

is likely that the distances for these CVs were underestimated by more than the standard 1.75 expected from this method, which would imply that the donors may contribute less than 30% of the light even in K -band. All four of the DN with $V_Q^{\text{lim},f} \gtrsim 14$, have short orbital periods (in the range 1.41–1.49 h), but are classified as SU UMa type CVs in RKCcat, so it is unlikely that these are extremely evolved, ultra-faint donor stars.

Figure 3.14 shows a dependence of $V_Q^{\text{lim},f}$ on P_{orb} of the form

$$V_Q^{\text{lim},f} = -6.6(\pm 0.5) \times \log(P_{\text{orb}}) + 12.7(\pm 0.2), \quad (3.3)$$

where P_{orb} is in hours. If the estimate V_Q^f is considered instead, the relationship is

$$V_Q^f = -6.6(\pm 0.5) \times \log(P_{\text{orb}}) + 12.7(\pm 0.2). \quad (3.4)$$

In both cases, the unphysical points for which $V_Q^{\text{lim},f} \gtrsim 14$ have been excluded from the fit. $V_Q^{\text{lim},b}$ was calculated using P_{orb} so it will show a dependence on P_{orb} – the trend, however, is in the same direction as that of V_Q^f . The quiescent absolute magnitude is thus fainter at shorter orbital periods.

In Figure 3.15, $V_Q^{\text{lim},b}$ shows a correlation (Spearman rank-order correlation coefficients are $\rho = 0.32$ and $p = 4.9 \times 10^{-5}$) with $t_{\text{recur}}^{\text{lim},u}$ of the form

$$V_Q^{\text{lim},b} = 0.64(\pm 0.17) \log(t_{\text{recur}}^{\text{lim},u}) + 5.89(\pm 0.38), \quad (3.5)$$

indicating that the systems with longer recurrence times are generally fainter. There were two DN with recurrence times of one day. In both cases the large scatter in the quiescent magnitude

led the classification script to erroneously split one outburst into two, so these are artifacts. $V_Q^{\text{lim},f}$ does not show a significant trend with $t_{\text{recur}}^{\text{lim},u}$.

Figure 3.16 shows that the limits for the quiescent absolute magnitude were correlated with the duty cycle. The Spearman rank-order correlation coefficients are $\rho = -0.32$ and $p = 0.0066$ for the faint-limit $V_Q^{\text{lim},f}$. The significance of the correlation for the bright-limit $V_Q^{\text{lim},b}$ is lower, as the coefficients are $\rho = -0.16$ and $p = 0.022$. As the estimates for the quiescent absolute magnitude differ from the limits by a constant factor (of less than 2), the functional form of the relation will be the same. This indicates that the quiescent absolute magnitude shows a marginal (but statistically significant) dependence on the duty cycle, with larger duty cycles producing a brighter quiescent state.

3.6 Conclusion

The Outburst Catalogue provides apparent outburst and quiescent V magnitudes, duty cycles, limits on the recurrence time, upper- and lower-limits on the distance and absolute quiescent magnitudes, colour information, orbital parameters, and X-ray counterparts where applicable for 722 dwarf novae (DN) and 309 other types of Cataclysmic Variable (CV), based on the Catalina Real-time Transient Survey (CRTS) ~ 9 year light curves. These properties were determined by means of a classification script, presented in this paper. This is the largest sample of DN with estimates for these properties to date.

Using the Outburst Catalogue we have found correlations between the duty cycle and the orbital period, as well as the outburst recurrence time. The quiescent absolute magnitude shows a correlation with the orbital period, and with the duty cycle. We also show the range, and distribution, of the outburst properties and distances in the CRTS dwarf nova population. In a subsequent paper we will address the issue of completeness, and estimate the space density.

Acknowledgements

Thank you to the referee, Michael Shara. The authors acknowledge funding from the Nederlandse Organisatie voor Wetenschappelijk Onderzoek and the Erasmus Mundus Programme SAPIENT. This paper uses data from the Catalina Sky Survey and Catalina Real Time Survey; the CSS is funded by the National Aeronautics and Space Administration under Grant No. NNG05GF22G issued through the Science Mission Directorate Near-Earth Objects Observations Program. The CRTS survey is supported by the U.S. National Science Foundation under grants AST-0909182.

This research has made use of NASA's Astrophysics Data System Bibliographic Services, as well as the SIMBAD database, operated at CDS, Strasbourg, France [Wenger et al., 2000].

Funding for SDSS-III has been provided by the Alfred P. Sloan Foundation, the Participating Institutions, the National Science Foundation, and the U.S. Department of Energy Office of Science. The SDSS-III web site is <http://www.sdss3.org/>. SDSS-III is managed by the Astrophysical Research Consortium for the Participating Institutions of the SDSS-III Collaboration including the University of Arizona, the Brazilian Participation Group, Brookhaven National Laboratory,

University of Cambridge, Carnegie Mellon University, University of Florida, the French Participation Group, the German Participation Group, Harvard University, the Instituto de Astrofísica de Canarias, the Michigan State/Notre Dame/JINA Participation Group, Johns Hopkins University, Lawrence Berkeley National Laboratory, Max Planck Institute for Astrophysics, Max Planck Institute for Extraterrestrial Physics, New Mexico State University, New York University, Ohio State University, Pennsylvania State University, University of Portsmouth, Princeton University, the Spanish Participation Group, University of Tokyo, University of Utah, Vanderbilt University, University of Virginia, University of Washington, and Yale University.

This publication makes use of data products from the Wide-field Infrared Survey Explorer, which is a joint project of the University of California, Los Angeles, and the Jet Propulsion Laboratory/California Institute of Technology, funded by the National Aeronautics and Space Administration. We have made use of the ROSAT Data Archive of the Max-Planck-Institut für extraterrestrische Physik (MPE) at Garching, Germany. Data products from the Two Micron All Sky Survey, which is a joint project of the University of Massachusetts and the Infrared Processing and Analysis Center/California Institute of Technology, funded by the National Aeronautics and Space Administration and the National Science Foundation are used. We have also made use of data products obtained with XMM-Newton, an ESA science mission with instruments and contributions directly funded by ESA Member States and NASA. This work is based in part on data obtained as part of the UKIRT Infrared Deep Sky Survey. This research has also used data obtained from the Chandra Source Catalog, provided by the Chandra X-ray Center (CXC) as part of the Chandra Data Archive.

3.A Determining the Distance Upper-limit (Column 33)

Empirically, the absolute magnitude of a DN in outburst (V_O) is related to the orbital period (P_{orb}) by

$$V_O = 5.70 - 0.287P_{\text{orb}},$$

where P_{orb} is in hours [Warner, 1987; Patterson, 2011]. This equation assumes a +0.8 mag correction to superoutbursts - larger amplitude outbursts that occur in a subclass of DN (the SU UMa stars) and have an additional source of emission possibly (believed to be from tidal heating, see Patterson [2011] for a discussion). As Patterson points out, it is not clear whether this correction is appropriate.

As the sampling of the CRTS data is not sufficient to differentiate outbursts and superoutbursts, we use the form of this equation that does not assume a correction for superoutbursts [Patterson, 2011],

$$V_O = 4.95 - 0.199P_{\text{orb}}. \quad (3.6)$$

The binary inclination (i) affects the observed V_O , so to adjust for this, the correction for a flat, limb-darkened accretion disc from Paczynski & Schwarzenberg-Czerny [1980] is applied:

$$\Delta V_i = -2.5 \log\left(\left(1 + \frac{3}{2} \times \cos i\right) \times \cos i\right). \quad (3.7)$$

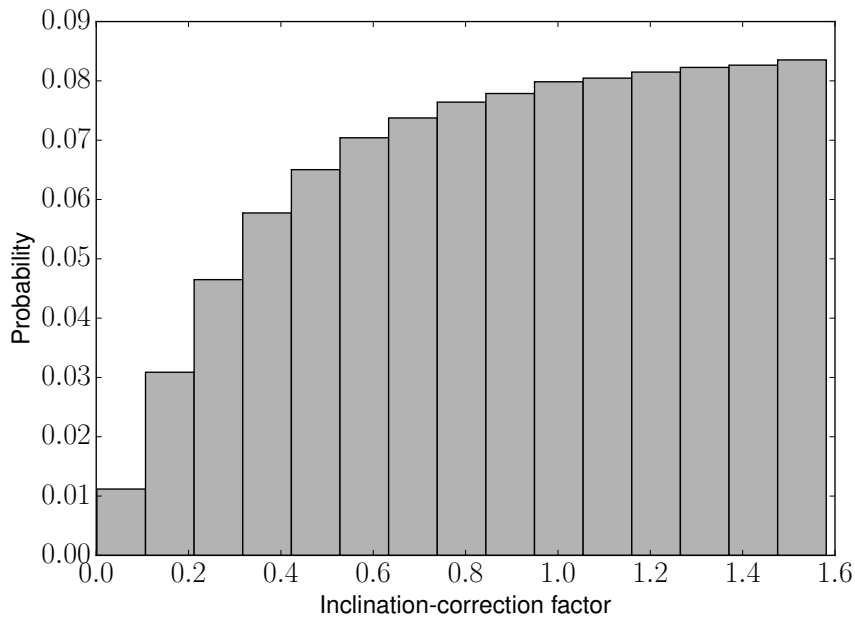


FIGURE 3.17: Probability that the estimated distance to a DN would need to be multiplied by a given inclination-correction factor to derive the true distance if an inclination of 56.7° is assumed. The distance can be over- or under-estimated, but will always be less than a factor 1.58 times further, if only inclination effects are considered.

Using the distance modulus, an estimate for the distance (d , in parsec) can thus be determined from P_{orb} and the apparent magnitude in outburst v_{O} via

$$d = 10^{(v_{\text{O}} - V_{\text{O}} + 5)/5} \times 10^{-\Delta V_i/5}, \quad (3.8)$$

where the last term is the inclination-correction factor. As it is difficult to determine the inclination angle of a CV (e.g. Littlefair et al. 2008), few have i estimates. Consequently we assume $i = 56.7^\circ$ (the average inclination) in cases where it is unknown.

We now discuss the uncertainties introduced by i , v_{O} and V_{O} to the distance estimate.

3.A.1 Inclination

Equation 3.7 shows that the correction to V_{O} is highly sensitive on i . By assuming $i = 56.7^\circ$, we have set the inclination-correction factor equal to one. Taking a uniform distribution of $\cos i$, Figure 3.17 shows that the true inclination-correction factor is in the range 0 to 1.58. Consequently the true distance is a factor 0 to 1.58 times the estimated distance.

The probability distribution is slightly skewed towards a closer distance than estimated, as there is a 55% probability of an inclination-correction factor of less than 1. However, the probability decreases rapidly to smaller factors. Equation 3.7 also becomes increasingly less reliable at large inclination angles (smaller inclination-correction factors), as the correction is for a flat disc and subsequently assumes an infinitely thin emission region at $i = 90^\circ$. At the high end, the distance can be underestimated by up to a factor 1.58 due to inclination effects.

3.A.2 Absolute Outburst Magnitude (V_O)

Equation 3.6 was determined empirically and has a rms of 0.41 mag [Patterson, 2011]. The uncertainty on P_{orb} is negligible, as it is typically known to an accuracy on the order of a few minutes or less. As mentioned previously, it is not clear if superoutbursts should have an additional correction to V_O and regardless, it is not possible to distinguish them from DN outbursts in the CRTS data. Equation 3.6 does not assume a correction and hence is appropriate.

3.A.3 Quiescent Outburst Magnitude (v_O)

$v_O^{\text{lim,f}}$ is a lower-limit (faint-limit) for the outburst maximum v_O , as the CRTS did not necessarily catch the DN at the peak of outburst. Outburst profiles and amplitudes vary between CVs and between outbursts of a single system, however the peak of outburst is typically a plateau phase that constitutes the most of the outburst. There is thus a large chance that it is detected at the peak, and this chance increases as more outbursts are sampled. As DN outbursts do not follow a standard template, it is not possible to estimate the uncertainty caused by assuming that v_O is the outburst maximum. However, since it is a faint-limit, the true distance will be closer than estimated.

Extinction will likewise make the estimate appear further than the true distance, as we cannot correct for it. As the CRTS does not observe within the galactic plane, it is not expected to produce a large uncertainty (in comparison to the inclination uncertainty).

3.A.4 Upper-limit Determination

The distance estimate derived in this manner should only be used as a rough estimate. Based on these arguments, however, it is possible to make a more robust estimate for the upper-limit. The uncertainty on v_O produces an under-estimate of the distance, and the inclination and uncertainty on V_O give upper-limits for the true distance. Substituting the maximum inclination-factor of 1.58, and $V_O = V_O + 0.41$ (the rms of Equation 3.6 is 0.41) into Equation 3.8 indicates that the true distance can be up to a factor 2 larger than estimated. An estimate for the upper-limit is thus be obtained by multiplying the distance estimate by a factor 2.

NOVALIKE CATAclySMIC VARIABLES ARE SIGNIFICANT RADIO EMITTERS

Deanne L. Coppejans, Elmar G. K rding, James C. A. Miller-Jones, Michael P. Rupen,
Christian Knigge, Gregory R. Sivakoff and Paul J. Groot

MNRAS 451, 3801–3813 (2015)

Abstract

Radio emission from non-magnetic cataclysmic variables (CVs, accreting white dwarfs) could allow detailed studies of outflows and possibly accretion flows in these nearby, numerous and non-relativistic compact accretors. Up to now, however, very few CVs have been detected in the radio.

We have conducted a VLA pilot survey of four close and optically-bright novalike CVs at 6 GHz, detecting three, and thereby doubling the number of radio detections of these systems. RW Sex, V603 Aql and the old nova TT Ari were detected in both of the epochs, while V1084 Her was not detected (to a 3σ upper-limit of $7.8 \mu\text{Jy beam}^{-1}$). These observations clearly show that the sensitivity of previous surveys was typically too low to detect these objects and that non-magnetic CVs can indeed be significant radio emitters.

The three detected sources show a range of properties, including flaring and variability on both short (~ 200 s) and longer-term (days) time-scales, as well as circular polarization levels of up to 100%. The spectral indices range from steep to inverted; TT Ari shows a spectral turnover at ~ 6.5 GHz, while the spectral index of V603 Aql flattened from $\alpha = 0.54 \pm 0.05$ to 0.16 ± 0.08 ($F_\nu \propto \nu^\alpha$) in the week between observations. This range of properties suggests that more than one emission process can be responsible for the radio emission in non-magnetic CVs. In this sample we find that individual systems are consistent with optically thick synchrotron emission, gyrosynchrotron emission or cyclotron maser emission.

4.1 Introduction

Radio emission is found, at least intermittently, from nearly all kinds of accreting objects. The most prominent radio emitters in the Universe are radio-loud Active Galactic Nuclei (AGN) - accreting supermassive black holes. AGN produce tightly collimated jets that are responsible for the majority of their radio emission. Accreting stellar mass black holes, the X-ray binaries (XRB), also show radio emission during particular stages of the outburst cycle [Fender, 2001; Fender et al., 2004]. The same holds true for neutron star XRBs [Migliari & Fender, 2006].

Scaling relations connecting different classes of black holes have been found [Merloni et al., 2003; Falcke et al., 2004]. This suggests that accretion and its associated phenomena can – at least to a first order approximation – be scaled from one source class to the other, and notably to accreting white dwarfs (WDs) [Körding et al., 2006, 2007; Körding, 2008]. As WDs are nearby, numerous and non-relativistic they are ideal laboratories for accretion studies in compact objects (see e.g. de Martino et al. 2015).

Cataclysmic variable stars (CVs) are the nearest examples of accreting compact objects. These binary star systems comprise a white dwarf that accretes matter from a red dwarf secondary star via Roche-lobe overflow (see Warner 1995). CVs are broadly classified according to their magnetic field strength (B) into the magnetic systems, namely polars ($B \gtrsim 10^7$ G) and intermediate polars ($10^6 \lesssim B \lesssim 10^7$ G), and non-magnetic systems ($B \lesssim 10^6$ G). The WDs in the non-magnetic systems accrete directly via an accretion disc onto the surface of the WD, but in the intermediate polars (IPs) the disc is truncated at the Alfvén radius and material is accreted onto the WD via magnetic field lines. In polars the Alfvén radius is large enough that no disc is formed and matter is fed directly onto the WD’s magnetic field lines.

The non-magnetic CVs are further divided into subclasses based on their long-term photometric behaviour. The accretion discs in some CVs undergo a thermal-viscous instability, which switches the disc between a low, faint state and a bright, hot state (Smak 1971; Osaki 1974; Höshi 1979). The bright states are known as dwarf nova outbursts and are 2–8 mag brighter at optical wavelengths than in the quiescent state. Similar outbursts are seen in X-ray binaries and the same mechanism is believed to be responsible [Lasota, 2001]. The dwarf nova outbursts typically last for a few days and recur on timescales of weeks to years. CVs that show such outbursts are known as dwarf novae (DN). Systems with a mass-transfer rate from the secondary that is high enough to maintain the accretion disc in a constant hot state are known as (non-magnetic) novalikes. Note that polars and intermediate polars are also sometimes referred to jointly as magnetic novalike systems.

CVs are well known for their variable optical, ultraviolet and X-ray emission, but their radio emission is less well studied. A few studies were performed in the 1980s, but their detection rates were low and the detections were unpredictable. Only three non-magnetic CVs (SU UMa, EM Cyg and TY Psc) were detected at radio wavelengths [Benz et al., 1983; Benz & Guedel, 1989; Turner, 1985]. Subsequent re-observations of the same sources with better sensitivities were usually not successful (typically 0.1 mJy upper-limits) and simply added to the large number of non-detections [Benz et al., 1983; Cordova et al., 1983; Fuerst et al., 1986; Echevarria, 1987; Nelson & Spencer, 1988].

Similarly, very few of the magnetic CVs have been detected at radio wavelengths, and of those

detected, only AM Her, AR UMa and AE Aqr are persistent radio emitters (see Mason & Gray 2007). The radio emission from the detected polars and intermediate polars (AM Her, V834 Cen, ST LMi, AR UMa, AE Aqr, DQ Her and BG CMi) was highly variable and often showed flares (e.g. Abada-Simon et al. 1993; Wright et al. 1988; Pavelin et al. 1994; Mason & Gray 2007). AM Her in particular, showed strong flares and even variable circular polarization that peaked at 100% during a 9.7 mJy flare [Dulk et al., 1983; Channugam, 1987]. The emission mechanism is not known, but in individual sources it has been suggested to be non-thermal emission from gyrosynchrotron or cyclotron maser radiation (e.g. Mason & Gray 2007; Meintjes & Venter 2005).

The lack of radio detections had implications for both CV studies and accretion theory. As radio emission is often taken as a tracer for jets, it was accepted that CVs do not launch jets, and this was used to constrain jet launching models [Livio, 1999; Soker & Lasota, 2004]. CVs would thus be the only accreting compact objects to not launch jets, as jets have been found in other compact accreting binaries, including those containing WDs (super soft sources, symbiotics and novae).

After a long hiatus in radio observations of non-magnetic CVs, K rding et al. [2008] and Miller-Jones et al. [2011] obtained radio light-curves during outbursts of the prototypical dwarf nova SS Cyg. It showed a bright radio flare (> 1 mJy) at the start of the outburst, followed by weaker radio emission (0.3-0.1 mJy) during the plateau phase of the optical outburst. This pattern was observed in multiple outbursts and a direct measurement of the distance to SS Cyg was determined using the radio parallax method [Miller-Jones et al., 2013]. In light of these detections, one can understand the earlier non-detections. Given the comparatively low sensitivity of radio telescopes at the time, the earlier observations needed to catch the flare by chance, as the plateau emission would have been undetectable. This may have been the case with EM Cyg [Benz & Guedel, 1989].

Besides this first secure detection of an outbursting (DN-type) CV, a nonmagnetic novalike CV has also been detected. K rding et al. [2011] detected the novalike V3885 Sgr at 6 GHz (C-Band) at a flux density of 0.16 mJy (distance of 110 ± 30 pc; Hartley et al. 2002). This flux is consistent with that of SS Cyg during the outburst plateau phase (0.15 to 0.5 mJy at 8.5 GHz), which given the similar distance (114 pc; Miller-Jones et al. 2013) implies a similar radio luminosity.

To establish the emission mechanism (or mechanisms) of the radio emission observed in non-magnetic CVs, one needs a larger sample of radio-detected CVs - particularly at higher sensitivity. In this paper we present the results of a pilot survey of 4 additional novalike cataclysmic variables conducted with the upgraded Very Large Array (VLA).

In Section 4.2 we present our targets. The VLA observations and data reduction are described in Section 4.3. In Section 4.4 we present the results and discuss them in Section 4.5.

4.2 Targets

We selected the four nearest and brightest novalike CVs from the Ritter & Kolb [2003] catalogue that are observable with the Karl G. Jansky Very Large Array (VLA). Preferentially we targeted non-magnetic novalikes, but also included SW Sex type novalikes, whose peculiar properties have been suggested to be associated with dynamically significant magnetic fields associated with their WDs.

TABLE 4.1: Properties of the target novalikes

Name	RA (J2000)	Dec. (J2000)	V-mag ^d	Distance (pc) ^e
RW Sex	10:19:56.62309±0.00201 ^a	-08:41:56.0867±0.00156	~10.7	150±37 ^{i,h,m}
V1084 Her	16:43:45.70±0.07 ^b	+34:02:39.7±0.06	~12.4	305±137 ^{j,h,m}
TT Ari	02:06:53.084±0.02 ^c	+15:17:41.81±0.026	~10.7	335±50 ^{g,k}
V603 Aql	18:48:54.63615±0.00223 ^a	+00:35:02.865±0.00182	~12	249+9-8 ^{f,l}

Notes: Optical coordinates retrieved via Simbad, from ^avan Leeuwen [2007], ^bCutri et al. [2003] and ^cHøg et al. [2000]. ^dV-mag at the time of the VLA observations, estimated from long-term AAVSO lightcurves. ^eFor each system, we adopted the best available distance estimate. These estimates were based on ^fthe observed parallax, ^gthe direct detection of the primary/secondary, ^hthe absolute infrared magnitude or the H α equivalent width, in that order. Distances from ⁱBeuermann et al. [1992], ^jAk et al. [2008], ^kGänsicke et al. [1999] and ^lHarrison et al. [2013]. ^mAs distance errors were not quoted for RW Sex and V1084 Her, we have made conservative error estimates based on the distance determination methods used (45% and 25% respectively).

The targets are RW Sex, V1084 Her, TT Ari and V603 Aql. Their V-band magnitudes and best distance estimates are given in Table 4.1. Each source is described briefly below so that the source properties can be compared with the radio observations in Section 4.4.

RW Sex

RW Sextantis (RW Sex) is an extremely bright novalike, as it has an apparent magnitude of $m_V \sim 10.6$ mag¹ in the V-band and absolute magnitude of $M_V = 4.8$ mag [Beuermann et al., 1992]. Beuermann et al. determined it to have an orbital period of 0.24507 ± 0.00020 d, an inclination of 28° to 40° and a mass ratio of $q = \frac{M_2}{M_1} = 0.74 \pm 0.05$ (where M_1 and M_2 are respectively the mass of the WD and secondary star). RW Sex is known to have a fast disc wind (up to 4500 km s⁻¹; e.g. Prinja & Rosen 1995; Prinja et al. 2003). Estimates for the mass-transfer rate from the secondary (\dot{M}_2) range between $10^{-9} M_\odot \text{ yr}^{-1}$ and $10^{-8} M_\odot \text{ yr}^{-1}$ [Linnell et al., 2010; Vitello & Shlosman, 1993; Greenstein & Oke, 1982].

Cordova et al. [1983] observed RW Sex in the radio with the VLA at 4885 MHz and a bandwidth of 50 MHz. This yielded a non-detection with an upper-limit of 0.15 mJy. No further radio observations were taken until now.

V1084 Her

V1084 Herculis (V1084 Her; RX J1643.7+3402) is a bright ($m_V \sim 12.6$), low-inclination novalike with an orbital period of 0.12056 ± 0.00001 d [Mickaelian et al., 2002; Patterson et al., 2002]. It is at a distance of ~ 305 pc [Ak et al., 2008] and is classified as a SW Sex type novalike [Mickaelian et al., 2002; Patterson et al., 2002].

There are a number of properties that define the SW Sex class, but the dominant characteristic is that the emission lines are single-peaked, despite the (mostly) high-inclination accretion discs – see Rodríguez-Gil et al. [2007] for an overview. Individual members of this class have shown evidence for having magnetic white dwarf primaries (e.g. Rodríguez-Gil et al. 2009, 2001;

¹according to the long-term AAVSO light curve

Rodríguez-Gil & Martínez-Pais 2002; Baskill et al. 2005), but it is not clear that this is the case for every SW Sex star (e.g. Dhillon et al. 2013). V1084 Her is not classified as an intermediate polar, but it has been argued that the WD in V1084 Her is magnetic [Rodríguez-Gil et al., 2009]. This is based on their discovery of modulated optical circular polarization at a period of 19.38 ± 0.39 min and emission line flaring at twice this polarimetric period.

V1084 Her has not been observed at radio wavelengths prior to this study.

TT Arietis

TT Arietis (TT Ari) has been observed and studied routinely since its discovery [Strohmeier et al., 1957]. It has an inclination of roughly 30° [Cowley et al., 1975], an orbital period of $0.13755040 \pm 0.00000017$ d [Wu et al., 2002], a 39,000 K WD and a M3.5 type secondary star [Gänssicke et al., 1999]. A rough estimate for the mass-accretion rate (\dot{M}_1) is $2.8\text{--}26.7 \times 10^{-8} M_\odot \text{ yr}^{-1}$ [Retter & Naylor, 2000] and far-ultraviolet observations indicate the presence of a fast and variable disc wind [Prinja & Rosen, 1995; Hutchings & Cowley, 2007].

Due to its long-term behaviour in the optical², TT Ari is classified as a VY Sculptoris (VY Scl) type novalike (see Shafter et al. 1985), as it spends most of the time in a high-state ($m_V \sim 12\text{--}14$ mag), but shows occasional low states ($m_V > 19$ mag) lasting a few hundred days.

Previously it was argued that TT Ari is an intermediate polar. First, it shows a high X-ray luminosity and variability [Robinson & Cordova, 1994]. Second, the photometric period – which differed from the spectroscopic period (Tremko et al. 1992 and Robinson & Cordova 1994) – was incorrectly taken as the spin period of the WD. It was subsequently shown that the photometric period was produced by a negative superhump (e.g. Vogt et al. 2013) and that the X-ray properties of TT Ari fit well into the properties of non-magnetic CVs [van Teeseling et al., 1996], thereby establishing TT Ari as a non-magnetic system.

Although TT Ari has been well studied at optical, X-ray and UV wavelengths, only one observation was taken in the radio. Cordova et al. [1983] observed it during an optical low-state with the VLA at 4885 MHz (50 MHz bandwidth), but did not detect it. The upper-limit they obtained was 0.44 mJy. No further radio observations were taken of it until now.

V603 Aql

V603 Aql is Nova Aquilae 1918 – the brightest nova eruption (thermo-nuclear runaway on the surface of the white dwarf) of the 20th century. The eruption began on June 4, 1918, peaked 6 days later at $m_V = -0.5$ mag and was back at pre-nova brightness ($m_B = 11.43 \pm 0.03$ mag) by February 1937 [Strope et al., 2010; Johnson et al., 2014a]. Since the eruption, it has been fading by 0.44 ± 0.04 mag century⁻¹ [Johnson et al., 2014a]; novae have been predicted to fade after outburst, as the outburst should widen the binary and consequently pause mass transfer (see e.g. Shara et al. 1986 and Patterson et al. 2013). By June 1982 only a very faint shell was still visible [Haefner & Metz, 1985].

The system parameters include an orbital period of 0.1385 ± 0.0002 d, inclination of $13^\circ \pm 2^\circ$, white dwarf mass $M_1 = 1.2 \pm 0.2 M_\odot$ and mass ratio $q = 0.24 \pm 0.05$ [Arenas et al., 2000]. It shows a

²See the AAVSO light curve at <http://www.aavso.org/data/lcg>

TABLE 4.2: Observing log

Name	Obs. No.	Date and Start Time (UT)	Integration Time (s)	Bandpass, Flux and Polarization Angle calibrator	Amplitude and Phase Calibrator	Polarization Leakage Calibrator
RW Sex	1	13/03/2014 08:17:09.0	2268	3C286	J0943-0819	J1407+2827
	2	15/03/2014 07:57:21.0	2264	3C286	J0943-0819	J1407+2827
V1084 Her	1	22/03/2014 07:40:37.0	2364	3C286	J1635+3808	J1407+2827
	2	31/03/2014 14:20:34	2126	3C286	J1635+3808	J1407+2827
TT Ari	1	02/04/2014 00:08:24	2138	3C48	J0203+1134	J0319+4130
	2	02/04/2014 18:56:25.0	2304	3C48	J0203+1134	J0319+4130
V603 Aql	1	07/04/2014 13:52:33.0	2144	3C48	J1851+0035	J2355+4950
	2	14/04/2014 14:09:57.0	2144	3C48	J1851+0035	J2355+4950

Observations were taken at 4226–8096 MHz (in C-band) with 4096 MHz of bandwidth (3-bit mode), in the VLA A-configuration.

time-variable wind and the mass accretion rate is estimated to be $\sim \dot{M}_1 = 9.2\text{--}94.7 \times 10^{-9} M_\odot \text{ yr}^{-1}$ [Retter & Naylor, 2000; Prinja et al., 2000].

As in the case of TT Ari, it was argued that V603 Aql could be an intermediate polar. This stemmed from detections of X-ray periodicities, linear and circular polarization and a differing photometric and spectroscopic period (e.g. Haefner & Metz 1985; Gnedin et al. 1990; Udalski & Schwarzenberg-Czerny 1989). Since then it has been confirmed that the photometric period is the permanent superhump period and that it shows no coherent sub-orbital period oscillations – thereby establishing V603 Aql as a non-magnetic CV [Patterson & Richman, 1991; Patterson et al., 1993; Naylor et al., 1996; Patterson et al., 1997; Borczyk et al., 2003; Andronov et al., 2005; Mukai & Orio, 2005]. Furthermore, Mukai & Orio [2005] state that V603 Aql does not show a strong energy dependence in X-ray variability, unlike what is seen in IPs.

No radio observations have been taken of V603 Aql prior to this study.

4.3 Observations

Two separate 1-hour observations with the VLA were taken of each target, both to look for variability and to facilitate easier scheduling. The log of the observations is given in Table 4.2.

The observations were taken in the most extended A-configuration (baselines ranging from 0.68 to 36 km) at 4 – 8 GHz (C-band), with 4 GHz bandwidth (3-bit samplers) for the highest

TABLE 4.3: Results

Name, Obs.	Beam Size ^a	PA ^b	RA Offset ^c	DEC Offset ^c	Peak Flux ^d	RMS ^d	CP ^d	LP ^d
RW Sex, 1	0.58'' × 0.33''	39°	0.016±0.02	0.26±0.02	33.6	3.7	<13.8	<7.2
RW Sex, 2	0.56'' × 0.33''	36°	0.018±0.02	0.18±0.03	26.8	3.3	<12.9	<8.4
V1084 Her, 1	0.43'' × 0.31''	-71°	-	-	<10.2	3.4	-	-
V1084 Her, 2	0.44'' × 0.32''	80°	-	-	<11.4	3.8	-	-
TT Ari, 1	0.67'' × 0.30''	64°	0.015±0.03	0.33±0.02	39.6	4.2	27.4±4.2	<8.1
TT Ari, 2	0.33'' × 0.30''	0°	0.013±0.003	0.300±0.004	239.1	5.5	22.8±4.8	<9.6
V603 Aql, 1	0.40'' × 0.38''	31°	0.010±0.003	0.095±0.003	178.2	4.3	<12.9	<8.7
V603 Aql, 2	0.46'' × 0.33''	33°	0.010±0.003	0.085±0.004	190.5	3.9	<12.0	<8.1

^aMajor and minor axis of the synthesized beam. ^bPosition angle of the beam. ^cOffset (in arcsec) from the optical position given in Table 4.1. ^dUnits are $\mu\text{Jy beam}^{-1}$. All detections were consistent with point sources. Upper-limits are quoted as 3σ .

sensitivity. This decision was based on the steep spectrum (spectral index of -0.7) of the only novalike for which the spectral index in the radio was known, namely V3885 Sgr [Körding et al., 2011]. The frequency tuning of the receivers was shifted to 4226–8096 MHz in order to avoid RFI from the Clarke belt. The 4 GHz bandwidth was split into two basebands, 4226–6246 MHz and 6176–8096 MHz, each of which was divided into 16 spectral windows comprising 64 channels. The observations were taken in standard phase referencing mode, where the phase calibrator was observed for 1 minute every 8 minutes.

The data were reduced with the VLA calibration pipeline v1.2.0 and the polarization calibration was performed in CASA³ v4.2.0 following standard procedures. The absolute flux density scale was set via observations of a standard flux calibrator source (3C286 or 3C48; see Table 2), using the Perley-Butler 2010 coefficients within CASA. No self-calibration was performed. For the imaging, two Taylor terms were used to model the frequency dependence, and Briggs weighting with robust parameter 1 was chosen to suppress bright source sidelobes and improve the resolution. Fitting was performed in the image plane using imfit task within CASA, and the RMS noise level for each image was calculated in the vicinity of the target.

4.4 Results

4.4.1 Total fluxes

Three out of the four systems were detected with $\geq 8\sigma$ significance – a 75% detection rate. RW Sex, TT Ari and V603 Aql were detected in both their observations, while V1084 Her was detected in neither. None of the sources were resolved (see Fig. 4.7) and their measured radio positions are consistent with the optical positions. These results are summarized in Table 4.3.

³Common Astronomy Software Applications package [McMullin et al., 2007]

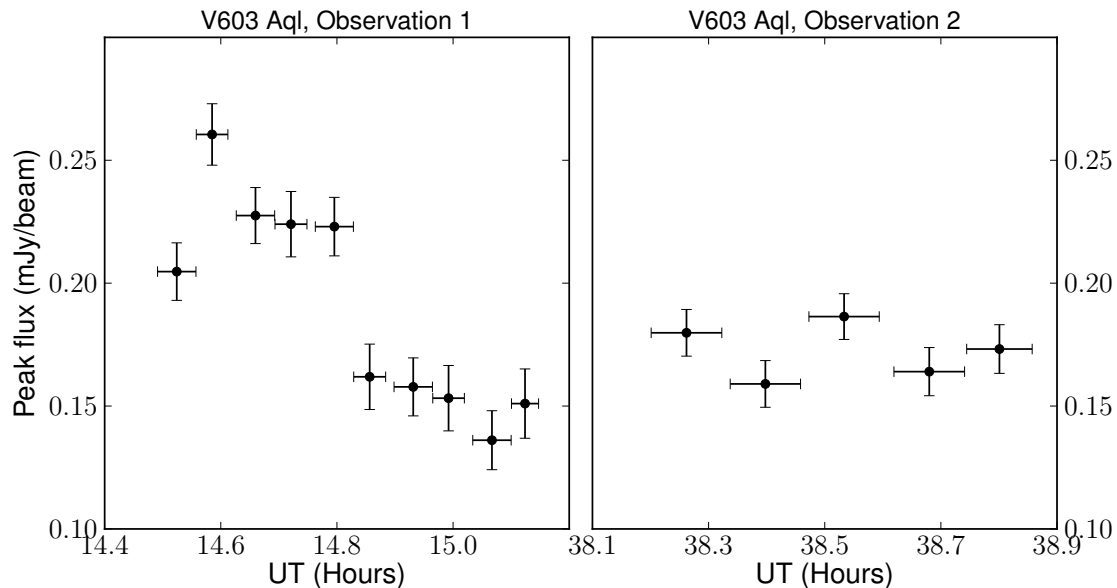


FIGURE 4.1: Total intensity (Stokes I) light curve for observations 1 and 2 of V603 Aql. There is clear variability in observation 1, but no such variability in observation 2. Error bars on the x-axis show the integration time for each point.

4.4.2 Polarization

We also imaged the target fields in all four Stokes parameters (I, Q, U and V) to determine the source polarization. TT Ari was the only source where circular polarization was measured and none of the sources were linearly polarized. Both observations of TT Ari showed circular polarization (CP, see Table 4.3 and Figure 4.8). The fractional polarization in observation 1 was 70%, whereas in observation 2 it was $\sim 10\%$. This difference in fractional polarizations was due to a large increase in unpolarized flux between the observations, as the polarized fluxes for the two observations were similar (at 27.4 ± 4.2 and $22.8 \pm 4.8 \mu\text{Jy beam}^{-1}$).

As the VLA has circular feeds, it is possible to produce instrumental CP, extrinsic to the source. We therefore ran a number of checks to test if this was the case. None of the other sources in the field show CP (the closest source is less than 2 arcsec from TT Ari and the brightest source is $58 \mu\text{Jy beam}^{-1}$). Neither the flux nor the gain calibrator show CP above 0.3% of the total intensity. Imaging the field with half of the antennas yields the same level of polarization as for the other half, so it is unlikely to be an antenna calibration problem. Similarly, when the two basebands are imaged separately they both show CP, so it is not a single-baseband effect. In the observational setup, the targets were offset 5 arcsec from the phase center to avoid correlator artifacts at the phase centre. Finally, both observations of TT Ari show circular polarization and none of the other novalikes (which were all observed with the same setup) showed CP. We therefore conclude that the CP is likely to be intrinsic to TT Ari and not an instrumental or calibration artifact.

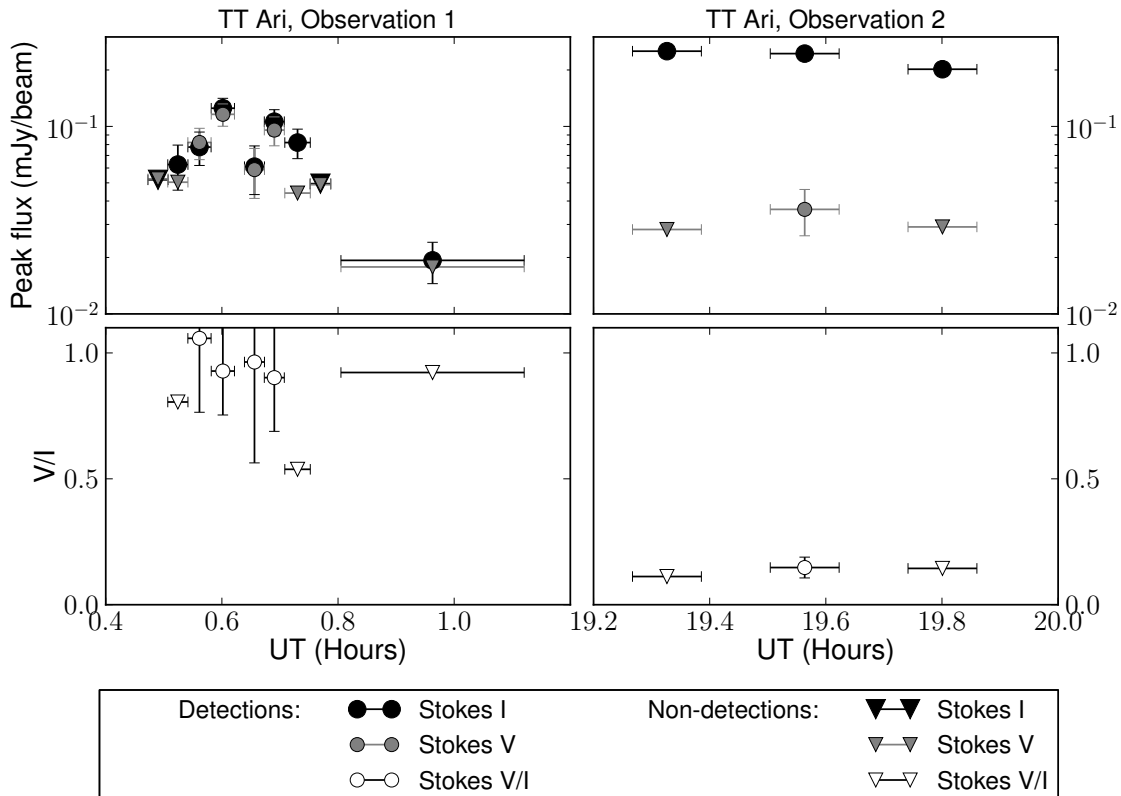


FIGURE 4.2: Total intensity (Stokes I) and circular polarization (Stokes V) light curves for observations 1 and 2 of TT Ari. The strong flare in Observation 1 of TT Ari is consistent with 100% circular polarization. 1-Sigma error bars are shown for the peak flux; they are too small to be seen in observation 2. The error bars on the x-axis give the integration time for each point.

4.4.3 Variability

TT Ari and V603 Aql were both variable on a timescale of minutes.

The total intensity light curve for V603 Aql is given in Figure 4.1. It peaked at $260.5 \pm 12.5 \mu\text{Jy beam}^{-1}$ during the first half of observation 1, but then dropped to approximately $170 \mu\text{Jy beam}^{-1}$ for the second half. We could detect variability on time-scales down to 217 s. In the second observation, V603 Aql was not variable.

In the 19 hours between observations 1 and 2 of TT Ari, its flux increased by a factor of 6 (39.6 ± 4.2 to $239.1 \pm 5.5 \mu\text{Jy beam}^{-1}$). Splitting the observations up in time (see Figure 4.2) shows that the variability is actually on shorter timescales (detected down to 144 s), and most of the flux from observation 1 was detected during a ~ 10 -min period. All the circularly polarized emission arose from a ~ 8 min flare during this time and the fractional polarization reached up to 100%. The flux dropped to $19.3 \pm 4.8 \mu\text{Jy beam}^{-1}$ in the second half of the observation.

Observation 2 was also variable (Figure 4.2), but at a higher total flux (201.8 ± 9.8 – $251.9 \pm 9.4 \mu\text{Jy beam}^{-1}$) and a lower CP fraction ($\leq 15\%$). As mentioned previously, the polarized flux for the two observations was similar (see Table 4.3 and Figure 4.8).

TABLE 4.4: Spectral indices

Object	Observation	Stokes	Spectral Index ($F=\nu^\alpha$)	Red. χ^2	Band (MHz)	Peak Flux ($\mu\text{Jy beam}^{-1}$)	RMS ($\mu\text{Jy beam}^{-1}$)
RW Sex	1 and 2 ^a	I	-0.5±0.7	-	4226–6274	36.2	5.4
					6176–8224	30.5	4.6
TT Ari	1	I	1.7±0.8	-	4226–6274	28.6	6.2
					6176–8224	49	5.8
TT Ari	1, during flare ^b	I	1.6±0.1	0.05	4226–5250	59.7	16.4
					5250–6274	74.0	19.2
					6176–7200	95.0	16.3
					7200–8224	123.0	11.3
TT Ari	1, during flare ^b	V	1.31±0.06	0.01	4226–5250	56.7	16.0
					5250–6274	73.3	18.7
					6176–7200	85.9	16.3
					7200–8224	106.9	11.1
TT Ari	2	I	0.7±0.3	4.9	4226–5250	173.4	10.5
					5250–6274	240.2	12.0
					6176–7200	264.9	11.8
					7200–8224	258.0	11.2
V603 Aql	1	I	0.54±0.05	0.15	4226–5250	152.7	7.7
					5250–6274	173.5	8.7
					6176–7200	189.6	9.5
					7200–8224	199.1	7.2
V603 Aql	2	I	0.16±0.08	0.2	4226–6274	178.9	8.9
					5250–6274	192.4	10.7
					6176–7200	189.0	15.0
					7200–8224	193.0	14.7

Notes: The spectral indices were obtained by fitting a power law to the measurements in different frequency sub-bands. ^aObservation 1 and 2 were combined to reduce the uncertainty in the spectral index. ^bIn the time range 00:32:30–00:42:28, during which CP was detected in the flare. The errors used in the fit were the RMS values.

Since the other sources in the field (in both cases) were not variable, we conclude this variability is intrinsic to TT Ari and V603 Aql.

The flux density of the first and second observation of RW Sex were consistent, but we checked for shorter time-scale variability by splitting the two observations into four epochs (each ~ 20 minutes long) and imaging each separately. As the flux densities were consistent in all four epochs, we conclude the RW Sex is not variable.

V1084 Her was not detected in either observation, but if it showed only a minor, short-duration flare (similar to TT Ari), this would not be detectable when integrated over the whole observation. In order to test if this was the case, we imaged the first and second halves of the two observations separately. We found no detections down to 3σ upper-limits of $\sim 17.5 \mu\text{Jy beam}^{-1}$ on ~ 20 minute timescales.

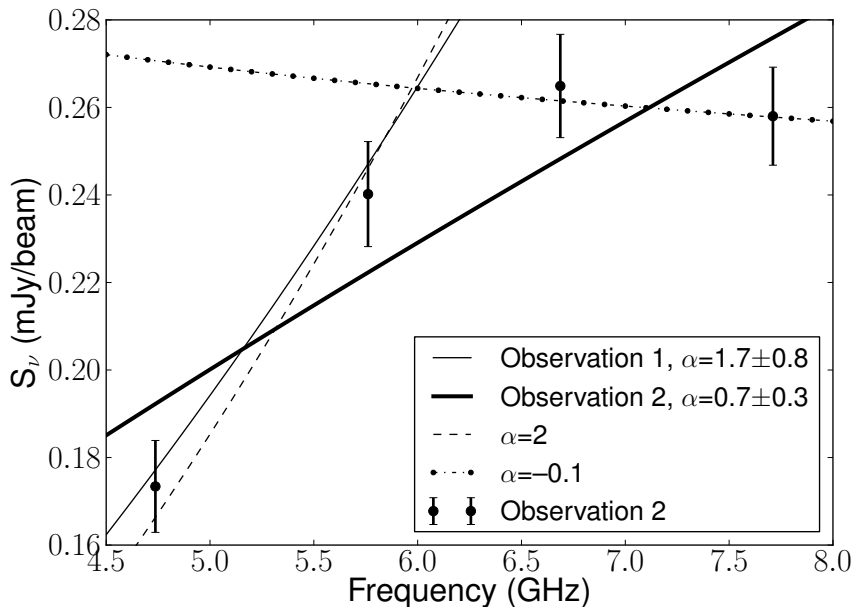


FIGURE 4.3: Spectrum of the second observation of TT Ari. The spectrum cannot be fitted with a single spectral index. The spectral index from the first observation, $\alpha=2$ and $\alpha=-0.1$ are shown for comparison.

4.4.4 Spectral Indices

The observations showed a spread of spectral indices (Table 4.4), from -0.5 ± 0.7 to 1.7 ± 0.8 .

As the total flux in the first observation of TT Ari was dominated by the ~ 10 minute flare, it is not surprising that the spectral index taken during the flare ($\alpha = 1.6 \pm 0.1$) is consistent with that taken over the whole of the observation. Unfortunately there was insufficient signal-to-noise to determine the spectral index after the flare. The circular polarization (which was only detected during the flare) had $\alpha = 1.31 \pm 0.06$. The second, brighter observation was not fitted well with a single power law, but rather showed a spectral turnover – this is plotted in Figure 4.3.

The spectrum of V603 Aql flattened from $\alpha = 0.54 \pm 0.05$ in the first observation to 0.16 ± 0.08 in the second (fainter) observation.

4.5 Discussion

Historically, non-magnetic CVs have not been considered to be significant radio emitters. This stems from the low detection rates in previous surveys. In the 1980s, more than 50 radio observations of non-magnetic CVs were taken and, as summed up by Benz et al. [1996], only two were detected, and only twice each. In contrast, we have obtained a 75% detection rate in this survey – strongly indicating that many novalikes are indeed significant radio emitters and that with modern radio telescopes we have the sensitivity required to detect them.

All the observations of non-magnetic CVs conducted since 2008 are plotted in Fig. 4.4. The radio fluxes are below the ~ 0.1 mJy detection limits of previous radio surveys.

There are not enough detections to test if there is a correlation between the radio flux and distance, as expected for a sample of uniform luminosity. Consequently, and due to the large

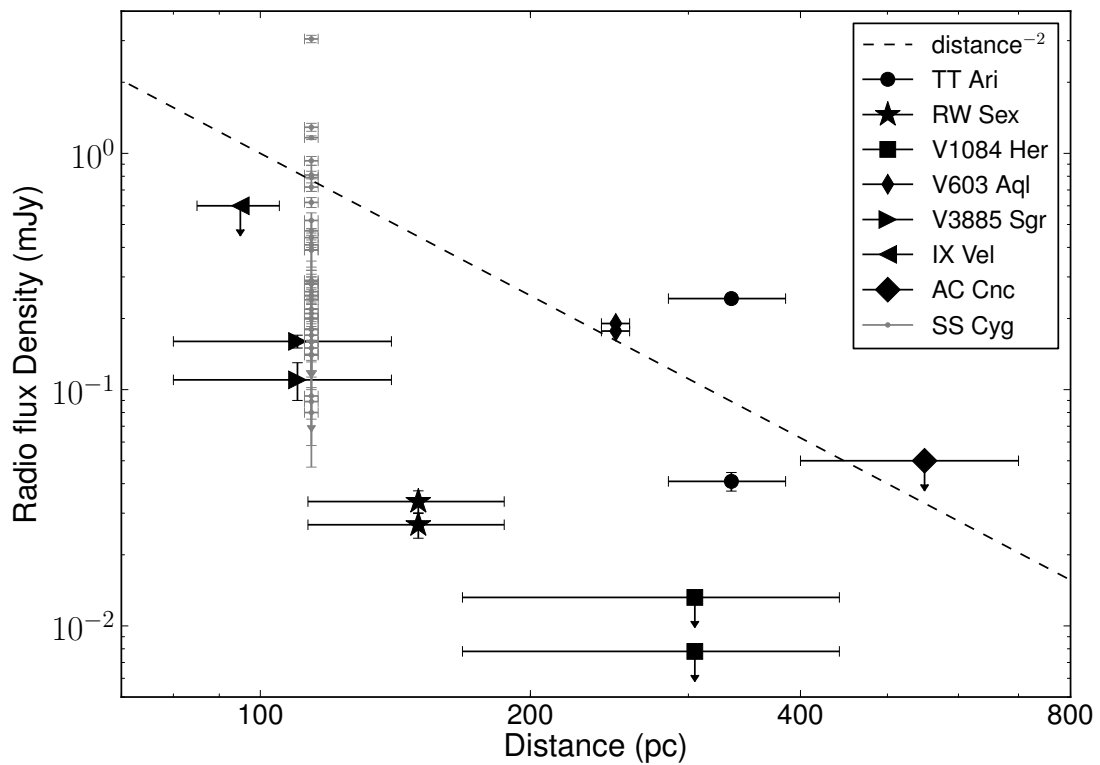


FIGURE 4.4: Radio flux density of all high-sensitivity observations of non-magnetic CVs, taken since 2008, as a function of distance (this work, K rding et al. 2008, 2011; Miller-Jones et al. 2011, 2013). The dotted line shows the expected trend ($1/d^2$) for sources with equal luminosities. Errors are calculated via standard error propagation techniques. Observations taken of the dwarf nova SS Cyg at various stages of outburst are plotted for comparison.

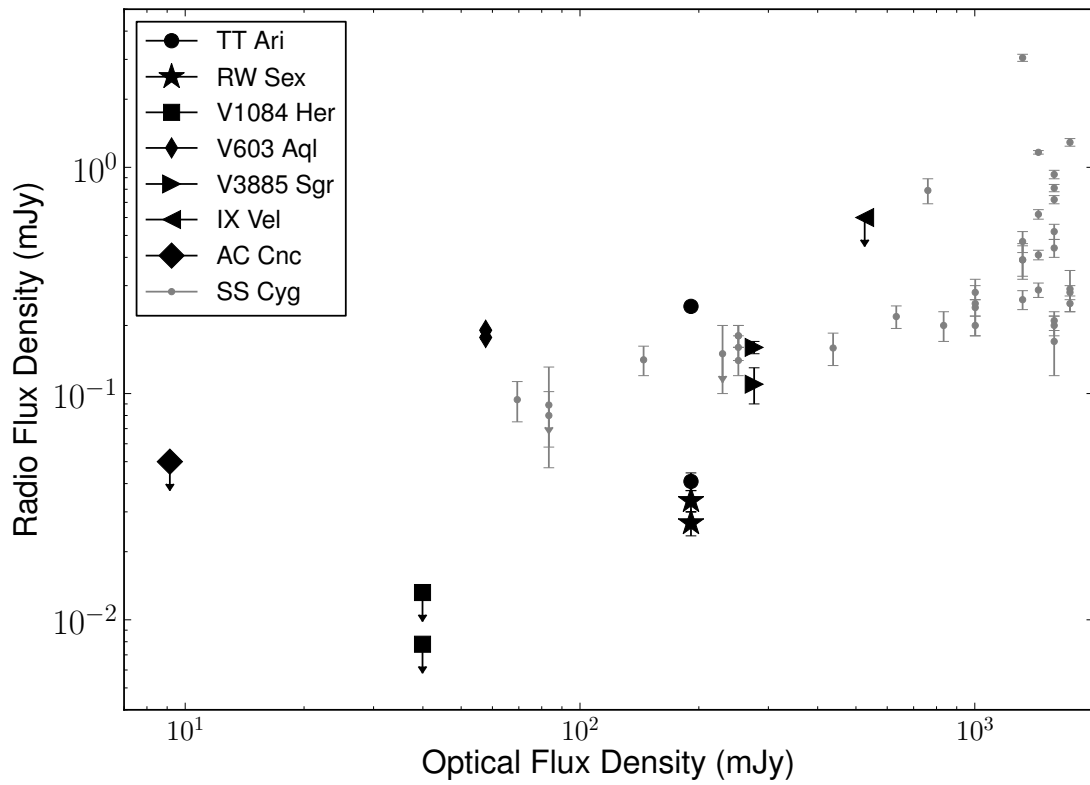


FIGURE 4.5: Radio and optical fluxes of all high-sensitivity (recent) detections and non-detections of non-magnetic CVs – with the dwarf nova SS Cyg plotted for comparison [Körding et al., 2008, 2011; Miller-Jones et al., 2011, 2013]. Using a rank test (Kendell’s tau), we find that there is no significant correlation between radio and optical fluxes for the given data (p value of 0.7)

distance uncertainty, we cannot say whether V1084 Her is simply too far away to detect or if it is intrinsically faint. At this stage there is also no correlation between the radio and optical fluxes of the novalikes (see Fig. 4.5). The dwarf nova SS Cyg does show a general positive correlation in radio flux with optical flux, but this is emission from a radio flare at the start of outburst, after which the radio flux was undetectable (Fig. 2 in K rding et al. 2008; Miller-Jones et al. 2011).

The range of different fluxes, variability, circular polarizations and spectra observed in this sample indicate there is likely more than one emission mechanism at work. Several explanations for the origin of the radio emission in non-magnetic CVs have been proposed over the years. These include thermal emission, synchrotron (possibly from jets) or gyrosynchrotron emission, and cyclotron maser emission.

4.5.1 Thermal Emission

Thermal emission could be produced by a large gas cloud surrounding the DN that is formed by the wind during outburst (e.g. Cordova et al. 1983; Fuerst et al. 1986). For the dwarf nova SS Cyg this suggestion was ruled out due to the observed brightness temperature, spectrum and coincidence with the optical outburst [K rding et al., 2008]. Thermal emission could produce the observed spectral indices in our sample.

As all of our detections are unresolved, we can place an upper-limit on the size of the emitting region. RW Sex is the closest CV and observation 1 had the largest beamwidth (150 pc and 0.58'' respectively); this gives an upper-limit on size of the emitting region of $\sim 1 \times 10^{15}$ cm for our sample.

The brightness temperature of a source is given by

$$T_b = \frac{S_\nu c^2}{2k_B \Omega \nu^2} \quad (4.1)$$

where S_ν is the specific flux, k_B is the Boltzmann constant, ν is the frequency and Ω is the solid beam angle.

For CVs with orbital periods in the range in this sample, the orbital radius is $r_{\text{orbit}} \sim 10^{11}$ cm. If we assume a circular source (as projected on the sky) that is the size of the binary, this gives a brightness temperature of

$$T_b \sim 1 \times 10^{12} \left(\frac{S_\nu}{\text{mJy}} \right) \left(\frac{\nu}{\text{GHz}} \right)^{-2} \left(\frac{r}{r_{\text{orbit}}} \right)^{-2} \text{ K}, \quad (4.2)$$

where r is the radius of the source.

If the emitting region is the size of the binary, then the brightness temperature for these observations is $\sim 1 \times 10^9$ K. As optically thick thermal emission from an ionized gas typically has brightness temperatures of $10^4 - 10^5$ K, this implies that any emission of order the size of the orbit must be non-thermal. The emitting region would need to have a radius of $\sim 10^2 - 10^3$ times the orbital radius if the observed emission is optically thick thermal emission, which is unlikely.

In the case of TT Ari and V603 Aql, optically thick thermal emission can be ruled out by the observed variability time-scales and causality arguments. CVs are non-relativistic, so heat transfer occurs at speeds significantly less than the speed of light. CV winds of up to 5000 km s⁻¹ have been detected [Kafka et al., 2009], so if we take an exceedingly fast CV wind of 1×10^4

km s⁻¹, then changes can only be propagated over the binary separation in ~ 200 s. V603 Aql is variable on time-scales down to 217 s and TT Ari to 144 s, so the emitting region would need to be smaller than the orbit, which (as shown above) cannot be the case for optically thick thermal emission. In addition to these arguments, in the case of TT Ari, thermal emission could also not account for the circular polarization.

The spectrum of observation 2 of TT Ari, however, is suggestive of thermal emission with a turnover at 6 GHz, so we now consider the possibility that there is a thermal component to the radio emission. Figure 4.3 shows the spectrum; it is consistent with $\alpha=2$ up to 6 GHz and $\alpha=-0.1$ at higher frequencies. This contrasts with the spectrum from observation 1, which was well fit with a single power-law ($\alpha = 1.7 \pm 0.8$, or $\alpha = 1.6 \pm 0.1$ during the flare). The variability and flux density also differed between the two observations, which suggests different emission mechanisms in the two epochs.

We now consider the properties of a possible thermal component in observation 2. For thermal opacity we have that

$$\tau_\nu \sim 8.235 \times 10^{-2} T_e^{-1.35} \nu^{-2.1} EM, \quad (4.3)$$

where the frequency ν is in GHz, T_e is the electron temperature (in K), and EM is the emission measure (pc cm⁻⁶), which is defined as the integral of the electron number density n_2 (in cm⁻³) along the line of sight

$$EM = \int n_2^2 dl. \quad (4.4)$$

For significant ionization T_e must be at least of order 10³ K. If we take $T_e=5000$ K and assume an emitting region that is Z times as large as the orbital radius, then we can estimate the electron density as follows:

$$\begin{aligned} EM &\sim \langle n_e^2 \rangle Z \left(\frac{r_{\text{orbit}}}{\text{pc}} \right) \\ \langle n_e^2 \rangle &\sim 4 \times 10^7 Z^{-0.5} \text{ cm}^{-3} \end{aligned} \quad (4.5)$$

Assuming a spherical emitting region with radius $r \sim 1 \times 10^{14}$ cm (the size restriction based on the brightness temperature) and width Z times the orbital radius ($dr = Z r_{\text{orbit}}$), we can estimate the total mass of a thermal emitting region as

$$\begin{aligned} M_t &= 4\pi r^2 n_e m_p dr \\ M_t &\sim 8 \times 10^{23} Z^{0.5} \text{ g}, \end{aligned} \quad (4.6)$$

where m_p is the mass of a proton (g). If the emission was indeed thermal, Z could be derived by watching the evolution of the radio light curve past epoch 2.

The observed spectrum with $\alpha=2$, and $\alpha=-0.1$ at higher frequencies is more compatible with a thin dense shell (e.g. of a nova) than an extended, centrally concentrated (r^{-2}) stellar wind. The latter would have $\alpha=0.6$ at lower frequencies, breaking to $\alpha=-0.1$ and would need a rather contrived geometry in order to reproduce the observed spectrum.

If there is a non-thermal component to the emission in the second observation of TT Ari, then more than one emission mechanism is necessary to produce the observed properties. Consequently we do not favour this scenario.

4.5.2 Non-thermal Emission

Non-thermal emission from CVs has been suggested by a number of authors (e.g. Fuerst et al. 1986; Benz & Guedel 1989; Benz et al. 1996; K rding et al. 2008) in the form of gyrosynchrotron and synchrotron emission, and maser emission.

4.5.2.1 Gyrosynchrotron Emission

Fuerst et al. [1986] concluded that either the magnetic field-strength is insufficient or the production rate of relativistic electrons is too low in non-magnetic CVs to produce gyrosynchrotron radiation, but this conclusion was based on the fact that they did not detect any of the eight non-magnetic CVs they observed at 5 GHz. Benz et al. [1983] had detected EM Cyg prior to this, but Fuerst et al. were unable to explain this discrepancy. Since then, SU UMa has been detected [Benz & Guedel, 1989] and so has V603 Aql (this work), so their conclusion needs revision.

Gyrosynchrotron emission is known to produce highly polarized CP, so it is a plausible emission mechanism for TT Ari. Although the 3σ upper-limits on the CP fraction in RW Sex and V603 Aql are 12.9% and 12.0% respectively, we cannot rule it out for these two sources.

Following the procedure in Benz & Guedel [1989], we can estimate the achievable brightness temperature for gyrosynchrotron emission of non-thermal electrons. For typical values of the power-law index of the electrons (~ 3) and an average angle between the magnetic field and the line of sight ($\sim 60^\circ$) we have

$$T_B < 2.8 \times 10^8 s^{0.755} \text{K}, \quad (4.7)$$

where s is the frequency in units of the gyro frequency $eB/m_e c$ and m_e is the electron mass. Thus, if the emission region is limited to the size of the binary, we find that we need a fairly low s factor just above 5, which corresponds to magnetic fields of $B < 100$ G. As argued by Benz & Guedel [1989], one can expect that at least in the case of low magnetic fields together with large emission regions (the size of the orbital separation), the electrons would be adiabatically outflowing and expansion would quench the emission. This could account for the observed flaring behavior in TT Ari.

4.5.2.2 Synchrotron Emission

The spectral index of TT Ari is consistent with optically thick (self-absorbed) synchrotron radiation, but it is circularly polarized and the CP fraction reached 100% during the flare in observation 1. High levels of linear polarization (LP) are possible, but typically LP levels for synchrotron radiation from astrophysical sources are lower, for example the compact jets in X-ray binaries typically have LP fractions of a few percent (e.g. Han & Hjellming 1992; Corbel et al. 2000; Russell et al. 2015). CP is suppressed in comparison to LP for synchrotron emission of relativistic particles (e.g. Longair 2011), so the 100% CP flare in TT Ari cannot be produced by synchrotron radiation.

V603 Aql and RW Sex both have spectral indices that are consistent with synchrotron radiation. Combined with the lack of strong CP, we could attribute V603 Aql to optically thick synchrotron emission and RW Sex to optically thin synchrotron emission.

K rding et al. [2008] suggested that radio emission in CVs could be due to synchrotron emission from a jet. This was supported by the observed CV outburst pattern, which has many features

in common with X-ray binaries. Jets have been detected in other accreting white dwarfs (symbiotics and novae). In the case of the dwarf nova SS Cyg, K rding et al. [2008] and Miller-Jones et al. [2011] concluded that the radio emission in outburst was most likely synchrotron radiation produced by a partially quenched optically thick synchrotron jet. This would be consistent with the observed emission from V603 Aql.

4.5.2.3 Cyclotron-Maser Emission

Benz & Guedel [1989] have suggested that the observed radio emission in CVs is due to a maser, or cyclotron instability, originating in the strong magnetic field and low densities near the white dwarf. They detected variability on time-scales of days and a CP fraction of 81% from the DN EM Cyg, and concluded that these properties support this model. Maser emission can produce high levels of CP and according to Benz et al. [1996], best explains the short, sporadic bursts of radio emission detected in DN. Our observations of TT Ari show this type of behaviour.

Benz & Guedel [1989] estimated the magnetic field strength necessary for EM Cyg to produce cyclotron-maser emission. They assumed a loss-cone velocity distribution for weakly relativistic electrons, the density profile for an isotropic outflow, and a dipole magnetic field for the WD of the form $B(r) = 10^5 \left(\frac{r_{\text{WD}}}{r}\right)^3$ G (where r is the radial distance from the WD) and estimated that a magnetic field strength of ~ 875 G or ~ 1750 G in the radio source region was necessary to produce cyclotron-maser emission. An electron density of $\geq 10^{11}$ cm $^{-3}$ requires the higher magnetic field strength (see the discussion in Section 4 of Benz & Guedel 1989). TT Ari shows the same radio properties as EM Cyg, and the assumptions and estimates made in Benz & Guedel are applicable to TT Ari.

4.5.3 Source of the Emission

Besides the sources mentioned above, radio emission could also be produced by the secondary star. Flare stars are isolated dwarfs (including K- or M-type dwarfs) that produce radio flares believed to be caused by magnetic reconnections in the star’s atmosphere (analogous to solar flares). As the secondary stars in CVs are K or M-type dwarfs, it is possible that the radio emission detected here could be from a flaring secondary – particularly in the case of TT Ari.

Figure 4.6 shows a histogram of the peak radio luminosities of the isolated flaring M dwarfs from McLean et al. [2012] and all the high-sensitivity radio observations of non-magnetic CVs. The dashed line at 10^{14} erg s $^{-1}$ Hz $^{-1}$ indicates the upper-edge of the radio emission from quiescent M-dwarfs from Gudel et al. [1993]. As RW Sex and V603 Aql are not flaring in our observations and have luminosities that are significantly higher than the quiescent flare stars, we conclude that their radio emission is not produced by a flaring secondary. TT Ari, however, is clearly flaring and the variability time-scales, high brightness temperature and circular polarization fit the properties of flare stars – particularly as they can produce flares that are up to 100% circularly polarized (e.g. Abada-Simon & Aubier 1997). Although there is some overlap between the maxima of some of the flare stars and the novalike luminosities, TT Ari peaked at around 3.3×10^{16} erg s $^{-1}$ Hz $^{-1}$ which is 38 times higher than the brightest flare in McLean et al. [2012]. We think that it is thus unlikely that the radio emission of TT Ari is produced by a flaring secondary.

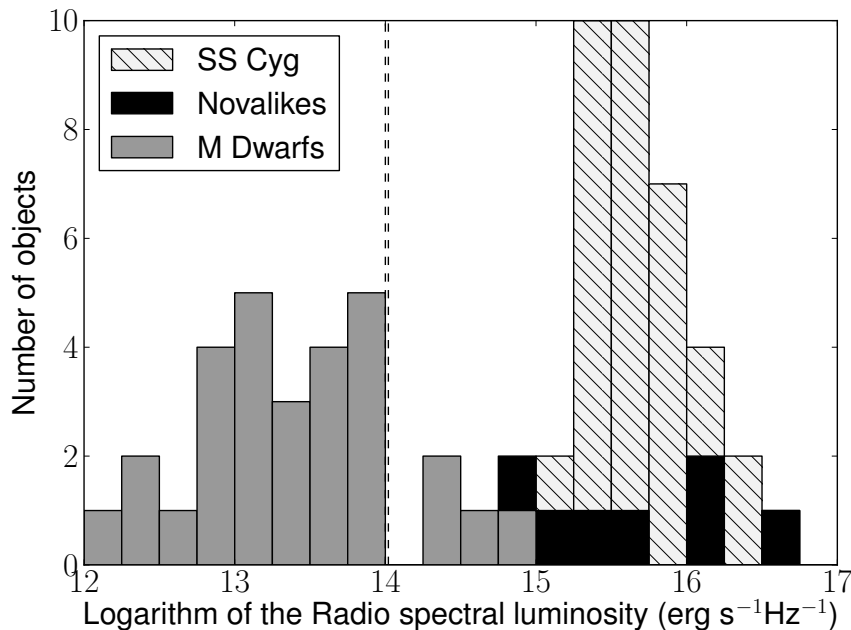


FIGURE 4.6: Histogram of the luminosities of all the flaring isolated M-dwarfs from McLean et al. [2012], as well as the CVs observed in the radio since 2008. The dashed line at $10^{14} \text{ erg s}^{-1} \text{ Hz}^{-1}$ indicates the upper edge of quiescence given by Gudel et al. [1993].

It should be noted that CV secondaries are tidally locked and have much higher rotation rates than isolated dwarfs, and that the impact of stellar rotation rates on magnetic fields is not well understood (see McLean et al. [2012] for a discussion). McLean et al., however, found that the radio emission of M0–M6 type dwarfs saturates at $10^{-7.5} L_{\text{bolometric}}$ for rotation rates larger than $v \sin i \simeq 5 \text{ km s}^{-1}$, so the comparison between CV secondaries and isolated dwarfs is appropriate.

A final consideration is whether TT Ari has actually been misclassified as non-magnetic and the (stronger) magnetic fields play a more significant role in generating the radio emission. Magnetic CVs have shown variable and highly circularly polarized emission just like that of TT Ari. For example, Dulk et al. [1983] detected a 9.7 mJy 100% circularly-polarized radio flare at 4.9 GHz from the polar AM Her, which they concluded was probably due to a cyclotron maser. As mentioned previously however, a similar flare at 81% CP was detected in the non-magnetic CV EM Cyg. Interestingly, the CV in our sample that is the most likely to be magnetic, V1084 Her, was the one source that was not detected. As CVs are not well studied in the radio, the radio properties of magnetic and non-magnetic CVs are not yet well defined and larger radio samples are needed.

4.6 Conclusion

We observed a sample of 4 novalikes at 6 GHz with the VLA and obtained a 75% detection rate, which doubles the number of detections of non-magnetic CVs. These observations show that the sensitivity of previous radio surveys ($\sim 1 \text{ mJy}$) was too low to detect non-magnetic CVs and that many novalikes are in fact significant radio emitters.

V603 Aql, RW Sex and the old nova TT Ari were each detected in two epochs, as point sources, while V1084 Her was detected in neither of the two epochs. The distance uncertainty on V1084

Her is too large to tell if it is intrinsically faint or too far away.

The observations show a range of properties that suggest that more than one emission mechanism is responsible for the radio emission in our sample. In the literature, emission mechanisms that have been suggested for non-magnetic CVs include thermal emission, gyrosynchrotron and synchrotron emission, and cyclotron maser emission.

RW Sex was detected at approximately the same flux density in both epochs ($33.6 \mu\text{Jy beam}^{-1}$) and with a spectral index $\alpha = -0.5 \pm 0.7$ ($F = \nu^\alpha$). It is unlikely the emission is thermal emission, as the emitting region would need to be a factor 10^2 – 10^3 times the orbital separation to produce the observed brightness temperature. Gyrosynchrotron and cyclotron maser emission are consistent with our observations, so we cannot rule these emission mechanisms out. As RW Sex has a 3σ CP fraction upper-limit of 12.9% and is not variable, however, we favour optically thin synchrotron emission.

V603 Aql was variable on timescales down to 217 s, with amplitudes of up to $61 \mu\text{Jy beam}^{-1}$ and had a spectral index $\alpha = 0.54 \pm 0.05$ in the first observation. In the second observation V603 Aql was not variable and the spectral index was flatter ($\alpha = 0.16 \pm 0.08$). The emission is unlikely to be thermal emission by the same argument as for RW Sex, and based on causality arguments and the observed variability timescales it cannot be optically thick thermal emission. The 3σ upper-limit on the CP fraction is 12% and the emission was variable, so we cannot rule out gyrosynchrotron or cyclotron maser emission. The radio detection is also consistent with optically thick synchrotron emission, which is consistent with the K rding et al. [2008] prediction of a partially quenched, optically thick synchrotron jet.

The two observations of TT Ari differed remarkably. The first showed a ~ 10 -minute flare with a peak flux density of $125.0 \pm 16.2 \mu\text{Jy beam}^{-1}$, that then declined to a 3σ upper-limit of $49.5 \mu\text{Jy beam}^{-1}$; ~ 8 mins of the flare was circularly polarized (CP) and peaked at a CP fraction of 100%. The flux in the second observation was higher (201.8 – $251.9 \mu\text{Jy beam}^{-1}$) and the highest CP detection was $36.1 \pm 10.0 \mu\text{Jy beam}^{-1}$ (polarization fraction of 15%). Radio behaviour like this has been seen in the magnetic CV AM Her [Dulk et al., 1983; Chanmugam, 1987] and in another non-magnetic CV (EM Cyg; Benz & Guedel 1989).

The observed CP fraction for TT Ari is too high to be produced by synchrotron emission, but can be explained by either gyrosynchrotron or cyclotron maser emission. By the same arguments as for V603 Aql and the additional fact that thermal emission cannot produce CP, we can rule out thermal emission in TT Ari. However, as the properties of the two epochs suggest different emission mechanisms, and the spectrum of the second epoch is consistent with $\alpha=2$ to 6 GHz and $\alpha=-0.1$ at higher frequencies (which could be indicative of thermal emission with a turnover frequency at 6 GHz), we did consider the possibility that there is a thermal component to the emission in the second epoch. If this is the case, the observed spectrum is more consistent with a thin, dense shell than an extended, centrally concentrated stellar wind, and we would need to observe the evolution of the spectrum over multiple epochs to derive the mass of the emitting region. As an additional non-thermal component is necessary to produce the CP and observed variability, we favour pure gyrosynchrotron or cyclotron maser emission as emission mechanisms.

The high CP levels and variability shown by TT Ari are also consistent with flare star behaviour. For all three novalikes however, we conclude that although it is possible, the emission is

unlikely to be produced in flares of the secondary star, as the luminosities are significantly higher than those seen in both flaring and quiescent flare stars.

We did not find a radio-optical flux relation or a radio flux-distance relation, but this may change as the sample of radio detections of non-magnetic CVs increases.

As we have demonstrated, it is now possible to detect non-magnetic CVs with the VLA. Further observations of CVs will help establish the nature of the radio emission, which could then be used to study accretion and possibly outflow physics in these nearby, numerous and non-relativistic compact accretors.

Acknowledgements

We thank the referee for their prompt and positive response. Thank you also to Cameron Van Eck for many helpful discussions.

This work is part of the research programme NWO VIDI grant Nr. 2013/15390/EW, which is financed by the Netherlands Organisation for Scientific Research (NWO, Nederlandse Organisatie voor Wetenschappelijk Onderzoek).

DLC gratefully acknowledges funding from the Erasmus Mundus Programme SAPIENT. JCAMJ is the recipient of an Australian Research Council Future Fellowship (FT140101082), and also acknowledges support from an Australian Research Council Discovery Grant (DP120102393). GRS acknowledges support from an NSERC Discovery Grant.

The National Radio Astronomy Observatory is a facility of the National Science Foundation operated under cooperative agreement by Associated Universities, Inc. This research has made use of NASA's Astrophysics Data System Bibliographic Services, as well as the SIMBAD database, operated at CDS, Strasbourg, France [Wenger et al., 2000].

4.A Subappendix

Here we show the total intensity and circular polarization maps (Figure 4.7 and Figure 4.8 respectively). See the captions for more information.

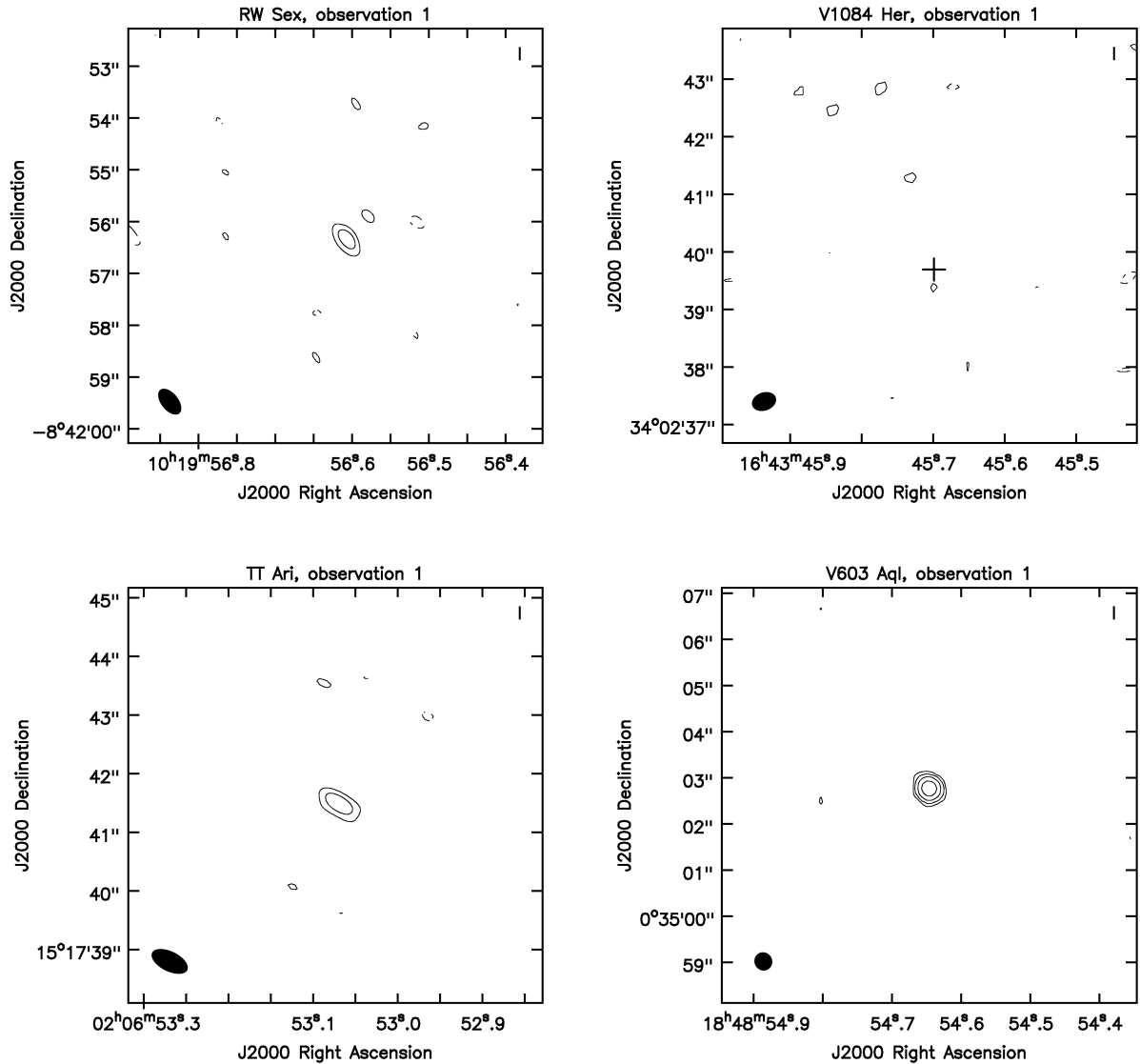


FIGURE 4.7: Stokes I (total intensity) maps for the first observation of each novalike. Contours are at ± 3 , ± 6 , ± 12 and ± 24 sigma. The beam (resolution) is given in the lower left corner of each image. None of the detections show extended emission; they are all point sources. RMS and peak flux values are given in Table 4.3. The cross indicates the optical position for the non-detection (V1084 Her) – the size is not indicative of the optical position error bars, as they are too small to be plotted here (see Table 4.1).

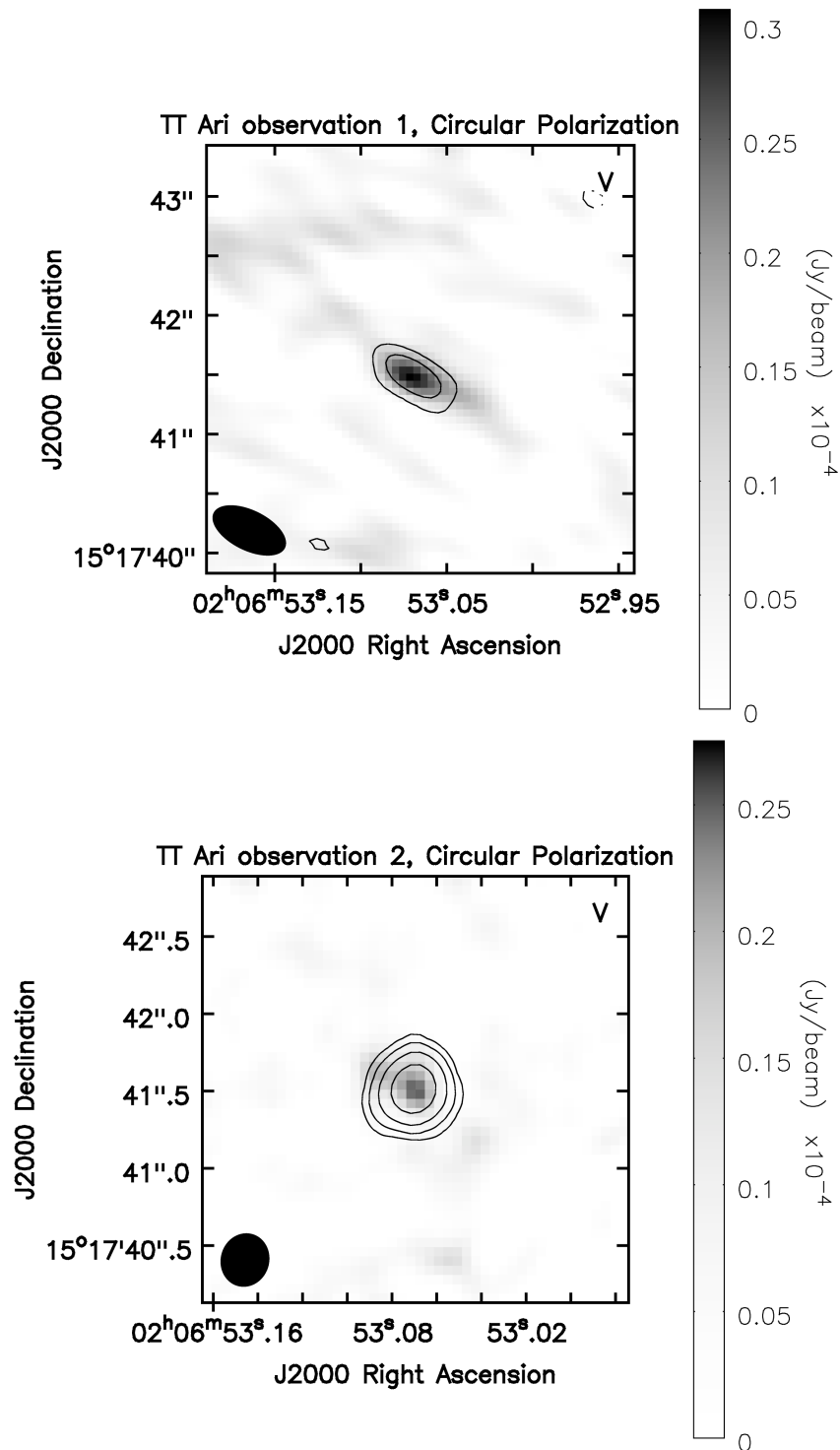


FIGURE 4.8: Stokes V (circular polarization) images for observation 1 (left) and 2 (right) of TT Ari. Stokes I contours are drawn at ± 3 , ± 6 , ± 12 and ± 24 sigma. For clarity purposes we do not show the left circularly polarized (negative) flux, as the detections were right circularly polarized (positive).

DWARF NOVA-TYPE CATAclySMIC VARIABLES ARE SIGNIFICANT RADIO EMITTERS

Deanne L. Coppejans, Elmar G. K rding, James C. A. Miller-Jones, Michael P. Rupen, Gregory R. Sivakoff, Christian Knigge, Paul J. Groot, Patrick A. Woudt, Elizabeth O. Waagen and Matthew Templeton

Submitted to MNRAS

Abstract

We present 8–12 GHz radio light curves of five dwarf nova (DN) type Cataclysmic Variable stars (CVs) in outburst (RX And, U Gem and Z Cam), or superoutburst (SU UMa and YZ Cnc), increasing the number of radio-detected DN by a factor of two. The observed radio emission was variable on time-scales of minutes to days, and we argue that it is likely to be synchrotron emission. This sample shows no correlation between the radio luminosity and optical luminosity, orbital period, CV class, or outburst type; however higher-cadence observations are necessary to test this, as the measured luminosity is dependent on the timing of the observations in these variable objects. The observations show that the previously detected radio emission from SS Cyg is not unique in type, luminosity (in the plateau phase of the outburst), or variability time-scales. Our results prove that DN, as a class, are radio emitters in outburst.

5.1 Introduction

Cataclysmic Variable stars (CVs) are binary systems consisting of a white dwarf that accretes matter from a main-sequence secondary star via Roche-lobe overflow [for a review, see Warner,

1995]. Systems in the dwarf nova (DN) class of CVs show episodic outbursts in which the optical emission of the system brightens by $\sim 2\text{--}8$ mag over a period of days to weeks. These outbursts develop when a build-up of matter in the accretion disc triggers a thermal-viscous instability and switches the disc to a hot, bright, viscous state [the Disc Instability Model (DIM); Smak, 1971; Osaki, 1974; Höshi, 1979; Lasota, 2001]. The interval between subsequent outbursts is weeks to years [e.g. Coppejans et al., 2015a].

One of the main questions in CV research is what role mass ejections (in the form of collimated jets or uncollimated winds) play during DN outbursts. Most other classes of accreting objects have been found to launch jets in at least some states. Jets have been found in the symbiotic systems (white dwarfs accreting from a red giant; e.g. Sokoloski et al. 2008), neutron star and black hole X-ray Binaries (XRBs; e.g. Russell et al. 2013), active galactic nuclei (AGN; e.g. King et al. 2011) and gamma-ray bursts (GRBs; e.g. Granot & van der Horst 2014). However, until recently it was commonly accepted that CVs do not launch jets. This was used to constrain jet-launching models [Livio, 1999; Soker & Lasota, 2004].

As radio emission is the best tracer for jets, it was the historical lack of detections of CVs at radio wavelengths that led to the conclusion that CVs do not launch jets. Although many surveys were conducted prior to 2008, only three non-magnetic CVs¹ were detected at radio wavelengths. EM Cyg [Benz & Guedel, 1989], SU UMa [Benz et al., 1983] and TY Psc [Turner, 1985] were detected in one set of observations, but were not detected in follow-up observations. Radio surveys of CVs were conducted by e.g. Benz et al. [1983], Benz & Guedel [1989], Cordova et al. [1983], Fuerst et al. [1986], Echevarria [1987], Nelson & Spencer [1988], Turner [1985], and Benz et al. [1996]. The detection rates were higher for the magnetic CVs², but to date only three persistent radio emitters have been identified in the literature, namely AE Aqr [e.g. Bookbinder & Lamb, 1987; Bastian et al., 1988; Abada-Simon et al., 1993; Meintjes & Venter, 2005], AR UMa [Mason & Gray, 2007], and AM Her [e.g. Chanmugam & Dulk, 1982; Chanmugam, 1987; Dulk et al., 1983; Mason & Gray, 2007].

Recently it has been shown that the timing [Körding et al., 2008], and sensitivity [Coppejans et al., 2015b], of previous observations were insufficient to detect the radio emission. Coppejans et al. [2015b] showed that CVs in a persistent high-accretion state (the novalike class) are radio emitters at a level that was below the sensitivity threshold of previous instruments. For the DN systems, none of the historical radio observations were taken in the early stages of the outburst. Through a comparison of the XRB and CV accretion states, Körding et al. [2008] showed that radio emission produced by a transient jet should flare shortly after the rise to outburst, and then subsequently drop to undetectable levels – explaining the lack of detections.

The XRBs show an empirical relation between the outflow properties (power, morphology) and the accretion state [e.g. Belloni et al., 2011; Fender et al., 2004; Migliari & Fender, 2006; Miller-Jones et al., 2012]. As outbursts of XRBs and CVs are described by the same model and they share similar phenomenology, Körding et al. [2008] mapped this relation onto the CVs. They predicted that DN should show a synchrotron radio flare from a transient jet on the rise

¹CVs in which the magnetic field strength of the white dwarf is $B \lesssim 10^6$ G, allowing matter to accrete onto the white dwarf via an accretion disc.

²CVs in which the magnetic field strength of the white dwarf is $B > 10^6$ G, which truncates the disc at the Alfvén radius.

to outburst, and they detected this in the DN SS Cyg. Miller-Jones et al. [2011] subsequently confirmed this behaviour in a separate outburst of SS Cyg, and Russell et al. [2016] proved that the radio outbursts of SS Cyg undergo similar evolution from outburst to outburst. Based on the timing, variability, spectral indices and brightness temperatures of the radio emission, and multi-wavelength data, K rding et al. [2008], Miller-Jones et al. [2011] and Russell et al. [2016] argue that the radio emission in SS Cyg is produced by a transient jet.

A number of other radio emission mechanisms have been suggested for non-magnetic CVs. Thermal emission from a large gas cloud surrounding the CV [e.g. Cordova et al., 1983] has been excluded in the detected CVs based on the spectral indices, brightness temperatures, or variability time-scales of the observed radio emission [Fuerst et al., 1986; K rding et al., 2008; Coppejans et al., 2015b]. Non-thermal emission in the form of synchrotron, or coherent emission has also been suggested to be produced through magnetic reconnections in the disc, reflection of electrons in the magnetic field near the surface of the white dwarf, or disruption of the magnetosphere [Fuerst et al., 1986; Benz & Guedel, 1989; Benz et al., 1996]. These coherent mechanisms have been ruled out for SS Cyg [K rding et al., 2008; Miller-Jones et al., 2011; Russell et al., 2016]. The radio emission from the novalike systems is either synchrotron or coherent emission [Coppejans et al., 2015b].

Only four DN (namely SU UMa, EM Cyg, TY PSc and SS Cyg) have been detected at radio wavelengths [Benz et al., 1983; Benz & Guedel, 1989; K rding et al., 2008; Miller-Jones et al., 2011; Russell et al., 2016]. The numerous other radio observations of DN in outburst yielded non-detections with upper-limits on the order of 0.1–0.3 mJy [Fuerst et al., 1986; Benz & Guedel, 1989; Echevarria, 1987]. Of the detected sources, only SS Cyg was observed with sufficient sensitivity, cadence, and timing, to look for radio emission from a transient jet.

In this paper we present 10-GHz Karl G. Jansky Very Large Array (VLA) light curves of five DN (U Gem, Z Cam, SU UMa, YZ Cnc and RX And) over the course of an outburst of each system. We detect radio emission from all five systems, proving that DN in outburst are radio emitters. Section 5.2 gives a brief description of the targets, and our selection criteria. The observations and results are given in Section 5.3 and 5.4 respectively.

5.2 Targets

There are three main subclasses of DN, namely the Z Cam, SU UMa and U Gem type DN. Each class is named after its prototype.

Z Cam type DN go through intervals which show DN outbursts, and intervals (known as “standstills”) during which the system remains at a constant optical brightness (intermediate between the quiescent and outburst levels) and does not show outbursts. According to the DIM, if the accretion rate exceeds a certain threshold, it is sufficient to maintain the accretion disc in a persistent high-state. This is the case for the novalike systems. The accretion rate of the Z Cam systems is believed to be close to this threshold, so minor accretion rate changes can shift the system in and out of standstill [e.g. Honeycutt et al., 1998].

SU UMa type DN show outbursts, as well as superoutbursts. Superoutbursts are brighter, and last longer than outbursts in a given system [e.g. Otulakowska-Hypka et al., 2016]. Three

TABLE 5.1: Properties of the target dwarf novae

Name	RA (J2000)	Dec. (J2000)	RA proper motion ^c (mas/y)	Dec. proper motion (mas/y)	DN type	P_{orb} (h)	Dist. (pc)	Incl. (deg)
Z Cam	08:25:13.201 \pm 0.002 ^a	+73:06:39.23 \pm 0.03 ^a	-8.1 \pm 2.5 ^a	-18.0 \pm 2.5 ^a	Z Cam	6.956174(5) ^f	163	62
RX And	01:04:35.538 \pm 0.004 ^b	+41:17:57.78 \pm 0.06 ^b	-	-	Z Cam	5.03743(2) ^g	200	55
SU UMa	08:12:28.264 \pm 0.004 ^b	+62:36:22.46 \pm 0.06 ^b	7.3 \pm 2.7 ^d	-30.3 \pm 6.9 ^d	SU UMa	1.832(1) ^h	260	42
YZ Cnc	08:10:56.645 \pm 0.004 ^b	+28:08:33.46 \pm 0.06 ^b	38 \pm 8 ^e	-58 \pm 8 ^e	SU UMa	2.0862(2) ⁱ	260	15
U Gem	07:55:05.235 \pm 0.005 ^b	+22:00:05.07 \pm 0.08 ^b	-26 \pm 8 ^e	-32 \pm 8 ^e	U Gem	4.246(7) ^j	102	70

Notes: Optical coordinates retrieved via Simbad from ^aHøg et al. [2000], ^bCutri et al. [2003]. ^c $\mu_{\text{RA}}\cos(\text{dec})$. Proper motions are from ^dMickaelian & Sinamyan [2010], ^eSkinner et al. [2014], ^aHøg et al. [2000]. Orbital periods from ^fThorstensen & Ringwald [1995], ^gKaitchuck [1989], ^hThorstensen et al. [1986], ⁱvan Paradijs et al. [1994] and ^jMarsh et al. [1990]. The error on the last digit is quoted in parenthesis; for example 0.2(3) is equivalent to 0.2 ± 0.3 . Distances from Patterson [2011], who estimate the uncertainty at 15-20%. Inclinations from Patterson [2011]. As a number of assumptions are necessary to determine the inclination (specifically for the low-inclination systems), the inclinations should be considered as rough estimates (see the discussion in Patterson 2011).

models have been proposed to explain superoutbursts. In the *Thermal Tidal Instability model* (TTI, Osaki 1989, 1996; Osaki & Meyer 2003), mass and angular momentum build up in the disc over successive DN outbursts and the disc radius increases. At a sufficiently large radius³, the orbital period of the outer disc material resonates with the orbit of the secondary star, and the outer disc material is driven into eccentric orbits. This increases the mass transfer rate through tidal dissipation and prolongs the outburst to form a superoutburst. In the *Enhanced Mass Transfer model* (EMT, Vogt 1983; Smak 1984; Osaki 1985), the secondary star is irradiated during the DN outburst, which increases the mass-transfer rate and produces a superoutburst. In the *Thermal-viscous Limit Cycle Instability model* [van Paradijs, 1983; Cannizzo et al., 2010, 2012], superoutbursts are triggered by the same thermal-viscous instability as the DN outbursts. The instability criterion is triggered in the inner disc, and a heating wave propagates outwards as the instability is triggered in annuli at increasingly larger radii. In DN outbursts, this wave does not reach the outer disc radius. In superoutbursts, the wave extends to larger disc radii and produces a longer, brighter outburst. For more discussions on the superoutburst models see e.g. Schreiber et al. [2004], Smak [2008] and Osaki & Kato [2013]. In some systems, DN outbursts are seen immediately prior to the superoutburst. These *precursor outbursts* are believed to trigger the superoutburst according to the TTI and EMT models [e.g. Osaki & Kato, 2013].

U Gem type DN show only normal outbursts. The build-up of a mass reservoir at the outer disc is prevented by the heating wave of a normal outburst reaching the outer regions every time.

We selected targets from each of the three classes. The selection criteria for the candidate sources were that they had to be nearby (≤ 260 pc in Patterson 2011) and optically bright in quiescence ($V \leq 15$ mag). This was to ensure that the American Association of Variable Star Observers (AAVSO) were able to easily monitor these targets. To guarantee that we were able to observe five systems in outburst during the observing semester, we monitored a sample of nine DN (Z Cam, RX And, SU UMa, YZ Cnc, U Gem, SY Cnc, EX Dra, EM Cyg and AB Dra). We

³The 3:1 resonance, which is approximately 0.46 times the orbital separation (see Osaki & Meyer 2003 and references therein).

triggered observations on Z Cam, RX And, SU UMa, YZ Cnc and U Gem. The properties of these targets are given in Table 5.1, and a short description of each is included below for reference.

5.2.1 Z Camelopardalis (Z Cam)

Z Cam is the prototype for the Z Cam class of DN. It has an orbital period of 0.2898406(2) d [Thorstensen & Ringwald, 1995], a $M_{\text{WD}} = 0.99 \pm 0.15 M_{\odot}$ white dwarf, a mass ratio of 1.4 ± 0.2 [Shafter, 1983], and a K7-type secondary star [Szkody & Wade, 1981]. Based on the observed variability in the mid-infrared lightcurve, Harrison [2014] conclude that Z Cam is a synchrotron source when it is near outburst maximum (this is discussed further in Section 5.5).

All previous radio observations of Z Cam have yielded non-detections. Fuerst et al. [1986] observed it during outburst at 4.885 GHz and obtained an upper-limit of 0.1 mJy. Further observations by Nelson & Spencer [1988] and Woodsworth & Hughes [1977] have produced 3σ upper-limits of 1.1 mJy (5 GHz), 4.6 mJy (5 GHz) and 25 mJy (10.6 GHz).

5.2.2 RX Andromedae (RX And)

RX And is classified as a Z Cam type DN as it shows long standstills. In the long-term optical light curve it also shows low states that are ~ 3.5 mag fainter than the standstills, during which time there are no outbursts [Schreiber et al., 2002]. It has an orbital period of 0.209893(1) d [Kaitchuck, 1989] and a $K5 \pm 2$ secondary star [Knigge, 2006].

Although RX And has been observed at radio wavelengths, there have been no prior detections. Benz & Guedel [1989] observed it during outburst at 1.49 and 4.86 GHz, and obtained 3σ upper-limits of 0.2 mJy. Nelson & Spencer [1988] and Woodsworth & Hughes [1977] also observed it and reported upper-limits of 2.6 mJy (at 5 GHz), 4.6 mJy (at 5 GHz) and 25 mJy (at 10.6 GHz).

5.2.3 SU Ursae Majoris (SU UMa)

SU UMa is the prototype of its subclass of outbursting DN. It was discovered by Ceraski [1908] and has an orbital period of 0.07635(4) d [Thorstensen et al., 1986]. Observations at 4.885 GHz by Fuerst et al. [1986] during the outburst maximum resulted in an upper-limit of 0.11 mJy. Effelsberg observations at 4.75 GHz by Benz et al. [1983] resulted in a 1.3 mJy detection 1–2 days after the rise of the outburst, and a 0.4 mJy upper-limit during a subsequent quiescent epoch. Further radio observations were attempted by Nelson & Spencer [1988], Echevarria [1987] and Fuerst et al. [1986], but no detections were reported.

5.2.4 YZ Cancri (YZ Cnc)

YZ Cnc is an eclipsing SU UMa-type DN system with an orbital period of 0.086924(7) d [van Paradijs et al., 1994]. Only upper-limits on the radio flux are known in the literature, despite observations during the rise and at the peak of super-outburst. Limits range from 0.11 mJy at 4.885 GHz [Fuerst et al., 1986], to 0.87, 0.6 and 0.96 mJy at 1.5, 4.9 and 0.15 GHz respectively [Nelson & Spencer, 1988].

TABLE 5.2: Observing log

Name	Obs.	VLA config.	Start Time (MJD)	Int. time ^a (s)	Bandpass, flux, & polarization angle calibrator	Amplitude & phase calibrator	Polarization & leakage calibrator
Z Cam	1	C	56986.11156	4905	3C48	J0721+7120	J0319+4130
Z Cam	2	C	56987.17184	2007	3C138	J0721+7120	J0319+4130
Z Cam	3	C	56988.14601	1770	3C48	J0721+7120	J0319+4130
RX And	1	C	56969.40396	5151	3C48	J0111+3906	J2355+4950
RX And	2	C	56970.35931	2181	3C48	J0111+3906	J2355+4950
RX And	3	C	56971.37201	2175	3C48	J0111+3906	J2355+4950
SU UMa	1	C	57027.15094	4902	3C138	J0805+6144	J0713+4349
SU UMa	2	C–CNB	57028.06830	1968	3C138	J0805+6144	J0713+4349
SU UMa	3	C–CNB	57029.43229	1995	3C286	J0805+6144	J0713+4349
YZ Cnc	1	C	56984.28431	4635	3C138	J0748+2400	J0713+4349
YZ Cnc	2	C	56985.22726	1854	3C138	J0748+2400	J0713+4349
YZ Cnc	3	C	56987.32938	1860	3C138	J0748+2400	J0713+4349
U Gem	1	B	57075.32906	4938	3C286	J0805+6144	J1407+2827
U Gem	2	B	57080.15337	1851	3C138	J0748+2400	J0713+4349
U Gem	3	B	57080.19420	1923	3C138	J0748+2400	J0713+4349

Observations were taken at 7976–12022 MHz (X-band) with 4046 MHz of bandwidth (3-bit mode). YZ Cnc and SU UMa were in superoutburst at the time of the observations. ^aTotal integration time on source, excluding calibration scans.

5.2.5 U Geminorum (U Gem)

U Geminorum (U Gem) is the ‘original’ cataclysmic variable [Hind, 1856], and one of the best-studied systems in the class. It is a partially eclipsing system where the accretion disc is eclipsed, but the white dwarf is unobscured. It shows outbursts with a recurrence time of ~ 150 days. Optical photometric and spectroscopic observations indicate that it develops spiral density waves in the accretion disk during outburst [Groot, 2001]. It has an orbital period of 0.1769(3) d [Marsh et al., 1990], and consists of a $1.20 \pm 0.05 M_{\odot}$ primary white dwarf and a $0.42 \pm 0.04 M_{\odot}$ late-type (M6) secondary star [Echevarria et al., 2007].

The first radio observations of U Gem were attempted by Woodsworth & Hughes [1977] at 10.6 GHz, which resulted in a 25 mJy upper-limit. Despite various attempts in the mid-1980s it was never detected at radio frequencies (neither in outburst nor quiescence). Upper-limits on the radio flux range from 1.3–2.9 mJy at 5 GHz [Nelson & Spencer, 1988], to 0.15 mJy at 4.885 GHz [Cordova et al., 1983], to 0.2 mJy during outburst at 1.49 and 4.86 GHz [Benz & Guedel, 1989].

5.3 Observations

DN outbursts and superoutbursts are not predictable and recur on timescales of weeks to months. Our program aimed to observe the targets immediately after the outburst rise to probe the same phase at which the radio emission flared in SS Cyg. This required the first VLA observation to be triggered during the rise from quiescence to peak outburst (which lasts approximately 24 hours). To trigger the observations at the correct time, we ran a campaign with the AAVSO. The

AAVSO monitored a sample of DN in the optical and alerted us when they detected an outburst⁴. We subsequently triggered VLA observations (project VLA/14B-177) on RX And, SU UMa, U Gem, YZ Cnc and Z Cam. For triggering purposes we defined the source to be in outburst when the optical *V*-band flux rose ~ 1 mag above the typical flickering and orbital modulations. To ensure that we observed superoutbursts in YZ Cnc and SU UMa, we waited until superhumps or a precursor outburst were detected⁵.

The observing log for the observations is given in Table 5.2. Three separate observations were taken of each source. The first was taken to coincide as closely as possible to the end of the outburst rise. The subsequent observations were taken on the next two days. This pattern was chosen to probe the same outburst phase at which radio emission was detected from SS Cyg [Körding et al., 2008], and to determine if our targets also showed a decline in the radio emission after the peak of outburst was reached. The deviations from this pattern were due to scheduling constraints at the VLA, or (in the case of SU UMa and YZ Cnc) to ensure that the outburst was a superoutburst.

All the observations were taken at 7976–12022 MHz (X-band) with a bandwidth of 4046 MHz (3-bit samplers). The bandwidth was split into two equal basebands, which were further subdivided into 16 spectral windows, each of which comprised 64 2-MHz channels. These observations were taken using the standard phase referencing mode; the phase and amplitude calibrator was observed for 1 minute, approximately every 4 minutes.

The data were reduced using CASA⁶ v4.4.0, following standard reduction techniques. Standard flux calibrators (see Table 5.2) and the Perley-Butler 2010 coefficients in CASA were used to set the absolute flux density scale. We did not perform any self-calibration. Two Taylor terms were used to model the frequency dependence of the sources, and Briggs weighting with a robust parameter of 1 was used. All fits were done in the image plane using the CASA IMFIT task and the quoted noise was determined in the vicinity of the target. Upper-limits are quoted as 3 times the noise level.

5.4 Results

5.4.1 Detections

We detected unresolved radio emission at the positions of all five DN (four of which have not been detected previously). This increases the number of radio-detected DN by a factor of two.

Table 5.3 gives a summary of the radio properties for each of the observations. Z Cam and SU UMa were detected in all three observations, and the remaining targets were detected in at least one observation. The flux densities of the detections were in the range of 20–60 μJy and the 3σ upper-limits on the non-detections were on the order of 17 μJy . The radio light curves are plotted with the AAVSO optical light curves in Figure 5.1, to show the outburst phase at which they were taken.

⁴For details of the campaign see <https://www.aavso.org/aavso-alert-notice-505>

⁵The average outburst level was estimated based on the long-term optical light curves.

⁶Common Astronomy Software Applications package [McMullin et al., 2007]

TABLE 5.3: Results

Name	Outburst type ^a	Obs.	Beam Size ^b (arcsec ²)	PA ^c (°)	RA ^d (J2000)	Dec. ^e (J2000)	Flux Density (μ Jy)	CP (μ Jy)	LP (μ Jy)
Z Cam	Normal	1	5.21×2.15	-54	08:25:13.149 ± 0.029	73:06:39.00 ± 0.44	25.0 ± 3.1	<10.2	<6.9
		2	4.54×2.08	-71	08:25:13.100 ± 0.025	73:06:39.13 ± 0.37	40.3 ± 5.2	<16.8	<11.1
		3	4.94×2.05	-62	08:25:13.067 ± 0.026	73:06:39.34 ± 0.39	33.1 ± 4.4	<16.5	<13.2
RX And	Normal	1	4.49×2.14	71	01:04:35.526 ± 0.030	41:17:57.73 ± 0.46	13.6 ± 3.2	<10.5	<6.0
		2	3.07×2.19	87	01:04:35.547 ± 0.020	41:17:57.22 ± 0.32	19.6 ± 4.4	<13.5	<8.7
		3	3.32×2.19	83	-	-	<14.4	-	-
SU UMa	Super	1	3.11×2.16	75	08:12:28.296 ± 0.012	62:36:21.89 ± 0.19	35.5 ± 3.8	<11.4	<7.2
		2	5.10×2.25	-75	08:12:28.232 ± 0.019	62:36:22.07 ± 0.29	58.1 ± 5.7	<17.7	<12.0
		3	2.86×1.79	-45	08:12:28.310 ± 0.027	62:36:22.32 ± 0.40	19.1 ± 4.9	<14.7	<9.9
YZ Cnc	Super	1	2.93×2.32	-72	08:10:56.692 ± 0.021	28:08:32.71 ± 0.32	17.4 ± 3.7	<10.5	<6.3
		2	5.73×2.25	-65	08:10:56.644 ± 0.045	28:08:32.86 ± 0.67	26.8 ± 5.2	<18.3	<10.8
		3	2.57×2.47	-23	-	-	<18.9	-	-
U Gem	Normal	1	0.96×0.65	64	07:55:05.2081 ± 0.0065	22:00:04.4106 ± 0.098	12.7 ± 2.8	<9.0	<7.8
		2	0.70×0.60	-3	-	-	<16.8	-	-
		3	0.72×0.60	-3	-	-	<17.5	-	-

Notes: All detections were consistent with point sources, and all upper-limits are 3σ . ^a‘Normal’ refers to a DN outburst, and ‘super’ refers to a super-outburst. ^bMajor and minor axis of the synthesized beam. ^cPosition angle of the beam. ^eEach radio position is consistent with the optical position and proper motion in Table 5.1.

5.4.2 Variability

U Gem, RX And and SU UMa all showed variability on the (approximately) one-day timescale between observations. As SS Cyg and the novalike systems showed faster-timescale variability [Körding et al., 2008; Coppejans et al., 2015b; Russell et al., 2016], we split the observations into finer segments to see if this is the case in the DN systems. The results are presented in Figure 5.2 and Table 5.5.

In RX And we detected variability on time-scales of minutes. The second observation showed a clear flare, rising from an undetectable level with a 3σ upper-limit of $40.2 \mu\text{Jy}$, to $95.0 \pm 15.0 \mu\text{Jy}$ in 4 minutes. As this flare occurred at the end of the observation, we can not constrain its duration.

SU UMa also showed a flare, and variability on time-scales of tens of minutes, during the second observation. The flux density dropped from 83.1 ± 8.7 to $33.4 \pm 9 \mu\text{Jy}$ in the first 27 minutes of the observation.

The shortest timescale on which U Gem showed significant variability was 69 minutes. It was detected at a flux density of $27.0 \pm 7.7 \mu\text{Jy}$, and in the subsequent 69 minutes dropped to undetectable levels (with a 3σ upper-limit of $17.5 \mu\text{Jy}$).

YZ Cnc and Z Cam were not significantly variable on timescales of minutes or days. Z Cam showed only 2-sigma variability (a 4% chance that it was non-variable according to the variability test in Bell et al. 2015). According to this same test, YZ Cnc was not variable.

In all cases the signal-to-noise ratio (SNR) was too low to test for variability on timescales shorter than minutes.

5.4.3 Spectral Indices and Polarization

The spectral indices of the radio emission are shown in Table 5.4. Unfortunately the SNR was not high enough to constrain the spectral indices well.

None of the observations showed circular or linear polarization. The 3σ upper-limits were on the order of 10-20% of the measured flux (see Table 5.3). Consequently there are only two non-magnetic CVs from which circular polarization has been detected, namely EM Cyg and TT Ari [Benz & Guedel, 1989; Coppejans et al., 2015b]. In both of these cases the circular polarization fraction was variable, and peaked at 81% and more than 75%, respectively.

5.5 Discussion

5.5.1 DN in Outburst as Radio Emitters

We detected 10 GHz radio emission from all five DN in outburst, with specific luminosities in the range $8 \times 10^{13} - 9 \times 10^{15} \text{ erg s}^{-1} \text{ Hz}^{-1}$, which correspond to luminosities of $8 \times 10^{23} - 9 \times 10^{25} \text{ erg s}^{-1}$ at 10 GHz. The radio emission is in excess of that expected from the known CV component (WD, disc and secondary star) spectra, and is variable on timescales of minutes to days in 3 of the 5 DN. The flux levels of our observations ($15 - 80 \mu\text{Jy}$) show that the sensitivity of previous instruments was insufficient to detect these objects, as historical non-detections had 3σ upper-limits in the range 0.1–0.3 mJy. All three classes of DN (U Gem, Z Cam and SU UMa-type DN)

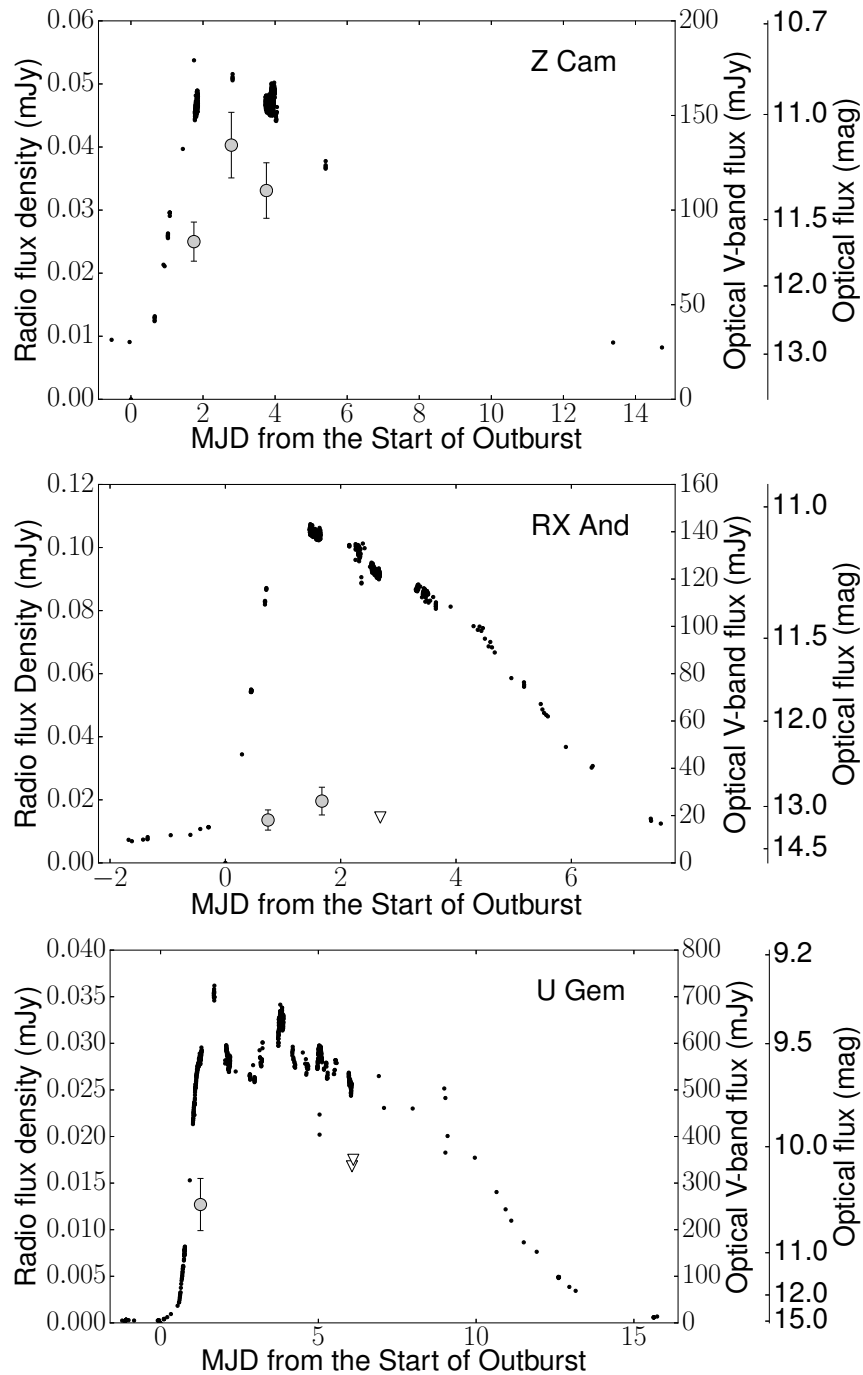


FIGURE 5.1: Radio (10 GHz) and optical (V-band) light curves of the outbursts of RX And, U Gem and Z Cam. The superoutbursts of SU UMa and YZ Cnc, as well as the legend, are shown on the following page. The fluxes and integration times for these light curves are given in Table 5.3. The precursor outburst of SU UMa has not been plotted for clarity. All optical observations are from the AAVSO International Database (see <http://www.aavso.org>).

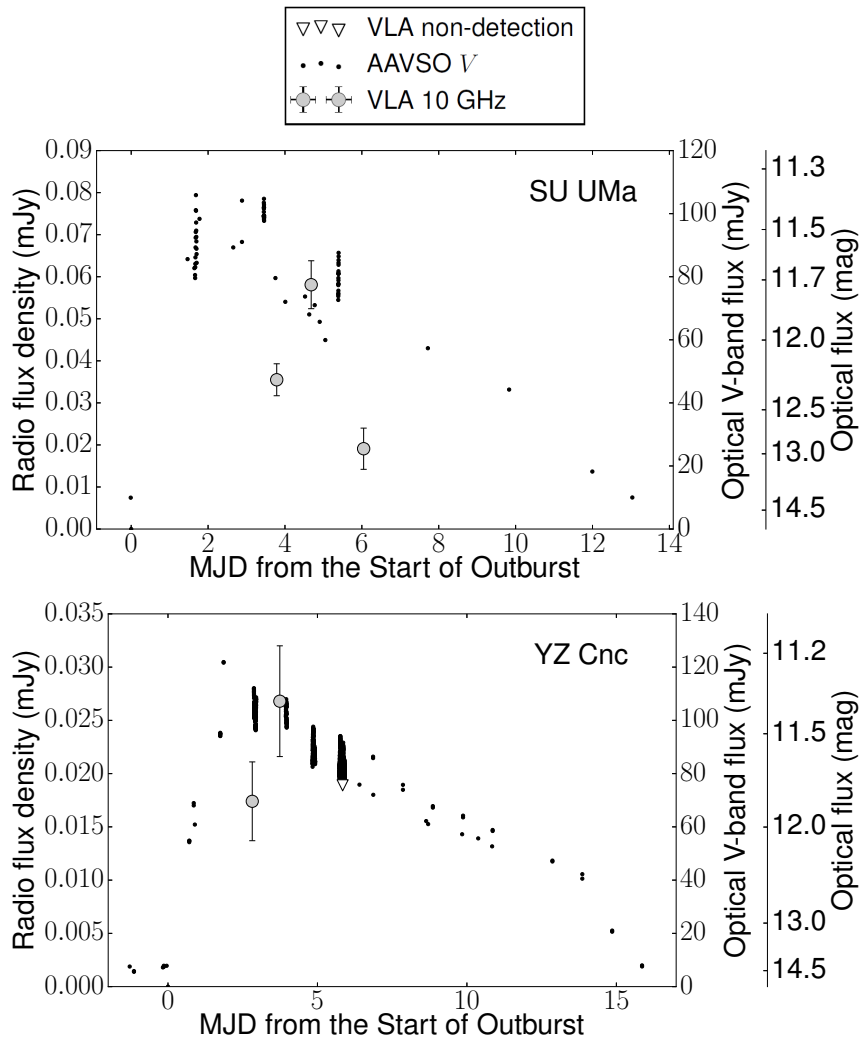


Figure 5.1 continued...

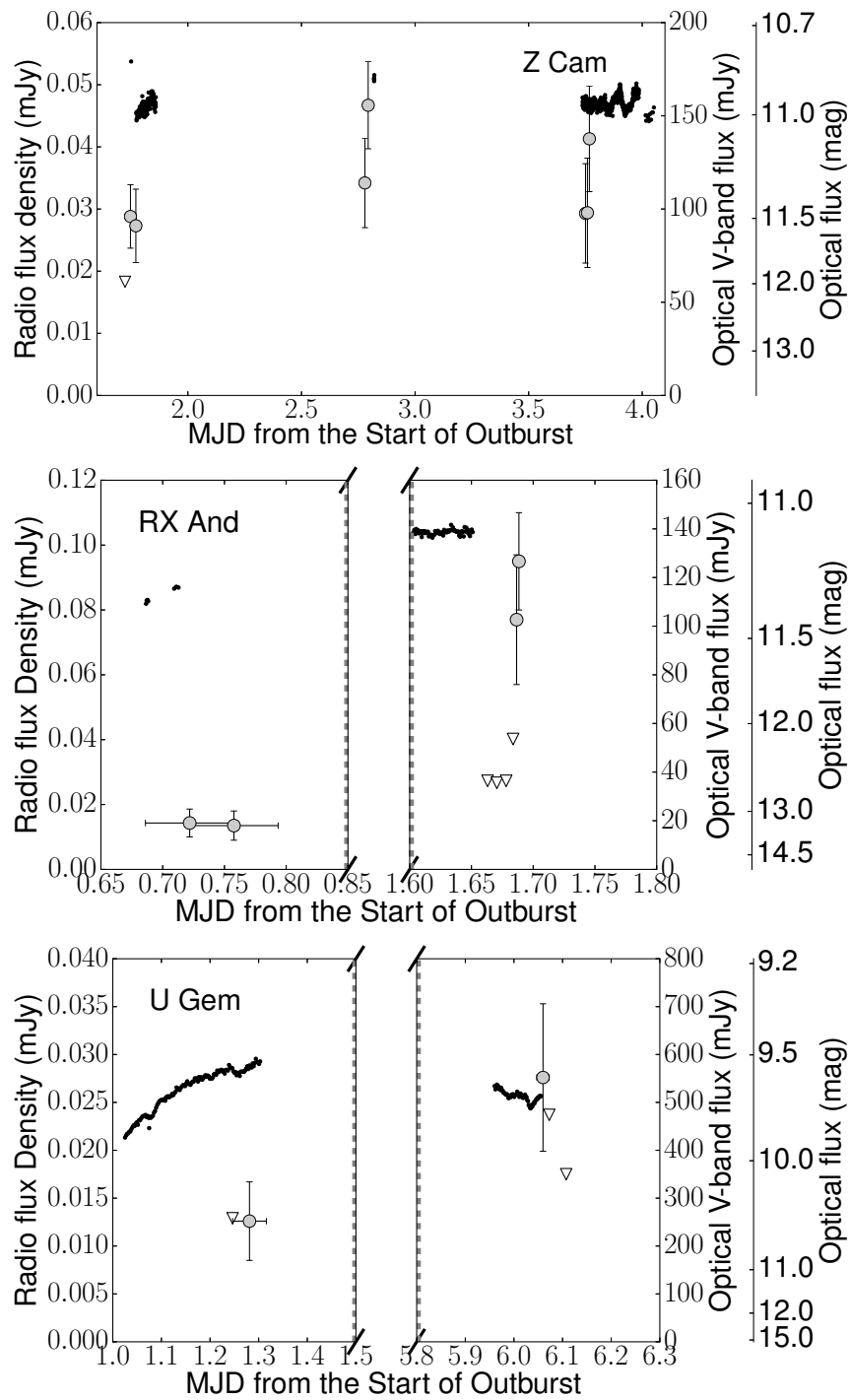


FIGURE 5.2: Radio (10 GHz) observations split into shorter integrations, to show the shorter timescale variability. SU UMA and YZ Cnc are shown on the following page. The fluxes and integration times for these light curves are given in Table 5.5. All optical V-band observations are from the AAVSO International Database (see <http://www.aavso.org>). Observation 3 of RX And and SU UMA have been omitted for clarity: The former was not detected and the latter did not show statistically significant variability.

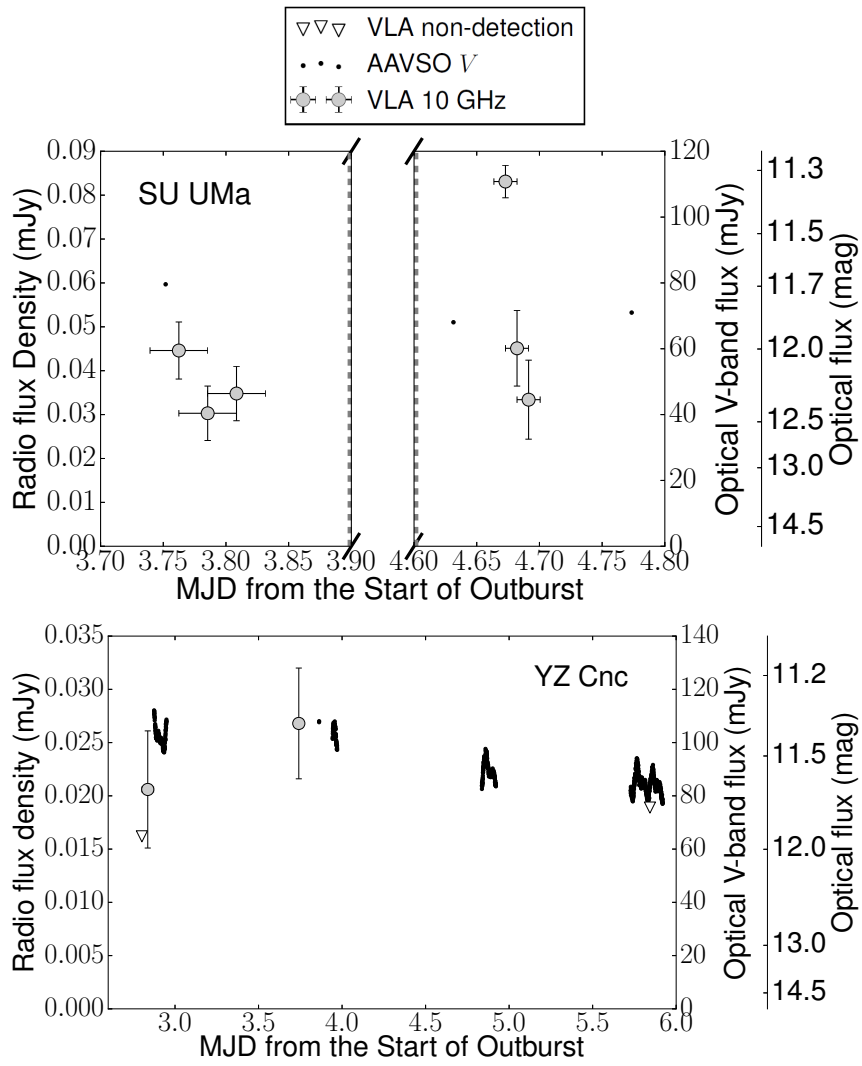


Figure 5.2 continued...

TABLE 5.4: Spectral indices

Object	Obs.	Band (MHz)	Flux Density (μJy)	Spectral Index ($F \propto \nu^\alpha$)	Reduced χ^2
Z Cam	1	7976 – 10024	24.2 ± 4.0	0.3 ± 1.2	-
		9976 – 12024	25.5 ± 4.7		
Z Cam	2	7976 – 10024	37.2 ± 6.7	0.9 ± 1.2	-
		9976 – 12024	44.6 ± 6.6		
Z Cam	3	7976 – 9000	38.5 ± 9.1	-0.1 ± 1.1	0.18
		9000 – 10024	39.0 ± 9.3		
		9976 – 11000	32.5 ± 9.2		
		11000 – 12024	41.0 ± 14.0		
RX And	2, flare ^a	7976 – 10024	10.3 ± 3.3	4.2 ± 1.3	-
		9976 – 12024	19.8 ± 4.2		
SU UMa	1	7976 – 9000	30.7 ± 7.0	1.0 ± 0.9	2.5
		9000 – 10024	31.7 ± 7.1		
		9976 – 11000	50.2 ± 6.9		
		11000 – 12024	32.0 ± 7.4		
SU UMa	2	7976 – 9000	60.7 ± 9.2	0.3 ± 0.6	0.84
		9000 – 10024	45.9 ± 9.5		
		9976 – 11000	59.8 ± 9.9		
		11000 – 12024	65.0 ± 9.9		
YZ Cnc	1, 2, 3	7976 – 10024	24.3 ± 3.6	-2.9 ± 1.5	-
		9976 – 12024	13.6 ± 3.7		

Spectral indices were calculated by fitting a power-law to the peak fluxes in the given frequency sub-bands. A 1σ error is given on the spectral index. U Gem did not have sufficient SNR to calculate the spectral index, and the observations of RX And (and YZ Cnc) were combined to increase SNR. ^aDuring the radio flare that occurred 1.7 days into the outburst (see Figure 5.2).

were represented in this sample, as well as systems in outburst and superoutburst. These results show that DN in outburst are radio emitters.

The maximum flux that SU UMa reached in our observations was $83.1 \pm 8.7 \mu\text{Jy}$, which is significantly fainter than the 1.3 mJy ⁷ detection of SU UMa in outburst by Benz et al. [1983]. Benz et al. observed SU UMa with Effelsberg at 4.75 GHz in two separate outbursts at 1–2 days after the optical peak (during the decline), and in quiescence. The combined outburst observations gave a detection at 1.3 mJy , and the quiescent observation produced an upper-limit of 0.4 mJy . Given the large discrepancy between the outburst flux measurements, we looked for sources of confusion within the $2.4'$ Effelsberg beamwidth in our higher resolution VLA images. One source⁸ (an unclassified object) with a flux density of $33 \pm 9 \mu\text{Jy}$ was within this beam, at $0.34'$ away from SU UMa. To produce a 1.3 mJy detection, this object would either need to have decreased in flux by a factor ~ 40 since 1982⁹, or have a spectral index of -3.7 ± 0.2 ($F_\nu \propto \nu^\alpha$). This source does not show variability on time-scales of days in our observations, but this does not eliminate the possibility that it was variable at the time of the Effelsberg observations. Nearby sources outside the beam were not sufficiently bright to account for the discrepancy. SU UMa was variable in our observations, and high-amplitude flares have been detected in SS Cyg [Körding et al., 2008; Miller-Jones et al., 2011; Russell et al., 2016]. It is therefore possible that SU UMa could have flared to 1.3 mJy , but as the Effelsberg detection was made in observations averaged from two separate outbursts, a flare should have been averaged out in these data. A decrease in flux over the decades between the observations could also explain the discrepancy, but the non-detections by Fuerst et al. [1986], Nelson & Spencer [1988] and Echevarria [1987] argue against this. It is also possible that our VLA observations resolved out some of the flux, as Effelsberg samples different spatial scales. Based on these arguments we cannot confirm, or refute, the validity of the historical 1.3 mJy outburst detection of SU UMa.

It is not yet clear whether DN are radio emitters in quiescence. The only CV for which we have high-sensitivity radio observations during quiescence is SS Cyg, and it was not detected down to a 3-sigma upper-limit of $89 \mu\text{Jy}$ [Körding et al., 2008]. All three historical radio detections (SU UMa, EM Cyg and TY PSc) were made during outburst, so there is circumstantial evidence indicating that the radio emission during outburst is brighter. High-sensitivity observations of quiescent DN are necessary to determine if the radio luminosities are fainter in quiescence.

5.5.2 Radio Emission Mechanism in DN Outbursts

As discussed in Section 5.1, various mechanisms to produce synchrotron, thermal and coherent radio emission in non-magnetic CVs have been suggested. In the novalikes, the radio emission is non-thermal, and is consistent with synchrotron or coherent emission [Coppejans et al., 2015b]. In the DN SS Cyg, the radio emission in outburst is explained as synchrotron emission from a transient jet [Körding et al., 2008; Miller-Jones et al., 2011; Russell et al., 2016]. We now discuss what type of radio emission is seen in our sample of DN.

⁷Based on Figure 2 in Benz et al. [1983] we judge the noise to be $\sim 230 \mu\text{Jy}/\text{beam}$

⁸at RA_{J2000} = 08:12:26, Dec_{J2000} = +62:36:36

⁹Assuming a flat spectral index between 4.75 and 10 GHz, and a gaussian fall-off in beam sensitivity

The emission region would need to have a radius that is $\sim 10^2 - 10^3$ larger than the orbital separation to produce the flux densities we observe, if it is optically thick thermal emission from an ionised gas at a typical brightness temperature of $10^4 - 10^5 \text{ K}$ ¹⁰. In this sample the smallest possible emission region would therefore be on the order of $1 \times 10^{13} \text{ cm}$. Wind speeds in CVs have been measured up to 5000 km s^{-1} [e.g. Kafka et al., 2009]. Even assuming an extremely fast wind of speed 10^4 km s^{-1} , the shortest time on which changes can be propagated over the emission region, is approximately 170 minutes. As we observe variability on timescales down to 4 minutes in this sample, the observed radio emission can not be optically thick thermal emission.

If it is optically thin thermal emission, it is unlikely to be reprocessed optical radiation from the CV (e.g. by a surrounding gas cloud), as the radio light curves do not follow the optical light curves. Following the arguments in K rding et al. [2008], the radio emission would need to be produced directly by an outflow (either a wind or jet). The upper-limit on the mass accretion rate in DN in outburst is $\sim 10^{-8} M_{\odot} \text{ y}^{-1}$, so this sets the maximum mass flow rate of the outflow (if none of the matter were accreted¹¹). From Equation 8 in Wright & Barlow [1975], the upper-limit on the optically thin thermal flux density from a uniform velocity wind (with a speed on the order of 10^3 km s^{-1}) with this flow rate is $\sim 1 \mu\text{Jy}$. Even if all the accreted material were carried off in a wind, the optically thin thermal emission would be insufficient to produce the flux densities we observe.

Synchrotron emission or coherent emission are both consistent with the observations, but as we detected no circular or linear polarization down to 3-sigma upper-limits of $\approx 10\%$, we conclude that the observed radio emission is more likely to be synchrotron. For Z Cam there is additional support for this, as Harrison [2014] found that Z Cam is a synchrotron source at mid-infrared frequencies, based on observations from the WISE mission [Wide-field Infrared Survey Explorer, Wright et al., 2010]. Near the peak of the visual outburst, they detected rapid variability with an amplitude of $\sim 2.5 \text{ mJy}$ at $12 \mu\text{m}$ (*W3* band), and only marginal variability at shorter wavelengths. Based on this, they concluded that the emission is most likely a synchrotron jet. The flux density of the $12 \mu\text{m}$ emission peaked at $5.0 \pm 0.5 \text{ mJy}$. In comparison, our 10 GHz radio observations were significantly fainter, peaking at a flux density of $0.0467 \pm 0.0007 \text{ mJy}$. If the $12 \mu\text{m}$ variability of $\sim 2.5 \text{ mJy}$ corresponds to a rise in the jet emission, this would suggest that the spectral index must be relatively inverted, $\alpha \gtrsim 0.6$. Spectral indices of 0.6–0.8 have been seen at some epochs for the synchrotron jets of MAXI J1836–194 [Russell et al., 2013]. Harrison [2014] also report a potential $160 \pm 50 \text{ mJy}$ detection with IRAS at $12 \mu\text{m}$ at the peak of a Z Cam outburst. If the marginal IRAS detection is real, the spectral index could be even more inverted. Given both the variable nature of the source, and the potential for a spectral break between radio and mid-IR wavelengths, we caution against over interpreting the spectral index.

For the DN SS Cyg (a U Gem-type DN), the synchrotron emission is produced by a transient jet [K rding et al., 2008; Miller-Jones et al., 2011; Russell et al., 2016]. Russell et al. [2016] compared the radio outbursts of SS Cyg over different outbursts and showed that the radio behaviour does not vary significantly between outbursts. The radio luminosity peaked on the rise to outburst (within 0.5-2 days after SS Cyg reached $V = 10 \text{ mag}$), decreased over the course of

¹⁰See Equation 4.5.1

¹¹and no additional matter from the WD were to be ejected

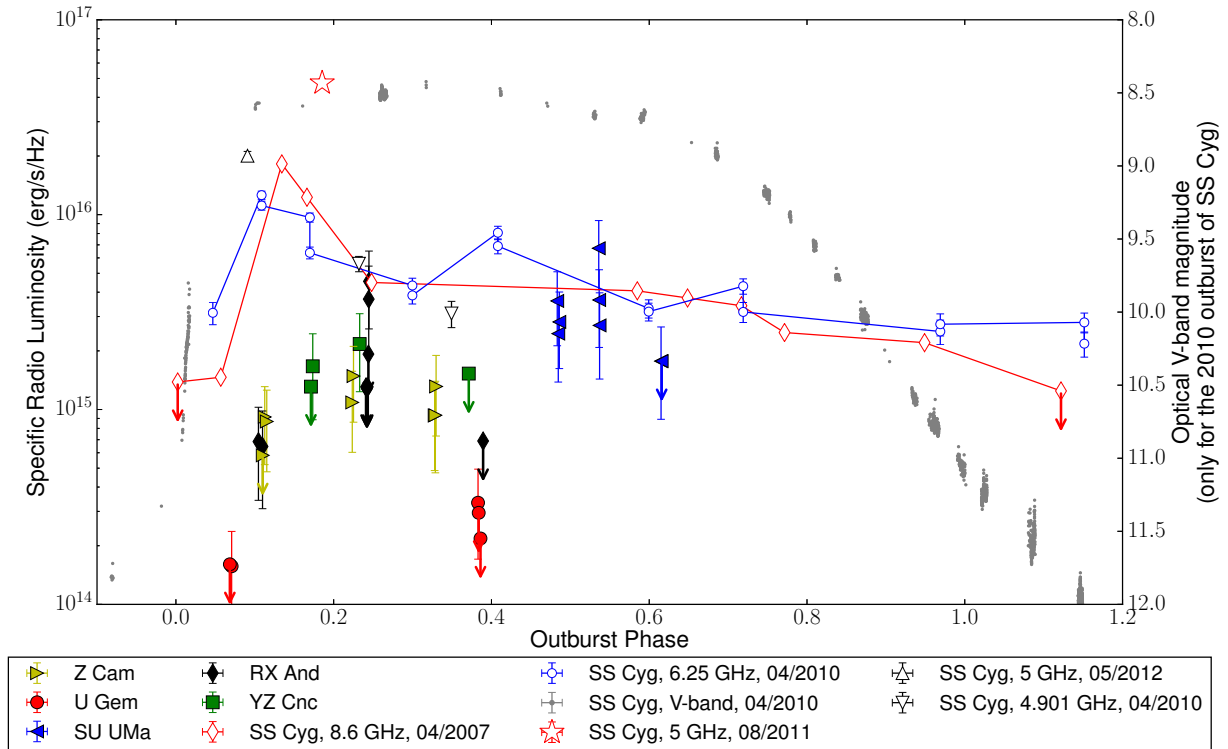
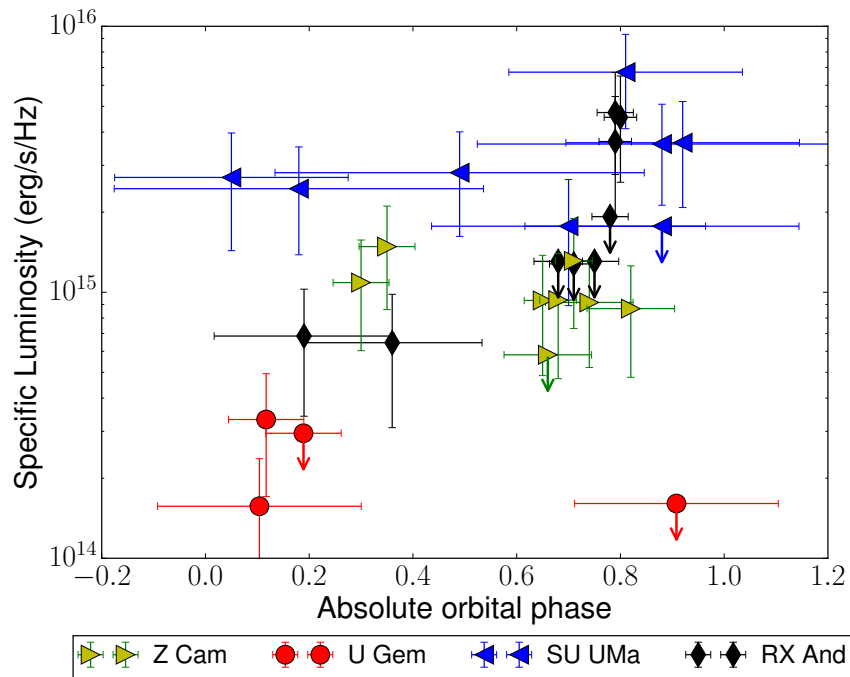


FIGURE 5.3: Specific radio luminosity of DN as a function of outburst phase. For comparison purposes, the start of the outburst (phase 0) is defined as the point on the rise to outburst at which it is $V = 1$ mag brighter than in quiescence, and the end (phase 1) is the equivalent point on the decline. In the two superoutbursts (SU UMa and YZ Cnc), phase zero is defined during the precursor outburst. The radio observations of SS Cyg are from K rding et al. [2008]; Miller-Jones et al. [2011, 2013] and Russell et al. [2016]. For clarity, not all previous radio observations of SS Cyg are plotted; the full light curve is in Russell et al. [2016]. Note that Russell et al. set phase 0 of the outburst to the time at which SS Cyg reached $V = 10$ mag (which is 2 mag brighter than the quiescence level), so our definitions of the outburst phase differ. We do not use the same phasing definition here, as the outburst magnitudes and amplitudes differed between the sources. The optical V -band data for SS Cyg are from the AAVSO international database. Note that the optical axis only refers to the V -band data for the 2010 outburst of SS Cyg; it does not give the simultaneous optical magnitude for any other outburst. For a colour version of this figure, please see the online material.



the outburst and was subsequently not detected in quiescence. Near the peak of an outburst, extreme radio flares (in excess of the already increased radio emission during the outburst) were detected. Based on the analogy between the outburst states in DN and XRBs, this behaviour is characteristic of a jet [Körding et al., 2008].

Figure 5.3 shows the radio lightcurves of our sample of DN with those of SS Cyg, as a function of the outburst phase. We now compare and contrast the radio lightcurves of the DN to SS Cyg.

In three of the DN we observed variability on time-scales of days to minutes. This is consistent with SS Cyg, which has been observed to vary on timescales of days down to 30 minutes [Russell et al., 2016]. The orbital period of DN is on the order of hours, and orbital modulations on shorter timescales are observed at other wavelengths in CVs. If the radio emission in the DN were to show an orbital phase dependence, it would isolate the emission region in the binary. Figure 5.4 shows the specific radio luminosity phased according to the orbital period (P_{orb}). As was the case for SS Cyg, the emission shows no orbital phase dependence.

SS Cyg shows increasing radio emission on the rise to optical outburst, followed by a radio flare that lasts a few hours [Russell et al., 2016]. We did not detect a high-amplitude radio flare like that of SS Cyg in our observations, but we could have missed it given our sampling cadence, as our observations were 1–2 hours long and separated by a day or two (see Table 5.2). U Gem was observed at a corresponding earlier phase in the outburst, and was then observed 5 days later. If the radio emission in U Gem followed the same template as SS Cyg, then the sampling could also explain the low luminosity. Note that we do not consider the brightening in RX And at 1.7 days into the outburst (phase 0.25) to be equivalent to the high-amplitude flare in SS Cyg. It has a comparatively lower amplitude to SS Cyg (although this could be explained by sampling), but more importantly it occurs later in the outburst. From simultaneous X-ray observations, Russell et al. [2016] found that the radio flare in SS Cyg was coincident with the initial disc material hitting the boundary layer. This condition occurs before phase 0.25 in the outburst.

For a full comparison to SS Cyg, higher-cadence radio observations throughout the outburst are necessary. From these observations it is clear that SS Cyg is not unique in the type of radio emission, the luminosity (in the plateau phase¹²), or the variability time-scales. Higher cadence observations during the rise phase, and during later phases, of the outburst are still needed to test the extent to which the radio emission in DN follows the SS Cyg synchrotron-jet template.

5.5.3 What Determines the Radio Luminosity?

It is not yet clear what parameter determines the radio luminosity of a non-magnetic CV. In the XRBs and AGN, the radio emission in the hard state is directly correlated with the power liberated in the accretion flow [Körding et al., 2006]. Körding et al. [2008] have suggested that the same is true in CVs.

One proxy for the liberated power is the optical luminosity of the CV. In Figure 5.5, the radio specific luminosity range is plotted as a function of the quasi-simultaneous optical specific luminosity. Contrary to what we would expect by analogy to the XRBs and AGN, the radio and optical luminosity are not correlated. As the radio emission in non-magnetic CVs can be highly

¹²After phase 0.3 in Figure 5.3

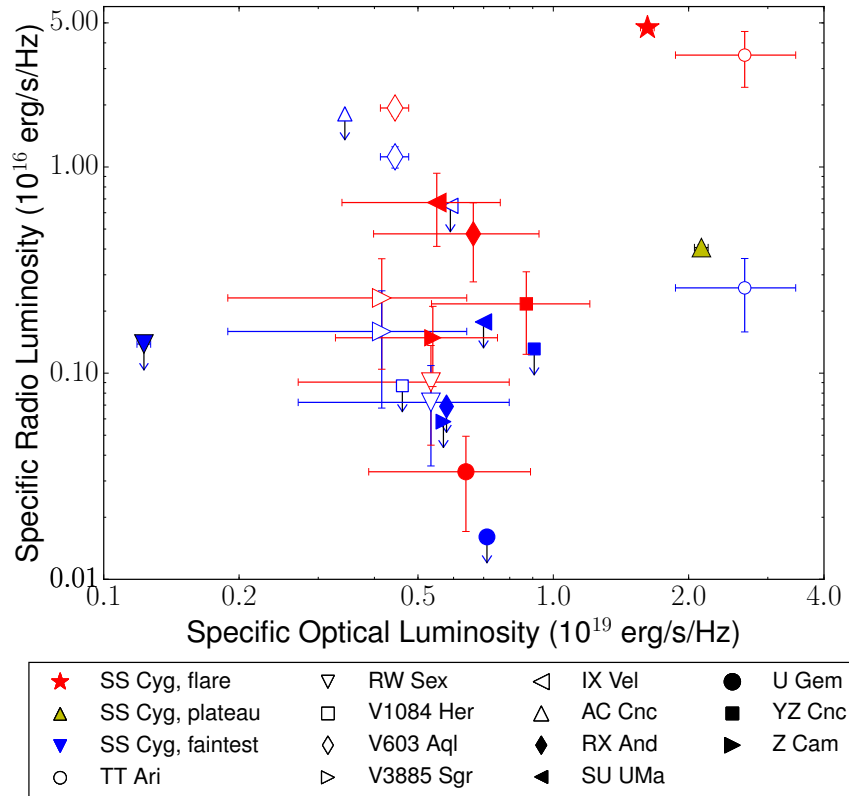


FIGURE 5.5: Distribution of the radio and quasi-simultaneous optical luminosities of all recent, high-sensitivity observations of non-magnetic CVs. The DN (solid symbols) and novalikes (empty symbols) occupy the same phase space. As most of the sources are variable, we plot only the brightest (red) and faintest (blue) radio detection (or most constraining upper-limit) for each source. The optical luminosities (from the AAVSO international database) are quasi-simultaneous to the radio observations. The brightest detection of TT Ari was during a flare with a circular polarization fraction of more than 75%, which is in contrast to the other sources which had circular polarization fraction upper-limits of $\sim 10\%$. Radio fluxes were taken from Miller-Jones et al. [2011], Körding et al. [2008] and Russell et al. [2016] (SS Cyg), Coppejans et al. [2015b] (V1084 Her, RW Sex, V603 Aql and TT Ari) and Körding et al. [2011] (V3885 Sgr and IX Vel). A colour version of this figure is available online.

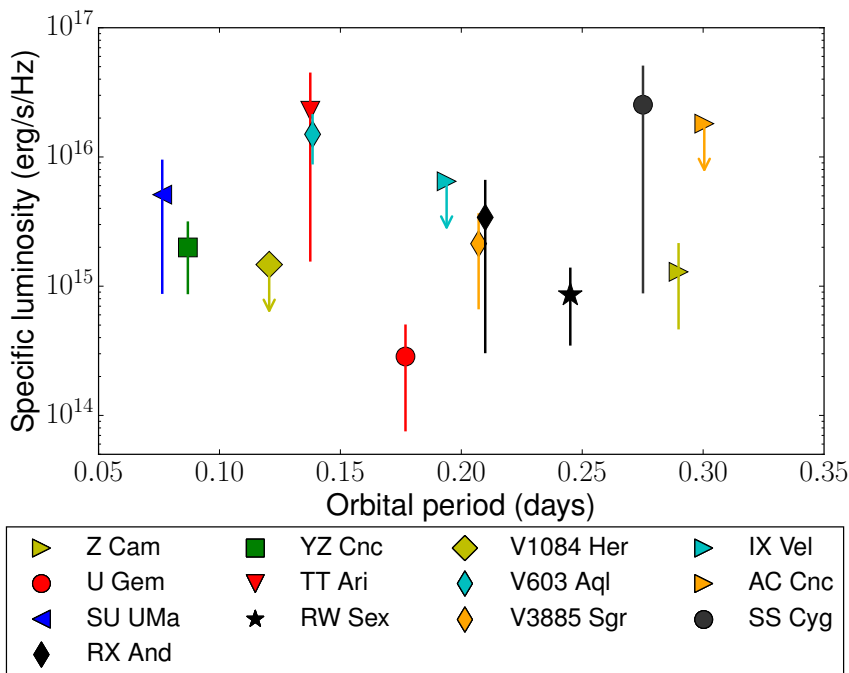


FIGURE 5.6: The radio luminosity of non-magnetic CVs is not correlated with orbital period. The error bars indicate the variability range. All high-sensitivity detections of non-magnetic CVs are plotted (this work, K rding et al. 2008; Miller-Jones et al. 2011, 2013; Coppejans et al. 2015b; Russell et al. 2016). For a colour version of this figure please see the online material.

variable however (see Section 5.4.2, Coppejans et al. 2015b; Russell et al. 2016), sampling effects could be masking an underlying correlation.

Extrapolating from the XRBs, K rding et al. [2008] estimated that the specific radio luminosity at 10 GHz ($L_{10\text{GHz}}$ in $\text{erg s}^{-1} \text{Hz}^{-1}$) should be related to the mass accretion rate (\dot{M}) by

$$L_{10\text{GHz}} \approx 1.5 \times 10^{24} \frac{\dot{M}}{M_{\odot} \text{y}^{-1}}. \quad (5.1)$$

The mass accretion rate for DN in outburst is estimated to be in the range 10^{-10} – $10^{-8} M_{\odot} \text{y}^{-1}$ (this is model-dependent and is a function of the orbital period, e.g. Knigge et al. 2011). This predicts a specific radio luminosity of 1×10^{14} – $1 \times 10^{16} \text{erg s}^{-1} \text{Hz}^{-1}$, which is consistent with the observed luminosities.

To establish whether the radio luminosity correlates with the power liberated in the accretion flow, a relative measure of the accretion rate of our systems is necessary. Unfortunately this is not known, as it is difficult to measure in DN.

In our sample we have DN from the three DN-subclasses (U Gem, Z Cam and SU UMa), the novalikes, and observations taken during outburst and superoutburst. As the different classes of CV are predicted to have different secular mass-accretion rates, we looked for a correlation between the radio luminosity and the CV-class. Figure 5.5 does not show this correlation. There were no clear distinctions in the luminosity between the three DN sub-classes, novalikes, or different outburst types, and there was no one class or outburst type that was consistently fainter or brighter. Similarly, plotting the radio luminosity range for each CV as a function of P_{orb} (Figure

5.6) does not show a correlation. The accretion rate in CVs, however, is known to vary significantly on time-scales that are significantly shorter than the secular time-scales [e.g. Livio & Pringle, 1994; Smak, 2004], due to e.g. variations in the mass transfer rate from the secondary star [King et al., 1995, 1996] or nova eruptions [MacDonald, 1986; Shara et al., 1986]. To determine if the radio luminosity is correlated with the accretion flow power, we consequently need measurements of the instantaneous accretion rate for these CVs.

For completeness, we also compared the radio emission properties in the different CV, and outburst, classes. In each class or outburst type there was at least one CV that was variable on timescales down to minutes (RX And, SU UMa, SS Cyg, TT Ari, V603 Aql). The spectral index was unfortunately not constrained in the DN, so we could not make a comparison on this basis. In all cases, the observed emission was non-thermal, and was consistent with synchrotron or coherent emission. High levels of circular polarization (CP) have been detected in two non-magnetic CVs in different classes. In the novalike TT Ari, the CP fraction peaked at more than 75% and lasted approximately 10 minutes [Coppejans et al., 2015b]. In the Z Cam-type DN EM Cyg [Benz & Guedel, 1989] the polarization fraction peaked at 81% in one of the two observations (which were separated by 37 hours). In both cases the radio emission was coherent. The rest of the recent, high-sensitivity observations of non-magnetic CVs have CP fractions $\leq 10\text{-}20\%$, and linear polarization fractions $\leq 6\text{-}15\%$. In this sample we do not see a difference in the radio luminosity or properties between the novalikes, different classes of DN, or different classes of outbursts.

Apart from the accretion flow power, other properties such as the WD mass, WD magnetic field strength, inclination angle, or the surrounding medium could affect the radio luminosity. These properties are insufficiently well-constrained in this sample to test this. To determine what property sets the radio luminosity, high cadence observations of a larger sample of CVs with well-determined properties are necessary.

5.6 Summary

Radio emission at a frequency of 8–12 GHz was detected in all five of the DN (Z Cam, RX And, SU UMa, YZ Cnc and U Gem) that we observed in outburst, which increases the number of radio-detected CVs by a factor of two and proves that DN in outburst are radio emitters with specific luminosities in the range $L_{10\text{GHz}} \sim 10^{14}\text{--}10^{16} \text{ erg s}^{-1} \text{ Hz}^{-1}$ at 10 GHz (luminosities of $10^{24}\text{--}10^{26} \text{ erg s}^{-1}$). The emission is variable, and is in excess of the radio emission expected from the CV components (WD, disc and secondary star). Previous radio surveys of DN did not have the sensitivity required to detect these objects, which explains why the detection rate was so low in historical surveys. Combined with the finding that the novalike systems are radio emitters [Coppejans et al., 2015b], this indicates that, as a class, non-magnetic CVs are radio emitters.

The emission is consistent with synchrotron or coherent emission, but it is more likely to be synchrotron emission, as the upper-limits on the polarization fraction are on the order of $\sim 10\%$, and coherent emission is associated with high levels of polarization. In Z Cam, there is additional support for this, as synchrotron emission at mid-infrared frequencies has been detected by Harrison [2014].

The DN SS Cyg is a radio synchrotron source in outburst [Körding et al., 2008; Miller-Jones

et al., 2011; Russell et al., 2016] and the emission has been found to originate from a transient jet [Körding et al., 2008; Miller-Jones et al., 2011; Russell et al., 2016]. We compared the radio emission of our sample of DN to that of SS Cyg, and found that SS Cyg is not unique in the type of radio emission, the luminosity (in the plateau phase), or the variability time-scales (minutes to days). SS Cyg shows rising radio emission on the rise to outburst followed by a radio flare (a key prediction of the jet-launching model, Körding et al. 2008). Although we did not detect a clear equivalent rise in our observations (or a high-amplitude flare), the sampling cadence was insufficient to rule it out. Higher cadence observations over the course of an outburst (and in quiescence) are necessary to establish the radio light-curve template for the DN as a class. High spatial resolution radio observations are needed to resolve extended emission and establish whether CVs, as a class, launch jets.

It is not yet clear what physical property is responsible for setting the radio luminosity. The observed radio luminosity of our sample is consistent with that predicted in Körding et al. [2008] from outflows based on the accretion-luminosity scaling relations in XRBs and AGN. Since the mass accretion rates in DN are not well determined, we could not test whether the accretion rate is correlated with the radio luminosity, as predicted for an outflow. In this sample there was no correlation between the radio luminosity and optical luminosity (a proxy for the outflow power), the orbital phase or the orbital period. Additionally we did not find any clear distinctions in the radio emission between the different DN classes, novalikes, or normal outbursts and super-outbursts. As our work and that of Körding et al. [2008], Coppejans et al. [2015b], Miller-Jones et al. [2011] and Russell et al. [2016] shows, CVs are highly variable and the measured luminosity depends on the sampling time. The low cadence of observations in our sample (relative to either the one well-sampled DN, SS Cyg, or the evolving physical parameters,) could consequently mask any underlying correlations.

Acknowledgements

This work is part of the research programme NWO VIDI grant No. 2013/15390/EW, which is financed by the Nederlandse Organisatie voor Wetenschappelijk Onderzoek (NWO). DLC gratefully acknowledges funding from the Erasmus Mundus Programme SAPIENT. JCAMJ is the recipient of an Australian Research Council Future Fellowship (FT140101082). GRS acknowledges support from an NSERC Discovery Grant. CK is grateful for support from the Science and Technology Facilities Council under grant ST/M001326/1 and from the Leverhulme Trust for the award of a Research Fellowship. PAW thanks UCT and the NRF for financial support.

The authors are grateful to the observers from the American Association of Variable Star Observers (AAVSO), whose observations and notifications were crucial to this research. We would like to especially thank the following observers for their significant contributions: Umair Asim, Douglas Barrett, Paul Benni, Richard Campbell, Shawn Dvorak, Tonis Eenmae, Steve Gagnon, Josch Hamsch, Dave Hinz, Laszlo Kocsmaros, Mike Linnolt, Walter MacDonald, Chris Maloney, Vance Petriew, Gary Poyner, Anthony Rodda, Paolo Ruscitti, Rod Stubbings, Glenn Thurman, John Toone, Brad Vietje and Brad Walter.

The National Radio Astronomy Observatory is a facility of the National Science Foundation

CHAPTER 5 : DWARF NOVAE ARE SIGNIFICANT RADIO EMITTERS

operated under cooperative agreement by Associated Universities, Inc. This research has made use of NASA's Astrophysics Data System Bibliographic Services, as well as the SIMBAD data base, operated at CDS, Strasbourg, France (Wenger et al. 2000).

5.A Subappendix

TABLE 5.5: Higher time resolution

Object	Obs.	MJD (mid-exposure)	Orbital phase ^a (mid-exposure)	Integration time (s)	Flux Density (μ Jy)
Z Cam	1	56986.12344	0.66 ± 0.02^b	2053	<18.3
	1	56986.14720	0.74 ± 0.02^b	2053	28.8 ± 5.1
	1	56986.17096	0.82 ± 0.02^b	2053	27.3 ± 5.9
Z Cam	2	56987.17910	0.30 ± 0.02^b	1254	34.2 ± 7.2
	2	56987.19361	0.35 ± 0.02^b	1254	46.7 ± 7.0
Z Cam	3	56988.15027	0.65 ± 0.02^b	737	29.3 ± 8.0
	3	56988.15880	0.68 ± 0.02^b	737	29.4 ± 8.8
	3	56988.16733	0.71 ± 0.02^b	737	41.3 ± 8.5
RX And	1	56969.42185	0.19 ± 0.03^c	3095	14.3 ± 4.3
	1	56969.45768	0.36 ± 0.03^c	3094	13.5 ± 4.5
RX And	2	56970.36307	0.68 ± 0.03^c	650	<27.3
	2	56970.37059	0.71 ± 0.03^c	650	<26.7
	2	56970.37811	0.75 ± 0.03^c	650	<27.3
	2	56970.38375	0.78 ± 0.03^c	325	<40.2
	2	56970.38657	0.79 ± 0.03^c	163	77.0 ± 20.0
	2	56970.38846	0.80 ± 0.03^c	163	95.0 ± 15.0
SU UMa	1	57027.16243	0.88 ± 0.19^d	1986	44.6 ± 6.5
	1	57027.18542	0.18 ± 0.19^d	1986	30.3 ± 6.2
	1	57027.20840	0.49 ± 0.19^d	1986	34.8 ± 6.2
SU UMa	2	57028.07291	0.81 ± 0.19^d	797	83.1 ± 8.7
	2	57028.08213	0.92 ± 0.19^d	797	45.1 ± 8.6
	2	57028.09135	0.05 ± 0.19^d	797	33.4 ± 9.0
SU UMa	3	57029.43929	0.70 ± 0.19^d	1210	21.9 ± 6.9
	3	57029.45330	0.88 ± 0.19^d	1210	<21.9
YZ Cnc	1	56984.30181	$0^{e,f}$	3024	<16.2
	1	56984.33681	$0.40265 \pm 0.00003^{e,f}$	3024	20.6 ± 5.5
U Gem	1	57075.34642	0.908 ± 0.002^g	3000	<12.9
	1	57075.38115	0.104 ± 0.002^g	3000	12.6 ± 4.1
U Gem	2	57080.15979	0.117 ± 0.002^g	1110	27.0 ± 7.7
	2	57080.17264	0.189 ± 0.002^g	1110	<23.7

Notes: When the SNR of an observation (in Table 5.3) was sufficiently high, we split it in time to probe the variability on shorter time-scales. Any observation not listed in the table did not have a sufficiently high SNR.

^aThe orbital phase is absolute unless indicated otherwise, and phase zero corresponds to inferior conjunction. Note that the uncertainty on the orbital phase is calculated at mid-exposure, it does not taken the integration time into account. The ephemerides used are from ^bThorstensen & Ringwald [1995], ^cKaitchuck [1989], ^dHJD = 2450247.986(3)+0.07637533(13) (updated ephemeris from Thorstensen et al. [1986], private communication with John Thorstensen), ^evan Paradijs et al. [1994] and ^gMarsh et al. [1990] updated in Echevarria et al. [2007]. ^fPhase relative to JD 2456984.801806, as the error on the absolute phase exceeds 0.5 and a recent ephemeris is not available.

BIBLIOGRAPHY

- Abada-Simon, M. & Aubier, M. 1997, *Radio burst statistics for M dwarf flare stars*, A&AS, 125, 511
- Abada-Simon, M., Lecacheux, A., Bastian, T. S., Bookbinder, J. A., & Dulk, G. A. 1993, *The spectrum and variability of radio emission from AE Aquarii*, ApJ, 406, 692
- Aihara, H., Allende Prieto, C., An, D., et al. 2011, *The Eighth Data Release of the Sloan Digital Sky Survey: First Data from SDSS-III*, ApJS, 193, 29
- Ak, T., Bilir, S., Ak, S., & Eker, Z. 2008, *Spatial distribution and galactic model parameters of cataclysmic variables*, New A, 13, 133
- Andronov, I. L., Ostrova, N. I., Kim, Y.-G., & Burwitz, V. 2005, *Two-Color VR CCD Photometry of Old Nova V603 Aquilae*, Journal of Astronomy and Space Sciences, 22, 211
- Andronov, N., Pinsonneault, M., & Sills, A. 2003, *Cataclysmic Variables: An Empirical Angular Momentum Loss Prescription from Open Cluster Data*, ApJ, 582, 358
- Arenas, J., Catalán, M. S., Augusteijn, T., & Retter, A. 2000, *A spectroscopic study of V603 Aquilae: stellar parameters and continuum-line variations*, MNRAS, 311, 135
- Balbus, S. A., Gammie, C. F., & Hawley, J. F. 1994, *Fluctuations, dissipation and turbulence in accretion discs*, MNRAS, 271
- Balbus, S. A. & Hawley, J. F. 1991, *A powerful local shear instability in weakly magnetized disks. I - Linear analysis. II - Nonlinear evolution*, ApJ, 376, 214
- Barnes, S. A. 2003, *On the Rotational Evolution of Solar- and Late-Type Stars, Its Magnetic Origins, and the Possibility of Stellar Gyrochronology*, ApJ, 586, 464
- Baskill, D. S., Wheatley, P. J., & Osborne, J. P. 2005, *The complete set of ASCA X-ray observations of non-magnetic cataclysmic variables*, MNRAS, 357, 626
- Bastian, T. S., Dulk, G. A., & Chanmugam, G. 1988, *Radio flares from AE Aquarii - A low-power analog to Cygnus X-3?*, ApJ, 324, 431
- Bath, G. T. 1975, *Dynamical instabilities and mass exchange in binary systems*, MNRAS, 171, 311
- Bath, G. T. & Pringle, J. E. 1981, *The evolution of viscous discs. I - Mass transfer variations*, MNRAS, 194, 967
- Bell, M. E., Huynh, M. T., Hancock, P., et al. 2015, *A search for variable and transient radio*

BIBLIOGRAPHY

- sources in the extended Chandra Deep Field South at 5.5 GHz*, MNRAS, 450, 4221
- Belloni, T. M., Motta, S. E., & Muñoz-Darias, T. 2011, *Black hole transients*, Bulletin of the Astronomical Society of India, 39, 409
- Benz, A. O., Fuerst, E., & Kiplinger, A. L. 1983, *First detection of radio emission from a dwarf nova*, Nature, 302, 45
- Benz, A. O., Gudel, M., & Mattei, J. A. 1996, *Radio Emission of Dwarf Novae*, in Astronomical Society of the Pacific Conference Series, Vol. 93, Radio Emission from the Stars and the Sun, ed. A. R. Taylor & J. M. Paredes, 188
- Benz, A. O. & Guedel, M. 1989, *VLA detection of radio emission from a dwarf nova*, A&A, 218, 137
- Bertin, E. & Arnouts, S. 1996, *SExtractor: Software for source extraction.*, A&AS, 117, 393
- Beuermann, K., Stasiewski, U., & Schwöpe, A. D. 1992, *Phase-resolved spectroscopy of the novalike cataclysmic variable RW Sextantis*, A&A, 256, 433
- Bode, M. F. 2010, *The outbursts of classical and recurrent novae*, Astronomische Nachrichten, 331, 160
- Bookbinder, J. A. & Lamb, D. Q. 1987, *Discovery of radio emission from AE Aquarii*, ApJ, 323, L131
- Borczyk, W., Schwarzenberg-Czerny, A., & Szkody, P. 2003, *Variability of The Old Nova V603 Aquilae in UV and X-ray bands*, A&A, 405, 663
- Borne, K. 2013, Virtual Observatories, Data Mining, and Astroinformatics, ed. T. D. Oswalt & H. E. Bond, 403
- Breedt, E., Gänsicke, B. T., Drake, A. J., et al. 2014, *1000 cataclysmic variables from the Catalina Real-time Transient Survey*, MNRAS, 443, 3174
- Britt, C. T., Maccarone, T., Pretorius, M. L., et al. 2015, *The relationship between X-ray luminosity and duty cycle for dwarf novae and their specific frequency in the inner Galaxy*, MNRAS, 448, 3455
- Brocksopp, C., Sokoloski, J. L., Kaiser, C., et al. 2004, *A radio jet in the prototypical symbiotic star Z And?*, MNRAS, 347, 430
- Cannizzo, J. K. 1984, *Accretion disk limit cycle mechanism in twin-degenerate interacting binaries*, Nature, 311, 443
- Cannizzo, J. K. 1993, *The Limit Cycle Instability in Dwarf Nova Accretion Disks*, Advanced Series in Astrophysics and Cosmology, 9, 6
- Cannizzo, J. K. & Nelemans, G. 2015, *Constraining the Physics of AM Canum Venaticorum Systems with the Accretion Disk Instability Model*, ApJ, 803, 19
- Cannizzo, J. K., Smale, A. P., Wood, M. A., Still, M. D., & Howell, S. B. 2012, *The Kepler Light Curves of V1504 Cygni and V344 Lyrae: A Study of the Outburst Properties*, ApJ, 747, 117
- Cannizzo, J. K., Still, M. D., Howell, S. B., Wood, M. A., & Smale, A. P. 2010, *The Kepler Light Curve of V344 Lyrae: Constraining the Thermal-viscous Limit Cycle Instability*, ApJ, 725, 1393
- Ceraski, W. 1908, *Une variable nouvelle 5.1908 Ursae majoris*, Astronomische Nachrichten, 177, 173
- Chanmugam, G. 1987, *Radio emission from cataclysmic variables*, Ap&SS, 130, 53
- Chanmugam, G. & Dulk, G. A. 1982, *Radio emission from AM Herculis-type binaries*, ApJ, 255,

- L107
- Christensen, E., Larson, S., Boattini, A., et al. 2012, *The Catalina Sky Survey: Current and Future Work*, in AAS/Division for Planetary Sciences Meeting Abstracts, Vol. 44, AAS/Division for Planetary Sciences Meeting Abstracts, 210.13
- Copeland, H., Jensen, J. O., & Jorgensen, H. E. 1970, *Homogeneous Models for Population I and Population II Compositions*, A&A, 5, 12
- Coppejans, D. L., Koerding, E. G., Knigge, C., et al. 2015a, *Statistical properties of dwarf nova-type cataclysmic variables: The Outburst Catalogue*, ArXiv e-prints
- Coppejans, D. L., Körding, E. G., Miller-Jones, J. C. A., et al. 2015b, *Novalike cataclysmic variables are significant radio emitters*, MNRAS, 451, 3801
- Coppejans, D. L., Woudt, P. A., Warner, B., et al. 2014, *High-speed photometry of faint cataclysmic variables - VIII. Targets from the Catalina Real-Time Transient Survey*, MNRAS, 437, 510
- Coppejans, R., Gulbis, A. A. S., Kotze, M. M., et al. 2013, *Characterizing and Commissioning the Sutherland High-Speed Optical Cameras (SHOC)*, PASP, 125, 976
- Corbel, S., Fender, R. P., Tzioumis, A. K., et al. 2000, *Coupling of the X-ray and radio emission in the black hole candidate and compact jet source GX 339-4*, A&A, 359, 251
- Corbel, S., Kaaret, P., Jain, R. K., et al. 2001, *X-Ray States and Radio Emission in the Black Hole Candidate XTE J1550-564*, ApJ, 554, 43
- Cordova, F. A., Hjellming, R. M., & Mason, K. O. 1983, *A radio survey of cataclysmic variable stars using the very large array*, PASP, 95, 69
- Cowley, A. P., Crampton, D., Hutchings, J. B., & Marlborough, J. M. 1975, *TT ARIETIS - an evolved, very short period binary*, ApJ, 195, 413
- Cutri, R. M. & et al. 2012, *VizieR Online Data Catalog: WISE All-Sky Data Release (Cutri+2012)*, VizieR Online Data Catalog, 2311, 0
- Cutri, R. M., Skrutskie, M. F., van Dyk, S., et al. 2003, *VizieR Online Data Catalog: 2MASS All-Sky Catalog of Point Sources*, VizieR Online Data Catalog, 2246, 0
- de Martino, D., Sala, G., Balman, S., et al. 2015, *Dissecting accretion and outflows in accreting white dwarf binaries*, ArXiv e-prints
- Deneva, J. S., Ray, P. S., Camilo, F., et al. 2016, *Multiwavelength Observations of the Redback Millisecond Pulsar J1048+2339*, ApJ, 823, 105
- Dhillon, V. S., Smith, D. A., & Marsh, T. R. 2013, *The SW Sex enigma*, MNRAS, 428, 3559
- Djorgovski, S. G., Baltay, C., Mahabal, A. A., et al. 2008, *The Palomar-Quest digital synoptic sky survey*, Astronomische Nachrichten, 329, 263
- Djorgovski, S. G., Drake, A. J., Mahabal, A. A., et al. 2010, *Exploring the Variable Sky with the Catalina Real-Time Transient Survey*, in The First Year of MAXI: Monitoring Variable X-ray Sources, 32
- Djorgovski, S. G., Drake, A. J., Mahabal, A. A., et al. 2011, *The Catalina Real-Time Transient Survey (CRTS)*, ArXiv e-prints
- Donati, J.-F. & Landstreet, J. D. 2009, *Magnetic Fields of Nondegenerate Stars*, ARA&A, 47, 333
- Drake, A. J., Catelan, M., Djorgovski, S. G., et al. 2013, *Probing the Outer Galactic Halo with*

BIBLIOGRAPHY

- RR Lyrae from the Catalina Surveys*, ApJ, 763, 32
- Drake, A. J., Djorgovski, S. G., Mahabal, A., et al. 2009, *First Results from the Catalina Real-Time Transient Survey*, ApJ, 696, 870
- Drake, A. J., Gänsicke, B. T., Djorgovski, S. G., et al. 2014, *Cataclysmic variables from the Catalina Real-time Transient Survey*, MNRAS, 441, 1186
- Dubus, G., Hameury, J.-M., & Lasota, J.-P. 2001, *The disc instability model for X-ray transients: Evidence for truncation and irradiation*, A&A, 373, 251
- Dulk, G. A., Bastian, T. S., & Chanmugam, G. 1983, *Radio emission from AM Herculis - The quiescent component and an outburst*, ApJ, 273, 249
- Echevarria, J. 1987, *Multi-wavelength observations of dwarf novae during outburst*, Ap&SS, 130, 103
- Echevarria, J., de la Fuente, E., & Costero, R. 2007, *U Geminorum: A Test Case for Orbital Parameter Determination*, AJ, 134, 262
- Efron, B. 1979, *Bootstrap Methods: Another Look at the Jackknife*, Ann. Stat., 7, 1
- Evans, I. N., Primini, F. A., Glotfelty, K. J., et al. 2010, *The Chandra Source Catalog*, ApJS, 189, 37
- Falcke, H., K rding, E., & Markoff, S. 2004, *A scheme to unify low-power accreting black holes. Jet-dominated accretion flows and the radio/X-ray correlation*, A&A, 414, 895
- Faulkner, J., Lin, D. N. C., & Papaloizou, J. 1983, *On the evolution of accretion disc flow in cataclysmic variables. I - The prospect of a limit cycle in dwarf nova systems*, MNRAS, 205, 359
- Fender, R. & Belloni, T. 2012, *Stellar-Mass Black Holes and Ultraluminous X-ray Sources*, Science, 337, 540
- Fender, R. P. 2001, *Powerful jets from black hole X-ray binaries in low/hard X-ray states*, MNRAS, 322, 31
- Fender, R. P., Belloni, T. M., & Gallo, E. 2004, *Towards a unified model for black hole X-ray binary jets*, MNRAS, 355, 1105
- Flannery, B. P. 1975, *Gas flow in cataclysmic variable stars*, ApJ, 201, 661
- Fuerst, E., Benz, A., Hirth, W., Kiplinger, A., & Geffert, M. 1986, *Radio emission of cataclysmic variable stars*, A&A, 154, 377
- G nsicke, B. T., Dillon, M., Southworth, J., et al. 2009, *SDSS unveils a population of intrinsically faint cataclysmic variables at the minimum orbital period*, MNRAS, 397, 2170
- G nsicke, B. T., Sion, E. M., Beuermann, K., et al. 1999, *TT Arietis: the low state revisited*, A&A, 347, 178
- Girven, J., G nsicke, B. T., Steeghs, D., & Koester, D. 2011, *DA white dwarfs in Sloan Digital Sky Survey Data Release 7 and a search for infrared excess emission*, MNRAS, 417, 1210
- Gnedin, Y. N., Borisov, N. V., & Natsvlishvili, T. M. 1990, *The Intermediate Polar V603-AQUILAE*, Soviet Astronomy Letters, 16, 272
- Gontikakis, C. & Hameury, J.-M. 1993, *Constraints on the illumination model for soft X-ray transients*, A&A, 271, 118
- Granot, J. & van der Horst, A. J. 2014, *Gamma-Ray Burst Jets and their Radio Observations*, PASA, 31, e008

- Gray, C. L. & Mason, P. A. 2005, *AR Ursae Majoris: A New Persistent Radio Emitter*, in Bulletin of the American Astronomical Society, Vol. 37, American Astronomical Society Meeting Abstracts #206, 496
- Greenstein, J. L. & Oke, J. B. 1982, *RW Sextantis, a disk with a hot, high-velocity wind*, ApJ, 258, 209
- Groot, P. J. 2001, *Evolution of Spiral Shocks in U Geminorum during Outburst*, ApJ, 551, L89
- Groot, P. J., Rutten, R. G. M., & van Paradijs, J. 2001, *SW Sextantis in an excited, low state*, A&A, 368, 183
- Gudel, M., Schmitt, J. H. M. M., Bookbinder, J. A., & Fleming, T. A. 1993, *A tight correlation between radio and X-ray luminosities of M dwarfs*, ApJ, 415, 236
- Gulbis, A. A. S., O'Donoghue, D., Fourie, P., et al. 2011, *SHOC: Sutherland High-speed Optical Cameras*, in EPSC-DPS Joint Meeting 2011, 1173
- Haefner, R. & Metz, K. 1985, *The old nova V 603 AQL - an intermediate polar?*, A&A, 145, 311
- Hameury, J.-M., Menou, K., Dubus, G., Lasota, J.-P., & Hure, J.-M. 1998, *Accretion disc outbursts: a new version of an old model*, MNRAS, 298, 1048
- Han, X. & Hjellming, R. M. 1992, *Radio observations of the 1989 transient event in V404 Cygni (=GS 2023+338)*, ApJ, 400, 304
- Harrison, T. E. 2014, *The WISE Light Curves of Z Camelopardalis during Outburst: Evidence for Synchrotron Emission?*, ApJ, 791, L18
- Harrison, T. E., Bornak, J., McArthur, B. E., & Benedict, G. F. 2013, *Hubble Space Telescope Fine Guidance Sensor Parallaxes for Four Classical Novae*, ApJ, 767, 7
- Hartley, L. E., Drew, J. E., Long, K. S., Knigge, C., & Proga, D. 2002, *Testing the line-driven disc wind model: time-resolved ultraviolet spectroscopy of IX Vel and V3885Sgr*, MNRAS, 332, 127
- Hastings, W. 1970, *Monte Carlo Sampling Methods Using Markov Chains and Their Applications*, Biometrika, 57, 97
- Hawley, J. F. & Balbus, S. A. 1991, *A Powerful Local Shear Instability in Weakly Magnetized Disks. II. Nonlinear Evolution*, ApJ, 376, 223
- Hawley, J. F. & Balbus, S. A. 1992, *A powerful local shear instability in weakly magnetized disks. III - Long-term evolution in a shearing sheet*, ApJ, 400, 595
- Hellier, C. 2001, *Cataclysmic Variable Stars*
- Hernández Santisteban, J. V., Knigge, C., Littlefair, S. P., et al. 2016, *An irradiated brown-dwarf companion to an accreting white dwarf*, Nature, 533, 366
- Hind, J. R. 1856, *On a new Variable Star*, MNRAS, 16, 56
- Hjellming, R. M., Johnston, K. J., & Miley, G. K. 1979, *The Radio Jets of SS433*, in BAAS, Vol. 11, Bulletin of the American Astronomical Society, 673
- Hjellming, R. M. & Wade, C. M. 1970, *Radio Novae*, ApJ, 162, L1
- Høg, E., Fabricius, C., Makarov, V. V., et al. 2000, *The Tycho-2 catalogue of the 2.5 million brightest stars*, A&A, 355, L27
- Honeycutt, R. K. & Kafka, S. 2004, *Characteristics of High-State/Low-State Transitions in VY Sculptoris Stars*, AJ, 128, 1279
- Honeycutt, R. K., Robertson, J. W., Turner, G. W., & Mattei, J. A. 1998, *Are Z Camelopardalis-*

BIBLIOGRAPHY

- Type Dwarf Novae Brighter at Standstill?*, PASP, 110, 676
- Höshi, R. 1979, *Accretion Model for Outbursts of Dwarf Nova*, Progress of Theoretical Physics, 61, 1307
- Howell, S. B. & Ciardi, D. R. 2001, *Spectroscopic Discovery of Brown Dwarf-like Secondary Stars in the Cataclysmic Variables LL Andromedae and EF Eridani*, ApJ, 550, L57
- Howell, S. B., Nelson, L. A., & Rappaport, S. 2001, *An Exploration of the Paradigm for the 2-3 Hour Period Gap in Cataclysmic Variables*, ApJ, 550, 897
- Hut, P. 1981, *Tidal evolution in close binary systems*, A&A, 99, 126
- Hutchings, J. B. & Cowley, A. P. 2007, *Far-Ultraviolet Spectra of TT Arietis*, AJ, 133, 1204
- Ichikawa, S. & Osaki, Y. 1992, *Time evolution of the accretion disk radius in a dwarf nova*, PASJ, 44, 15
- Ivanova, N. & Taam, R. E. 2003, *Magnetic Braking Revisited*, ApJ, 599, 516
- Jester, S., Schneider, D. P., Richards, G. T., et al. 2005, *The Sloan Digital Sky Survey View of the Palomar-Green Bright Quasar Survey*, AJ, 130, 873
- Johnson, C. B., Schaefer, B. E., Kroll, P., & Henden, A. A. 2014a, *Nova Aquilae 1918 (V603 Aql) Faded by 0.44 MAG Per Century from 1938 to 2013*, ApJ, 780, L25
- Johnson, J. A., Christensen, E. J., Gibbs, A. R., et al. 2014b, *The Catalina Sky Survey: Status, Discoveries and the Future*, in AAS/Division for Planetary Sciences Meeting Abstracts, Vol. 46, AAS/Division for Planetary Sciences Meeting Abstracts, 414.09
- Kafka, S., Hoard, D. W., Honeycutt, R. K., & Deliyannis, C. P. 2009, *Observations of V592 Cas – an Outflow at Optical Wavelengths*, AJ, 137, 197
- Kaitchuck, R. H. 1989, *The Orbital Period of RX Andromedae*, PASP, 101, 1129
- Kato, T. 2013, available at: <http://ooruri.kusastro.kyoto-u.ac.jp/mailarchive/vsnet-alert/15618>
- Kato, T., Hamsch, F.-J., Maehara, H., et al. 2013, *Survey of Period Variations of Superhumps in SU UMa-Type Dwarf Novae. IV. The Fourth Year (2011-2012)*, PASJ, 65, 23
- Kato, T., Pavlenko, E. P., Maehara, H., et al. 2009, *SDSS J080434.20+510349.2: Eclipsing WZ Sge-Type Dwarf Nova with Multiple Rebrightenings*, PASJ, 61, 601
- King, A. L., Miller, J. M., Cackett, E. M., et al. 2011, *A Distinctive Disk-Jet Coupling in the Seyfert-1 Active Galactic Nucleus NGC 4051*, ApJ, 729, 19
- King, A. R., Frank, J., Kolb, U., & Ritter, H. 1995, *Mass transfer cycles in cataclysmic variables*, ApJ, 444, L37
- King, A. R., Frank, J., Kolb, U., & Ritter, H. 1996, *Global Analysis of Mass Transfer Cycles in Cataclysmic Variables*, ApJ, 467, 761
- King, A. R. & Schenker, K. 2002, *A new evolutionary picture for CVs and LMXBs*, in Astronomical Society of the Pacific Conference Series, Vol. 261, The Physics of Cataclysmic Variables and Related Objects, ed. B. T. Gänsicke, K. Beuermann, & K. Reinsch, 233
- Knigge, C. 2006, *The donor stars of cataclysmic variables*, MNRAS, 373, 484
- Knigge, C., Baraffe, I., & Patterson, J. 2011, *The Evolution of Cataclysmic Variables as Revealed by Their Donor Stars*, ApJS, 194, 28
- Kolb, U. 1993, *A model for the intrinsic population of cataclysmic variables*, A&A, 271, 149
- Kolb, U. & Baraffe, I. 1999, *Brown dwarfs and the cataclysmic variable period minimum*, MNRAS, 309, 1034

- Körding, E. 2008, *Connections from supermassive black holes to white dwarfs*, in *Microquasars and Beyond*, 23
- Körding, E., Rupen, M., Knigge, C., et al. 2008, *A Transient Radio Jet in an Erupting Dwarf Nova*, *Science*, 320, 1318
- Körding, E. G., Fender, R. P., & Migliari, S. 2006, *Jet-dominated advective systems: radio and X-ray luminosity dependence on the accretion rate*, *MNRAS*, 369, 1451
- Körding, E. G., Knigge, C., Tzioumis, T., & Fender, R. 2011, *Detection of radio emission from a nova-like cataclysmic variable: evidence of jets?*, *MNRAS*, 418, L129
- Körding, E. G., Migliari, S., Fender, R., et al. 2007, *The variability plane of accreting compact objects*, *MNRAS*, 380, 301
- Kotko, I., Lasota, J.-P., Dubus, G., & Hameury, J.-M. 2012, *Models of AM Canum Venaticorum star outbursts*, *A&A*, 544, A13
- Kraft, R. P., Mathews, J., & Greenstein, J. L. 1962, *Binary Stars among Cataclysmic Variables. II. Nova WZ Sagittae: a Possible Radiator of Gravitational Waves.*, *ApJ*, 136, 312
- Kraus, A. L. & Hillenbrand, L. A. 2007, *The Stellar Populations of Praesepe and Coma Berenices*, *AJ*, 134, 2340
- Kunze, S., Speith, R., & Hessman, F. V. 2001, *Substantial stream-disc overflow found in three-dimensional SPH simulations of cataclysmic variables*, *MNRAS*, 322, 499
- Landolt, A. U. 1992, *Broadband UBVR photometry of the Baldwin-Stone Southern Hemisphere spectrophotometric standards*, *AJ*, 104, 372
- Larson, S., Beshore, E., Hill, R., et al. 2003, *The CSS and SSS NEO surveys*, in *Bulletin of the American Astronomical Society*, Vol. 35, AAS/Division for Planetary Sciences Meeting Abstracts #35, 982
- Larson, S., Brownlee, J., Hergenrother, C., & Spahr, T. 1998, *The Catalina Sky Survey for NEOs*, in *Bulletin of the American Astronomical Society*, Vol. 30, *Bulletin of the American Astronomical Society*, 1037
- Lasota, J.-P. 2001, *The disc instability model of dwarf novae and low-mass X-ray binary transients*, *New Astron. Rev.*, 45, 449
- Law, N. M., Kulkarni, S. R., Dekany, R. G., et al. 2009, *The Palomar Transient Factory: System Overview, Performance, and First Results*, *PASP*, 121, 1395
- Lawrence, A., Warren, S. J., Almaini, O., et al. 2007, *The UKIRT Infrared Deep Sky Survey (UKIDSS)*, *MNRAS*, 379, 1599
- Levitan, D., Groot, P. J., Prince, T. A., et al. 2015, *Long-term photometric behaviour of outbursting AM CVn systems*, *MNRAS*, 446, 391
- Lin, D. N. C., Faulkner, J., & Papaloizou, J. 1985, *On the evolution of accretion disc flow in cataclysmic variables. III - Outburst properties of constant and uniform-alpha model discs*, *MNRAS*, 212, 105
- Linnell, A. P., Godon, P., Hubeny, I., Sion, E. M., & Szkody, P. 2010, *The Anomalous Accretion Disk of the Cataclysmic Variable RW Sextantis*, *ApJ*, 719, 271
- Linnell Nemec, A. F. & Nemec, J. M. 1985, *A test of significance for periods derived using phase-dispersion-minimization techniques*, *AJ*, 90, 2317
- Littlefair, S. P., Dhillon, V. S., Marsh, T. R., et al. 2008, *On the evolutionary status of short-period*

BIBLIOGRAPHY

- cataclysmic variables*, MNRAS, 388, 1582
- Livio, M. 1999, *Astrophysical jets: a phenomenological examination of acceleration and collimation.*, Phys. Rep., 311, 225
- Livio, M. & Pringle, J. E. 1994, *Star spots and the period gap in cataclysmic variables*, ApJ, 427, 956
- Longair, M. S. 2011, High Energy Astrophysics
- MacDonald, J. 1986, *Postthermonuclear runaway angular momentum loss in cataclysmic binaries*, ApJ, 305, 251
- Marsh, T. R., Horne, K., Schlegel, E. M., Honeycutt, R. K., & Kaitchuck, R. H. 1990, *Doppler imaging of the dwarf nova U Geminorum*, ApJ, 364, 637
- Mason, P. A. & Gray, C. L. 2007, *AR Ursae Majoris Discovered to Be a Persistent Radio Polar: Results from a VLA Survey of Magnetic Cataclysmic Variables*, ApJ, 660, 662
- McLean, M., Berger, E., & Reiners, A. 2012, *The Radio Activity-Rotation Relation of Ultracool Dwarfs*, ApJ, 746, 23
- McMullin, J. P., Waters, B., Schiebel, D., Young, W., & Golap, K. 2007, *CASA Architecture and Applications*, in Astronomical Society of the Pacific Conference Series, Vol. 376, Astronomical Data Analysis Software and Systems XVI, ed. R. A. Shaw, F. Hill, & D. J. Bell, 127
- Meintjes, P. J. & Venter, L. A. 2005, *The diamagnetic blob propeller in AE Aquarii and non-thermal radio to mid-infrared emission*, MNRAS, 360, 573
- Merloni, A., Heinz, S., & di Matteo, T. 2003, *A Fundamental Plane of black hole activity*, MNRAS, 345, 1057
- Metropolis, N., Rosenbluth, A., Teller, A., & Teller, E. 1953, *Equation of State Calculations by Fast Computing Machines*, J. Chem. Phys., 21, 1087
- Meyer, F. 1984, *Transition waves in accretion disks*, A&A, 131, 303
- Meyer, F. & Meyer-Hofmeister, E. 1981, *On the Elusive Cause of Cataclysmic Variable Outbursts*, A&A, 104, L10
- Mickaelian, A. M., Balayan, S. K., Ilovaisky, S. A., et al. 2002, *RX J1643.7+3402: A new bright cataclysmic variable*, A&A, 381, 894
- Mickaelian, A. M. & Sinamyan, P. K. 2010, *Proper motions and natures of First Byurakan Survey blue stellar objects*, MNRAS, 407, 681
- Migliari, S. & Fender, R. P. 2006, *Jets in neutron star X-ray binaries: a comparison with black holes*, MNRAS, 366, 79
- Miller-Jones, J. C. A., Sivakoff, G. R., Altamirano, D., et al. 2012, *Disc-jet coupling in the 2009 outburst of the black hole candidate H1743-322*, MNRAS, 421, 468
- Miller-Jones, J. C. A., Sivakoff, G. R., Altamirano, D., et al. 2011, *Investigating accretion disk - radio jet coupling across the stellar mass scale*, in IAU Symposium, Vol. 275, IAU Symposium, ed. G. E. Romero, R. A. Sunyaev, & T. Belloni, 224-232
- Miller-Jones, J. C. A., Sivakoff, G. R., Knigge, C., et al. 2013, *An Accurate Geometric Distance to the Compact Binary SS Cygni Vindicates Accretion Disc Theory*, Science, 340, 950
- Miller-Jones, J. C. A., Strader, J., Heinke, C. O., et al. 2015, *Deep radio imaging of 47 Tuc identifies the peculiar X-ray source X9 as a new black hole candidate*, MNRAS, 453, 3918
- Mineshige, S. & Osaki, Y. 1985, *Disk-instability model for outbursts of dwarf novae. II Full-disk*

- calculations*, PASJ, 37, 1
- Monet, D. G., Levine, S. E., Canzian, B., et al. 2003, *The USNO-B Catalog*, AJ, 125, 984
- Mukai, K. & Orio, M. 2005, *X-Ray Observations of the Bright Old Nova V603 Aquilae*, ApJ, 622, 602
- Nakata, C., Ohshima, T., Kato, T., et al. 2013, *WZ Sge-Type Dwarf Novae with Multiple Re-brightenings: MASTER OT J211258.65+242145.4 and MASTER OT J203749.39+552210.3*, PASJ, 65, 117
- Naylor, T., Koch-Miramond, L., Ringwald, F. A., & Evans, A. 1996, *The linear polarization of non-magnetic cataclysmic variables*, MNRAS, 282, 873
- Nelson, R. F. & Spencer, R. E. 1988, *A search for radio emission from X-ray binaries and related objects*, MNRAS, 234, 1105
- Nomoto, K. 1982, *Accreting white dwarf models for type I supernovae. I - Presupernova evolution and triggering mechanisms*, ApJ, 253, 798
- O'Donoghue, D. 1995, *High Speed CCD Photometry*, Baltic Astronomy, 4, 519
- Osaki, Y. 1974, *An accretion model for the outbursts of U Geminorum stars*, PASJ, 26, 429
- Osaki, Y. 1985, *Irradiation-induced mass-overflow instability as a possible cause of superoutbursts in SU UMa stars*, A&A, 144, 369
- Osaki, Y. 1989, *A model for the superoutburst phenomenon of SU Ursae Majoris stars*, PASJ, 41, 1005
- Osaki, Y. 1996, *Dwarf-Nova Outbursts*, PASP, 108, 39
- Osaki, Y. & Kato, T. 2013, *The Cause of the Superoutburst in SU UMa Stars is Finally Revealed by Kepler Light Curve of V1504 Cygni*, PASJ, 65
- Osaki, Y. & Meyer, F. 2003, *Is evidence for enhanced mass transfer during dwarf-nova outbursts well substantiated?*, A&A, 401, 325
- Oshima, T. 2012a, available at: <http://ooruri.kusastro.kyoto-u.ac.jp/mailarchive/vsnet-alert/14406>
- Oshima, T. 2012b, available at: <http://ooruri.kusastro.kyoto-u.ac.jp/mailarchive/vsnet-alert/14416>
- Otulakowska-Hypka, M. & Olech, A. 2013, *On supercycle lengths of active SU UMa stars*, MNRAS, 433, 1338
- Otulakowska-Hypka, M., Olech, A., & Patterson, J. 2016, *Statistical analysis of properties of dwarf novae outbursts*, ArXiv e-prints
- Paczyński, B. 1967, *Gravitational Waves and the Evolution of Close Binaries*, Acta Astron., 17, 287
- Paczynski, B. 1976, *Common Envelope Binaries*, in IAU Symposium, Vol. 73, Structure and Evolution of Close Binary Systems, ed. P. Eggleton, S. Mitton, & J. Whelan, 75
- Paczynski, B. & Schwarzenberg-Czerny, A. 1980, *Disk accretion in U Geminorum*, Acta Astron., 30, 127
- Paczynski, B. & Sienkiewicz, R. 1981, *Gravitational radiation and the evolution of cataclysmic binaries*, ApJ, 248, L27
- Paczyński, B., Ziolkowski, J., & Zytkow, A. 1969, *On the Time-Scale of the Mass Transfer in Close Binaries*, in Astrophysics and Space Science Library, Vol. 13, Mass Loss from Stars, ed.

BIBLIOGRAPHY

- M. Hack, 237
- Papaloizou, J. C. B. & Bath, G. T. 1975, *Stellar stability in close binary systems*, MNRAS, 172, 339
- Patterson, J. 1998, *Late Evolution of Cataclysmic Variables*, PASP, 110, 1132
- Patterson, J. 2011, *Distances and absolute magnitudes of dwarf novae: murmurs of period bounce*, MNRAS, 411, 2695
- Patterson, J., Fenton, W. H., Thorstensen, J. R., et al. 2002, *Superhumps in Cataclysmic Binaries. XXIII. V442 Ophiuchi and RX J1643.7+3402*, PASP, 114, 1364
- Patterson, J., Kemp, J., Saad, J., et al. 1997, *Superhumps in Cataclysmic Binaries. XI. V603 Aquilae Revisited*, PASP, 109, 468
- Patterson, J. & Raymond, J. C. 1985, *X-ray emission from cataclysmic variables with accretion disks. I - Hard X-rays. II - EUV/soft X-ray radiation*, ApJ, 292, 535
- Patterson, J. & Richman, H. 1991, *Permanent superhumps in V603 Aquilae*, PASP, 103, 735
- Patterson, J., Thomas, G., Skillman, D. R., & Diaz, M. 1993, *The 1991 V603 Aquilae campaign - Superhumps and P-dots*, ApJS, 86, 235
- Patterson, J., Uthas, H., Kemp, J., et al. 2013, *BK Lyncis: the oldest old nova and a Bellwether for cataclysmic variable evolution*, MNRAS, 434, 1902
- Pavelin, P. E., Spencer, R. E., & Davis, R. J. 1994, *A 5-GHZ Radio Survey of Magnetic Cataclysmic Variables*, MNRAS, 269, 779
- Plotkin, R. M., Gallo, E., Jonker, P. G., et al. 2016, *A clean sightline to quiescence: multiwavelength observations of the high Galactic latitude black hole X-ray binary Swift J1357.2-0933*, MNRAS, 456, 2707
- Pojmanski, G. 1986, *Structure of the accretion disks in the cataclysmic variables*, Acta Astron., 36, 69
- Pretorius, M. L. & Knigge, C. 2008a, *An H α -selected sample of cataclysmic variables - I. Observations of newly discovered systems*, MNRAS, 385, 1471
- Pretorius, M. L. & Knigge, C. 2008b, *An H α -selected sample of cataclysmic variables - II. Implications for CV evolution*, MNRAS
- Pretorius, M. L., Knigge, C., & Kolb, U. 2007, *The influence of selection effects on the observed cataclysmic variable population: modelling and application to the Palomar-Green sample*, MNRAS, 374, 1495
- Pretorius, M. L., Knigge, C., & Schwöpe, A. D. 2013, *The space density of magnetic cataclysmic variables*, MNRAS, 432, 570
- Pringle, J. E. 1977, *Soft X-ray emission from dwarf novae*, MNRAS, 178, 195
- Pringle, J. E. & Savonije, G. J. 1979, *X-ray emission from dwarf novae*, MNRAS, 187, 777
- Prinja, R. K., Knigge, C., Ringwald, F. A., & Wade, R. A. 2000, *Episodic absorption in the outflow of the old nova V603 Aquilae*, MNRAS, 318, 368
- Prinja, R. K., Long, K. S., Froning, C. S., et al. 2003, *FUSE and HST ultraviolet observations of the disc wind of RW Sextantis*, MNRAS, 340, 551
- Prinja, R. K. & Rosen, R. 1995, *High-resolution IUE spectroscopy of fast winds from cataclysmic variables*, MNRAS, 273, 461
- Quinn, P. J., Barnes, D. G., Csabai, I., et al. 2004, *The International Virtual Observatory Alliance:*

- recent technical developments and the road ahead*, in Society of Photo-Optical Instrumentation Engineers (SPIE) Conference Series, Vol. 5493, *Optimizing Scientific Return for Astronomy through Information Technologies*, ed. P. J. Quinn & A. Bridger, 137–145
- Ramsay, G., Brocksopp, C., Wu, K., Slee, B., & Saxton, C. J. 2007, *A search for electron cyclotron maser emission from compact binaries*, MNRAS, 382, 461
- Rappaport, S., Joss, P. C., & Webbink, R. F. 1982, *The evolution of highly compact binary stellar systems*, ApJ, 254, 616
- Rappaport, S., Verbunt, F., & Joss, P. C. 1983, *A new technique for calculations of binary stellar evolution, with application to magnetic braking*, ApJ, 275, 713
- Rau, A., Kulkarni, S. R., Law, N. M., et al. 2009, *Exploring the Optical Transient Sky with the Palomar Transient Factory*, PASP, 121, 1334
- Rebassa-Mansergas, A., Agurto-Gangas, C., Schreiber, M. R., Gänsicke, B. T., & Koester, D. 2013, *White dwarf main-sequence binaries from SDSS DR 8: unveiling the cool white dwarf population*, MNRAS, 433, 3398
- Reiners, A. & Basri, G. 2008, *Chromospheric Activity, Rotation, and Rotational Braking in M and L Dwarfs*, ApJ, 684, 1390
- Reiners, A. & Basri, G. 2009, *On the magnetic topology of partially and fully convective stars*, A&A, 496, 787
- Retter, A. 2004, *Constraining Jet Theories Using Nova Outbursts*, ApJ, 615, L125
- Retter, A. & Naylor, T. 2000, *Thermal stability and nova cycles in permanent superhump systems*, MNRAS, 319, 510
- Ritter, H. & Kolb, U. 2003, *Catalogue of cataclysmic binaries, low-mass X-ray binaries and related objects (Seventh edition)*, A&A, 404, 301
- Robinson, C. R. & Cordova, F. A. 1994, *The X-ray Behavior of Two CVs: TT Ari and DP Leo*, in Astronomical Society of the Pacific Conference Series, Vol. 56, *Interacting Binary Stars*, ed. A. W. Shafter, 146
- Rodríguez-Gil, P., Casares, J., Martínez-Pais, I. G., Hakala, P., & Steeghs, D. 2001, *Evidence of Magnetic Accretion in an SW Sextantis Star: Discovery of Variable Circular Polarization in LS Pegasi*, ApJ, 548, L49
- Rodríguez-Gil, P., Gänsicke, B. T., Hagen, H.-J., et al. 2007, *SW Sextantis stars: the dominant population of cataclysmic variables with orbital periods between 3 and 4h*, MNRAS, 377, 1747
- Rodríguez-Gil, P. & Martínez-Pais, I. G. 2002, *V533 Herculis: the second SW Sex old nova displaying emission-line flaring*, MNRAS, 337, 209
- Rodríguez-Gil, P., Martínez-Pais, I. G., & de la Cruz Rodríguez, J. 2009, *The magnetic SW Sextantis star RXJ1643.7+3402*, MNRAS, 395, 973
- Rosen, S. R., Webb, N. A., Watson, M. G., et al. 2015, *The XMM-Newton serendipitous survey. VII. The third XMM-Newton serendipitous source catalogue*, ArXiv e-prints
- Rupen, M. P., Mioduszewski, A. J., & Sokolowski, J. L. 2008, *An Expanding Shell and Synchrotron Jet in RS Ophiuchi*, ApJ, 688, 559
- Russell, D. M., Russell, T. D., Miller-Jones, J. C. A., et al. 2013, *An Evolving Compact Jet in the Black Hole X-Ray Binary MAXI J1836-194*, ApJ, 768, L35
- Russell, T. D., Miller-Jones, J. C. A., Curran, P. A., et al. 2015, *Radio monitoring of the hard*

BIBLIOGRAPHY

- state jets in the 2011 outburst of MAXI J1836-194*, MNRAS, 450, 1745
- Russell, T. D., Miller-Jones, J. C. A., Sivakoff, G. R., et al. 2016, *The reproducible radio outbursts of SS Cygni*, ArXiv e-prints
- Scaringi, S. 2014, *A physical model for the flickering variability in cataclysmic variables*, MNRAS, 438, 1233
- Schreiber, M. R., Gänsicke, B. T., & Mattei, J. A. 2002, *RX And: An intermediate between Z Cam and VY Scl stars*, A&A, 384, L6
- Schreiber, M. R., Hameury, J.-M., & Lasota, J.-P. 2004, *Delays in dwarf novae II: VW Hyi, the tidal instability and enhanced mass transfer models*, A&A, 427, 621
- Shafter, A. W. 1983, PhD thesis, California Univ., Los Angeles.
- Shafter, A. W., Szkody, P., Liebert, J., et al. 1985, *TT ARIETIS - The low state*, ApJ, 290, 707
- Shara, M. M., Livio, M., Moffat, A. F. J., & Orio, M. 1986, *Do novae hibernate during most of the millenia between eruptions? Links between dwarf and classical novae, and implications for the space densities and evolution of cataclysmic binaries*, ApJ, 311, 163
- Skinner, J. N., Thorstensen, J. R., & Lépine, S. 2014, *Cataclysmic Variables in the Superblink Proper Motion Survey*, AJ, 148, 115
- Skrutskie, M. F., Cutri, R. M., Stiening, R., et al. 2006, *The Two Micron All Sky Survey (2MASS)*, AJ, 131, 1163
- Slee, O. B., Wilson, W., & Ramsay, G. 2008, *The Coherent Radio Emission from the RS CVn Binary HR 1099*, PASA, 25, 94
- Smak, J. 1971, *Eruptive Binaries. II. U Geminorum*, Acta Astron., 21, 15
- Smak, J. 1984, *Outbursts of dwarf novae*, PASP, 96, 5
- Smak, J. 2000, *Unsolved problems of dwarf nova outbursts*, New A Rev., 44, 171
- Smak, J. 2004, *Irradiation of Secondary Components and Enhanced Mass Outflow in Dwarf Novae during Outbursts*, Acta Astron., 54, 181
- Smak, J. 2008, *Superoutbursts of Z Cha and their Interpretation*, Acta Astron., 58, 55
- Smak, J. 2009, *New Interpretation of Superhumps*, Acta Astron., 59, 121
- Soker, N. & Lasota, J.-P. 2004, *The absence of jets in cataclysmic variable stars*, A&A, 422, 1039
- Sokoloski, J. L., Rupen, M. P., & Mioduszewski, A. J. 2008, *Uncovering the Nature of Nova Jets: A Radio Image of Highly Collimated Outflows from RS Ophiuchi*, ApJ, 685, L137
- Spruit, H. C. & Ritter, H. 1983, *Stellar activity and the period gap in cataclysmic variables*, A&A, 124, 267
- Stellingwerf, R. F. 1978, *Period determination using phase dispersion minimization*, ApJ, 224, 953
- Strohmeier, W., Kippenhahn, R., & Geyer, E. 1957, K1. Veröff. Sternwarte Bamberg Nr. 18
- Strömgren, B. 1939, *Book Review: An Introduction to the Study of Stellar Structure, by S. Chandrasekhar*, Popular Astronomy, 47, 287
- Strope, R. J., Schaefer, B. E., & Henden, A. A. 2010, *Catalog of 93 Nova Light Curves: Classification and Properties*, AJ, 140, 34
- Sweeney, D., Tyson, J. A., Axelrod, T., et al. 2009, *Overview of the LSST Observatory System*, in Bulletin of the American Astronomical Society, Vol. 41, American Astronomical Society Meeting Abstracts #213, 366

- Szkody, P., Everett, M. E., Howell, S. B., et al. 2014, *Follow up Observations of SDSS and CRTS Candidate Cataclysmic Variables*, AJ, 148, 63
- Szkody, P. & Wade, R. A. 1981, *Z Camelopardalis at standstill*, ApJ, 251, 201
- Tetarenko, B. E., Bahramian, A., Arnason, R. M., et al. 2016, *The First Low-mass Black Hole X-Ray Binary Identified in Quiescence Outside of a Globular Cluster*, ApJ, 825, 10
- Thorstensen, J. R. & Ringwald, F. A. 1995, *An Improved Ephemeris for Z Camelopardalis*, Information Bulletin on Variable Stars, 4249
- Thorstensen, J. R. & Skinner, J. N. 2012, *Spectroscopy and Photometry of Cataclysmic Variable Candidates from the Catalina Real Time Survey*, AJ, 144, 81
- Thorstensen, J. R. & Taylor, C. J. 2000, *Spectroscopy and orbital periods of the old novae V533 Herculis, V446 Herculis and X Serpentis*, MNRAS, 312, 629
- Thorstensen, J. R., Wade, R. A., & Oke, J. B. 1986, *A spectroscopic study of the cataclysmic binary star SU Ursae Majoris*, ApJ, 309, 721
- Tody, D. 1986, *The IRAF Data Reduction and Analysis System*, in Proc. SPIE, Vol. 627, Instrumentation in astronomy VI, ed. D. L. Crawford, 733
- Toonen, S., Voss, R., & Knigge, C. 2014, *The influence of mass-transfer variability on the growth of white dwarfs, and the implications for Type Ia supernova rates*, MNRAS, 441, 354
- Tremko, J., Andronov, I. L., Luthardt, R., et al. 1992, *On Hour-Scale Photometric Variations of TT Arietis*, Information Bulletin on Variable Stars, 3763, 1
- Turner, K. C. 1985, *12 cm Observations of Stellar Radio Sources*, in Astrophysics and Space Science Library, Vol. 116, Radio Stars, ed. R. M. Hjellming & D. M. Gibson, 283
- Tylenda, R. 1981, *Viscous Boundary Layer and Hard X-Rays from Dwarf Novae*, Acta Astron., 31, 267
- Tyson, J. A. 2002, *Large Synoptic Survey Telescope: Overview*, in Society of Photo-Optical Instrumentation Engineers (SPIE) Conference Series, Vol. 4836, Survey and Other Telescope Technologies and Discoveries, ed. J. A. Tyson & S. Wolff, 10–20
- Udalski, A. & Schwarzenberg-Czerny, A. 1989, *Photometry of cataclysmic variables. IV - Nova V603 Aquilae: Discovery of a magnetic rotator*, Acta Astron., 39, 125
- Unda-Sanzana, E., Marsh, T. R., & Morales-Rueda, L. 2006, *Optical spectroscopy of the dwarf nova U Geminorum*, MNRAS, 369, 805
- van der Sluys, M. 2006, PhD thesis, Utrecht University, Netherlands
- van Leeuwen, F. 2007, *Validation of the new Hipparcos reduction*, A&A, 474, 653
- van Paradijs, J. 1983, *Superoutbursts - A general phenomenon in dwarf novae*, A&A, 125, L16
- van Paradijs, J., Charles, P. A., Harlaftis, E. T., et al. 1994, *A 60-NIGHT Campaign on Dwarf Novae - Part One - Photometric Variability of Su-Ursae and Yz-Cancri*, MNRAS, 267, 465
- van Teeseling, A., Beuermann, K., & Verbunt, F. 1996, *The X-ray source in non-magnetic cataclysmic variables.*, A&A, 315, 467
- Verbunt, F. & Zwaan, C. 1981, *Magnetic braking in low-mass X-ray binaries*, A&A, 100, L7
- Viallet, M. & Hameury, J.-M. 2007, *Hydrodynamic simulations of irradiated secondaries in dwarf novae*, A&A, 475, 597
- Viallet, M. & Hameury, J.-M. 2008, *Mass transfer variation in the outburst model of dwarf novae and soft X-ray transients*, A&A, 489, 699

BIBLIOGRAPHY

- Vitello, P. & Shlosman, I. 1993, *Ultraviolet line diagnostics of accretion disk winds in cataclysmic variables*, ApJ, 410, 815
- Voges, W., Aschenbach, B., Boller, T., et al. 2000, *Rosat All-Sky Survey Faint Source Catalogue*, IAU Circ., 7432, 3
- Voges, W., Aschenbach, B., Boller, T., et al. 1999, *The ROSAT all-sky survey bright source catalogue*, A&A, 349, 389
- Vogt, N. 1983, *VW Hydri revisited - Conclusions on dwarf nova outburst models*, A&A, 118, 95
- Vogt, N., Chené, A.-N., Moffat, A. F. J., et al. 2013, *A photometric study of the nova-like variable TT Arietis with the MOST satellite*, Astronomische Nachrichten, 334, 1101
- Warner, B. 1987, *Absolute magnitudes of cataclysmic variables*, MNRAS, 227, 23
- Warner, B. 1995, *Cataclysmic variable stars.*, Cambridge Astrophysics Series, 28
- Warner, B. 2004, *Rapid Oscillations in Cataclysmic Variables*, PASP, 116, 115
- Warner, B. & Nather, R. E. 1971, *Observations of rapid blue variables - II. U Geminorum.*, MNRAS, 152, 219
- Watson, M. G., Schröder, A. C., Fyfe, D., et al. 2009, *The XMM-Newton serendipitous survey. V. The Second XMM-Newton serendipitous source catalogue*, A&A, 493, 339
- Wenger, M., Ochsenbein, F., Egret, D., et al. 2000, *The SIMBAD astronomical database. The CDS reference database for astronomical objects*, A&AS, 143, 9
- Weston, J. H. S., Sokoloski, J. L., Metzger, B. D., et al. 2016, *Non-thermal radio emission from colliding flows in classical nova V1723 Aql*, MNRAS, 457, 887
- Whelan, J. & Iben, Jr., I. 1973, *Binaries and Supernovae of Type I*, ApJ, 186, 1007
- Whitehurst, R. 1988, *Numerical simulations of accretion disks. I - Superhumps - A tidal phenomenon of accretion disks*, MNRAS, 232, 35
- Wils, P., Gänsicke, B. T., Drake, A. J., & Southworth, J. 2010, *Data mining for dwarf novae in SDSS, GALEX and astrometric catalogues*, MNRAS, 402, 436
- Woodsworth, A. W. & Hughes, V. A. 1977, *Observations of radio stars at 10.6 GHz*, A&A, 58, 105
- Woudt, P. A. & Warner, B. 2002, *Dwarf nova oscillations and quasi-periodic oscillations in cataclysmic variables - I. Observations of VW Hyi*, MNRAS, 333, 411
- Woudt, P. A., Warner, B., de Budé, D., et al. 2012, *High-speed photometry of faint cataclysmic variables - VII. Targets selected from the Sloan Digital Sky Survey and the Catalina Real-time Transient Survey*, MNRAS, 421, 2414
- Wright, A. E. & Barlow, M. J. 1975, *The radio and infrared spectrum of early-type stars undergoing mass loss*, MNRAS, 170, 41
- Wright, A. E., Stewart, R. T., Nelson, G. J., Slee, O. B., & Cropper, M. 1988, *Detection of the AM HER type cataclysmic variable V834 CEN at radio wavelengths*, MNRAS, 231, 319
- Wright, E. L., Eisenhardt, P. R. M., Mainzer, A. K., et al. 2010, *The Wide-field Infrared Survey Explorer (WISE): Mission Description and Initial On-orbit Performance*, AJ, 140, 1868
- Wu, X., Li, Z., Ding, Y., Zhang, Z., & Li, Z. 2002, *TT Arietis: Spectroscopy and Photometry*, ApJ, 569, 418
- Wynn, G. A., King, A. R., & Horne, K. 1997, *A magnetic propeller in the cataclysmic variable AE Aquarii*, MNRAS, 286, 436

- Zhang, E.-H. & Robinson, E. L. 1987, *The eclipses of cataclysmic variables. II - U Geminorum*, ApJ, 321, 813
- Zhilkin, A. G., Bisikalo, D. V., & Mason, P. A. 2012, *Full 3D MHD calculations of accretion flow structure in magnetic cataclysmic variables with strong, complex magnetic fields*, Astronomy Reports, 56, 257
- Zorotovic, M., Schreiber, M. R., & Gänsicke, B. T. 2011, *Post common envelope binaries from SDSS. XI. The white dwarf mass distributions of CVs and pre-CVs*, A&A, 536, A42

SUMMARY

Recent developments in the field of Cataclysmic Variable stars (CVs) have highlighted the need for large (more unbiased) samples of CVs with known properties, as well as the need for multi-wavelength studies to determine the accretion-outflow connection. In this thesis I have presented radio observations of non-magnetic CVs, proving them to be significant radio emitters. I have also presented optical follow-up studies of CVs, and developed an algorithm that automatically classifies these objects based on photometric data from large surveys. This was applied to the Catalina Real-time Transient Survey to produce a catalogue of accretion properties for 1031 CVs.

Optical CV Population Studies

To effectively constrain models for the evolution and outbursts of CVs, large, statistically-significant, and less-biased samples of characterised CVs are necessary. Surveys such as the Catalina Real-time Transient Survey (CRTS), and the Sloan Digital Sky Survey (SDSS) are detecting, and identifying, large numbers of new (typically fainter) CVs and greatly expanding the known CV population. To include these newly identified CVs in population studies however, they first need to be classified and characterised.

In Chapter 2, I present optical photometric follow-up observations of a sample of 20 faint CVs identified by the CRTS. The main objectives of this work were to determine orbital periods (which are particularly necessary for evolutionary studies), classify the CVs, and identify magnetic and eclipsing systems¹³. In this work we determined orbital periods for 14 of the systems, and independently found a further two. Additionally we identified six SU UMa-type DN, one polar, and eight eclipsing systems. This work forms part of the University of Cape Town CCD survey [Woudt et al., 2012, and references therein], which (including this work), has published optical photometry of 91 CVs, and determined orbital periods for 57 systems.

The large surveys are adroit at detecting new CVs, but more importantly, they provide valuable observations of large samples of CVs. These data can be used to answer a multitude of different science questions, and often probe time-scales that are difficult to observe with tradi-

¹³Eclipse deconvolution studies of the eclipsing systems can be used to determine properties such as the mass ratio and inclination angle [e.g Littlefair et al., 2008], which makes them valuable targets for population studies.

tional targetted observations. As the detection rates of new CVs (and transients in general) are expected to exceed the rate at which we can conduct targetted follow-up studies (which are expensive in terms of telescope time) in the near-future, there is a growing need to develop algorithms to automatically classify and characterise systems based directly on the survey data.

In Chapter 3, I present a script that automatically classifies and characterizes CVs based on long-term photometric data from the CRTS, and then use the script (in combination with multi-wavelength data from other large surveys) to produce a catalogue of properties for 1031 CVs. The catalogue contains fields for the apparent outburst and quiescent V -band magnitude, duty cycle, limit on the outburst recurrence time, upper- and lower-limits on the distance, absolute quiescent magnitudes, orbital parameters, colour information, and X-ray counterparts. This is the largest catalogue of these properties to date. In this sample we found a correlation between the outburst duty cycle and orbital period (and outburst recurrence time), and between the quiescent absolute magnitude and the orbital period (and duty cycle).

Radio Emission from Non-magnetic CVs

Prior to this thesis work, radio emission had only been detected in five non-magnetic CVs (SU UMa, EM Cyg, TY PSc, V3885 Sgr, and SS Cyg), and only one of these (SS Cyg) had been detected in more than one set of observations. The poor detection rates of these objects in historical radio surveys cemented their reputation as non-radio emitters, and established the idea that CVs are one of the few classes of accreting objects to not launch collimated outflows (jets). The subsequent use of CVs to put constraints on jet-launching models [e.g. Livio, 1999; Soker & Lasota, 2004] was brought into sharp question when Körding et al. [2008] predicted that CVs should produce synchrotron emission from a transient jet during outburst, and detected this emission in SS Cyg. Observations of subsequent outbursts of SS Cyg confirmed this behaviour, and also concluded that the radio emission stemmed from a transient jet [Miller-Jones et al., 2011; Russell et al., 2016]. Arguments that SS Cyg was unique (due to an exceedingly high mass accretion rate) were set aside when Miller-Jones et al. [2013] proved that the measured distance was incorrect, and the mass accretion rate was consistent with other DN systems. It was however, still not clear what the radio emission properties and mechanism were in the non-magnetic CVs as a class.

In Chapter 4 and 5, I present radio observations of a sample of non-magnetic CVs (novalikes and dwarf novae) and prove that these systems are significant radio emitters (in excess of the thermal contributions of the disc, the white dwarf, and the secondary). The previous lack of detections was due to a lack of sensitivity, as the detected fluxes are below historical detection thresholds.

The specific luminosity of the radio emission is in the range 10^{14} – 10^{16} erg s $^{-1}$ Hz $^{-1}$ (luminosities of 10^{24} – 10^{26} erg s $^{-1}$ at 10 GHz). In all the sources, the radio emission was non-thermal, and in individual sources was consistent with synchrotron or coherent emission. We detected variability time-scales of minutes to days, different polarization fractions (non-detections to $\geq 75\%$), and a range of spectral indices. We did not find a clear distinction in the radio emission between the novalikes and dwarf novae, the different classes of dwarf novae, or between the different classes

of outburst. This sample did not show a correlation between the radio and optical luminosity, or between the radio luminosity and orbital period. The variability in these objects could be masking an underlying correlation however.

Additionally, we compared the radio emission of dwarf novae to that of SS Cyg, and conclude that SS Cyg is not unique in the luminosity of the radio emission during the plateau phase of the outburst, the type of emission, or the variability time-scales. Higher cadence observations are necessary, however, to compare the evolution of the radio emission over the course of an outburst to that of SS Cyg. High-spatial resolution radio observations are necessary to confirm whether CVs, as a class, launch jets.

Looking Forward

A number of large surveys, such as the LSST (Large Synoptic Survey Telescope) are set to come online in the following years. Automatic classification scripts (such as the one presented in Chapter 3) can be used on this data to detect larger (and less-biased) populations of CVs. The next necessary step in these optical population studies of CVs, is to determine the ‘completeness’ of the survey samples. Surveys (such as the CRTS) have numerous selection effects that produce a bias in the observed population. Before these populations are used to constrain evolutionary models, the biases need to be understood and counteracted.

Having established non-magnetic CVs as radio emitters, the next important steps in this research are to determine the radio emission mechanism(s), and establish whether CVs (as a class) launch jets. This will require a combination of targetted high-cadence, multi-wavelength observations, as well as large-scale population studies using multi-wavelength surveys.

The Square Kilometer Array (SKA) precursor instrument, MeerKAT, is expected to start observations with the full array in 2017. One of the MeerKAT key science projects, ThunderKAT (The Hunt for Dynamic and Explosive Radio Transients with MeerKAT), has been awarded commensal access to the data taken for the large surveys in addition to targetted observing time. Importantly, one of the key science areas for ThunderKAT is the accretion/outflow connection in CVs. To answer the science questions stated previously, we will consequently have high-sensitivity radio observations of large samples of CVs, with cadences and durations that were previously not accessible. In addition to this, the MeerLICHT telescope will provide simultaneous optical observations for all MeerKAT observations. Using algorithms such as the one presented in Chapter 3 on this data, we can determine the accretion state at the time of the radio observations – knowledge that is important in answering these science questions.

In preparation for these surveys, this thesis work has established that non-magnetic CVs are radio emitters, and determined the radio properties necessary to plan for these surveys (e.g. ThunderKAT). In addition to effectively planning a survey, these properties are necessary to classify newly identified objects. For example, Russell et al. [2016] have found that the DN SS Cyg would be a source of confusion for the neutron star X-ray Binaries. By extension, this might be the case for the general CV population. The CV radio properties identified in this thesis work have already been used in classification efforts [Miller-Jones et al., 2015; Tetarenko et al., 2016].

Numerous multi-wavelength surveys are set to come online in the near future, and will provide

SUMMARY

the data to answer these, and other, questions related to the accretion physics in CVs and related objects. The radio observations, in particular, are likely to provide exciting insights into the accretion and outflow processes in these accreting binaries.

SAMENVATTING

Cataclysmische Variabelen (CVs) zijn dubbelstersystemen waarin een lage-massa hoofdreeksster (een rode dwerg) massa overdraagt aan een witte dwerg. Deze massa-overdracht verloopt via zogeheten 'Roche-lobe overflow', doordat de rode dwerg zijn beschikbare volume in het gezamenlijke zwaartekrachtspotentiaal veld van de dubbelster volledig vult. Het overgedragen gas accreteert op de witte dwerg via een accretieschijf. Eén van de openstaande vragen in het onderzoek naar CVs is of deze systemen wel of geen straalstromen vertonen die gelanceerd worden in het interactiegebied tussen de accretieschijf en de witte dwerg. Deze straalstromen worden onder andere verwacht tijdens periodes van verhoogde accretie op de witte dwerg doordat de accretieschijven een instabiliteit ondergaan die we waarnemen als 'dwergnova uitbarstingen'. In vergelijkbare nauwe dubbelstersystemen zijn deze straalstromen met name gedetecteerd in radiostraling doordat de elektronen in deze straalstromen straling uitzenden via het synchrotron mechanisme.

Recente ontwikkelingen op het gebied van CVs benadrukken de behoefte aan grote (meer homogene) catalogi van CVs met goed-gekaracteriseerde eigenschappen, alsmede de behoefte aan simultane waarnemingen op meerdere golflengtes om het verband tussen accretie en uitstroming in straalstromen te onderzoeken. In dit proefschrift heb ik radio-waarnemingen van niet-magnetische CVs gepresenteerd, en bewezen dat zij significante radiobronnen zijn. Ook heb ik optische vervolgwarnemingen van CVs gepresenteerd, en heb ik een algoritme ontwikkeld dat deze objecten automatisch klassificeert, gebaseerd op helderheidsgegevens uit grootschalige onderzoeken. Dit algoritme werd vervolgens toegepast op de Catalina Real-time Transient Survey om een catalogus te ontwikkelen van accretie-eigenschappen van 1031 CVs.

Optical CV Population Studies

Om effectief onderscheid te maken tussen modellen voor de evolutie en dwergnova uitbarstingen van CVs is er behoefte aan grote, statistisch significante, en homogene catalogi van nauwkeurig gekarakteriseerde CVs. Projecten zoals de Catalina Real-time Transient Survey (CRTS) en de Sloan Digital Sky Survey (SDSS) detecteren en identificeren grote aantallen nieuwe (meestal vrij zwakke) CVs, waarmee ze de populatie van bekende CVs sterk uitbreiden. Om deze nieuwe CVs in populatie-onderzoeken te betrekken, moeten zij echter eerst worden geklassificeerd en hun

eigenschappen vastgelegd.

In Hoofdstuk 2 presenteer ik optische waarnemingen van de helderheidsvariaties van een steekproef van 20 zwakke CVs die zijn geïdentificeerd tijdens de CRTS. De hoofddoelen van dit werk zijn om de baanperioden van de CVs vast te leggen (die cruciaal zijn voor evolutionaire onderzoeken), om de CVs te classificeren, en om magnetische en eclipserende systemen te detecteren¹⁴. In dit werk leggen we de baanperioden vast voor 16 CVs. Daarnaast identificeren we zes SU UMa-type dwerg novae, een magnetische systeem (polar) waarbij accretie via het magneetveld verloopt en niet via een accretieschijf en acht eclipserende CVs. Dit werk vormt een deel van de University of Cape Town CCD survey [Woudt et al., 2012, en de daarin aangetroffen referenties], welke (inclusief dit werk) optische helderheidsdata heeft gepubliceerd van 91 CVs en de periode van 57 systemen heeft bepaald.

Grootschalige onderzoeken (surveys) zijn goed in het detecteren van nieuwe CVs. Ze leveren waardevolle waarnemingen van grote aantallen CVs. Deze data kunnen worden gebruikt om een veelvoud aan wetenschappelijke vragen te beantwoorden, en vaak zijn de waarnemingen gedaan op tijdschalen die moeilijk zijn te verkrijgen met traditionele, waarnemingen met een kleiner blikveld. Aangezien de detectiesnelheid van nieuwe CVs vermoedelijk de snelheid waarmee we gedetailleerde vervolgwaarnemingen kunnen doen (die kostbaar zijn qua telescooptijd) zal overstijgen in de nabije toekomst, is er een groeiende behoefte aan het ontwikkelen van algoritmes die systemen automatisch kunnen classificeren en beschrijven op basis van data uit surveys.

In Hoofdstuk 3 presenteer ik een computerprogramma dat automatisch CVs klassificeert en beschrijft op basis van lange-termijn helderheidswaarnemingen uit de CRTS; vervolgens gebruik ik dit programma (in combinatie met data op meerdere golflengten uit andere surveys) om een catalogus te produceren met eigenschappen van 1031 CVs. De catalogus bevat informatie over de uitbarstingen en de kalme *V*-band helderheid, waarneemtijden, limieten op de herhalingsstijd van uitbarstingen, limieten op de afstand, absolute helderheid in kalme toestand, baan-parameters, kleurinformatie, en röntgen-tegenhangers. Dit is de grootste catalogus van deze eigenschappen tot nu toe. In dit onderzoek vonden we een verband tussen de tijdstippen en lengtes van uitbarstingen en de baanperiode (en herhalingsstijd van uitbarstingen), alsmede tussen de absolute helderheid in kalme toestand en de baanperiode (en herhalingsstijd).

Radiostraling van Niet-magnetische CVs

Vóór dit proefschrift was radiostraling slechts gedetecteerd in vijf niet-magnetische CVs (SU UMa, EM Cyg, TY PSc, V3885 Sgr, en SS Cyg), en slechts één van deze bronnen (SS Cyg) werd gedetecteerd in meer dan één set waarnemingen. De moeilijkheid van het detecteren van deze objecten in traditionele radio surveys versterkte hun reputatie als bronnen die niet in radio-golflengten schijnen, alsmede het idee dat CVs één van de weinige klassen van objecten met accretieschijven zijn die geen gecollimeerde straalstromen (jets) produceren. Daaropvolgend gebruik van CVs om limieten te vinden voor modellen met jets [e.g. Livio, 1999; Soker & Lasota, 2004] werd in twijfel

¹⁴Nauwkeurige studies van de eclipserende systemen kunnen worden gebruikt om eigenschappen zoals de massa-verhouding en de baan-inclinatie vast te leggen [o.a. Littlefair et al., 2008], hetgeen ze waardevolle doelwitten maakt voor populatie-onderzoeken.

getrokken toen Körding et al. [2008] voorspelde dat CVs synchrotronstraling zouden moeten produceren door middel van een tijdelijke jet tijdens uitbarstingen, en deze straling vervolgens heeft waargenomen in SS Cyg. Waarnemingen van verdere uitbarstingen van SS Cyg bevestigden dit gedrag, alsmede het feit dat de radiostraling uit een tijdelijke jet voortkwam [Miller-Jones et al., 2011; Russell et al., 2016]. Argumenten dat SS Cyg een uniek geval was (door een zeer hoog tempo van massa-accretie) werden opzij gezet toen Miller-Jones et al. [2013] bewees dat de gemeten afstand tot de bron incorrect was, en dat het tempo van accretie consistent was met andere DN systemen. Het was echter nog altijd niet duidelijk door welk mechanisme de radiostraling werd gegenereerd in niet-magnetische CVs, of wat de eigenschappen van deze straling waren.

In Hoofdstukken 4 en 5 presenteer ik radio-waarnemingen van een steekproef van niet-magnetische CVs (zogenaamde novalikes en dwerg novae), en bewijs ik dat deze systemen significante bronnen van radiostraling zijn: zij produceren meer radiostraling dan de bijdrage door thermische straling in de accretieschijf, de witte dwerg, en haar compagnon. Het voormalige gebrek aan detecties kwam door een gebrek aan gevoeligheid van de waarnemingen; de gedetecteerde flux ligt onder de historische detectiedrempels.

De specifieke lichtkracht van de radiostraling ligt in het bereik 10^{14} – 10^{16} erg s⁻¹ Hz⁻¹ (een lichtkracht van 10^{24} – 10^{26} erg s⁻¹ op 10 GHz). In alle bronnen was de radio-straling non-thermisch, en in individuele bronnen was zij consistent met synchrotronstraling of coherente straling. We namen tijdschalen van variabiliteit waar van minuten tot dagen, alsmede verschillende polarisatiefracties (non-detecties tot $\geq 75\%$), en een reeks spectrale indices. We vonden geen duidelijk onderscheid in de radiostraling afkomstig van novalikes en dwerg novae, de verschillende klassen van dwerg novae, of de verschillende klassen van uitbarstingen. Deze steekproef toonde geen correlatie tussen de radio- en optische lichtkracht, of tussen de radio-helderheid en de baanperiode. De variabiliteit in deze objecten kunnen echter een onderliggende correlatie maskeren.

Ook hebben we de radiostraling van dwerg novae vergeleken met die van SS Cyg. We concluderen dat SS Cyg niet uniek is in de lichtkracht van de radiostraling tijdens de plateau-fase van de uitbarsting, het type straling, of de tijdschalen van variabiliteit. Waarnemingen met hogere cadans zijn echter noodzakelijk om de evolutie van de radiostraling tijdens een uitbarsting te vergelijken met die van SS Cyg. Radio-waarnemingen met hoge ruimtelijke resolutie zijn vereist om te bevestigen of te weerleggen dat CVs jets lanceren.

Vooruit Kijken

Een aantal grootschalige surveys, zoals de LSST (Large Synoptic Survey Telescope), komen tijdens de komende jaren op gang. Automatische classificatie-algoritmen (zoals het algoritme dat in Hoofdstuk 3 wordt gepresenteerd) kunnen op deze data worden toegepast om grotere, beter gebalanceerde populaties van CVs te detecteren. De volgende noodzakelijke stap in deze optische populatie-studies van CVs is om de volledigheid van de surveys te achterhalen. Surveys zoals de CRTS hebben vele selectie-effecten die een bias introduceren in de waargenomen populatie. Voordat deze populaties kunnen worden gebruikt om evolutionaire modellen te evalueren moet deze bias worden begrepen en gecorrigeerd.

Nadat we hebben bevestigd dat niet-magnetische CVs bronnen zijn van radiostraling is de

volgende belangrijke stap in dit onderzoek om te bepalen welk(e) mechanisme(n) verantwoordelijk is/zijn voor de straling, en om te bepalen of CVs in het algemeen jets produceren. Dit zal een combinatie van doelgerichte, hoge-cadans, multi-golflengte-waarnemingen vereisen, alsmede een grootschalige populatie-studie die gebruik maakt van multi-golflengte surveys.

De Zuid-Afrikaanse voorganger van de Square Kilometer Array (SKA), MeerKAT, zal beginnen met waarnemingen in 2017. Één van de belangrijkste wetenschappelijke projecten van MeerKAT, ThunderKAT (The Hunt for Dynamic and Explosive Radio Transients with MeerKAT), heeft toegang gekregen tot data vergaard in grootschalige surveys alsmede doelgerichte waarneemtijd. Belangrijk hierbij is dat één van de belangrijkste aandachtsgebieden van ThunderKAT de accretie en uitstroming van CVs behelst. Om de wetenschappelijke vragen die hierboven worden gesteld te beantwoorden zullen we daarom radio-waarnemingen van hoge kwaliteit hebben van grote hoeveelheden CVs, met een cadans en waarneemtijd die voorheen niet te realiseren waren. Bovendien zal de MeerLICHT telescoop simultaan optische waarnemingen leveren voor alle MeerKAT waarnemingen. Door algoritmes zoals het algoritme dat in Hoofdstuk 3 wordt gepresenteerd toe te passen op deze data kunnen we de accretie-toestand vaststellen tijdens de radio-waarnemingen – kennis die belangrijk is voor het beantwoorden van deze wetenschappelijke vragen.

Als voorbereiding op deze surveys hebben we in dit proefschrift vastgesteld dat niet-magnetische CVs bronnen van radiostraling zijn, en hebben we de eigenschappen vastgelegd van een radio-instrument dat deze surveys kan uitvoeren (zoals ThunderKAT). Naast het effectief plannen van een survey zijn deze eigenschappen nodig om nieuwe objecten te klassificeren. Ter voorbeeld: Russell et al. [2016] ontdekte dat de DN SS Cyg een bron van verwarring zou zijn voor de neutronenster-röntgendubbelsterren. Dit kan ook het geval zijn voor de algemene CV populatie. De radio-eigenschappen van CVs die in dit proefschrift worden gerapporteerd worden reeds gebruikt voor het klassificeren van zulke objecten [Miller-Jones et al., 2015; Tetarenko et al., 2016].

Verscheidene multi-golflengte surveys zullen in de nabije toekomst uitgevoerd worden, en zij zullen de data leveren die deze en andere vragen, gerelateerd aan de accretie-fysica van CVs en verwante objecten, kunnen beantwoorden. Vooral de radio-waarnemingen zullen waarschijnlijk interessante inzichten leveren in de accretie en uitstromingsprocessen in deze accreterende binaire systemen.

PUBLICATION LIST

- **Coppejans D.L.**, Körding E.G., Miller-Jones J.C.A., Rupen M.P., Sivakoff G.R., Knigge C., Groot P.J., Woudt P.A., Waagen E.O., Templeton M., 2016, MNRAS [accepted], “*Dwarf nova-type cataclysmic variable stars are significant radio emitters*”
- **Coppejans D.L.**, Körding E.G., Knigge C., Pretorius M.L., Woudt P.A., Groot P.J., Van Eck C., Drake A.J., 2016, MNRAS, 456, 4441 – 4454, “*Statistical properties of dwarf novae type cataclysmic variables: The outburst catalogue*”
- **Coppejans D.L.**, Körding E.G., Miller-Jones J.C.A., Rupen M.P., Knigge C., Sivakoff G.R., 2015, MNRAS, 451, 3801 – 3813, “*Novalike cataclysmic variables are significant radio emitters*”
- **Coppejans D.L.**, Woudt P. A., Warner B., Körding E., Macfarlane S.A., Schurch M.P.E., Kotze M.M., Breytenbach H.B., Gulbis A.A.S., Coppejans R., 2014, MNRAS, 437, 510 – 523, “*High-speed photometry of faint cataclysmic variables - VIII. Targets from the Catalina Real-Time Transient Survey*”
- Coppejans R., Gulbis A.A.S., Kotze M.M., **Coppejans D.L.**, Worters H.L., Woudt P.A., Whittal H., Cloete, J., Fourie P., 2013, PASP, 125, 930, 976 – 988, “*Characterizing and Commissioning the Sutherland High-Speed Optical Cameras (SHOC)*”
- Woudt P. A., Warner B., **de Bude D.** (*maiden name*), Macfarlane S., Schurch M.P.E., Zietsman E., 2012, MNRAS, 421, 2414 – 2429, “*High-speed photometry of faint cataclysmic variables - VII. Targets selected from the Sloan Digital Sky Survey and the Catalina Real-time Transient Survey*”

Proceedings

- **Coppejans D.**, Koerding E., Groot P., Knigge C., Pretorius R., Woudt P., Drake A., 2014, in *The X-ray Universe 2014*, Jan-Uwe Ness (ed.), “*Dwarf Novae of the Catalina Real-time Transient Survey*”

PUBLICATION LIST

- **de Bude D.**, Woudt P., Warner B., 2012, in *New Horizons in Time-Domain Astronomy*, Proceedings of the IAU, Griffin E., Hanisch R., Seaman, R. (eds.), 285, 301, “*Characterising the Dwarf Nova Population of the Catalina Real-time Transient Survey*”
- **de Bude D.**, Woudt P., Warner B., Macfarlane S.A., 2012, *African Skies*, 16, 111 – 113, “*Ultra-Compact Binaries in the Galaxy*”
- Woudt P.A., Warner B., **de Bude D.**, 2012, *African Skies*, 16,141, “*Orbital Period Distribution of Cataclysmic Variables in the Catalina Real-time Transient Survey*”

CURRICULUM VITAE

Deanne Coppejans was born in Johannesburg (South Africa), and attended school at Halfway House Primary School and Midrand High School. To pursue her interest in science, mathematics and computers, Deanne completed a BSc Physics (with distinction) at the University of Pretoria in 2008. It was during these studies that she became fascinated with astrophysics (compact stars in particular), and decided to specialise in this field.

The South African Square Kilometre Array (SKA) project funded Deanne's subsequent studies at the University of Cape Town. In 2009 she obtained a BSc Honours degree in Theoretical Physics, and in 2011 she completed a MSc Astronomy degree (with distinction). Her MSc project was supervised by Prof. Patrick Woudt and Em. Dist. Prof. Brian Warner, and involved using optical photometric observations to classify and characterise Cataclysmic Variable stars (CVs). During this time she spent a total of 12 (very enjoyable) weeks observing at the Sutherland site of the South African Astronomical Observatory.

In December 2011, Deanne moved to the Netherlands to begin a PhD Astrophysics at Radboud University. Dr. Elmar K rding, and Professors Paul Groot and Patrick Woudt, supervised this PhD. It was partially funded by the Erasmus Mundus programme SAPIENT. During her PhD, she used radio and optical observations, combined with multi-wavelength large survey data, to study the accretion properties of CVs. The main projects and results of this research are presented in this thesis.

Over the course of her studies, Deanne has tutored courses (Introductory Physics, Stellar Astrophysics, An Introduction to Modern Astrophysics, Radio Astronomy, and Observational Astronomy) at all three of the universities she attended. She enjoys outreach, and has given telescope tours and public talks, participated in public observing nights, and contributed to the Siyavula open source textbooks in South Africa.

After her PhD, Deanne will begin a postdoctoral position at Northwestern University, to work on multi-wavelength observations of supernovae and CVs with Dr Raffaella Margutti.

ACKNOWLEDGEMENTS

Thank you to every one of the many people who have helped and supported me over the years. It feels wonderful to finally see this thesis in print, and your support has made it possible. There are a few people in particular that I would like to mention...

To my amazing supervisor, Elmar: You have always made time to help me, even when your family was very young and you were tired from travelling. You have helped me through this PhD in so many ways – the most memorable of which was when you saw that there was one particularly difficult task that I kept on pushing backwards on my ‘to do’ list, and you ‘paid’ me a chocolate coin to drop everything else and finish it first. As the task proved easier than I thought, and I kept this in mind when faced with subsequent difficult tasks, this was a highly successful exercise. I think you will also be pleased to hear that whenever I feel the need to nitpick finished work, I hear the words ‘stop polishing it’ in your voice – and they get increasingly louder and more insistent if I ignore them. Thank you so much for everything.

Paul and Patrick, thank you for all the great discussions, comments, help and advice – I have learned so much during this PhD. I also want to thank you for all the work you put into setting the PhD up, especially considering all the organisational work between SAPIENT, Radboud and UCT.

Thank you to all my collaborators for your contributions to the articles in this thesis. Especially thank you to James, Christian, Greg, Michael, Retha and Brian, whose constructive comments, questions, and feedback have taught me so much.

To my manuscript and examination committee: Thank you for the time and effort you have put into evaluating this thesis, I really appreciate it.

Over the years I have received funding for my studies from a number of institutions that I would like to thank: Midrand High School, McCarthy Toyota Midrand, the University of Pretoria, the University of Cape Town, the South African Square Kilometre Array Project, Radboud University, and the Erasmus Mundus project SAPIENT.

There have been many other people who have been important in completing this PhD. Thank you Thomas for translating my summary, Pim for your countless hours sorting out the cluster, and Martin for your great thesis template. Cameron, thank you for all your help and the many discussions about statistics, radio astronomy principles, polar bears, and English grammar. Let

ACKNOWLEDGEMENTS

me say here (officially on the record), that despite your protests to the contrary, you were deeply involved in all the office pranks. To all my wonderful office mates, you have made the office a fun (if somewhat perilous) place to work. Wendy and Kosma, the Python support and the motivation fairies/llamas you have sent me over the years have been a real help in finishing this thesis. Your support has been really amazing. To the rest of my friends/colleagues thank you so much for the myriad ways you have helped me complete this thesis.

Sally, we moved country together, have survived gale force winds and glaciers together, and somehow got through this PhD together, and I am really going to miss you. Your monumentally hyperbolised renditions of awkward moments have helped me to laugh through some tough times. Keep in touch.

To my family, you have always believed in me – something that means more to me than I can express. Even though you are far away, please know that your support helps me through the hard times, and the good times.

Rocco, jy weet wat jy vir my beteken. Vir al die kere wat jy jou arms om my gesit het en my die krag gegee het om aan te gaan - hierdie tesis is opgedra aan jou.